South Eastern Australian

Climate Initiative

Program Annual Report 2010/11

October 2011

Citation
CSIRO (2011) South Eastern Australian Climate Initiative Program Annual Report 2010/11. CSIRO, Australia.

Program management

Program Director David Post
Program Coordinator Therese McGillion
Program Communicator Laura Wynne (to March 2011), Heidi Dennis (July 2011 onwards)
Theme Leaders Bertrand Timbal (Theme 1), Francis Chiew (Theme 2), Harry Hendon (Theme 3)
Finance Officer Suzanne Blankley
Data Manager Steve Marvanek
Administration Assistant Kieran O'Shea

Report production

Scientific Editor Becky Schmidt
Production Assistants Simon Gallant, Ben Wurcker
Designer Siobhan Duffy

Projects

Project Leaders Bertrand Timbal (Project 1.1), Peter Briggs and Mike Raupach (Project 1.2), Dewi Kirono (Project 2.1), Cuan Petheram (Project 2.2), Harry Hendon (Project 3.1), QJ Wang (Project 3.2)

Project Team Members (by organisation)

CSIRO: Wenju Cai, Tim Cowan, Marie Ekstrom, Vanessa Haverd, Sandra Hawthorne, David Kent, Yun Li, Matt Paget, Prafulla Pokhrel, Nicholas Potter, David Robertson, Jin Teng, Peter van Rensch, Biao Wang, Kirien Whan, Lu Zhang

Bureau of Meteorology: Oscar Alves, Morwenna Griffiths, Sally Langford, Eun-Pa Lim, Guo Liu, Chris Lucas, Hanh Nguyen, Guomin Wang, Yang Wang

Program governance

Steering Committee Campbell Fitzpatrick (Chair, Victorian Department of Sustainability and Environment), Jody Swirepik (Murray–Darling Basin Authority), Chris Johnston / Kushla Munro (Department of Climate Change and Energy Efficiency), Neville Smith (Bureau of Meteorology), and Ian Prosser (CSIRO)

Science Panel Graeme Pearman (Independent Chairperson), Michael Manton (Independent), Jason Alexandra (Murray–Darling Basin Authority), Rae Moran (Victorian Department of Sustainability and Environment), Anthony Swirepik (Department of Climate Change and Energy Efficiency), Tom Keenan / Peter May (Bureau of Meteorology), and Glen Walker (CSIRO)

Address and contact details:
CSIRO Water for a Healthy Country Flagship
Ph (+61 2) 62465617 Fax (+61 2) 62465800
Email: seaci@csiro.au

EXECUTIVE SUMMARY

The South Eastern Australian Climate Initiative (SEACI) was established in 2005 to investigate the causes, impacts and prediction of climate variability and change in south-eastern Australia. The first three years of SEACI made progress in characterising and explaining the nature and causes of the recent drought, produced climate and runoff projections out to 2030, and improved seasonal forecasts of rainfall and runoff across south-eastern Australia.

These research findings are summarised in the report Climate variability and change in south-eastern Australia: A synthesis of findings from Phase 1 of the South Eastern Australian Climate Initiative (SEACI) available for download from <http://www.seaci.org>.

Research in Phase 2 of SEACI is building on the findings of Phase 1. It is a three-year, $9 million research partnership between the Murray–Darling Basin Authority, the Victorian Government Department of Sustainability and Environment, CSIRO Water for a Healthy Country Flagship, the Bureau of Meteorology and the Australian Government Department of Climate Change and Energy Efficiency. The SEACI study area incorporates the Murray–Darling Basin, the state of Victoria and southern South Australia, including the Eyre Peninsula.

Research in Phase 2 of SEACI is conducted through three related themes. This report summarises the progress made in the second year (2010/11) of Phase 2 of SEACI. Progress made in the first year of Phase 2 is summarised in the Program Annual Report 2009/10 (CSIRO, 2010a).

Theme 1: Understanding past hydroclimate variability and change in south-eastern Australia

Research in Theme 1 is contributing to a better understanding of the factors that influence climate and streamflow within south-eastern Australia (SEA). Having previously established the relationship between south-eastern Australian rainfall and the Sub-Tropical Ridge (STR) intensity and position, the focus this year has been to investigate the relationship between this key controller of SEA rainfall and large-scale indices of the Mean Meridional Circulation such the Australian Monsoon Index and the intensity and latitudinal extent of the Hadley circulation.. The overall picture emerging is that the changes seen across SEA are part of changes in large-scale atmospheric circulation patterns and, in turn, in climate affecting the entire southern hemisphere. For example, a range of datasets and methods indicate that the tropics are expanding, pushing the downward descending arm of the Hadley circulation further south. Although not very large (of the order of 0.5° per decade), evidence for this expansion appears very robust. One important finding was that changes in both the Sub Tropical Ridge intensity (STR-I) and Sub Tropical Ridge position (STR-P) are related to the expansion of the Hadley circulation. While this was anticipated for the STR-P, this is a surprise for the STR-I, which was expected to relate more to the intensity of the Hadley cell. These observed changes are changing the nature of the rainfall across SEA: rain bearing systems affecting SEA are less often due to mid latitude cyclones and increasingly due to larger systems located further north. This signal is seasonally dependent and peaks during summer and autumn, providing insight into the observed autumn rainfall deficit. Finally, a climate model reproduced the expansion of the Hadley circulation only if anthropogenic influences on atmospheric greenhouse gas and particle concentrations were included in the model. Furthermore, the model also related the strengthening of the STR to the expansion and not the intensity of the Hadley circulation.

Research has also continued into understanding the relationship between hydrological drivers and responses using the CableDyn model. The latest model results show that precipitation is the dominant determinate of discharge with an increase/decrease in rainfall being amplified by a factor of 3 for wetter catchments in SEA and

8 for drier catchments. Temperature and CO_2 concentrations have smaller, but still significant impacts on runoff with discharge reducing by 4 to 9 percent per degree temperature increase. The effects of CO_2 on runoff are still being investigated.

Theme 2: Long-term hydroclimate projections in south-eastern Australia

Research in Theme 2 aims to improve long-term projections of climate and streamflow for south-eastern Australia. In 2010/11, we assessed the ability of the 24 IPCC AR4 global climate models to represent a range of selected climate variables and large-scale climate drivers across SEA. Having done this, we selected the better performing models and explored the implications of weighting and/or selection for future rainfall projections for the region. Results showed that the CSIRO-MK3.0 and MIROC3.2-MEDRES models were the best performing across SEA, followed by CGCM-T47, CSIRO_MK3.5, IPSL-CM4, INM-CM3.0, MRI-CGCM2.3, and CNRM-CM3 (see main text for explanation of these acronyms). Other models i.e. MIROC3.2.-HIRES, NCAR-CCSM, GFDL-CM2.0, ECHAM-MPI, NCAR-PCM, UKMO-HadCM3 and GFDL-CM2.1, are also classified as 'best performing' but they do not have the required data for the analogue downscaling technique or potential evapotranspiration data. The median annual rainfall projections from the first eight best models are drier than the median from all 24 models. Work also began on assessing a range of downscaling methods across SEA, including pattern scaling, dynamic downscaling using the Weather Research and Forecasting (WRF) model and analogue downscaling. Initial results suggest that the analogue downscaling technique may be useful; however more work is required in order for the method to produce daily rainfall time series that are sufficiently similar to the observed daily rainfalls for direct use in hydrological models. Research into the potential use of WRF is continuing. However, at this point in time, the pattern scaling technique is still the most robust for use in climate-change studies with an emphasis on hydrology. One note of caution is that the current generation of pattern-scaled results are based on climate model projections which only cover up to around 2.0 °C of global warming. Extrapolation beyond this range therefore should be undertaken with caution.

Research was also carried out to determine if observations demonstrated changes in the rainfall-temperature-runoff relationship for 34 catchments in SEA. Of these 34 catchments, 22 had a statistically significantly different rainfall-streamflow relationship during the recent drought, and 18 had a statistically significantly different temperature-streamflow relationship. Of the average 46 percent reduction in streamflow during the recent drought, 65 percent was accounted for by reductions in annual rainfall, 7 percent by increases in temperature, and 28 percent was unexplained. Further analysis of these catchments suggested that runoff-generating processes have changed to a greater extent in the low-rainfall catchments of the southern SEACI region than in the high-rainfall catchments due to a change to the aquifer storage – outflow relationship in these (low-rainfall) catchments. To investigate this further, 17 catchments with streamflow and groundwater data prior to and during the recent drought were examined in more detail. This analysis suggests that that the majority of the reduction in streamflow in these catchments was due to an unprecedented deepening and drying of the unsaturated zone. However, there is still uncertainty as to whether there had been an increase in the number of farm dams during the recent drought which would act to confound these results.

Theme 3: Seasonal hydroclimate prediction in south-eastern Australia

Research in Theme 3 is exploring the potential for improved seasonal forecasts of climate and streamflow. In 2010/11, we assessed the improvements in climate forecasting obtained by using the new version of the Predictive Ocean Atmosphere Model for Australia (POAMA2) system by comparison with results obtained from POAMA1.5, focussing on the representation and prediction of the main climate drivers of rainfall in SEA. Our investigation showed that the influence of the Indian Ocean Dipole (IOD) is dominant in southern SEA in winter and early spring whereas the influence of central Pacific El Niño is strong in northern SEA in autumn to spring. POAMA2 demonstrates improved skill in predicting the variability of different types of El Niño – Southern Oscillation (ENSO) and sea-surface temperatures over the eastern Indian Ocean (the eastern pole of the IOD). POAMA2 demonstrates good skill at short lead times (zero to one month) in predicting rainfall in SEA for all seasons except for late autumn and summer. POAMA2 shows good skill in late winter to early summer at lead times of up to 2 to 4 months. Further improvements may come from using a dynamical multi-model ensemble which has been demonstrated to improve all aspects of forecast quality: accuracy, reliability, resolution and sharpness.

We also investigated the use of dynamical model outputs as an alternative to the existing predictors in the Bayesian joint probability approach for forecasting seasonal streamflows. In particular, we used simulations from the Water Balance and Partition (WAPABA) model and rainfall forecasts from POAMA2. This new statistical-dynamical modelling approach was applied to produce seasonal streamflow forecasts in 21 catchments with different climatic and catchment characteristics, on the eastern coast of Australia. The results indicate that forecasts produced using the outputs from the dynamic hydrologic model, are as good as those produced using the antecedent observations. However, the use of hydrological modelling outputs as a predictor is attractive for operational forecasting because it eliminates the need for selecting predictors related to the initial catchment condition, thereby reducing the computational requirements to establish forecast models. In addition, the skill estimates based on forecasts of historical events are not artificially inflated as can occur with predictor selection. The streamflow forecasts produced using POAMA2 rainfall forecasts as predictors do not outperform, on average, forecasts made using climate indices. For many locations and seasons, POAMA rainfall forecasts introduce noise and reduce the forecast skill. However, for some catchments and seasons, inclusion of POAMA does improve the forecast skill. We suggest that Bayesian model averaging, over a range of models, using both climate indices and POAMA rainfall as predictors, could be a way to make use of the best available information.

A highlight of 2010/11 is the adoption of the Bayesian joint probability approach by the Australian Bureau of Meteorology, with seasonal streamflow forecasts for 21 locations in SEA released to the public as of December 2010.

CONTENTS

FIGURES

TABLES

ACRONYMS

AWAP	Australian Water Availability Project
BJP	Bayesian joint probability
BoM	Bureau of Meteorology
CAWCR	Centre for Australian Weather and Climate Research
CCAM	cubic conformal atmospheric model
DDD	drought depth duration
DMI	Indian Ocean Dipole Mode Index
EMI	El Niño Modoki Index
ENSO	El Niño – Southern Oscillation
Ep	potential evaporation
ESCCI	Eastern Seaboard Climate Change Initiative
GCM	global climate model
IOD	Indian Ocean Dipole
IPCC AR4	Intergovernmental Panel on Climate Change Fourth Assessment Report
MDB	Murray–Darling Basin
MMC	mean meridional circulation
MME	multi-model ensemble
MSLP	mean sea-level pressure
NCC	National Climate Centre
NCEP	National Center for Environmental Prediction
NHMM	non-homogenous hidden Markov Model
NSE	Nash-Sutcliffe efficiency
PEODAS	POAMA Ensemble Ocean Data Assimilation System
POAMA	Predictive Ocean Atmosphere Model for Australia
PPE	physics parameter ensemble
PsBF	pseudo Bayes factor
SAM	Southern Annular Mode
SEA	south-eastern Australia
SEACI	South Eastern Australian Climate Initiative
SST	sea-surface temperature
STR	sub-tropical ridge
Tmax	maximum temperature
WRF	Weather Research Forecasting
WIRADA	Water Information Research and Development Alliance

CHAPTER 1: INTRODUCTION

The South Eastern Australian Climate Initiative

Phase 2 of the South Eastern Australian Climate Initiative (SEACI) is a three-year, $9 million research program investigating the causes and impacts of climate change and climate variability across south-eastern Australia. The SEACI geographical study area incorporates the Murray–Darling Basin, the state of Victoria and southern South Australia, including the Eyre Peninsula, as shown in Figure 1.

Planning for future management of Australia's water resources requires an understanding of the future state of Australia's climate. This program aims to deliver a holistic and better integrated understanding of climate change and climate variability across south-eastern Australia to support water managers and policy makers.

The research program includes studies of the nature and causes of climate variability on time scales from weeks to decades. This range of scales is relevant to the stakeholders. Issues on short-term time scales (weeks and months) arise in the operational management of water, while horizons for water resources planning and policy are of a long-term nature (years and decades).

SEACI is a partnership between CSIRO Water for a Healthy Country Flagship, the Australian Government Bureau of Meteorology, the Murray-Darling Basin Authority, the Victorian Department of Sustainability and Environment, and the Australian Government Department of Climate Change and Energy Efficiency. CSIRO is the managing agency.

A Steering Committee, comprising representatives of each partner agency, sets and monitors the strategic direction of SEACI. In 2010/11 a representative from the Victorian Department of Sustainability and Environment chaired the Steering Committee (Campbell Fitzpatrick). The Steering Committee is supported by a Science Panel, which provides advice on implementation of the initiative. The Science Panel is chaired by an independent expert, Dr Graeme Pearman.

In 2010/11 Dr David Post from CSIRO continued his role as SEACI Program Director.

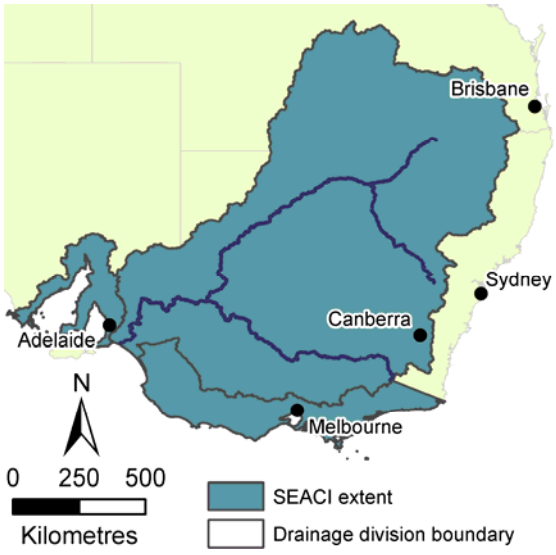

Figure 1. The study area of the South Eastern Australian Climate Initiative

Research context

The variability of Australia's climate has always been a challenge for water management and agricultural industries. Global climate change is now recognised as a threat to water resources, agriculture and natural ecosystems in many parts of the world. In south-eastern Australia, temperatures have been rising steadily and with the exception of 2010/11, rainfall has been low since the 1990s. Similar rainfall declines started in the mid-1970s in south-west Western Australia, prompting the establishment of the Indian Ocean Climate Initiative (IOCI) in 1997. IOCI research focused on understanding variability and change in the region's climate, and showed that climate change is likely to be a significant factor in the observed changes in the region. The clear benefits of IOCI motivated the establishment of SEACI.

Findings from Phase 1 of the South Eastern Australian Climate Initiative

Research in Phase 1 of SEACI included an investigation into the nature and causes of the Millennium Drought which occurred from 1997 to 2009 in SEA. Research concluded that this drought is unprecedented with regards to its extent, the low degree of inter-annual rainfall variability, and the seasons in which the rainfall has declined. In particular, SEACI research found that throughout the drought the rainfall decline was greatest in the autumn months, unlike in previous droughts where the rainfall decline was greatest in winter and spring.

The STR is a band of high pressure which affects rainfall across southern Australia. SEACI research found a strong relationship between increased pressures along the STR and the recent rainfall decline. Further modelling studies conducted within SEACI showed that this observed intensification of the STR could only be reproduced when human influences on atmospheric greenhouse-gas and particle concentrations were included. This suggests a link between global warming and the recent rainfall decline in SEA.

Research throughout Phase 1 of SEACI also showed that the 13 percent decline in rainfall in the southern Murray–Darling Basin during the Millennium Drought led to a 44 percent reduction in streamflow. The magnitude of this reduction in streamflow was greater than expected. This is thought to be likely due to the absence of wet years over the decade, and to the seasons in which the rainfall has declined. The decline in autumn rainfall has meant that winter rains must moisten the soil before any useful streamflow can begin. It is expected that in the future this effect will be amplified as average temperatures across the region continue to rise due to climate change.

Phase 1 of SEACI also achieved improvements to the coupled atmosphere–ocean–land climate model (POAMA) to increase the accuracy of seasonal forecasting, especially for SEA. Ongoing research efforts will further refine POAMA and aim to increase the accuracy of prediction at longer lead times.

Research in Phase 2 of SEACI is building upon the findings and progress made in Phase 1. Phase 2 is addressing key research questions through three linked research themes, described below.

Details of the findings of Phase 1 of SEACI can be found in:

CSIRO (2010) Climate variability and change in south-eastern Australia: a synthesis of findings from Phase 1 of the South Eastern Australian Climate Initiative (SEACI). SEACI report, 36 pp. <http://www.seaci.org/publications/documents/SEACI-1%20Reports/Phase1_SynthesisReport.pdf>

Research themes

Theme 1: Understanding past hydroclimate variability and change in south-eastern Australia

Research in Theme 1 will lead to a better understanding of the factors that drive changes in both climate and streamflow within the region. The projects aim to understand and attribute causes of observed climate change in SEA, as well as diagnose the relationships between climate variability and the water balance.

The projects in Theme 1 are:

Project 1.1: Understanding and attributing climate change in SEA.

Project 1.2: Impact of climate variability and change on the water balance.

Theme 2: Long-term hydroclimate projections in south-eastern Australia

Research in Theme 2 will lead to improved hydroclimate projections for SEA. The research aims to identify the most suitable global climate models assess methods for downscaling projections from these models to obtain catchment-scale climate series, and adapt hydrological models to represent changed rainfall–temperature–streamflow relationships and dominant hydrological processes in a warmer, drier environment with increased levels of CO_2.

The projects in Theme 2 are:

Project 2.1: Climate change projections.

Project 2.2: Hydroclimate impacts for SEA.

Theme 3: Seasonal hydroclimate prediction in south-eastern Australia

Theme 3 is aiming to improve predictions of rainfall and streamflow on timescales of around 1 to 12 months in SEA, extending to the development of operational products. It assesses the skill of models in producing useful predictions of streamflow. Additionally, it is further developing modelling approaches and assessing the utility of seasonal forecasts in improving the skill of hydrological modelling for SEA.

The projects in Theme 3 are:

Project 3.1: Advancing seasonal predictions for SEA.

Project 3.2: Hydrological application of seasonal predictions.

About this report

This report provides detailed information about the progress made in each of the six SEACI research projects in the 2010/11 financial year. Publications arising from this year's research are listed at the end of the document.

CHAPTER 2: PROJECT 1.1

Understanding and attributing climate change in south-eastern Australia

Bertrand Timbal, Hanh Nguyen, Chris Lucas, Morwenna Griffiths, Kirien Whan, Robert Fawcett, Harry Hendon, Wenju Cai, Tim Cowan and Peter van Rensch.

Abstract

Across the many activities undertaken as part of this project, a clear focus on the meridional circulation and its various components is emerging. This is particularly true for autumn, the key season of the on-going rainfall deficit. The project has seen a large number of new developments investigating new or existing datasets using novel approaches and methodologies. Having established the relationship between SEA rainfall and the Sub-Tropical Ridge (STR) intensity and position, the focus this year has been to investigate the relationship between this key controller of SEA rainfall and large-scale indices of the Mean Meridional Circulation (MMC) such as the intensity and latitudinal extent of the Hadley circulation, and a Northern Australian Circulation Index based on lower tropospheric zonal winds. A particular effort has been made to access all existing global reanalyses of the atmosphere to ensure an appropriate sampling of the errors in our knowledge of the climate mean state. In particular, as it is well recognised that global observing systems markedly improved in the late 1970s, many analyses presented here focus on the period from 1980 to the present when satellite data are widely used.

The picture emerging across the entire project is that SEA has been affected by large-scale changes that are affecting the entire Southern Hemisphere. It was found across a range of datasets and methods that the tropics are expanding. This is changing the nature of the rainfall across SEA: rain bearing systems affecting SEA are less often due to mid-latitude cyclones forming part of the storm track but increasingly due to larger systems centred further north, hence increasing the relationship between SEA rainfall and the northern half of the continent. The broadening of the tropics is one aspect of the broadening of the MMC which is apparent in all existing reanalyses. Although not very large (of the order of 0.5° per decade), evidence for this expansion appears very robust. The extent of the broadening of the tropics is seasonally dependent and peaks during summer and autumn. This provides insight into the observed autumn rainfall deficit. It appears to be the critical period in which the peak of the MMC changes (i.e. summer and autumn) overlaps with the period during which the relationship between the STR (the surface signature of the MMC) and SEA rainfall is strongest (this relationship peaks during winter but starts to be significant from April). One important finding was that both changes in STR-I and STR-P are related to the expansion of the Hadley cell. While this was anticipated for the STR-P, this is a surprise for the STR-I, which was expected to relate more to the intensity of the Hadley cell.

Finally, these changes were investigated using a climate model. It was found that the model reproduces an extension of the cell only if human influences on atmospheric greenhouse-gas and particle concentrations were used, either alone or combined with natural external influences. The widening of the southern hemisphere cell is a highly likely feature since it is reproduced in every single climate model simulation that includes these human effects (10 in total). Furthermore, the model also related the strengthening of the STR (observed in the model as well) to the expansion and not the intensity of the cell.

Background

Phase 1 of SEACI made substantial progress in documenting recent climate change in SEA and identifying the large-scale circulations that control the regional climate of SEA including the El Niño – Southern Oscillation (ENSO), the Indian Ocean Dipole (IOD), and the Southern Annular Mode (SAM). Key findings were that the recently observed decline in rainfall in SEA has occurred predominantly in the autumn and early winter, and that much of this decline is accounted for by an increased intensity of the STR. In addition, it was established that the rise in the STR-I followed the rise of global temperature. Although the STR-I and STR-P are convenient diagnostics closely linked to rainfall in SEA, the causality of the global temperature–STR relationship remains to be established and requires further investigation.

During the first year of Phase 2 of SEACI, further progress was made in better understanding and attributing the ongoing rainfall deficiency in SEA. The characterisation of the severity of the recent drought was improved by analysis of a longer set of data from the instrumental record. This provided a better comparison of the severity of the rainfall deficiency in the recent drought relative to that of the Federation drought. The annual cycle of the natural variability of rainfall in SEA and its relationship with the annual cycle of the ongoing rainfall deficiency was analysed, quantifying identifying the amount of natural variability which is not due to large-scale forcings but weather noise. Finally, an important contribution was to review the existing literature regarding the MMC of the atmosphere, its observed changes, and likely response to global warming with a focus on relevant features for climate in SEA.

Objectives

The objectives for 2010/11 were to:

- refine the analysis of SEA rainfall using daily rainfall statistics and fine-scale features: defining rainfall entities, tracking their directions and identifying relationships between temperature and rainfall
- identify synoptic systems using the cyclone tracking package developed at the University of Melbourne, but not following the traditional grouping of months into seasons, so as to capture any robust fine temporal structure in the available data
- continue to evaluate the combined roles of the changes in STR-I and STR-P in the autumn rainfall decline with a focus on the interactions between the two using non-linear statistics
- diagnose aspects of the meridional circulation and its trends from observations: tropopause height (as a proxy for the edge of the Tropics as derived from radiosonde data) and MMC intensity and extent using the latest reanalyses (ERA-interim and others as they become available)
- analyse existing climate simulations (ensembles with external influencing factors included with the CCSM3 model) to (i) evaluate the climate model's ability to reproduce the meridional circulation changes, and (ii) the possible attribution of these changes
- evaluate the interactions between the reversal of the Australian monsoon and SEA rainfall.

Methods

Refined analysis of SEA rainfall (Objective 1)

Additional work on describing the rainfall decline in SEA was again carried out using the Australian Water Availability Project (AWAP) rainfall data. SEA was defined as continental Australia south of 33.5 °S and east of 135.5 °E. The work previously performed with a limited station network to capture SEA rainfall variability and extend the record back in time was revisited. A more limited network was created (Figure 2) which allowed us to extend the record as far back as 1865, while still reproducing 95 percent of the month-to-month variability of the AWAP-based rainfall average across SEA.

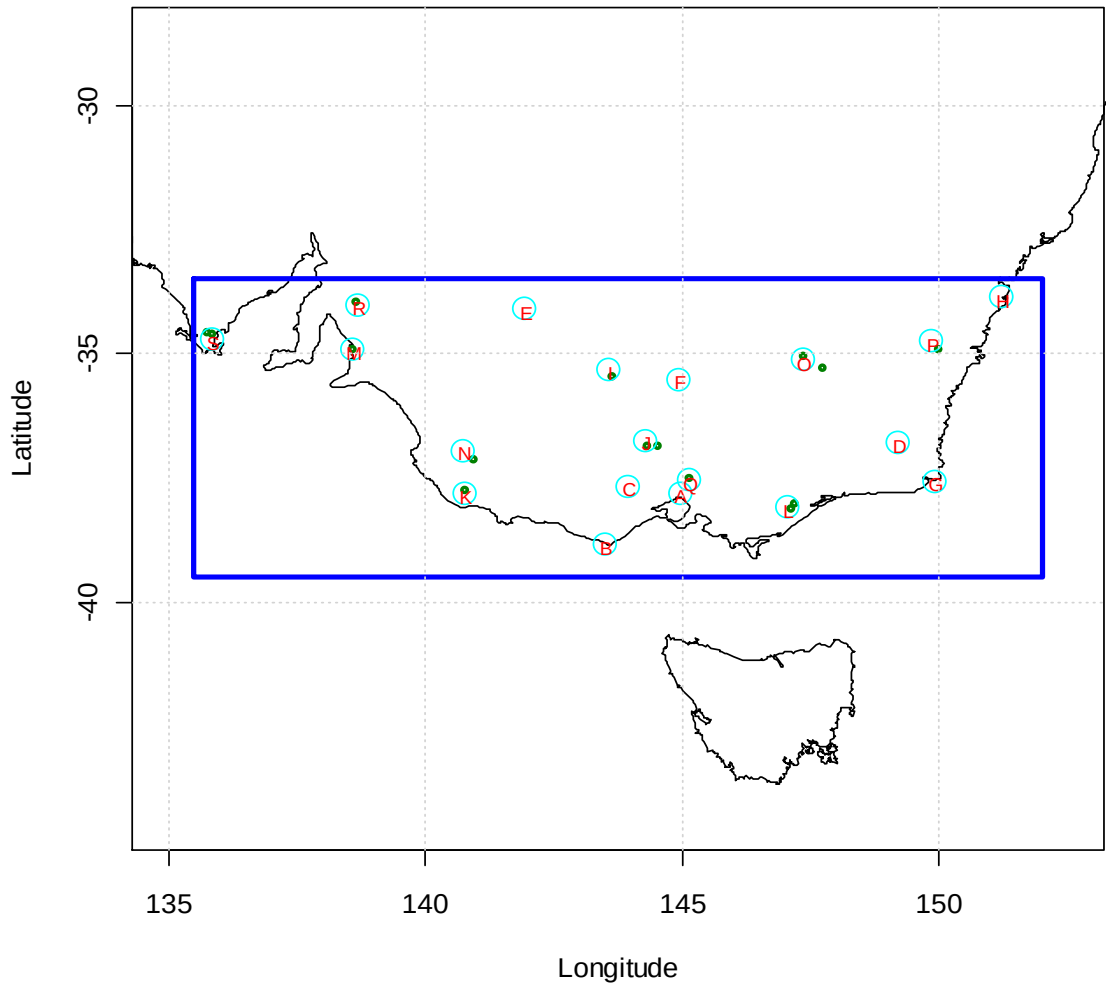

Figure 2. All sites considered to reconstruct SEA rainfall: Melbourne (A), Cape Otway (B), Mount Buninyong (C), Bukalong (D), Wentworth (E), Deniliquin (F), Gabo Island (G), Sydney (H), Swan Hill (I), Bendigo (J), Mount Gambier (K), Sale (L), Adelaide (M), Naracoorte (N), Wagga Wagga (O), Goulburn (P), Yan Yean (Q), Auburn (R) and Port Lincoln (S). Letters indicate the primary sites, the small green circles indicate location of actual stations when composites are used. The chosen network to extend records back to 1865 was based on 11 sites: M, A, Q, C, D, H, K, J, B, I and P.

In addition to rainfall in SEA, additional analysis was performed on a small area in Victoria strategically located to depict the fine details of the large-scale influences affecting rainfall in SEA. This analysis contributes to understanding the interactions between the orography and the large-scale influences. The area is the Eildon catchment on the north side of the Great Dividing Range and Melbourne Water's main catchment area on the south side (Figure 3). In the analysis, Melbourne Water catchments were further sub-divided between the Western catchment area and the Thomson catchment which is located on the Eastern side of the vertical ridge line connecting to the Great Dividing Range at a location known as 'The Triangle'. Rainfall and streamflows on the three sides of this triangle were analysed. Streamflow data were sourced from the Victoria Department of Sustainability and Environment for the Eildon catchment and Melbourne Water for the other catchments.

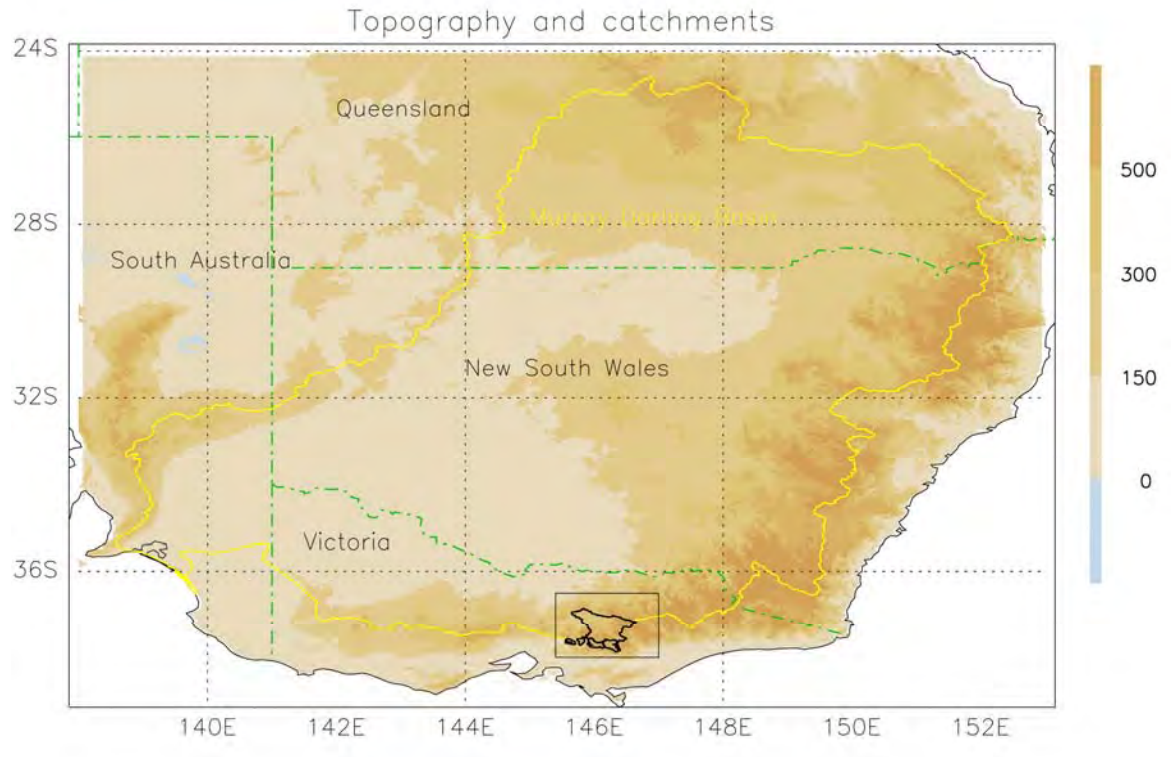

Figure 3. Topographic map of SEA showing the Murray-Darling Basin (yellow line) and the small catchments for which rainfall variability and trend were analysed in detail (black lines)

Daily rainfall "entities" (ie contiguous area experiencing rainfall on a particular day) were developed using based on an objective analysis of Australian Water Availability Project (AWAP) daily rainfall maps. Several techniques were evaluated to identify spatially consistent rainfall patterns on a daily timescale and aggregate them into a single entity. These techniques are commonly used in radar-based rainfall analysis and for the evaluation of high-resolution Numerical Weather Predictions. Several criteria were developed and tested to define these climate entities and to answer questions such as:

The maximum distance between two rainfall systems (i.e. within a close contour) allowed for these two system to be part of the same "entity"? The answer to this question is related to the contour level chosen and also to the next question:

What total rainfall value within a close contour is sufficient to be meaningful and included into a bigger structure?

In the course of the development of the method to define rainfall entities, smoothing techniques (Fast Fourier Transformed of the original Australian Water Availability Project daily field) were tried and found helpful in defining the entities and in defining thresholds objectively. Cases of rainfall entities emerging from daily rainfall maps are illustrated in Figure 4. Using this method, several data series have been created to describe these entities based on the:

- centre of the rainfall entities using weighted rainfall amount
- total rainfall volume of each entity
- total coverage space of each entity.

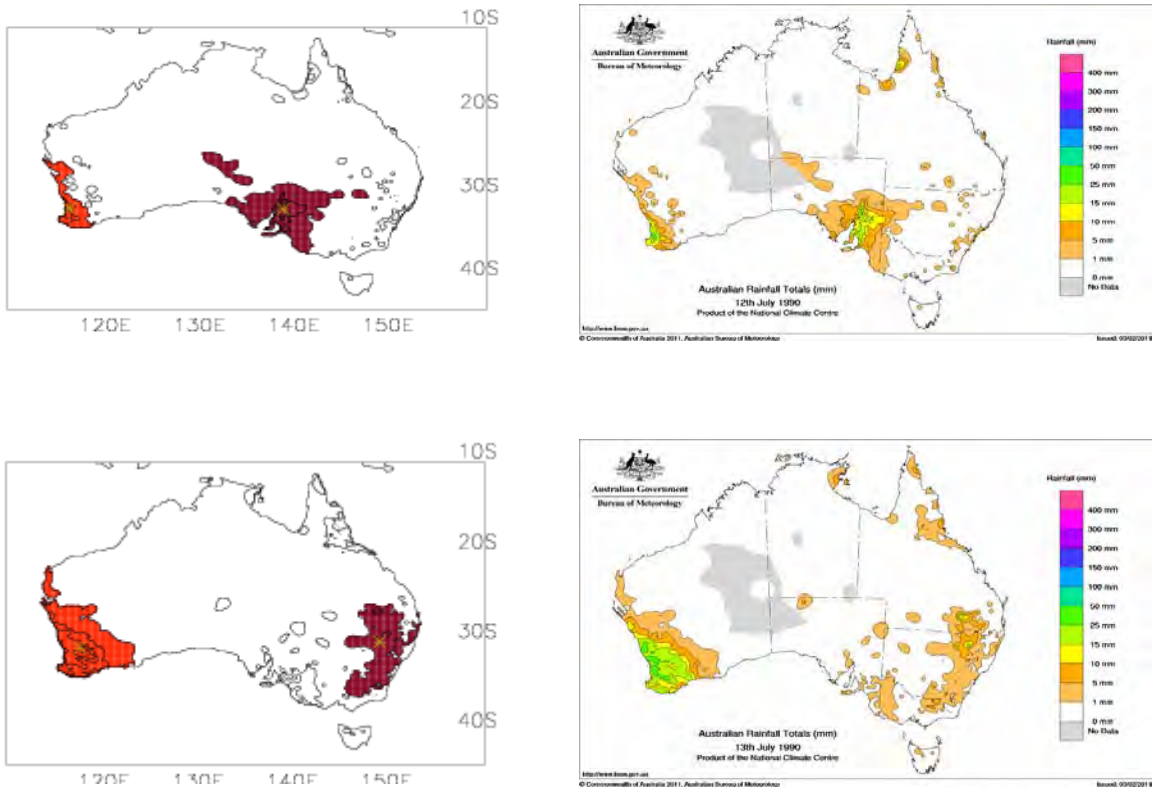

Figure 4. Examples illustrating the definition of rainfall entities (left maps) compared to the daily Australian Water Availability Project rainfall (right) on the 12th (upper) and 13th (lower) July 1990. In both days, two entities were identified (red in the west, brown in the east). Note that small localised rainfall patterns are omitted from the entities.

From these series, it is possible to derive additional quantities (e.g. mean intensity) and relate them to particular regions (e.g. SEA). As an illustration, the climatology of the centre of the rainfall entities from 1990 to 1998 is shown for the four calendar seasons (Figure 5). At this stage, the analysis of the 110-year climatology of daily rainfall entities identified across the Australian continent has started focusing on the entities relevant to rainfall observed in SEA. This work is to be extended by adding a tracking capability to the developed software.

Relationship between STR-I and STR-P (Objective 3)

The non-linear analysis of the interplay between STR-I and STR-P was performed using Classification and Regression Trees (CART), a binary recursive partitioning technique first developed in the 1980s. CART has been employed in many research fields including ecology and genetics but rarely in climatology. Decision trees are constructed that seek to describe the variability of one response variable with respect to several predictor variables. These trees are particularly useful for multiple correlated predictor variables, such as has been shown with STR-I and STR-P. Seasonal average rainfall in SEA based on the AWAP dataset was separated in three terciles (below, normal and above) and classification trees were constructed using STR-P and STR-I as two predictors. This method allows the evaluation of the relative importance of the two predictors (e.g. which one is identified first in the tree) and how the two predictors combine (e.g. the non-linear interactions of the two predictors of rainfall in SEA) in succeeding splits of the tree.

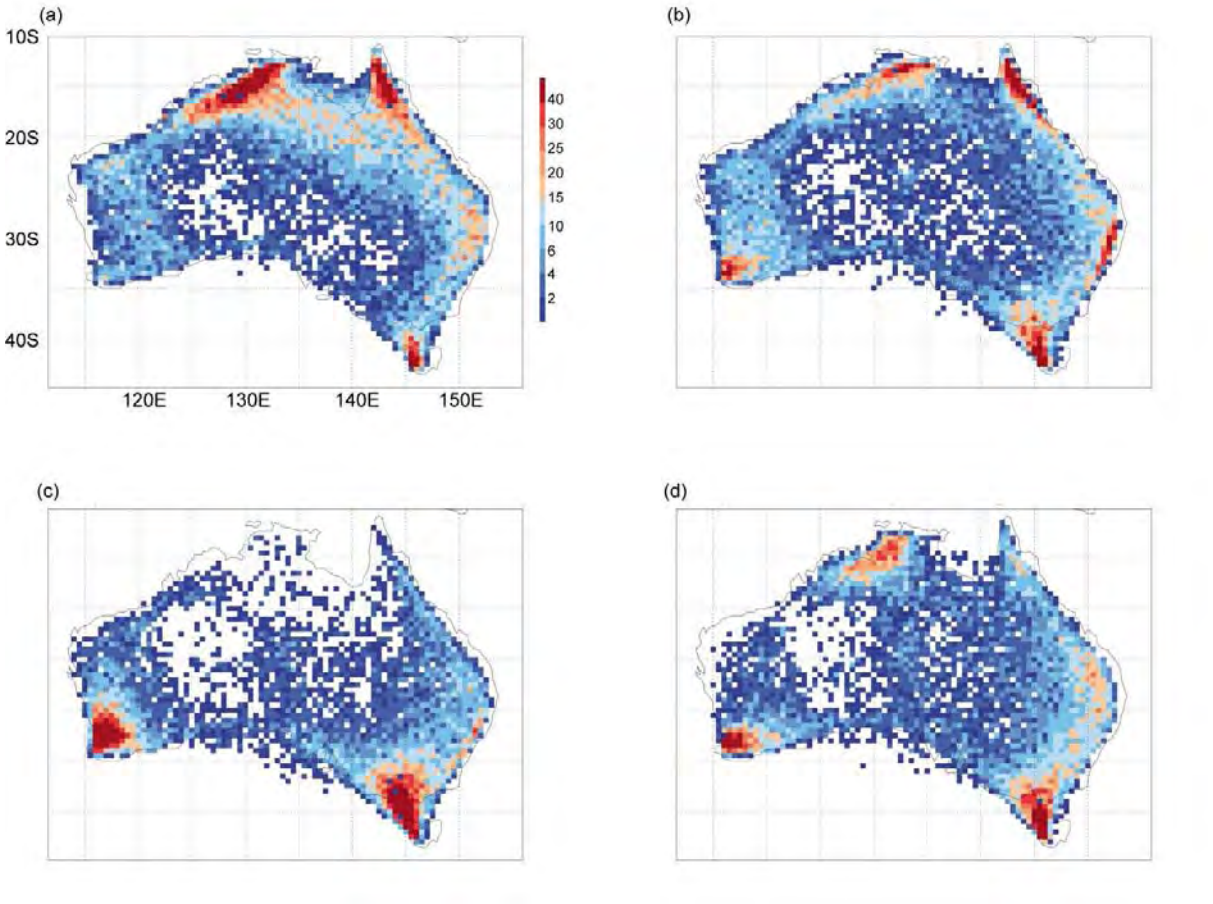

Figure 5. The 111-year climatology of the location of the geographical centre of daily rainfall entities across Australia in the four calendar seasons. Every pixel is a 50 by 50-km box and the numbers are expressed as a total for the calendar season.

Investigation of the MMC and Attribution of Changes (Objectives 4 and 5)

The MMC was investigated using all existing reanalysis datasets. These include:

- three versions from the NCEP (NCEP-NCAR, hereafter NCEP; NCEP-DOE II, hereafter NCEP2; and CFSR)
- two versions from the ECMWF (ERA40 and ERA-Interim)
- the NASA reanalysis (MERRA)
- the Japanese 25-year Reanalysis Project (JRA-25).

From these datasets we are using monthly mean. These products have different spatial and vertical resolutions:

- NCEP and NCEP2 : 2.5°, 17 levels
- CFSR: 0.5°, 36 levels
- ERA40: 2.5°, 23 levels
- ERA-Interim: 0.75°, 37 levels
- MERRA: 2/3° x 1/2°, 42 levels
- JRA25: 1.25°, 23 levels.

The common period of study is 1979–2009 except for ERA40 which ends in August 2002 and ERA-Interim which starts in 1989. For these latter datasets, the missing periods were filled using a linear scaling from the other five datasets by performing a basic multiple linear regression.

The Hadley cells are defined in terms of the intensity and extent of the zonal mean meridional streamfunction (ZMPSI) as displayed in Figure 6. We define the extent of the Hadley cells by the zero line of the ZMPSI on the poleward side of these cells averaged between 400 and 600 hPa. The zero line is obtained after linear interpolation of the vertically averaged ZMPSI with a 0.5° latitudinal resolution. The intensity of the Hadley cells is defined by the vertical mean of maximum ZMPSI defined for each pressure level within the cells.

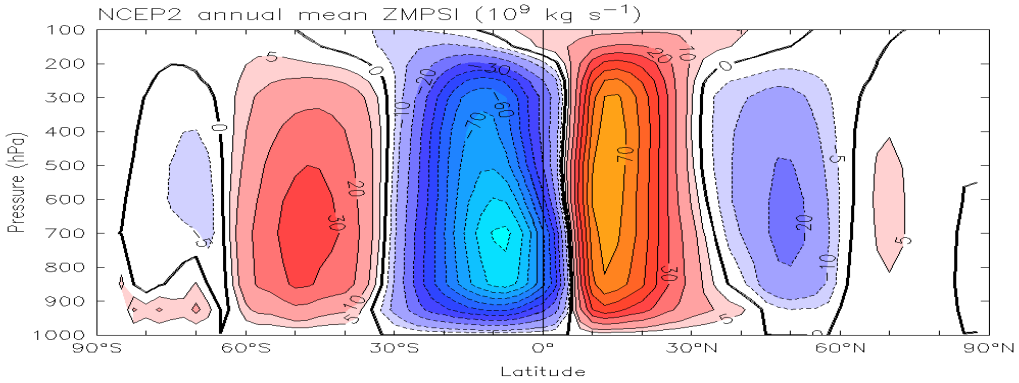

Figure 6. Cross section of the zonal mean mass streamfunction averaged over 1979-2009 used to diagnose the Mean Meridional Circulation (units are 10^9 kg s^{-1}). The Southern Hemisphere is toward the left, positive values indicate clockwise rotation. On both sides of the Equator, the two largest cells are the Hadley cells (blue in the Southern Hemisphere as it rotates anti-clockwise). The width of the cell was measured by the average location of the average zero line between 400 and 600 hPa. The intensity of the cell was computed as the vertical average along the profile of maximum value.

The MMC was also investigated in simulations with the Community Climate System Model version 3 (CCSM3), developed at the National Center for Atmospheric Research (Colorado). The model was run with well-defined external forcing separated in three groups (Meehl et al., 2006):

1. anthropogenic forcing AF), which includes greenhouse gases, aerosols and stratospheric ozone
2. natural forcing (NF), which includes variations of the solar constant and volcanic eruptions
3. full forcing (FF), which combines (1) and (2).

Each ensemble consists of five simulations with slightly different initial conditions (starting around 1850) enabling an estimation of the uncertainty of the climate signals. All 20th century simulations were run until the end of 1999.

A largely independent source of data that has been poorly exploited in understanding tropical expansion is the radiosonde data. On a global scale, the radiosonde sampling of the atmosphere is poor, particularly in the Southern Hemisphere. However, on regional scales the sounding network is dense and, after extensive data treatment, we believe adequate to the task. In this study, tropical expansion in the Southern Hemisphere is examined using the historical radiosonde network over the broader Australia – New Zealand region and South America over the period 1979–2010 (Figure 7). The radiosonde data from Australia – New Zealand are very good, with good spatial coverage and largely complete records; the South American data have poorer coverage in both time and space. The tropopause height-frequency technique is used to identify the edge of the tropics. Annual time series of the number of days with tropopause height exceeding 14.5 km at individual stations for each region are combined into zonal averages over latitude bands of 3 to 5 degrees. A technique to account for the 'sampling bias' introduced by uneven and/or incomplete sampling of the annual cycle is applied and provides consistency to the results, particularly over South America where these issues are more significant. The time-latitude field of tropopause height above 14.5 km is contoured, and changes in the position of the contours are used to identify the trend.

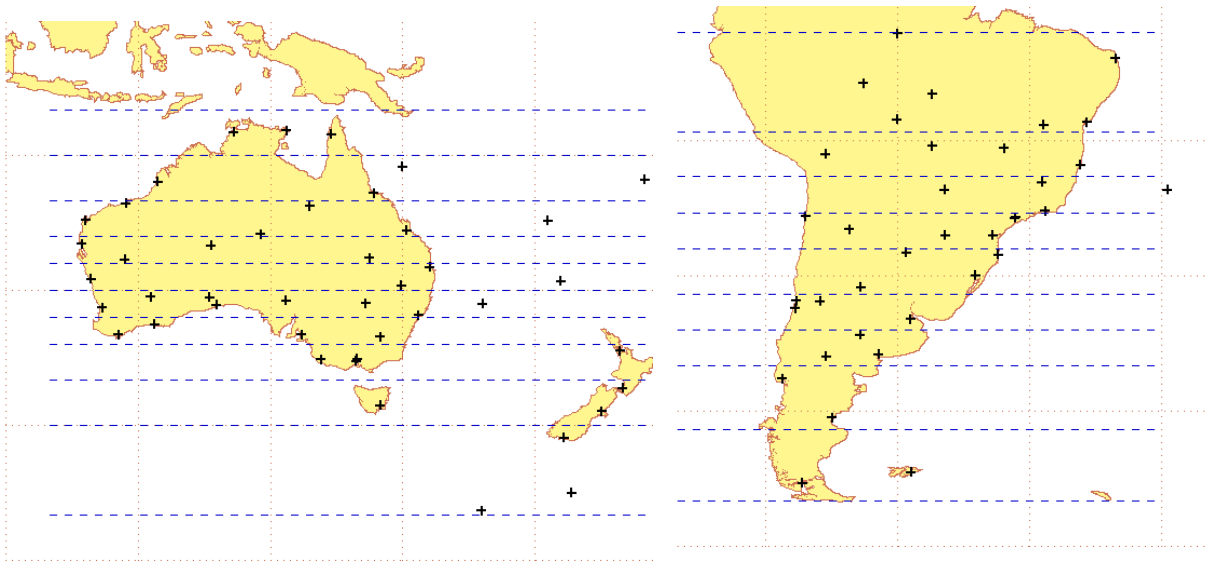

Figure 7. Location of the upper air sounding data used in the Australian – New Zealand (left) and the South America (right) sectors. The dashed line indicates the latitude bands used to separate the data.

Role of the Monsoon Reversal (Objective 6)

In evaluating the role of the reversal of the Australian monsoon as a controller of autumn rainfall in SEA, we construct an index by averaging zonal winds of the lower troposphere (850 mb) over the area 0-15S and 110-150E (using NCEP-NCAR reanalyses). We refer to this index as the Northern Australia Circulation index (NACI), where a positive index represents an areal average westerly, associated with low surface pressure. The NACI definition combines two summer monsoon regions, as described in Wang et al. (2004) and Kajikawa et al. (2010). The focus is on two periods, 1948–1979 and 1980–2010, to highlight the circulation differences in the pre- and post-autumn rainfall reduction across SEA and the emerging influence of the NACI (e.g. Figure 22). The justification of this method of comparing two periods using NCEP reanalysis is robust and has been employed in previous studies (e.g. Frederiksen and Frederiksen, 2007); however, some concern still exists with using pressure data from NCEP in the high southern latitudes prior to 1979 (Marshall,

2003) due to the existence of spurious trends. Along with the expanding tropics is a poleward shift of the dominant processes controlling autumn rainfall variability in SEA. To derive these dominant processes, we apply a statistical treatment, referred to as Empirical Orthogonal Function (EOF) analysis, on extra-tropical 500 mb geopotential height (from NCEP-NCAR reanalyses) in the pre- and post-1980 period. The analysis separates the circulation field into several dominant spatial patterns, each having a time series that describe the evolution of the pattern.

Results

Long historical record of rainfall in south eastern Australia (objective 1)

The network developed in the previous year of SEACI research was simplified further in order to extend the record back in time. The latest constructed network is based on only 11 sites with long continuous records all extending as far back as 1865, thus extending the previous record by 8 years. As was the case for the previous network, this latest network captures 95 percent of the month-to-month variability of rainfall in SEA as obtained by a straight averaging of the 0.05° AWAP analyses across SEA during the overlapping period, 1900–2010. Annual values for the SEA network and the AWAP average are very close and 11-year running means for the two methods are nearly indistinguishable (Figure 8).

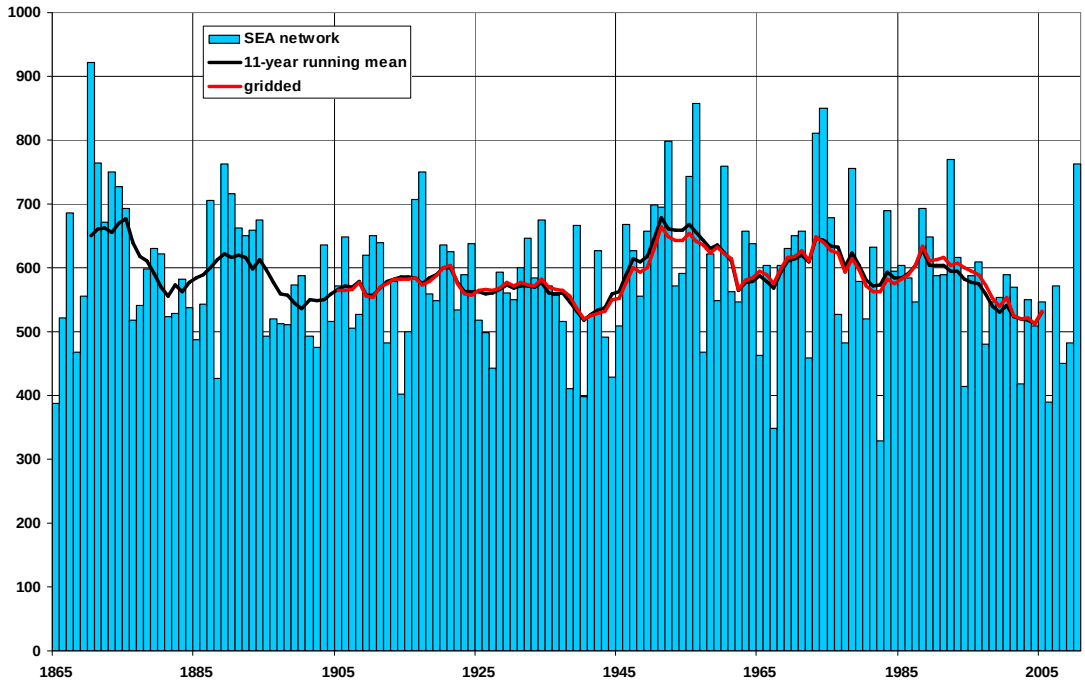

Figure 8. Annual SEA rainfall totals (blue bars) from 1865 to 2010 based on the 11-site network. Also shown are the 11-year running mean for the network (black line) and from the high-resolution AWAP rainfall analyses averaged over the SEA region (red line). The wettest year in the reconstruction is 1870 (922 mm). The driest year is 1982 (329 mm).

This record provides a good depiction of the drought at the time of Federation, thus confirming that the recent drought experienced in SEA is the worst on record. In addition, extending the record back by nearly a decade captures a new wettest decade on record -the 1870s- which appeared as wet as the recent wet decades in the 1950s and 1970s. This result is consistent with the argument developed in Phase 1 of SEACI, that:

> The period with the very high rainfall during the 1950s to the 1970s coincides with a period when the global temperature of the planet was stable (a pause amidst the 20th-century global warming). Very high rainfall observed at that time was due to that stability (see Timbal et al. 2010 for details).

The argument is based on the relationship between rainfall, STR and global warming. Therefore it is interesting to observe that during the latter part of the 19th century, when no global warming was occurring, similar high-rainfall decades (e.g. 1870s and early 1890s) were observed on par with those observed in the 1950s to 1970s.

The interplay between orography and large-scale influences (objective 1)

In this analysis, three catchment areas north-east of Melbourne in the Great Dividing Range were considered – Eildon (to the north), Thomson (to the east) and other Melbourne Water catchments: Watts river, Graceburn creek, O'Shannassy and upper Yarra) (to the south). The three Victorian catchment areas were also compared to the broader Murray Darling Basin). All three Victorian areas showed record breaking rainfall deficits in the 11 years prior to 2010 (Figure 9).

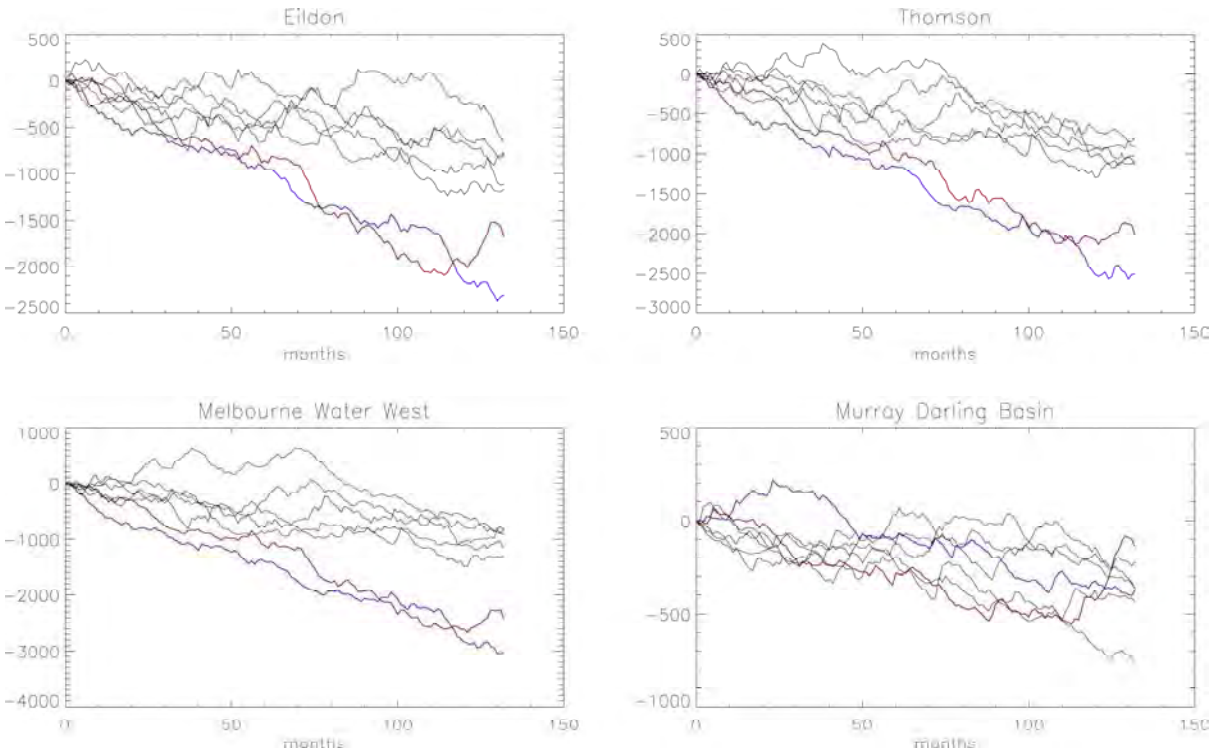

Figure 9. 11-year month-by-month accumulated rainfall deficit for the four catchment areas. The blue line shows the deficit for the most recent dry period. The other five lines show the next 5 dry non-overlapping dry decades from the historical record. The red line shows the accumulated deficit for the 11 years ending May 2011. Note the recovery of the accumulated amount of rainfall in all regions but more pronounced north of the Great Dividing Range (MDB and Eildon).

2010 saw a recovery in all regions. The recovery of the accumulated amount of rainfall is far larger north of the Great Dividing Range. This is due to 2010-11 being a typical wet year driven by tropical modes of variability and their associated influences (using the Tripole developed earlier in this project) with the impact diminishing on the southern side of the Divide. While the 2010 rainfall average for the entire MDB was the highest on record (807 mm, larger than the previous record of 784 mm in 1956) due to the large La Niña event in the Pacific and other positive large-scale influences, it was only the 7th highest value on record for the Eildon catchment (1516 mm, 12 percent lower than the 1956 record of 1724 mm), the 25th highest value for Melbourne Water west catchment (1702 mm, 25 percent lower than the 1952 record of 2275 mm) and the 32nd highest value for Thomson catchment (1557 mm, 30 percent lower than the 1952 record of 2245 mm).

Despite very favourable large-scale influences observed in 2010, rainfall across the all Melbourne Water catchment considered (Thomson and the western catchments) did not reach the record values observed in the 1950s. This is consistent with the fact that since the observed rainfall deficit started in 1997, while tropical modes of variability continue to explain the inter-annual variability between high and low runoff years within the Melbourne Water catchment as it did prior to 1997, it is centred around a reduced mean inflow (Figure 10). In the recent period, a favourable year due to tropical influence (positive tripole) provides less runoff within the Melbourne Water system than an unfavourable (negative tripole year) prior to 1997. This provides a clear example within SEA that tropical modes of variability (including ENSO and the IOD) do not account for the reduction in inflow since 1997.

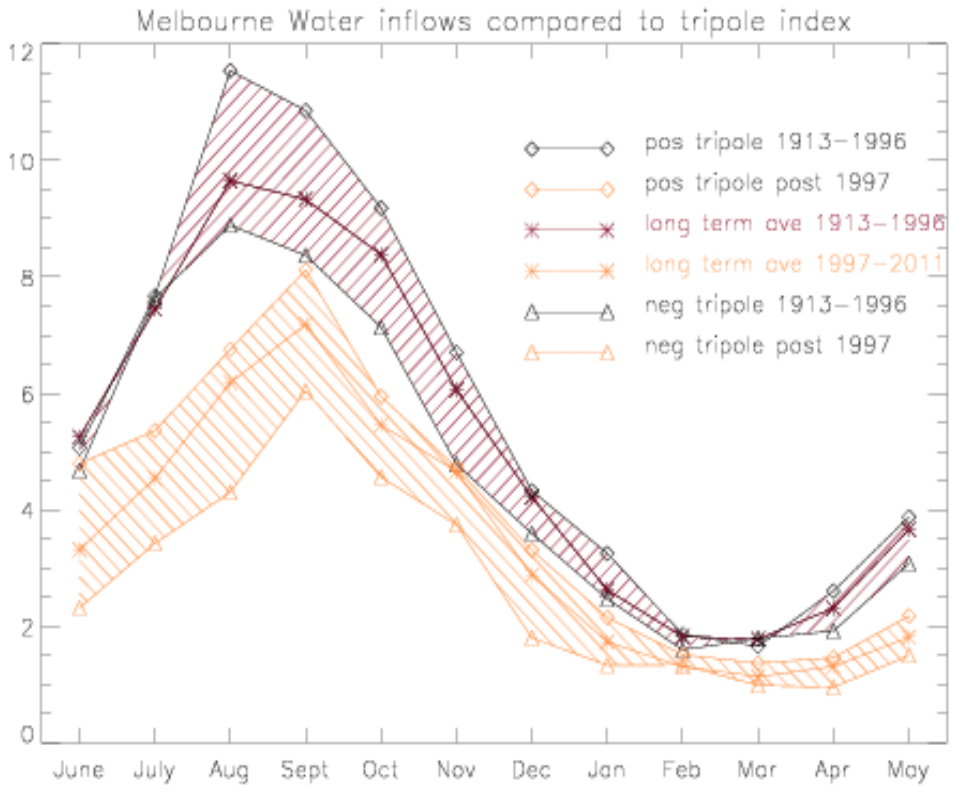

Figure 10. Average monthly inflow for all Melbourne water catchment considered before 1997 (1913-1996 shown by red stars) and after 1997 (1997-2010 shown by orange stars). For both periods, diamonds (triangles) show the positive (negative) tripole years in that period. The results are almost identical when a La Nina / El Nino classification is used.

Daily rainfall statistics: a new methodology to define rainfall entities and synoptic analysis (objective 1)

This newly developed approach aims to describe rainfall in Australia and more particularly SEA from a daily perspective, but from a system approach rather than using station data. It is expected to provide additional insight about the rainfall-producing synoptic systems, in particular when at a later stage, additional functionality to track the rainfall entities will be developed and results will be compared to synoptic tracking system based on mean sea-level pressure field.

The climatology of the location of the centre of rainfall entities (Figure 5) is consistent with our understanding of the mean annual cycle of rainfall across the continent. An early result worth mentioning is the proportion of the rainfall in SEA accounted for by entities with their centre located within the region (Figure11). (Note: it is possible that the percentages exceed 100 percent as the total rainfall amount is counted for every rainfall entity which is centred within the SEA region but some of this rainfall may have been experienced outside the SEA region). This proportion measures the amount of SEA rainfall which is due to localised rain bearing systems with geographical centres in the south (these systems are dominant in winter) versus broader rain bearing systems with geographical centres further north toward the tropics. This ratio has very large inter-annual variability but also a marked and highly significant downward trend, suggesting that recent daily rainfall systems tend to be larger and centred further north. In particular, 2010 was the lowest proportion on record, with only 40 percent of the rainfall in SEA accounted for by systems centred in SEA, suggesting that in most instances rainfall in SEA during this large La Niña event was produced by large rainfall entities with strong tropical connections.

Using the Melbourne University automatic tracking scheme to calculate cyclone trajectories in NCEP/NCAR reanalysis, it was found that events that have directly influenced SEA (here defined as the region from 135 °E to 150 °E and from 33 °S to 45 °S) have decreased in frequency and appear to originate from higher latitudes, particularly in April and May (Figure 12). This result is consistent with a poleward shift of the meridional circulation discussed in the later part of this report.

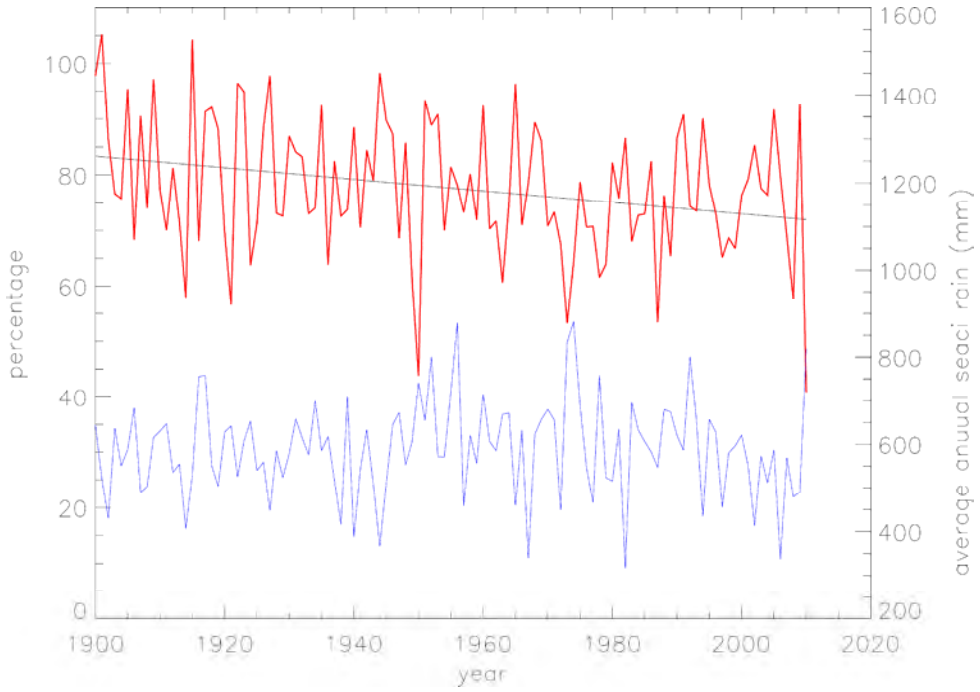

Figure11. SEA annual rainfall (lower curve) and the percentage of the rainfall accounted for by rainfall entities for which the weighted centred falls within the SEA box (red curve) with the long-term linear trend fitted to the annual data (black line). Note that 2010 has the lowest value on record at 40 percent.

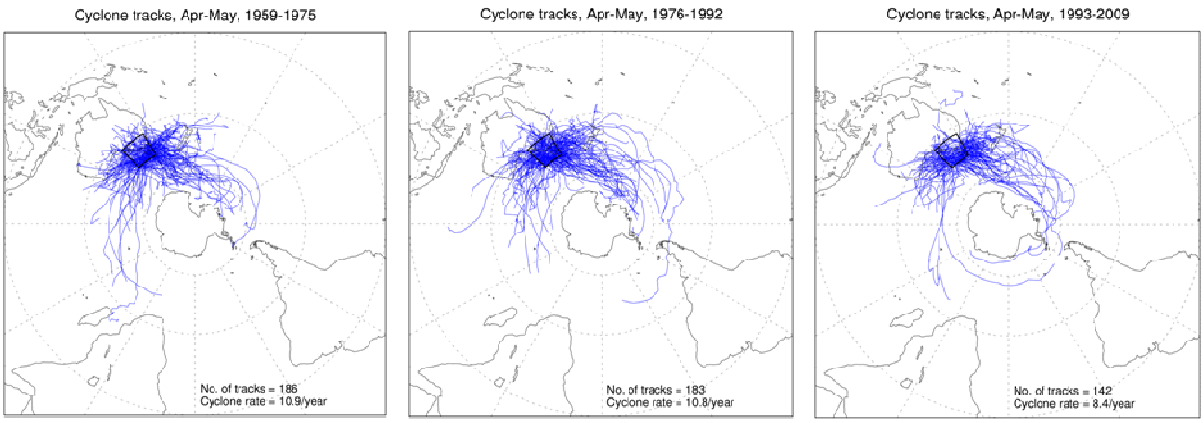

Figure 12. All cyclone tracks propagating through the box 135-150°E, 33-45°S (highlighted) occurring during April and May during the periods 1959-1975, 1976-1992, and 1993-2009.

Joint effect of changes in the STR-I and STR-P in autumn: a non-linear perspective (objective 3)

The STR – principally the STR-I but STR-P as well – has a strong and significant (at the 95 percent level) relationship with rainfall variability in southern Australia from April to November for the STR-I, and May through September for the STR-P (Table 1). However, it was shown during Phase 1 of SEACI using only linear statistics, that there was no combined effect of intensity and position, in autumn and winter, on rainfall in SEA due to the strong relationship between the two quantities. STR-I and STR-P are related for most of the year, with a significant correlation from April to December (Table 1).

Table 1. Monthly correlation coefficients between STR-I and STR-P and SEA rainfall (SEA-R). Correlations with rainfall are calculated using detrended monthly means from 1900 to 2009, and from 1890 between the two STR series. Statistically significant (at the 95 percent level) values are in bold.

Correlation coefficients	STR-I and SEA-R	STR-P and SEA-R	STR_I and STR_P
January	0.21	0.21	0.18
February	0.00	0.35	0.05
March	0.01	0.10	0.09
April	-0.48	-0.12	0.47
May	-0.71	-0.29	0.48
June	-0.64	-0.28	0.39
July	-0.60	-0.46	0.64
August	-0.69	-0.51	0.62
September	-0.42	-0.31	0.62
October	-0.39	-0.16	0.58
November	-0.30	-0.06	0.57
December	0.05	0.04	0.47
Annual mean	-0.48	-0.20	0.53

The 30-year correlations between rainfall in SEA and the STR computed for each calendar month show that while the relationship with the STR-I is stable over time, this is not the case for the relationship with STR-P, for which large swings are observed as the STR shifts in position over time (not shown). In autumn, the key season of the rainfall decline in SEA, it interesting to note that as the STR has been moving south during the 20th century, the negative relationship with rainfall in SEA has been contracting south for the STR-P but on the contrary expanding across most of eastern Australia for the STR-I (Figure 13).

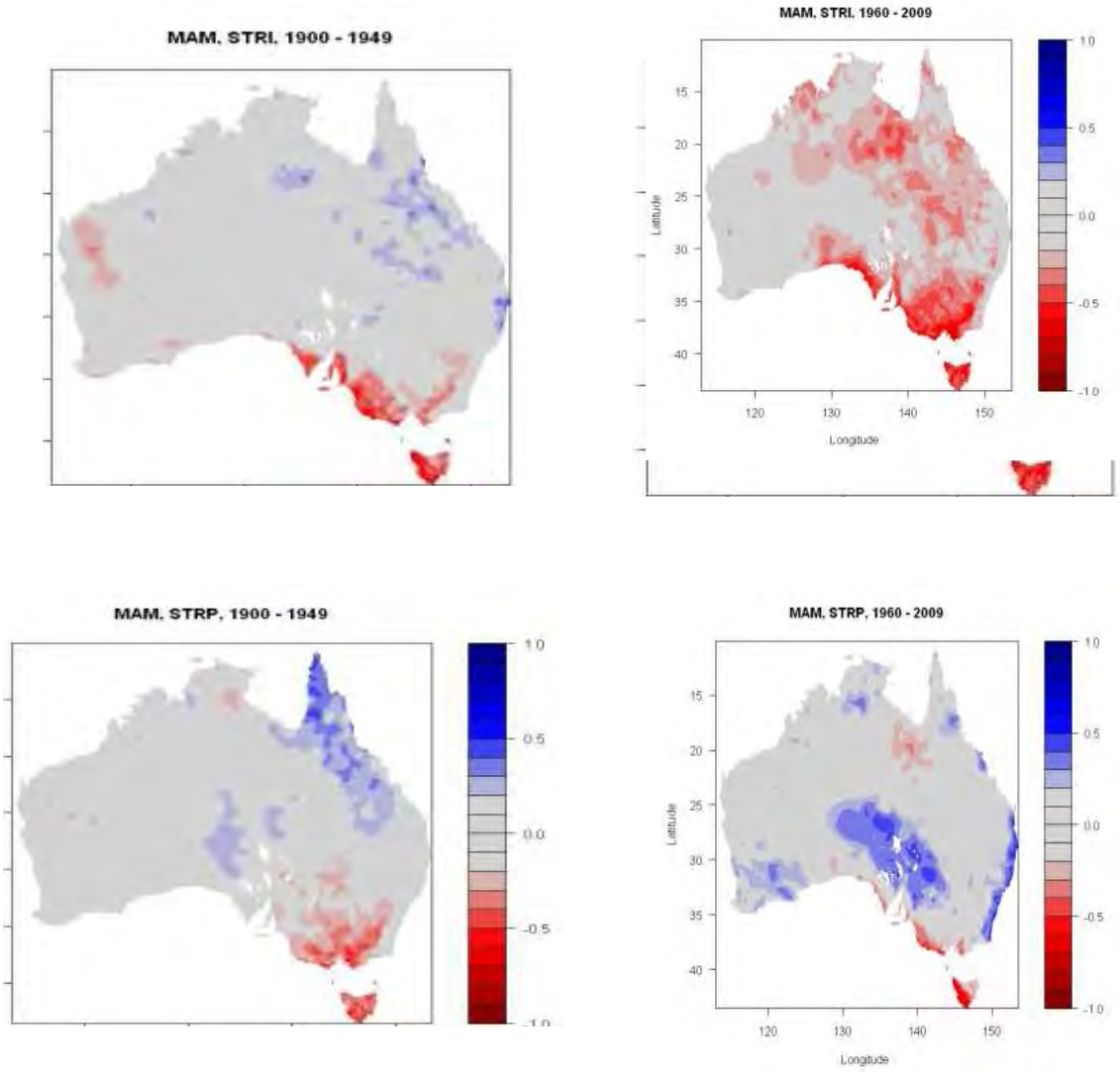

Figure 13. Correlation coefficients between STR-I (top row) and position (bottom row), in autumn (March through May) over 50-year epochs: 1900 – 1949 (Epoch 1) and 1960 – 2009 (Epoch 2).

These non-linearities were investigated further using the CART approach. Area-averaged precipitation data (terciles) for south-west eastern Australia were classified on the basis of STR-I and STR-P. In both seasons, STR-I was identified by the classification tree as the primary partition identifying the dry group, confirming the linear analysis. In the transition season of autumn, the time of year when the mean position of the ridge is on average over SEA, the position is important in distinguishing winter and summer-like wet rainfall groups, providing the STR-I is low (Figure 14). Vector wind analysis explains the composite of seasonal precipitation in terms of the different circulation patterns associated with these two wet groups and show that the two wet nodes (7 and 13) correspond to very different wind and moisture transport anomalies: stronger westerlies extending further north in the case of Node 13 (a winter-like wet autumn) and stronger easterlies north of SEA in Node 7 (a summer-like wet autumn).

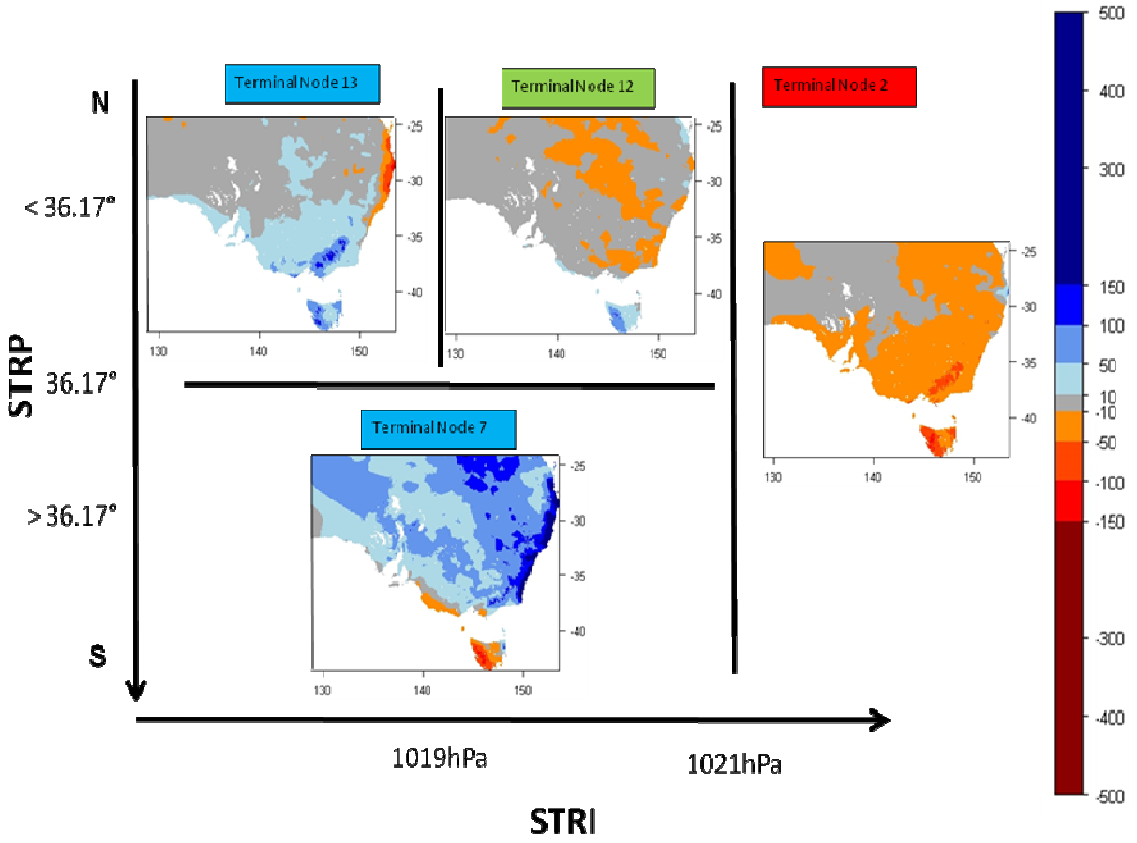

Figure 14. Anomaly maps displaying the seasonal precipitation composite (mm/year) in autumn (March through May) obtained using a CART analysis of the influence of the STR-I and STR-P on rainfall. Composites are based on seasonal means from 1900 to 2009.

The frequency of wet and dry cases in each group was examined, with changes evident over recent years. Node 13, which was not uncommon during the wet 1950s and 1970s, has only been observed once in the last 13 years, since the March through May autumn rainfall decline in SEA started (1995). This contrasts with the summer-like wet autumn Node 13, which is a rare occurrence during the entire record. The research confirms that intensity of the ridge is the most important factor in explaining inter-annual rainfall variability across southern Australia but also demonstrates the additional role of STR-P in autumn. When the intensity of the ridge is high (Node 2), autumn rainfall is very likely to be low, but for the years when the ridge is not very strong, a shift further south of the ridge will in fact more likely bring a wet autumn (Node 7), while a more northerly position will prevent this and results in a average autumn (Node 12). These results explain the low correlation between rainfall and STR-P and why this relationship has evolved during the 20th century as the mean location of the ridge has shifted south in autumn. For that reason, linear statistics based on a century-long relationship will underestimate the combined effect of the STR-I and STR-P on rainfall in SEA due to these non-linear effects. Using linear statistics on shorter periods is not a solution either, as the relationship becomes insignificant as shorter periods are considered.

Table 2. Autumn classification from 1900 to 2009 in each terminal node; colour code for the year indicates dry (red), average (black) or wet (blue) years.

Node 2	1902 1904 1910 1912 1918 1919 1920 1930 1934 1936 1939 1940 1941 1945 1947 1949 1959 1961 1967 1972 1976 1980 1984 1985 1987 1988 1991 1992 1993 1994 1996 1997 1998 1999 2000 2002 2003 2004 2005 2008
Node 12	1901 1914 1915 1921 1922 1923 1924 1925 1928 1931 1937 1938 1942 1943 1946 1948 1953 1954 1955 1957 1958 1962 1964 1965 1966 1969 1973 1975 1981 1982 1983 1986 2001 2006 2009
Node 13	1900 1903 1906 1907 1909 1911 1916 1917 1926 1927 1929 1932 1933 1935 1944 1951 1952 1956 1960 1968 1970 1971 1977 1978 1995
Node 7	1905 1908 1913 1950 1963 1974 1979 1989 1990 2007

Expansion of the Tropics: a perspective from radiosonde data (objectives 4 and 5)

In 2009/10, an extensive review of the existing literature was carried out. Recent studies have observed an expansion of the tropics or widening of the Hadley cell in multiple datasets, including the various global reanalyses (e.g. Birner, 2010; Hu and Fu, 2007) and satellite data (e.g. Fu et al., 2006). Reanalysis 'observations' have been the primary source of data, although different metrics have been used to identify the widening, including the tropopause height frequency distribution methodology described by Siedel and Randel (2007), trends in the position of the jet stream (e.g. Archer and Caldeira, 2008), and the changing isobaric streamfunction (e.g. Hu and Fu 2007). These studies generally suggest that tropical widening is larger in the Southern Hemisphere, although the amount of widening indicated by the different studies shows considerable variation, depending on the methodology and dataset. The cause of this expansion is hypothesised to be an effect of enhanced greenhouse gases (e.g. Lu et al., 2009). The likely impacts of this expansion, particularly in the subtropics, are poorly understood beyond a general drying trend over the next century.

In 2010/11 tropical expansion was investigated using upper-air sounding data. A key component of the work was to evaluate the data-quality issues and ensure that important issues were properly addressed. That work will not be covered in detail here, but rather this section will focus on the results obtained. Both the South American (SA) and Australia-New Zealand (ANZ) regions show a general poleward trend in position, i.e. an expansion of the tropics as evidenced by a general increase in latitude (i.e. a southerly trend) for the various contours of numbers of high tropopause days (Figure 15). This is overlain with inter-annual variability. With the exception of the 300-day contour, the regions show a good correspondence both in position and variability. The offset in the 300-day contour is apparently real, a regional feature of South America. Depending on the contour and region, expansion trends range from 0.2 to 1.2 degrees per decade, with most values in the 0.4 to 0.8 range. After accounting for measurement uncertainties, these trends are in most instances significant, exceeding the 2-σ contour intervals in 6 of 8 cases. Overall, the trends are also greatest in the early portion of the record, and 'level off' over approximately the last decade. In the South America region, trends are consistently larger and show less levelling off. In Figure 15, the annual data are grouped from June through May to better correspond with the annual ENSO cycle. A correlation analysis using the de-trended position data and annual Multivariate ENSO Index suggests that much of the inter-annual variability is related to the ENSO cycle. During La Niña years, the tropics expand. This is more prominent in the 100-day and 50-daycontours (where correlations are between 0.4 and 0.7). The large volcanic eruptions of El Chichón in 1982 and Mt Pinatubo in 1991 are also apparent as a reduction in the width of the tropics, more pronounced over the South American region.

The results suggest that some of the larger trends identified in the studies of tropical expansion mentioned earlier may be too large; our values are firmly in the low-to-moderate end of the spectrum that can be inferred from a review of the scientific literature. Further comparison with the various reanalysis data will give some insight into which reanalysis data should be used to more fully explore the observed impacts of this expansion, as well as some of the limitations and uncertainties in the reanalysis data. A better understanding of the sources of the inter-annual and regional variability in tropical expansion can provide information into the mechanisms involved and provide some understanding of what future climate changes might hold in store for SEA.

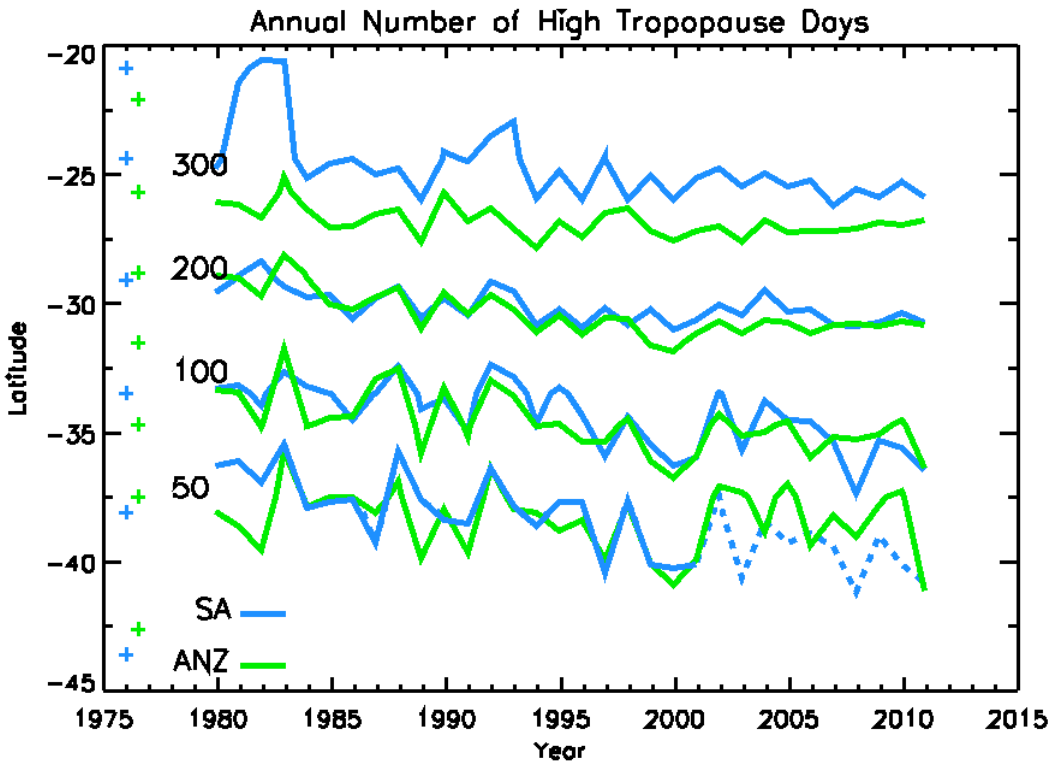

Figure 15 . The positions of contours (300, 200, 100 and 50 days per year) for both the South America and Australia-New Zealand sector analyses. The plus signs on the left locate the mean position of the contours computed from 1979 to 2010.

Representation of the Hadley circulation in the reanalyses (objectives 4 and 5)

Firstly, the MMC is analysed across the seven reanalyses (Figure 16). All datasets exhibit comparable annual cycle. A marked seasonality of the cells in both hemispheres is observed in all datasets. These cells vary out of phase, maximising in hemispheric winter; the Southern-Hemisphere cell is generally more intense during this season. In addition the seasonal migration of the southern cell extent is less marked than its counterpart. The Northern-Hemisphere cell cycle has a triangular shape. In contrast, the annual cycle of the southern cell is more complex, tending to have a 'figure eight' shape. These hemispheric differences reflect the asymmetry of the Hadley cells, probably due to the different distribution of land and ocean in each hemisphere. There is also the hypothesis of unequal observation coverage, with the Northern Hemisphere being more important because of a larger land surface, which induces a less realistic feature of the Southern-Hemisphere cell.

Differences between the datasets are particularly noticeable in the amplitudes. Namely, JRA-25 and NCEP are the most extreme. In NCEP, the northern cell maximum intensity is roughly $50x10^9$ kg s^{-1} smaller and the minimum extent in spring is roughly 3° wider than the others. Note that the maximum extent in August is the largest of the seven datasets. The southern cell also differs in NCEP from the others, especially during the phase of intensity strengthening and extent narrowing between February and July. The narrowing is more rapid and more marked. The intensity associated with this is generally weaker; the maximum in July is about $100x10^9$ kg s^{-1} smaller. This also affects the July to December part of the annual cycle, with the intensity-weakening rate being less marked. In JRA-25, the northern cell tends to have comparable features to NCEP with notably the minimum extent in spring and the maximum extent in August being the widest. In contrast, the maximum intensity in winter is similar to the others. The whole annual cycle of the southern cell is shifted roughly 2° poleward compared to the others, although the intensity is of comparable amplitude.

In spite of this, the differences in representing the mean state, inter-annual variability of extent and intensity of the Hadley cells are similar amongst all the products (Figure 17), with variability in the extent being more consistent. However, as for the mean state, NCEP reanalyses appear to be an outlier exhibiting lowest variability in intensity, in contrast to MERRA or ERA40, which show strongest variability. Overall, they all show large variability of these variables in both hemispheres, and the intensity tends to show larger variability than the extent. Note that these variables evolve symmetrically in each hemisphere. Longer timescale variability is also clearly observed, especially the strong expansion and intensification of the Hadley cells and remaining so from 1998 to present. Finally, it is noted that there is no significant correlation between the time series of extent and intensity anomalies.

We also noted that this inter-annual variability is seasonally dependent (not shown). For example, the extent in the Southern-Hemisphere cell shows a marked negative trend in December through February and March through May; the variability in September through November resembles the annual mean; and variability in June-July-August is negligible. Variability in intensity shows a semi-annual feature, with strongest anomalies not only in winter hemisphere but also in spring hemisphere when the mean intensity tends to be weakest.

As mentioned earlier, a large part of the inter-annual variability in the MMC is likely to be related to ENSO. All datasets highlight significant (greater or equal than 90 percent) correlations between the ENSO index in December through February and the Hadley-cell extent: positive in the Southern Hemisphere and negative in the Northern Hemisphere. This suggests that warm episodes of ENSO are associated with shrinking Hadley cells and vice versa. In contrast, no relationship was found with the South Hemisphere intensity, as noted above. In the Northern Hemisphere, only three datasets (NCEP2, CFSR and ERAI) show significant positive correlation between ENSO index and Hadley cell intensity.

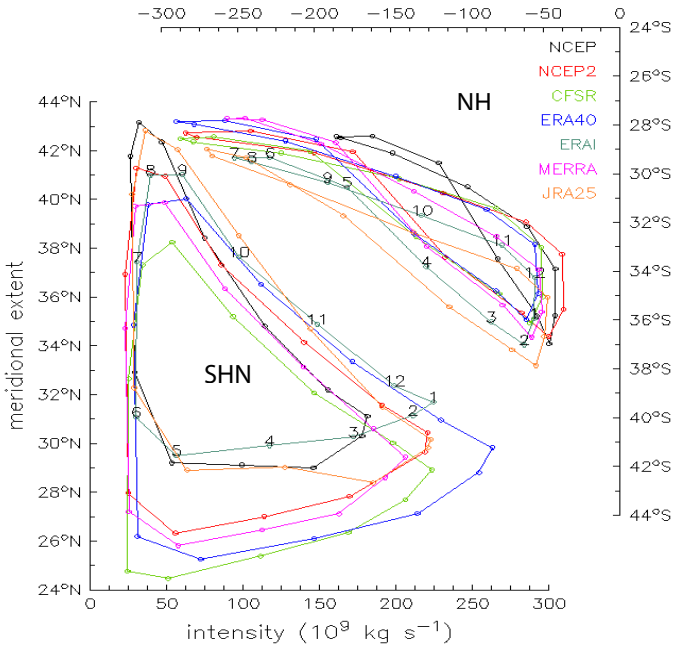

Figure 16. Annual cycle of the Northern and Southern Hemisphere Hadley cells intensity (negative numbers in the Southern Hemisphere indicated that the cell rotates anticlockwise) vs. extent across the seven reanalyses (shown in colour code). Months of the year are indicated by numbers.

In the Southern Hemisphere, significant positive correlation is obtained between summer ENSO index and Hadley-cell extent in summer and autumn for all datasets, in the preceding spring as well but only for five of the 7 reanalyses (CFSR and JRA25 are the exceptions). This suggests that the ENSO influence in the Southern Hemisphere is marked for all seasons, except in austral winter, when the variability in the Hadley-cell extent is negligible. This result is somewhat counterintuitive since ENSO variability has a peak influence in subtropics such as Australia in winter and spring.

Trends in the MMC are presented in Figure 18. All datasets show an expansion of the MMC of 0.5° per decade in the Southern Hemisphere (0.6° per decade in the Northern Hemisphere), consistent with the observed widening of the tropics from radiosonde data (Figure 15). However, there is a marked variability of the trends, ranging from 0.13° per decade in CFSR to 0.79° per decade in JRA25 (0.09° per decade also in CFSR to 1.08° per decade in MERRA for the Northern Hemisphere). That consistent result confirms the consensus found during the review of the literature on that issue. It was, however, often observed that earlier results based on reanalyses were questionable since they were often obtained on longer period including the pre-satellite era and that could lead to spurious trends. This rigorous analysis (with a focus on the post-satellite era and sampling the uncertainties in the reconstruction of the atmosphere using reanalyses across 7 products raises the likelihood that these trends (consistent in sign and ranging from 0.1 to 1.1° per decade) are real. They are lower than many prior estimates but consistent with our analysis based on upper air sounding. Nevertheless, it is worth pointing out that it is not possible to rule out the impact of changes in the global observing system (i.e. different satellites) which could still have an impact on these trends.

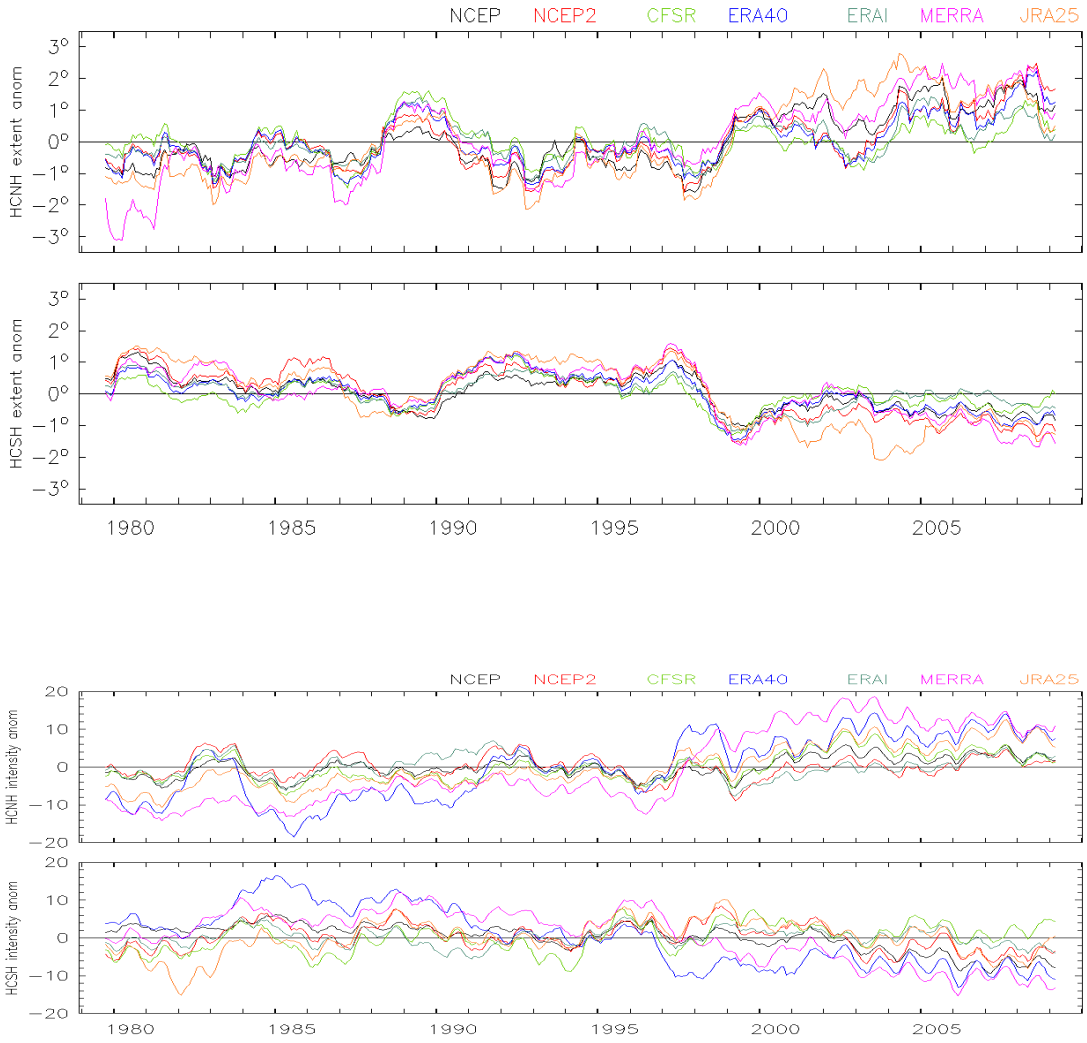

Figure 17. The 19-month running mean anomalies of the Southern Hemisphere Hadley cells extent (top two panels) and intensity (bottom two panels).

In contrast to the consistent expansion, trends in intensity are inconsistent amongst the reanalyses (Figure 18b). In the Southern Hemisphere, four datasets show strengthening against three weakening. The weakening is found in CFSR, ERAI and JRA25 reanalyses, with trend values ranging from 0.17 percent per decade for NCE2 to 8.3 percent per decade for ERA40. In the Northern Hemisphere, only two datasets show a slight weakening (NCEP2 and ERAI) against the other five. The strengthening obtained in MERRA is particularly large (15.3 percent per decade). In contrast, NCEP2 and ERAI show a very weak negative trend. Previous studies suggested a strengthening of the northern cell in boreal winter. The results here further suggest the strengthening of the northern cell throughout the year.

These trends also show a marked seasonality – as indicated in Table 3 for the extent and Table 4 for the intensity – in the Southern Hemisphere. The expansion tendency is observed in all seasons except winter, consistent with Hu and Fu (2007). The expansion is most pronounced during summer (0.93° per decade) and autumn (0.64 per decade). The range of expansion amongst the data is very large in summer, exceeding 1° per decade across the 7 products, less so in the other seasons (about 0.5° per decade across the 7 reanalyses).

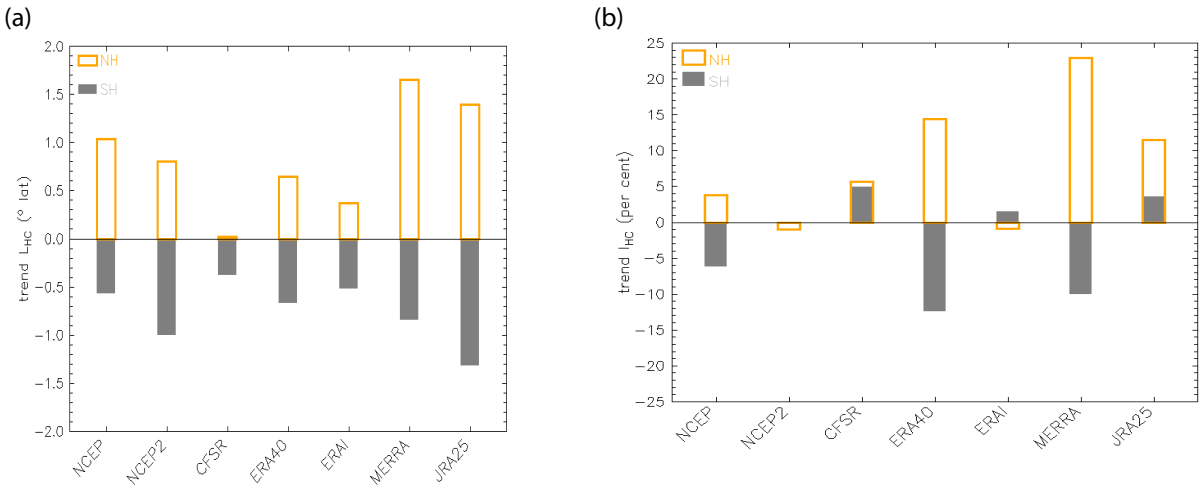

Figure 18. Trends in Hadley circulation extent (a) and intensity (b) from the seven reanalysis datasets computed as a difference of two 15 year periods (1980-1994 and 1995-2009). Results are shown for the Southern (grey filled bars) and Northern (orange empty bars) Hemispheres.

Table 3. Seasonal trends of Hadley circulation extent (degrees) in the Southern Hemisphere as determined from 7 different reanalysis data sets. The trends are computed as a difference of two 15 year periods (1980-1994 and 1995-2009).

Reanalysis data set	December-February	March - May	June-August	September-November
NCEP	-1.17	-0.98	0.15	-0.3
NCEP2	-2.24	-1.31	0.14	-0.62
CFSR	-0.73	-0.7	0.009	-0.11
ERA40	-1.35	-0.96	0.1	-0.49
ERAI	-0.85	-0.77	-0.01	-0.44
MERRA	-1.73	-1.06	0.34	-0.96
JRA25	-1.73	-2	-0.36	-1.2

In terms of intensity, the trends in summer are strongest (6.4 percent per decade) and generally show a weakening except for ERAI. The other seasons exhibit more inconsistency, although NCEP, ERA40 and MERRA exhibit weakening while CFSR and JRA exhibit strengthening.

To summarise, the trend analysis suggests that both cells are widening and that is consistent across all products. In contrast, not all datasets agree on long-term trends in the intensity, although most of them suggest a strengthening. The Northern Hemisphere cell tends to widen and strengthen more than the Southern Hemisphere cell. There also seems to be more agreement in the Northern Hemisphere, possibly related to the better *in situ* data coverage. It is worth noting however, that theories about the MMC tend to suggest that the cells should widen and weaken together, and this is certainly the case when the annual cycle is considered. The results here suggest the cells are widening and strengthening. What causes both characteristics to evolve in the same direction has yet to be investigated.

Table 4. As in Table 3 but for the intensity (percent with respect to the mean).

Reanalysis data set	December-February	March-May	June-August	September-November
NCEP	-10.09	-2.3	-5.42	-8.54
NCEP2	-12.42	0.71	3.12	-3.74
CFSR	-1.09	5.34	7.33	2.62
ERA40	-25.83	-13.4	-6.53	-17.03
ERAI	5.78	-0.62	1.77	1.11
MERRA	-11.15	-1.28	-7.29	-13.24
JRA25	-12.44	3.16	6.99	3.52

Relationship between the Hadley cells and the STR

Strong and significant correlation between the extent of the Hadley cell in the Southern Hemisphere and STR in all datasets suggests that the extent of the Hadley cell is associated with both STR-I and STR-P (Figure 19). The relationship between the expansion of the cell and the shift poleward of the STR was expected since the extent corresponds to the descending branch of the Hadley cell, which would correspond to high-pressure anomalies at the surface. The surprise is that the STR-I is only poorly associated (low and non-significant correlation) with the intensity of the cell. A stronger link is found between the Hadley cell expansion and the STR-I. This is likely to have important implications for climate variability in SEA, in particular in light of the high consistency amongst all reanalyses (and in the literature) on the expansion of the cells.

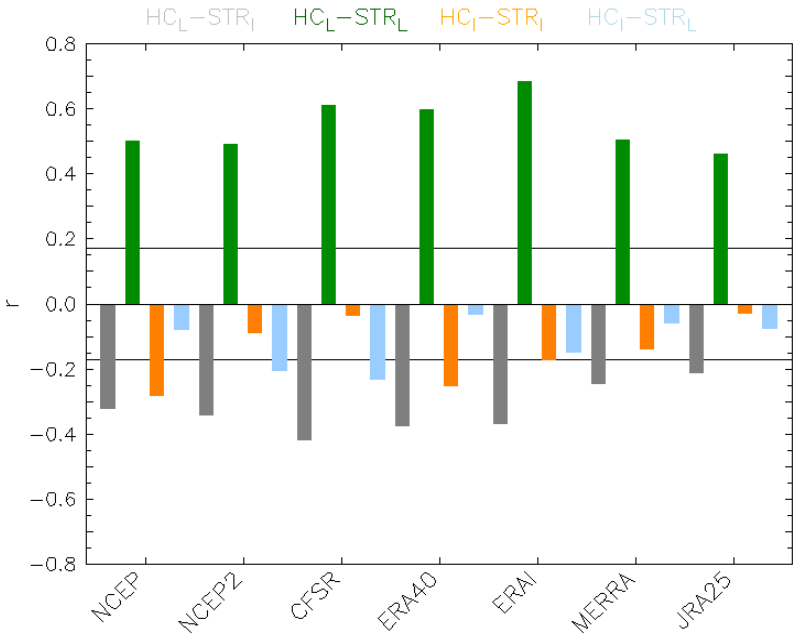

Figure 19. Correlation between the Hadley circulation, extent (L) and intensity (I) and STR location (L) and intensity (I) anomalies in the Southern Hemisphere. Black horizontal lines represent the 99 percent significance levels.

Attribution of the changes in meridional circulation to external forcings (objective 5)

Using the CCSM3 set of model experiments, we found that there is a general expansion of both cells observed in both all and human influences on atmospheric greenhouse-gas and particle concentrations (Figure 20a). This is particularly true in the Southern Hemisphere, where all five members in the two model sets display an expansion of the cells. While this result is consistent with the reanalyses, it is worth noting that the trends in CCSM3 are only about one-half to one-third of those in the reanalyses. This sort of ratio was also found in earlier SEACI work regarding the strengthening of the STR which was captured by the CCSM3 model provided that human releted effects were used (either alone or in the fossil fuel experiments). As it was the case for the STR, the trends in the experiments with human related effects are equally toward an expansion or a contraction with no trend for the ensemble mean. This is a strong suggestion that the observed expansion of the Hadley cell is mainly attributable to human influences.

Trends in Hadley-cell intensity show weakening of the cells in almost all model experiments in which the impact of human activities are tested, in contrast to the reanalyses (Figure 20b). Note also that, unlike in the reanalyses, in the model a weakening is noted associated with the expansion, that behaviour is in agreement with the theory. The amplitudes of the trends in the model are about 10 times weaker than in the reanalyses.

Finally, as in the reanalyses, the CCSM3 model related the STR-I and STR-P to the Hadley-cell expansion (Figure 21). This result makes sense in the light of the results published during Phase 1 of SEACI: the intensification of the STR is only observed in the CCSM3 simulations with the impact of human activities included. This can now be related to the expansion of the Hadley cell, through the linkage between the cell expansion and the STR-I.

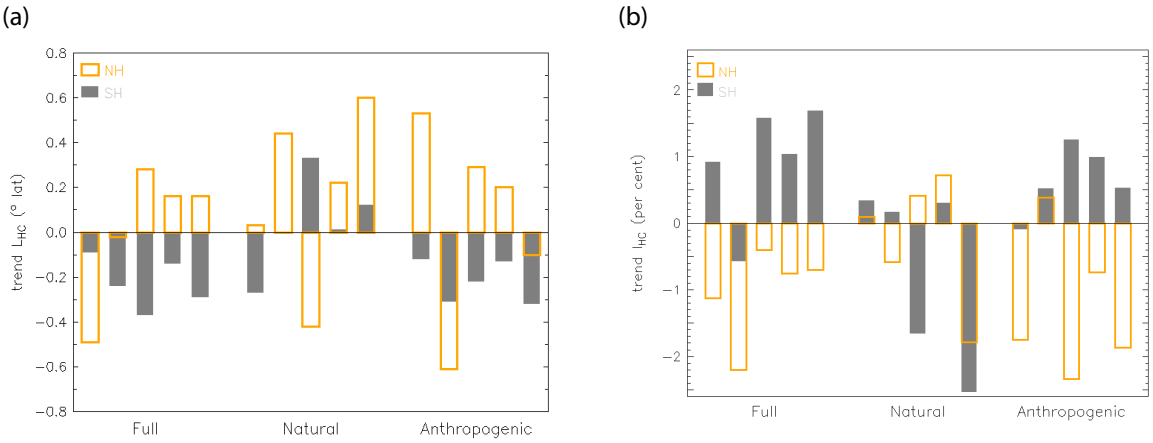

Figure 20. Same as in Fig. 17 but from three different set of climate model simulations with different external forcings (anthropogenic forcings –AF-, Natural forcings –BF-, and both forcings together –FF-) of the CCSM3 model.

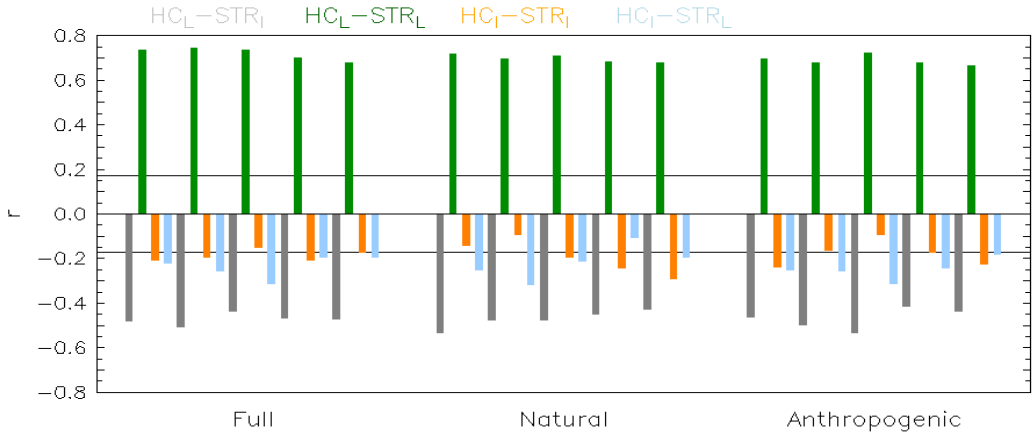

Figure 21. Same as in Fig. 18 from three different ensemble runs (FF, NF and AF) of the CCSM3 model.

Interactions between the northern Australian circulation, extratropical weather systems, and SEA rainfall (objective 6)

Since the 1980s, autumn (March though May) rainfall across SEA, extending to much of eastern Australia has shown a strong decline. Despite the numerous studies researching the autumn rainfall reduction (e.g. Cai and Cowan, 2008; Nicholls, 2009; Timbal, 2009), the causes of the change and mechanism(s) remain elusive. In fact, processes controlling variability of autumn rainfall variability in SEA are not well understood. Prior to the 1980s, a strong relationship existed between the STR-I and SEA rainfall (Figure 22a), and between STR-I and STR-P (Figure 22b). Historically, when the relationship between the intensity and position of the STR is strong (i.e., a well-established STR), the influence of the STR-I on SEA rainfall strengthens. Around 1980, this relationship declined, offering an important clue for understanding the dynamics of the SEA autumn rainfall reduction. One such process that can influence the establishment of the STR is the poleward expansion of the tropical circulation over northern Australia, including the reversal of the monsoonal winds.

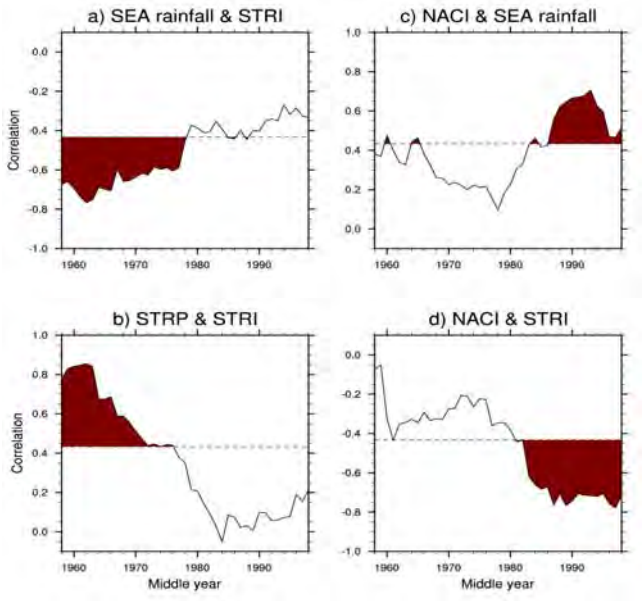

Figure 22. The 21-year sliding window March through May correlations over the period 1948-2008 of (a) SEA rainfall and STR-I, (b) STR-P and STR-I, (c) Northern Australian Circulation Index and SEA rainfall, and (d) Northern Australian Circulation Index and STR-I. Shaded regions are significant at the 95 percent confidence level.

Given that the Hadley cell is expanding poleward, will the relationship between the northern Australian circulation and SEA autumn rainfall change? Using the NACI to describe the circulation in tropical regions north of Australia, we find that there is a strengthening correlation between NACI and SEA rainfall and between NACI and the STR-I (Figures 22c and 22d). The correlations become statistically significant at the 95 percent confidence level in the post-1980 period. This strengthening influence from the north is further supported by the difference in the surface pressure patterns associated with NACI in the pre- and post-1980 period (Figures 23a and 23b), suggesting that the influence of the dry season in the north has extended to the SEA region. Further to this, previous studies have shown that the transition to the northern Australia dry season has occurred earlier, leading to stronger easterlies in the NACI region in MAM, which could contribute to a lower autumn rainfall over SEA, as indicated in the NACI-SEA rainfall relationship shown in Figure 22c.

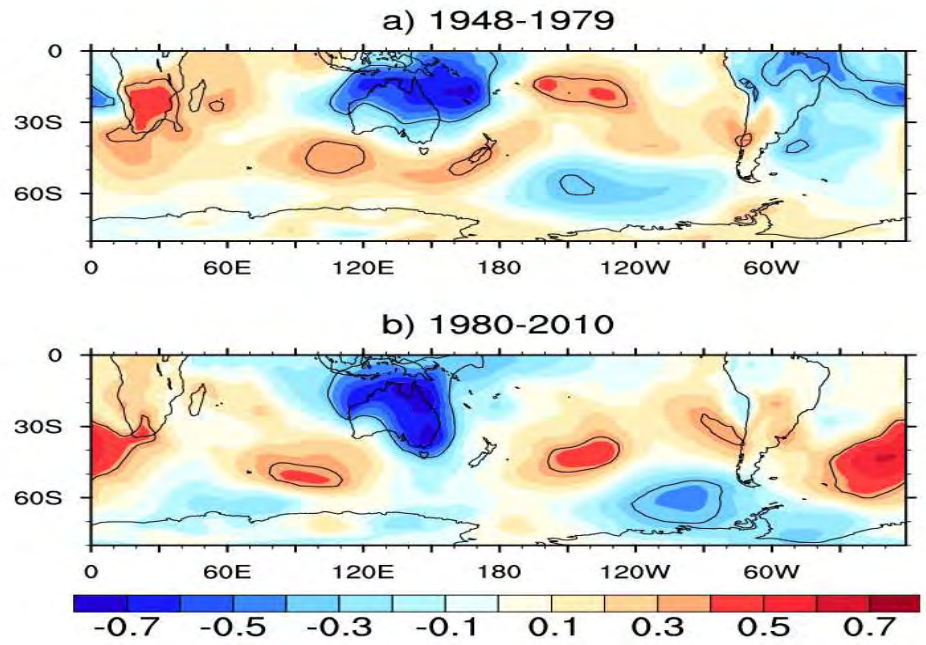

Figure 23. The March –May correlation of Northern Australian Circulation Index with mean sea level pressure, for the periods (a) 1948-1979 and (b) 1980-2010. Significant correlations at the 95 percent confidence level are within the black contours.

Associated with the Hadley cell poleward expansion is a poleward shift of the dominant process controlling autumn rainfall variability in SEA, which we derive through EOF analysis. Prior to 1980, the first and third EOFs of the 500 mb geopotential height reflect the aggregated weather systems emanating from the north-west and the west (Figure 24a and Figure 24b), which affect variability of autumn rainfall in SEA, across north-west Victoria and western New South Wales (Figure 25a) and Tasmania (Figure 25b). The second EOF mode broadly represents the index of the state of the Southern Hemisphere climate system, the SAM that, over the past 30-years, has shown little influence on southern Australia autumn rainfall. In the post-1980 period, these systems shift poleward (Figure 24c and Figure 24d, with the associated rainfall impacts in Figure 25c and Figure 25d). The influence from the northern Australia is embedded in the shifted pattern of the post-1980 period (Figure 24c), and its impact on Australian rainfall is shown in Figure 25c.

Over the pre-1980 period, the weather systems emanating from the tropical Indian Ocean and the Southern Ocean influenced southern Australia rainfall in autumn. As the circulation system shifts poleward, so do the 'centres of action' of these modes. Given that the upward trend of the SAM and the poleward shift of the mean circulation are shown to be induced by climate change (e.g., stratospheric ozone depletion, see Cai (2006), it follows that the poleward shift of these modes and the strengthen influence from the north is at least in part attributable to climate change.

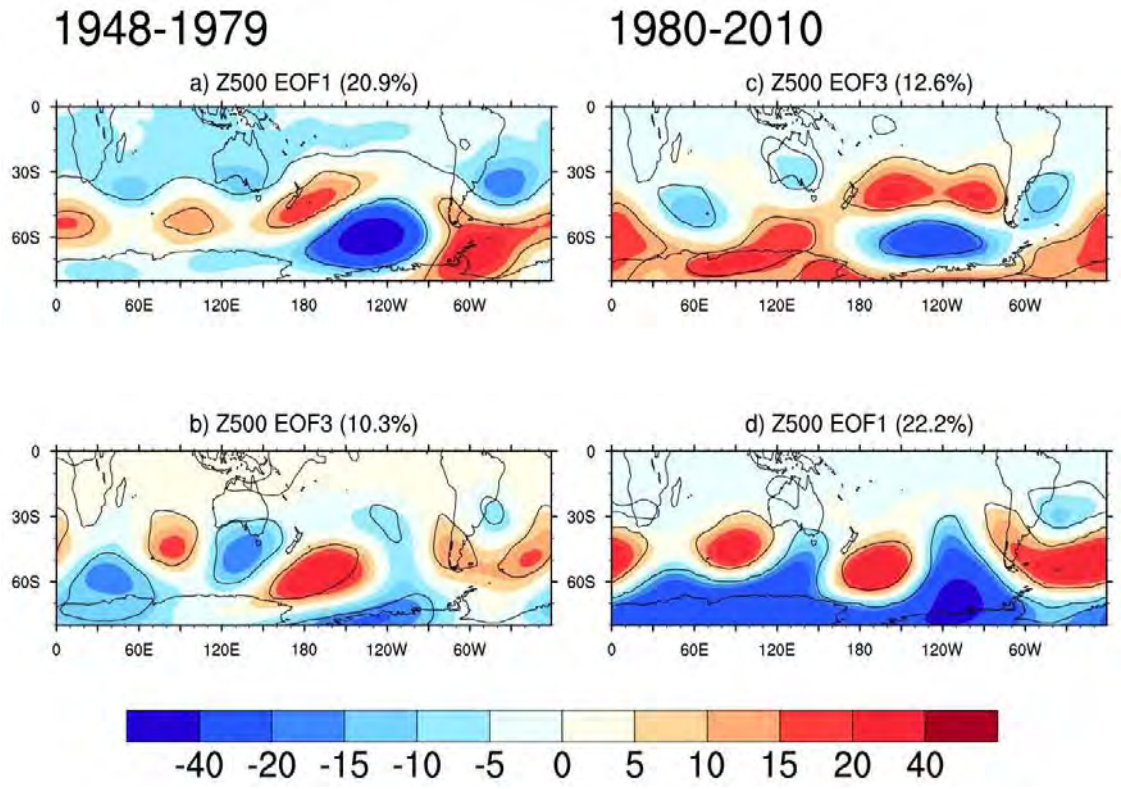

Figure 24. The March-May one-standard deviation anomaly pattern of 500 mb geopotential height associated with its respective (a) EOF1 and (b) EOF3, over 25-70°S latitude band for 1948-1979. (c) and (d) are EOF3 and EOF1 for 1980-2010, respectively. The variance explained by each mode is shown in brackets in the figure headings. Significant correlations at the 95 percent confidence level are within the black contours

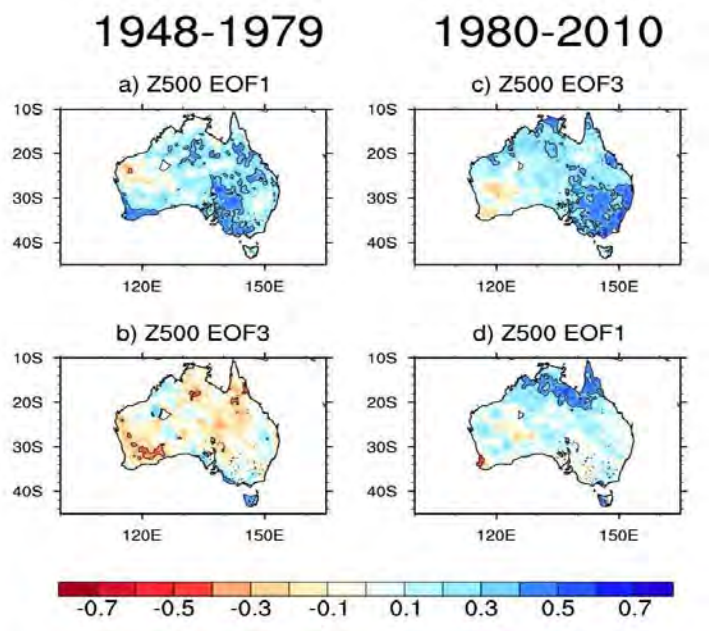

Figure 25. March-May maps of correlations between Australian rainfall and (a) EOF1 and (b) EOF3 of 500 mb geopotential height for 1948-1979. (c) and (d) are the correlation maps of EOF3 and EOF1, with rainfall, respectively, for 1980-2010. Significant correlations at the 95 percent confidence level within the black contours

Conclusions

In 2010/11, Project 1.1 has had a strong focus on the key season of autumn, when most of the long-term deficiency in rainfall has occurred. The project has seen a large number of new developments investigating new or existing datasets using novel approaches and methodologies.

In terms of improving the characterisation of the severity of the recent drought using surface data, using the AWAP daily gridded rainfall shows that rainfall entities have become larger events more connected to the tropics; streamflow data from selected catchments within SEA were found useful due to the amplification of the rainfall decline signal. The STR has continued to be used as a convenient proxy for the rainfall in SEA across the wet months from autumn to spring, either by relating changes in STR-P and STR-I and their joint effects on rainfall in SEA, or by relating these series to large-scale circulation indices such as the Hadley Circulation or the Australian Monsoon Index.

As part of the effort to strengthen our conclusions about changes in atmospheric circulation patterns, all available reanalyses (seven) were accessed. Some of the calculations presented were performed across all products, thus ensuring an appropriate sampling of the error in our knowledge of the climate mean state due to the global observing systems. It is a useful approach due to the lingering doubts about using reanalyses for extended periods due to the increased reliance on satellite information within the reanalyses and the resulting spurious non-stationarity – a problem which is acute in the Southern Hemisphere and aggravated at higher latitudes. In particular, it was found beneficial to focus on the post-satellite era (1979 onwards). This approach, whilst not without shortcomings as there is a continuum of changes in the global satellite coverage, is expected to alleviate some of the concerns about stationarity within the climatological record. In addition, upper air soundings were also explored to corroborate some of the results obtained from reanalyses.

Alongside the traditional and well-known large-scale indicators of the state of the global climate (e.g. the STR-I, STR-P and Australian Monsoon Index), new diagnostics were developed such as the number of days when the tropopause height is above 14.5 km (as a proxy of the extension of the tropics) and an index measuring the strength and extent of the MMC (e.g. Hadley cells). As with classical indices, the relationships of these indices with SEA surface climate were explored.

Finally, two new methods were investigated to update previous research . Firstly, non-linear statistics (i.e. a CART approach) were used to explore the joint effect of the STR intensification and shift poleward on autumn and winter rainfall in SEA. While linear statistics suggested that both could have contributed to the observed rainfall deficit, no additional effects were found when their combined influence was considered. The CART analysis provides an understanding for why this is the case and helps explain the subtlety of the influence of the STR in autumn. Secondly, while monthly to seasonal rainfall in SEA has been extensively explored in the past, daily rainfall was rarely touched on. A new approach was developed to evaluate continuous daily rainfall entities in order to evaluate how rain-bearing systems affecting SEA have evolved. This was done in conjunction with a more classical approach using synoptic tracking software.

The picture emerging across the entire project is consistent and informative. SEA has been affected by large-scale climate changes which are much broader than the direct vicinity of the Australian continent. The entire Southern Hemisphere is affected.

The case for the abnormality of rainfall during the last 20 years has been strengthened by extending the instrumental record back in time (as far back as the mid 1860s). Analysis of this extended record has shown that the recent drought was clearly unprecedented in the historical record; it also adds evidence to the statement that very wet decades tend to be observed when global warming levels off, in contrast to very dry decades (the recent decade and the 1930s-1940s) which were observed at times of accelerated global warming.

Despite the very large La Nina event in 2010/11 which had Australia-wide impacts and resulted in a substantial recovery across the MDB, catchments south of the Divide nevertheless remain in an unprecedented long-term rainfall deficit compared to any period of the 20th century. In addition, the mean inflow into the Melbourne catchment dams has seen a step reduction since 1997 that is not related to the influence of the tropical modes of variability affecting SEA. It is also noticeable that most of the rainfall increases above average were observed in spring and summer, outside the peak of the observed rainfall deficiency in autumn and winter. In fact, for the core months of April, May, June and July in 2010 and in 2011, the 20 percent deficit observed in rainfall since 1997 has continued unabated.

It has been observed that rain-bearing systems affecting SEA year-round are increasingly larger systems centred further north than SEA; this is corroborated by the observation that in autumn, rainfall in SEA is increasingly correlated with Australia-wide rainfall. In addition, in the key months of April and May, it was found that extra-tropical cyclones affecting SEA were strongly reduced and appear to originate from higher latitudes upstream. These two results, coupled with the CART analysis of the STR influence on autumn rainfall, suggest that as the STR has moved poleward, it has reduced the possibility for high-latitude fronts and lows to affect SEA, while allowing tropically-generated rain-bearing systems to penetrate further south. This is a secondary effect from the intensification of the STR which acts as a barrier for both types (high latitude and tropical) of systems affecting SEA In this context, while the STR has shifted south, the strengthening of the ridge can have a positive effect by slowing down systems with tropical origins or preventing them from "escaping" once connected to the fast moving mid-latitude storm-track leading to increased precipitation across SEA.

These large-scale changes observed at the earth's surface were related to upper-level changes affecting the MMC: Hadley cell strength and extent, and the Australian Monsoon Index. It was found across a range of datasets and methods (e.g. analyses of tropopause height and the relationship between the Australian Monsoon Index and surface climate) that the tropics are expanding. This is also apparent from the diagnosed MMC in all existing reanalyses. Although not very large (of the order of 0.5 degrees per decade), this expansion appears very robust. The signal is seasonally dependent and peaks during summer and autumn. This provides insight into the observed autumn rainfall deficit, as this season overlaps the period in which the MMC changes peak (i.e. summer and autumn) and also the period during which the relationship between the STR (the surface signature of the MMC) and SEA rainfall is strongest (this relationship peaks during winter but starts to be significant from April). In addition, while the large meridional circulation expansion in autumn drives both the intensification and shift poleward of the STR (both are most notable in autumn), for the reasons discussed earlier, this is only partially captured when linear statistics are used to reconstruct the rainfall deficit in SEA.

One important finding was that both changes in STR-I and STR-P are related to the expansion of the Hadley cell. This result was anticipated for the STR-P but is a surprise for the STR-I since its correlation with the intensity of the Hadley cell is weak and insignificant across all reanalyses. Regarding the consistent and significant intensification of the STR as observed during the 20th century (in response to increases in global temperature), it makes sense that the STR-I is more related to the widening of the cells (which is consistently observed) rather than the intensity of the cells (for which there is limited evidence).

Finally, the possibility of attributing these observed changes (global warming, widening of the Hadley cell/tropical expansion, strengthening of the STR, and reduction of the rainfall in SEA) was investigated using the CCSM3 model. Complementing results presented during SEACI-1, it was found that the model reproduces an extension of the Hadley cell only if the impact of human activities are incorporated either alone or combined with natural external factors. The widening of the Southern Hemisphere cell is a highly robust feature since it is produced in every single model experiment including the impact of human activities (10 in total). Furthermore, the model also relates the strengthening of the STR (observed in the model as well) to the expansion of the cell and not the intensity of the cell. The cell intensity was found to weaken in response to anthropogenic forcings leading to global warming, in agreement with the theory about the MMC, thus casting further doubt on the magnitude of the strengthening of the Hadley cell observed in some of the reanalyses.

Links to other projects

In 2010/11, the findings on the STR–rainfall relationship that underpin our current understanding of the rainfall decline in SEA have been used by Project 2.1 to evaluate the reliability of climate models' future projections and similarity with observed features. It is planned that the recently described sea-surface temperature tripole – which describes the tropical influences on rainfall in SEA – will now be used to evaluate climate models' future projections as part of the same project.

Findings from this project were also used to describe the impact of large-scale influences on the hydrological cycle in SEA (Project 1.2).

CHAPTER 3: PROJECT 1.2

Impact of climate variability and change on the water balance
Peter Briggs, Michael Raupach, Vanessa Haverd, Kirien Whan and Matt Paget

Abstract

Work in Project 1.2 has delivered results in three areas.

Develop, maintain and document the gridded hydrometeorological data flowing from the Australian Water Availability Project

Release of research-quality monthly historical time series and all spatial parameter datasets, for the continent and a SEACI subset, along with area-average Australian Water Availability Project (AWAP) time series for the 245 Australian Water Resources Council drainage basins and major drainage divisions, available to SEACI partners

Improved metadata

Successful AWAP validation against GRACE gravimetric data (independent work).

Model statistical climate–water relationships using Australian Water Availability Project gridded data

In work by Kirien Whan, correlation and regression tree (CART) and random forest analyses were used to classify spring hydrometeorological state for the whole of the Murray–Darling Basin (MDB) (the whole-MDB average rainfall and upper-layer soil moisture in September through November) against the Indo-Pacific sea-surface temperature up to 6 months previously – with a view to determining whether sea temperature has predictive skill at lead times of up to 6 months. Preliminary results indicate significant predictive skill (around 70 percent) for whole-MDB spring rainfall at lead times of up to 6 months. These skills are far higher than those achieved with linear models.

Understand the relationship between hydrological drivers and responses

This work now uses a modelling framework called CableDyn. This framework is based on AWAP but replaces the simple water balance model for AWAP (WaterDyn) with the model CABLE-SLI-CASACNP, developed from CABLE (Community Atmosphere-Biosphere-Land Exchanges), the CSIRO land-surface model developed over many years. Compared to WaterDyn, CABLE-SLI-CASACNP includes far more sophisticated descriptions of critical biological processes, such as the effect of water stress, temperature changes and CO_2 changes on evapotranspiration.

Without tuning, CABLE-SLI-CASACNP performs as well as or better than WaterDyn for predicting local discharge at annual to decadal time scales.

In three test catchments, CABLE-SLI-CASACNP has been used to analyse the sensitivity of water balance responses (local discharge, transpiration, soil evaporation and wet canopy evaporation) to perturbations in hydrometeorological drivers.

The sensitivity of local discharge to temperature ranges from –4 to –9 percent per °C across the three catchments; results are strongly dependent on the concurrent water vapour perturbation.

Sensitivity of local discharge to precipitation is consistent with an amplification factor (proportional response / proportional forcing perturbation) of 3 for the wetter catchments to 8 for the drier catchments.

Initial results suggest that rising CO_2 increases discharge by 0.5 to 2 percent per ppm CO_2, the result of decreased stomatal conductance and hence decreased transpiration as CO_2 increases. This is a significant effect, However, additional feedbacks associated with plant growth and structure are likely to modify this result, with overall consequences that are under investigation in current work.

Background

This project arose from the Australian Water Availability Project (AWAP), which aimed to monitor the state and trend of the terrestrial water balance of the Australian continent, and specifically to determine the past history and present state of soil moisture and all water fluxes contributing to changes in soil moisture (rainfall, transpiration, soil evaporation, surface runoff and deep drainage), across the entire Australian continent at a spatial resolution of 5 km. Past work in the AWAP has provided a 111-year (1900–present and ongoing) record of soil moisture and all terrestrial water fluxes over the Australian continent at 5-km spatial and daily temporal resolution (with monthly archiving).

As originally framed at the outset of Phase 2 of SEACI, the focus of Project 1.2 was to (i) maintain the AWAP data stream, (ii) apply it to model statistical climate–water relationships, and (iii) use the AWAP framework to understand the relationship between climatological drivers (precipitation, temperature etc) and hydrological responses (runoff, evaporation etc).

All of these lines of work have been delivered, but the priorities and modelling approaches have evolved. Through work by Vanessa Haverd (with support from Peter Briggs and Mike Raupach), we have now developed a modelling framework called CableDyn. This is based on AWAP, and uses the same driving data and computational infrastructure, but replaces the simple water balance model for AWAP (called WaterDyn) with CABLE, the land surface model developed over many years in CSIRO by numerous workers (Wang, Leuning, Raupach, Kowalczyk and others). CABLE describes not only energy and water exchanges but also carbon exchanges and carbon pool dynamics, and includes far more sophisticated descriptions of critical biological processes (such as the effect of water stress, temperature changes and CO_2 changes on evapotranspiration) than WaterDyn. In the version used in CableDyn, CABLE has been greatly extended and improved by Vanessa Haverd to further improve and test the representations of these processes. CABLE is also the land surface model used in most CSIRO climate models.

The development of CableDyn has opened a new method for investigating the third area in our workplan, the relationship between climatological drivers and responses. This has been our main focus in 2010/11.

Work in the first area (maintenance of the AWAP data stream by Peter Briggs and Matt Paget) has continued as before, because these data are essential for (and identical with) the driving data for CableDyn. We also continue to operate the existing AWAP website (Matt Paget). AWAP (with WaterDyn) continues to be a respected and widely used modelling framework, which performs against independent benchmarks at least as well as other systems developed after AWAP, such as Australian Water Resources Assessment.

Our work in the second area (application of AWAP to model statistical climate–water relationships) has proceeded mainly through the role of Mike Raupach in supervising PhD student Kirien Whan.

Objectives

The research in Project 1.2 falls into three main categories.

Develop, maintain and document the gridded hydrometeorological data flowing from the Australian Water Availability Project

The objectives were to:

- maintain and enhance the AWAP hydrometeorological data stream, including gridded meteorological data and modelled water-balance outputs
- from the AWAP dataset, produce time series of hydrological responses (soil moisture, runoff components and evaporation components) and proximate drivers of relevance to the hydrometeorology (rainfall, solar radiation, temperatures etc) over the whole of Australia (including masked outputs for SEA as required elsewhere).

Model statistical climate–water relationships using Australian Water Availability Project gridded data

The objectives were to:

- apply a general statistical model (linear with non-linear variants) to relate water balance responses over Australia to a set of indices that reflect the state of the climate
- determine the parameters in the statistical model over the whole of Australia (including SEA).

Understand the relationship between hydrological drivers and responses

The objective was to:

- apply the AWAP datasets to identify mechanisms causing hydrological responses (soil moisture, runoff and evaporation) to differ from hydrological drivers, thus to investigate the critical question: what determines the gain of the rainfall-runoff amplifier (whereby a given percentage change in rainfall leads to a larger percentage change in runoff)?

Results

Develop, maintain and document the Australian Water Availability Project gridded hydrometeorological data

This year significant milestones were achieved with the update and enhancement of the principal AWAP data stream the development of new data products, including SEACI-specific ones, and the release of important new documentation. Key outputs from these activities include:

- the public release of research-quality monthly historical time series for the continent: AWAP WaterDyn 26M, Run 26c, incorporating the latest updates (March 2011) of Bureau of Meteorology (BoM) Version 3 meteorology for January 1900 to February 2011. Importantly, the updated series covers the return to wet conditions in most of the SEACI region occasioned by the La Niña summer of 2010/11

- the public release of all spatial parameter datasets, with accompanying map graphics
- a SEACI subset of the full Run 26c, including map graphics for the period January 1997 to February 2011, the span of the south-eastern drought. A time series of thumbnail images of the percentile ranks for rainfall and upper- and lower-layer soil moisture for this period are shown as Figure 26a to Figure 26c. In Figure 26, percentile ranks show the conditions at each location relative to the climatology of conditions for the same place at the same time of year during the standard period 1961 to 1990. Percentile rank maps give a concise visual overview of anomaly patterns, but should be interpreted with care since they do not show the magnitude of the quantities involved. The patterns of upper-layer (Figure 26b) and lower-layer (Figure 26c) soil moisture tell different stories due to the different timescales on which they respond to precipitation (Figure 26a). The upper-layer soil moisture responds quickly and will often have a pattern that reflects the rainfall and temperature events of the same or the preceding month. Lower-layer soil moisture (Figure 26c) is a larger, deeper store that is slow to respond and tends to reflect accumulated events over seasonal and longer timescales. Discharge (Figure 26d) refers to the water available to rivers through surface runoff and deep drainage. Because deep drainage (not shown) is closely linked to lower-layer soil moisture, discharge shows a similar pattern of drought persistence to lower-layer soil moisture (Figure 26c), interrupted occasionally by wet months involving significant surface runoff
- area-average AWAP time series for the 245 Australian Water Resources Council drainage basins and major drainage divisions, which were made available to SEACI partners and used as inputs to the statistical modelling (Project 2.1). Sample plots of all AWAP quantities for wet, moderate and semi-arid regions of the MDB (Figure 27) for the period January 1997 to February 2011 are shown in Figure 28. Excel and comma-delimited files of the complete time series for all basins and all quantities from 1900 are available at the AWAP website <www.csiro.au/awap>.

Accompanying the new data release were updates to the CSIRO AWAP web and ftp sites including:

- thumbnail and full-size Run 26c imagery, which are now available at the website above. The most noticeable improvement is in the spatial structure of monthly model results in data-sparse areas, which now transition smoothly to denser-gauged areas due to the use of recalibrated daily rainfall (Jones et al. 2009) supplemented in regions of interpolation failure by monthly rainfall totals disaggregated to daily rainfall (Briggs et al. 2011a). Water balance components in data-sparse areas are now, therefore, generated from quasi-realistic forcing, replacing the artefacts in the previous Run 25a data (Raupach et al. 2009).
- historical data at the ftp site are now organised by individual variable to better fit the requirements of most users.

Metadata documentation has been redesigned to better reflect the topics of greatest interest to users, including:

CSIRO AWAP Run 26c historical monthly and annual model results for 1900-2011/02: AWAP 26c using improved Bureau of Meteorology AWAP Version 3 meteorological data is a concise guide to the new historical data, including a comprehensive FAQ about the new meteorology and its preparation for use by the WaterDyn and CableDyn models (including new information since Jones et al. 2009). This accompanied the March 2011 announcement of the 1900–2009 series and has been updated to reflect the 1900 to 2011/02 data (Briggs et al. 2011a). The original document was reviewed by members of the Bureau of Meteorology AWAP team.

Spatial soil and vegetation parameters for AWAP modelling is a set of maps with brief descriptions of the spatially varying parameter datasets used by AWAP WaterDyn (Briggs et al. 2011b). This package provides an important interpretation aid for users wishing to understand how the soil and vegetation parameters influence the response of the model to meteorological forcing. It supplements the spatial parameter description in Raupach et al. (2009).

Version 5 of the AWAP readme file has been updated to reflect the changes associated with Run 26c.

These documents are available though links at the *Additional Information* section at <www.csiro.au/awap>.

Updates and improvements to the BoM Version 3 data[1] and the creation of Run 26c have allowed useful progress on the core paper for the AWAP model, primarily in the area of updated calibration-validation against the Vaze et al. (2011) streamflow dataset supplemented by additional catchments from Neil Viney (unpublished). We have also obtained updated streamflow records (early December 2010) for the Burdekin, Fitzroy and Murray rivers at Wentworth gauging stations to expand the scope of the flow cascade work in Raupach et al. (2009).

This year we have been pleased to receive unsolicited assistance with AWAP calibration-validation courtesy of two independent comparisons of Run 26c soil moisture surfaces with GRACE gravimetric data by Munier et al. (2011, submitted) for the Canning Basin and continentally by García-García et al. (2011), who found 'remarkable' agreement between GRACE, GLDAS and AWAP data in analyses linking GRACE data to Indo-Pacific climate variability in the period 2002 to 2010.

Evaluation of the model results shown in Figures 26-28 has been extensive, including tests summarised above and described in more detail in Raupach et al. (2009).

[1] Improvements since Jones et al. (2009), mainly to the Australian Data Archive for Meteorology (ADAM) source data for the BoM AWAP surfaces, have been documented informally by the BoM but are described in the Run 26c data announcement.

(a) Precipitation percentile ranks

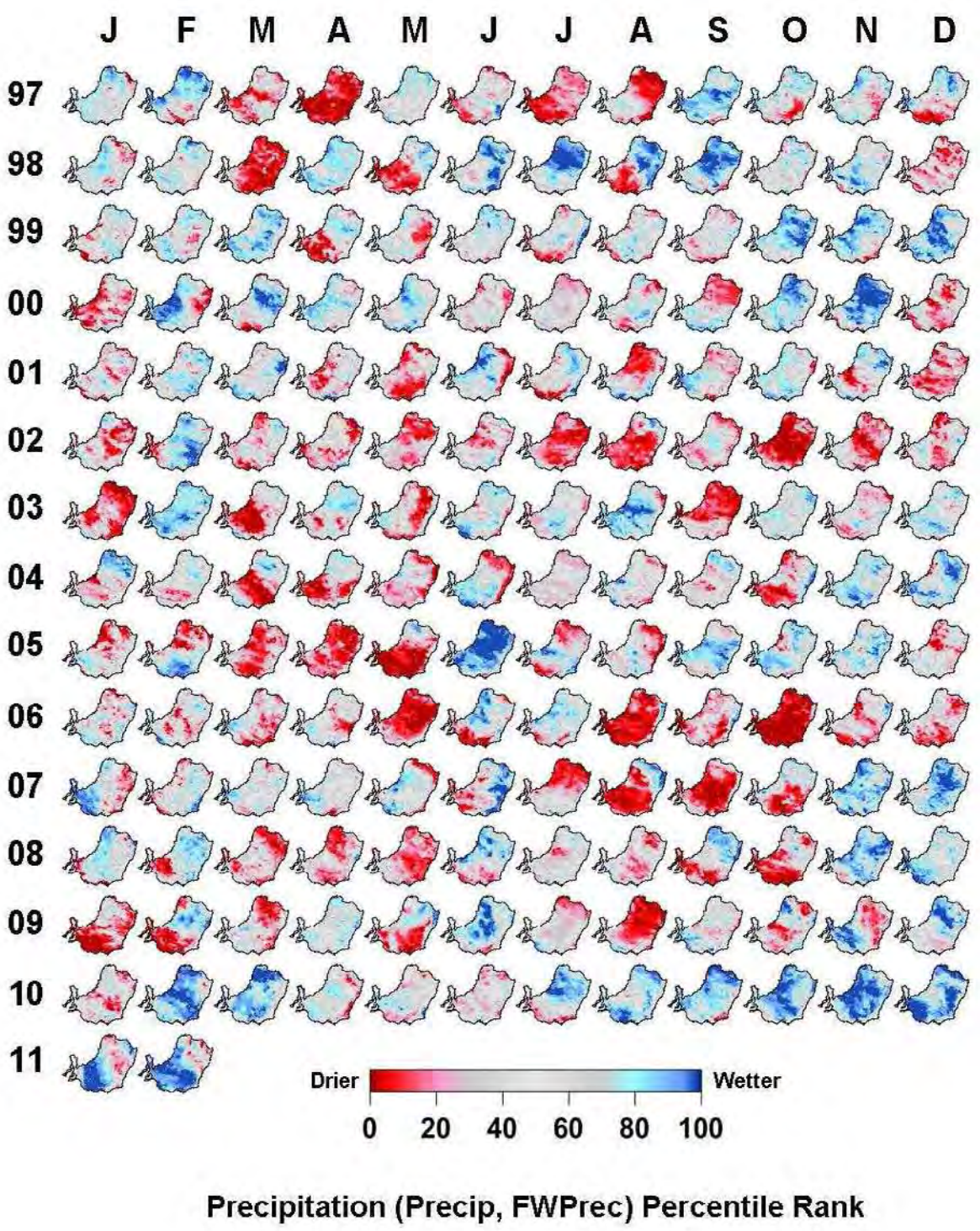

Figure 26. SEACI region monthly time series of (a) precipitation, (b) upper-layer soil moisture, (c) lower-layer soil moisture, and (d) discharge (surface runoff and deep drainage) for the period January 1997 to February 2011, expressed as percentile ranks

(b) Upper-layer relative soil moisture percentile ranks, showing a broadly similar pattern to precipitation, with lags evident after notably wet months.

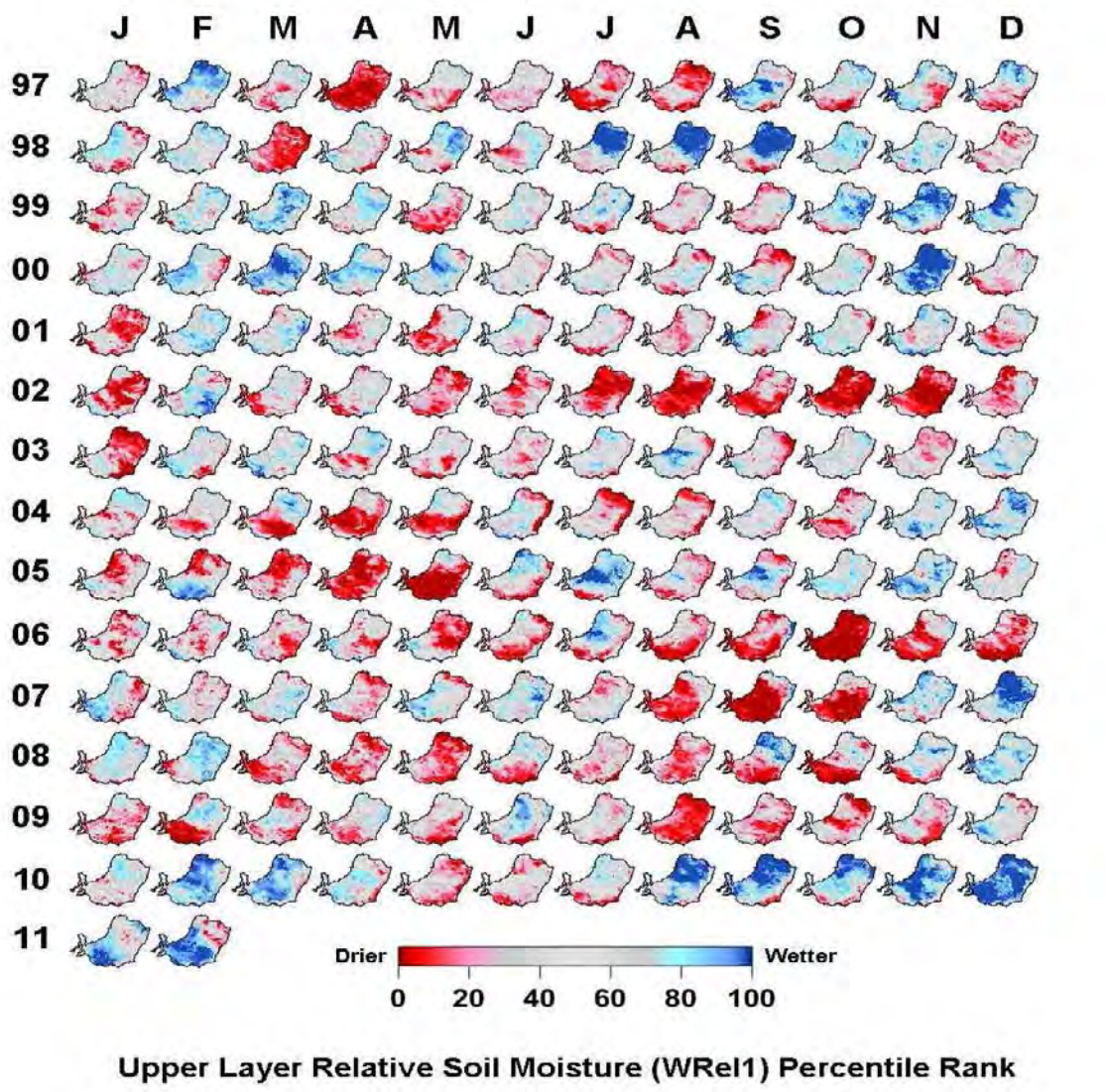

Figure 26 (cont.) SEACI region monthly time series of (a) precipitation, (b) upper-layer soil moisture, (c) lower-layer soil moisture, and (d) discharge (surface runoff and deep drainage) for the period January 1997 to February 2011, expressed as percentile ranks

(c) Lower-layer relative soil moisture percentile ranks. The early development of the drought in the southern part of the SEACI region can be seen in 1997, with a persistence of drier than normal conditions in that area through the continentally-wet year 2000. In 2002, the drought becomes widespread, contracting to the south through 2008–2010, finally breaking in most areas in the wet summer of 2010–2011

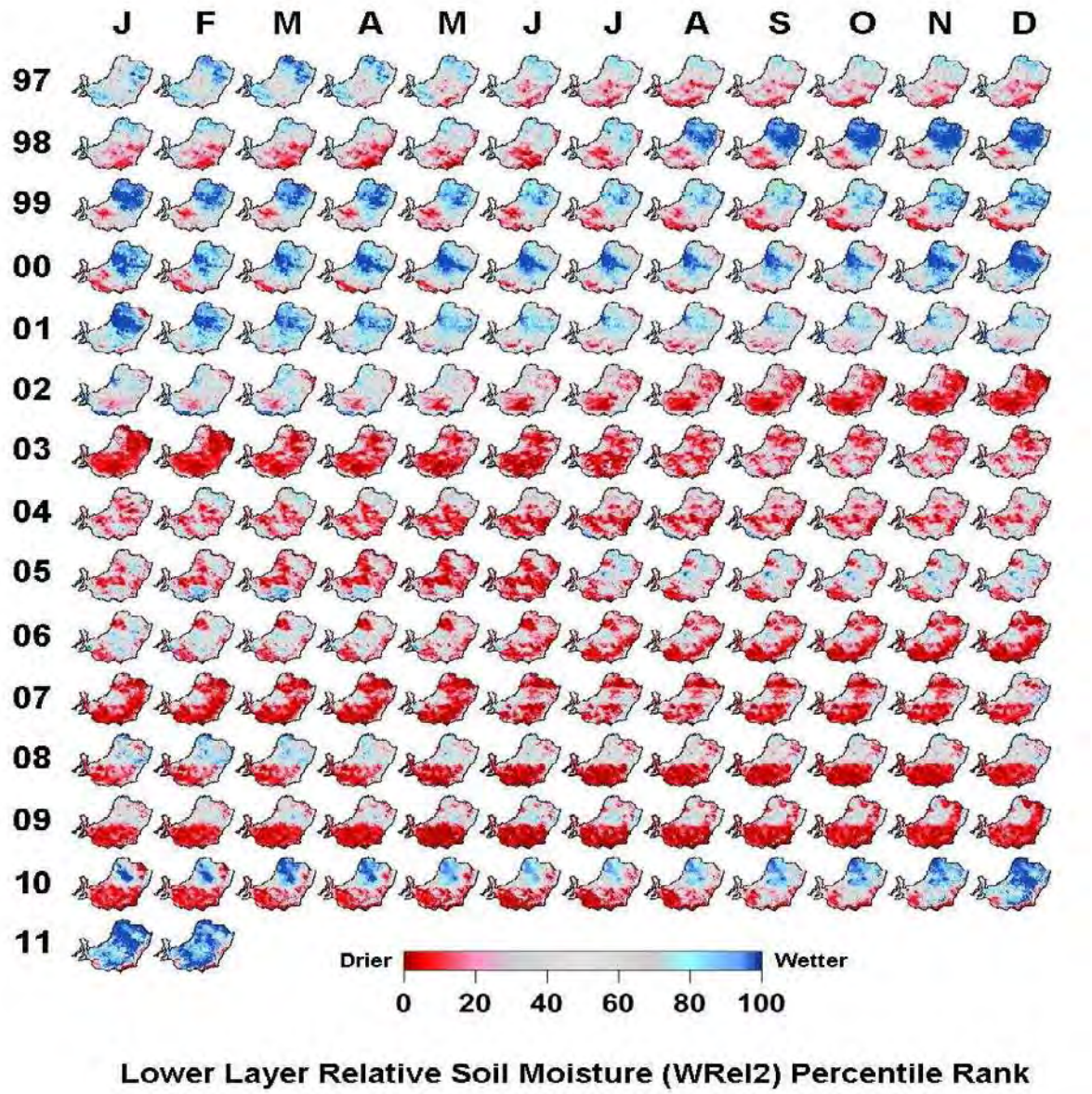

Figure 26 (cont.) SEACI region monthly time series of (a) precipitation, (b) upper-layer soil moisture, (c) lower-layer soil moisture, and (d) discharge (surface runoff and deep drainage) for the period January 1997 to February 2011, expressed as percentile ranks

(d) Discharge percentile ranks. In AWAP WaterDyn, discharge is the sum of contributions to streamflow from surface runoff (FWRun) and deep drainage (FWLch2), and shows a similar pattern of slow evolution to lower-layer soil moisture. Occasional departures occur when significant rain events lead to discharges with a large surface runoff component such as the central northern SEACI region in June 2005. This event is not observed in the lower layer soil moisture map for that month (see c)

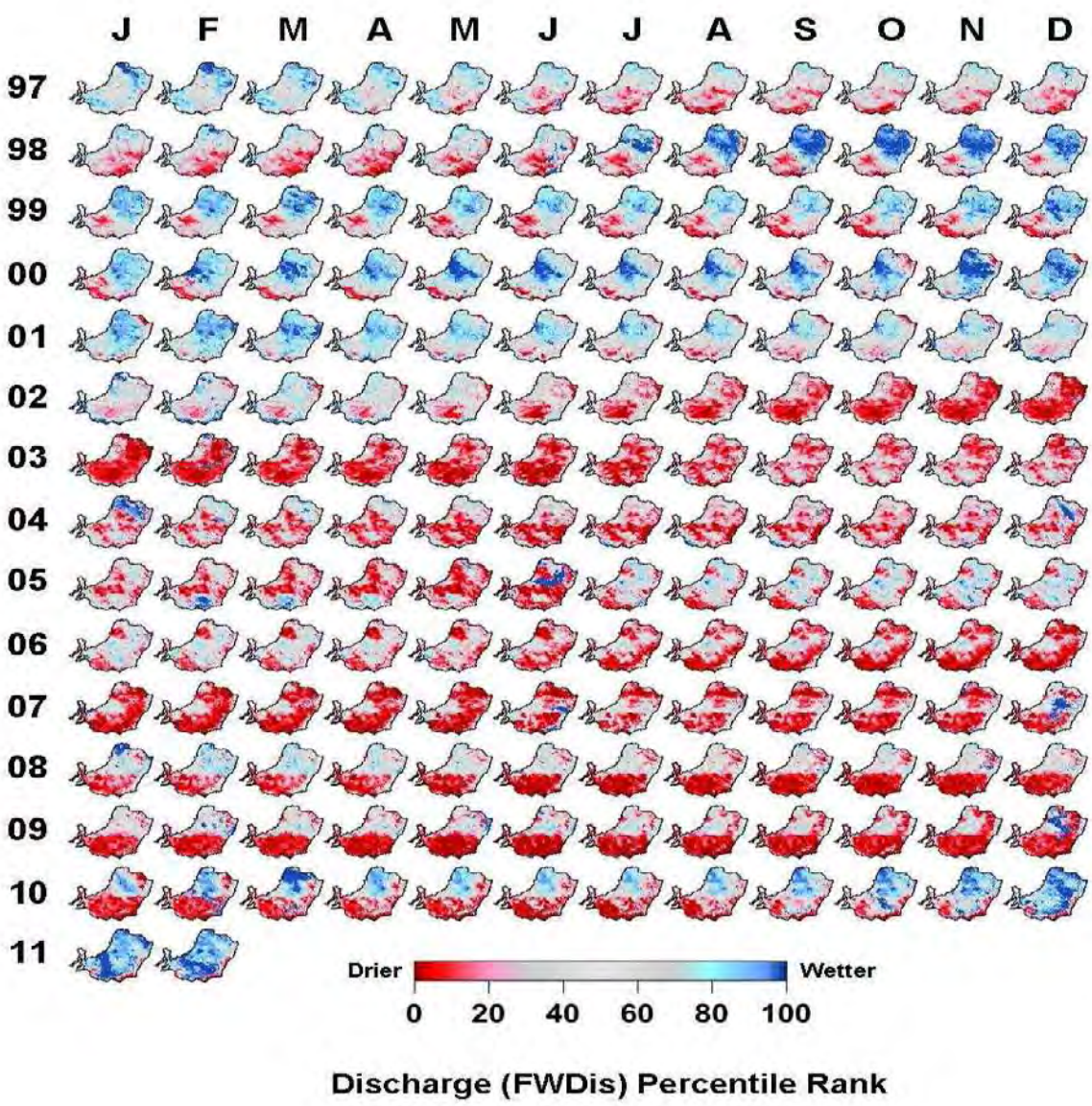

Figure 26 (cont.) SEACI region monthly time series of (a) precipitation, (b) upper-layer soil moisture, (c) lower-layer soil moisture, and (d) discharge (surface runoff and deep drainage) for the period January 1997 to February 2011, expressed as percentile ranks

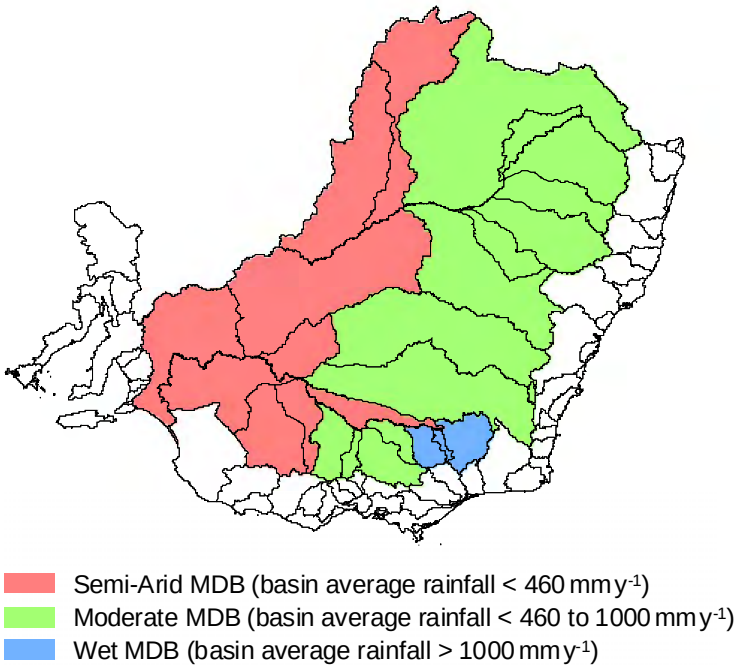

Figure 27. Within the SEACI region, the Murray–Darling Basin (coloured) can be sub-divided into three regions based on the mean annual rainfall of the constituent basins. The green basins are broadly suited to agricultural activity

(a) Precipitation and relative soil moisture

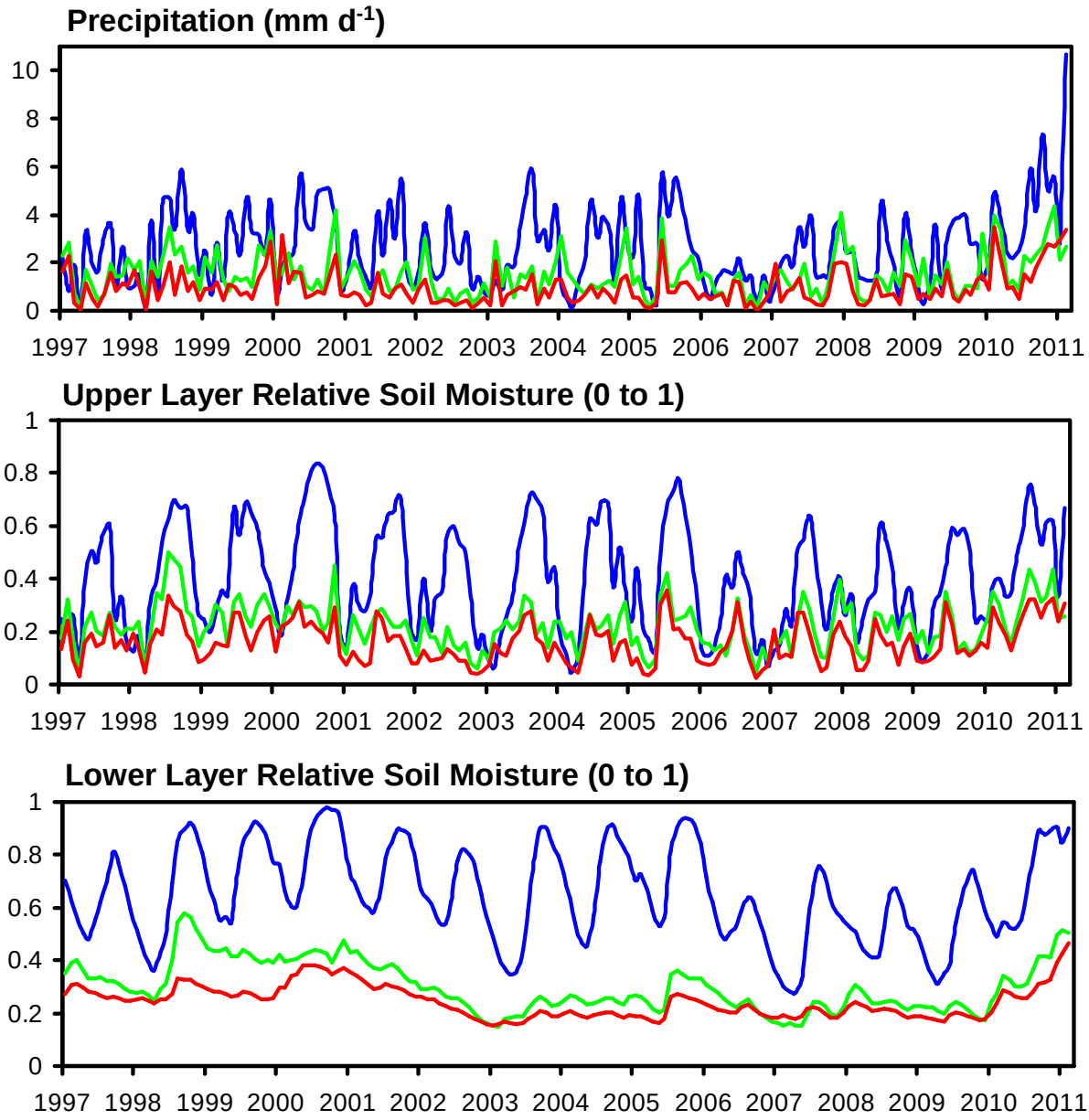

Figure 28. Regionally-averaged monthly time series of water and energy balance components and meteorological forcings (the Australian Water Availability Project product suite), January 1997 to February 2011, for semi-arid (red), moderate (green), and wet (blue) sub-divisions of the Murray–Darling Basin (Figure 27). Plots of precipitation are repeated for ease of comparison

(b) Precipitation and local discharge components

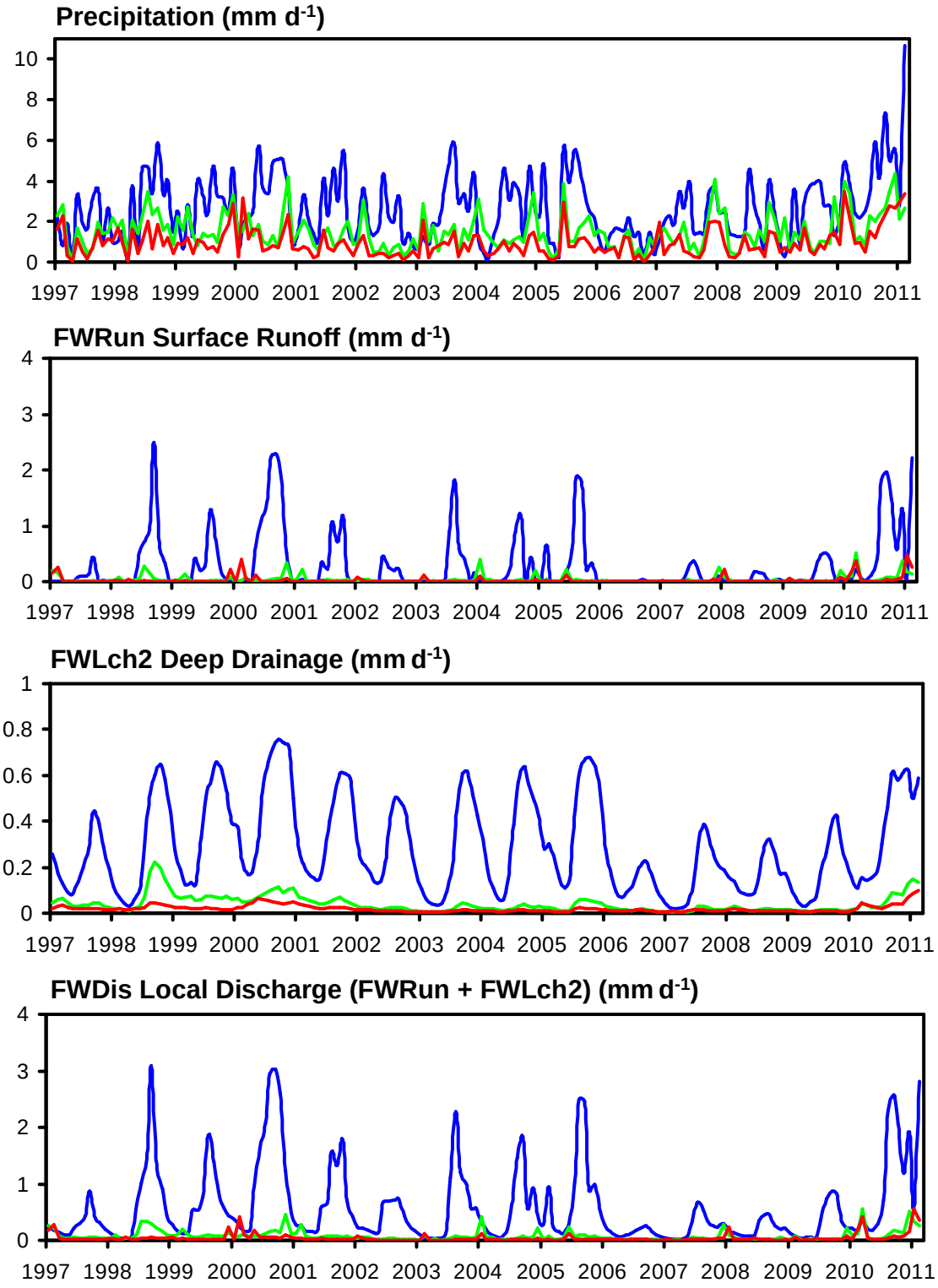

Figure 28 (cont). Regionally-averaged monthly time series of water and energy balance components and meteorological forcings (the Australian Water Availability Project product suite), January 1997 to February 2011, for semi-arid (red), moderate (green), and wet (blue) sub-divisions of the Murray–Darling Basin (Figure 27). Plots of precipitation are repeated for ease of comparison

(c) Evaporation components and potential evaporation

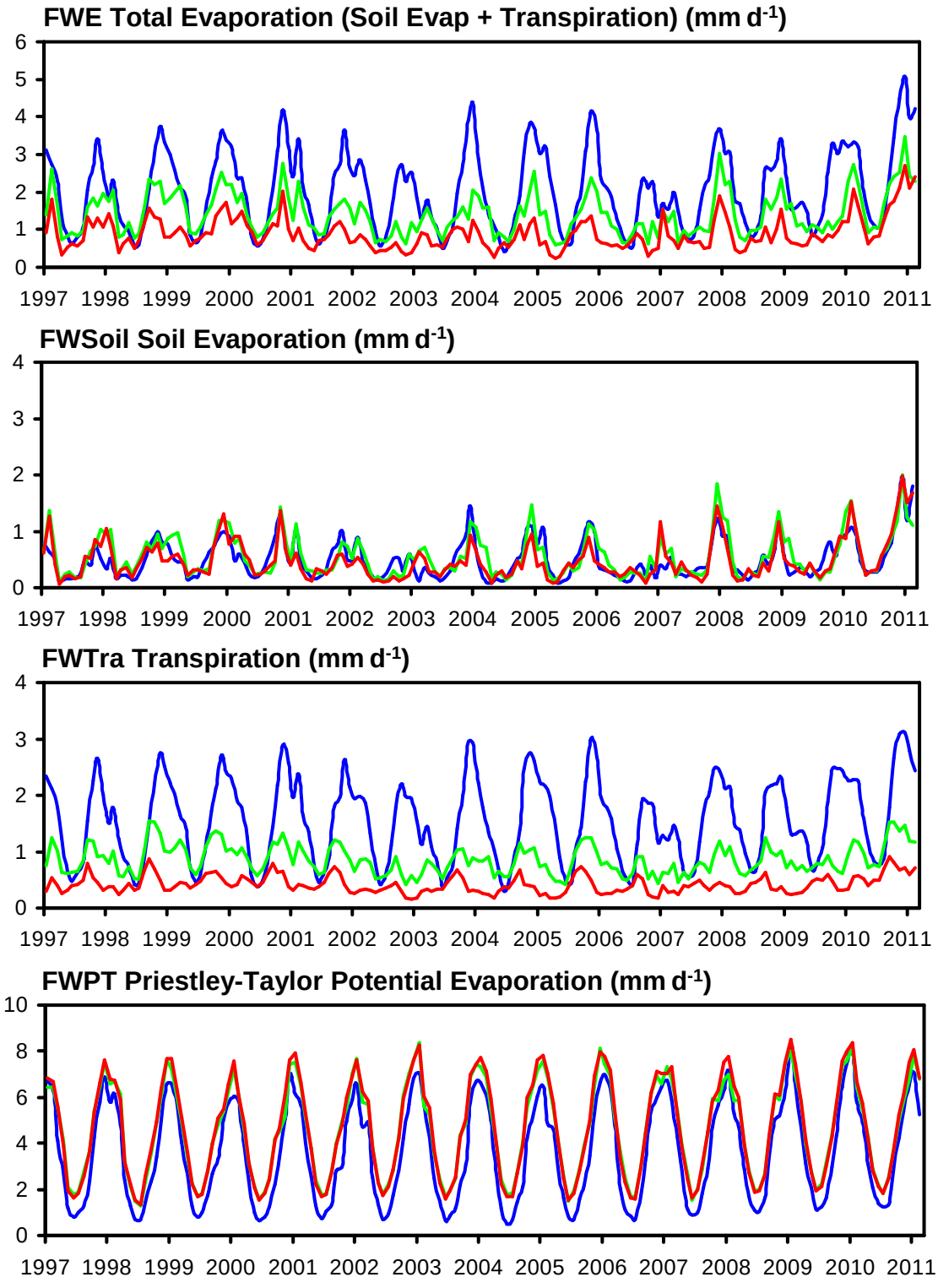

Figure 28 (cont). Regionally-averaged monthly time series of water and energy balance components and meteorological forcings (the Australian Water Availability Project product suite), January 1997 to February 2011, for semi-arid (red), moderate (green), and wet (blue) sub-divisions of the Murray–Darling Basin (Figure 27). Plots of precipitation are repeated for ease of comparison

(d) Precipitation, energy partitioning and open water (pan) evaporation (modelled)

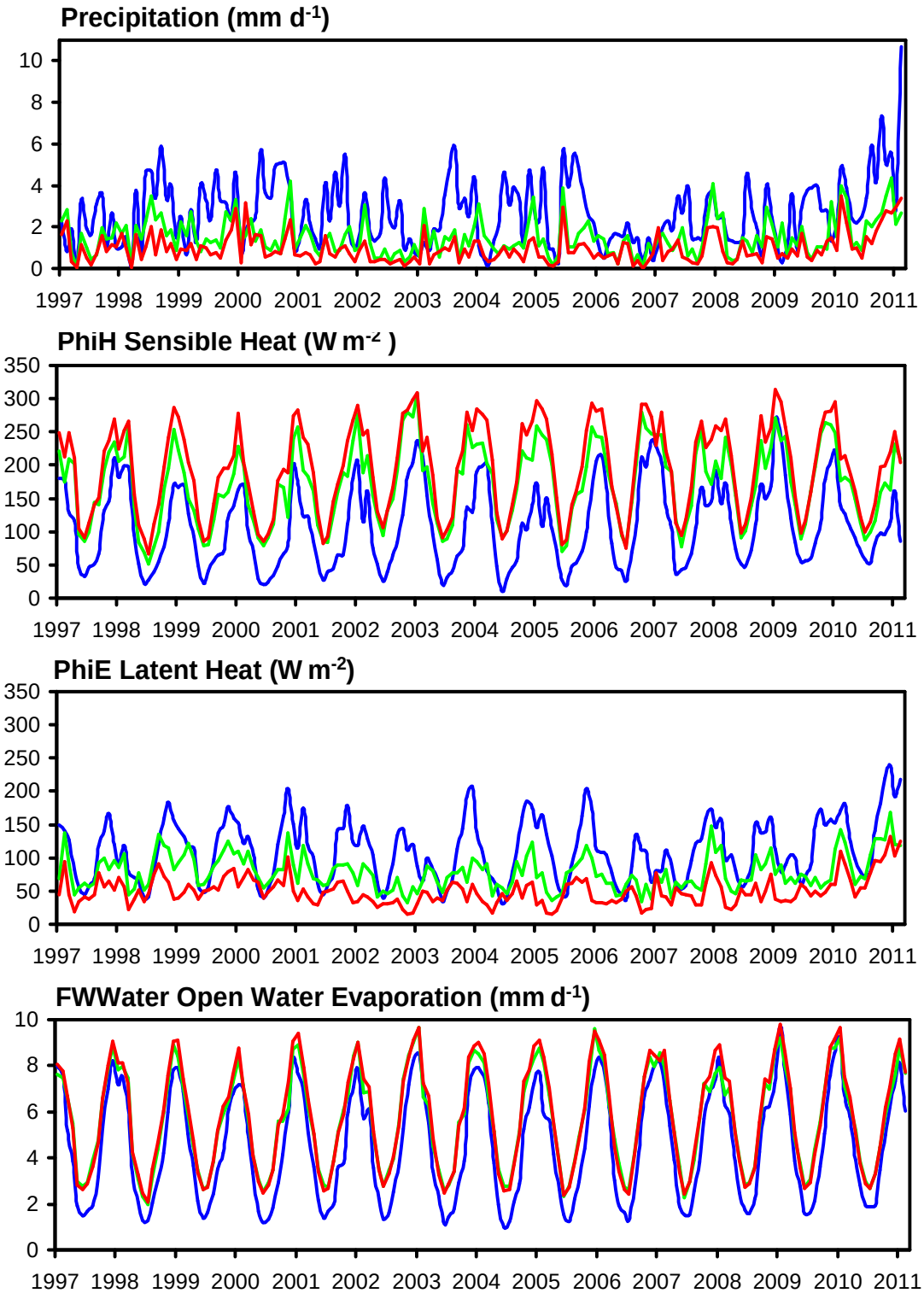

Figure 28 (cont). Regionally-averaged monthly time series of water and energy balance components and meteorological forcings (the Australian Water Availability Project product suite), January 1997 to February 2011, for semi-arid (red), moderate (green), and wet (blue) sub-divisions of the Murray–Darling Basin (Figure 27). Plots of precipitation are repeated for ease of comparison

(e) Relevant meteorological forcings (Bureau of Meteorology Australian Water Availability Project Version 3)

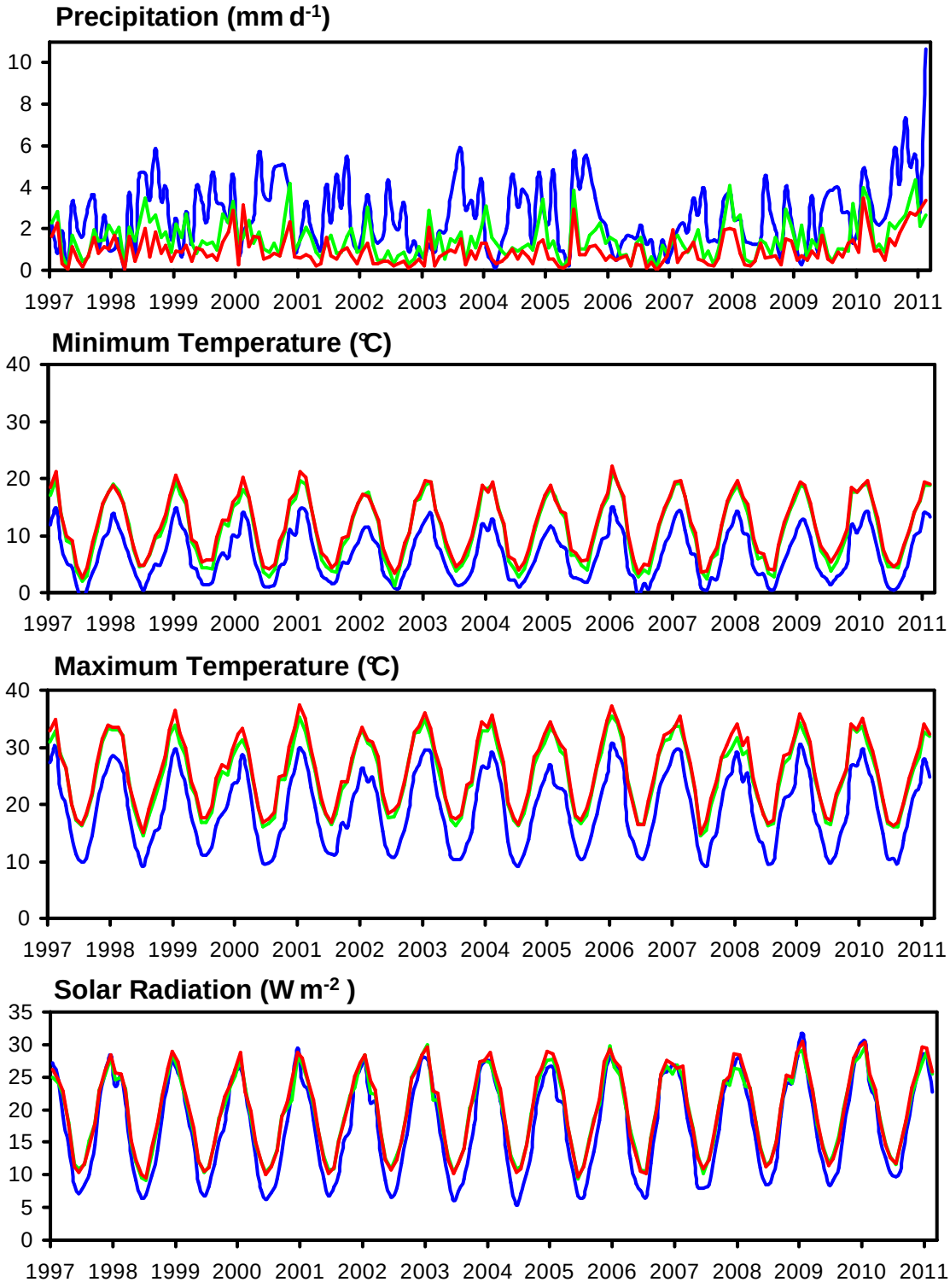

Figure 28 (cont). Regionally-averaged monthly time series of water and energy balance components and meteorological forcings (the Australian Water Availability Project product suite), January 1997 to February 2011, for semi-arid (red), moderate (green), and wet (blue) sub-divisions of the Murray–Darling Basin (Figure 27). Plots of precipitation are repeated for ease of comparison

Model statistical climate–water relationships using Australian Water Availability Project gridded data

In work by Kirien Whan, CART analyses have been used to explore the relationship between Indo-Pacific equatorial sea-surface temperature with upper-level soil moisture in the MDB. Both linear and non-linear analyses confirm that sea surface temperatures in the waters north of Australia (100 °E to 140 °E) have the strongest relationship with upper-layer soil moisture.

Key outputs this year include:

We have classified hydrometeorological state in the MDB with respect to the state of the Indo-Pacific region, using several hydrometeorological variables (precipitation, upper- and lower- layer soil moisture, potential evaporation and local discharge) in the four regular seasons.

Predictive classification-based models for spring hydrometeorological state, based on the state of the Indo-Pacific region in the preceding six 3-month seasons (ASO, JAS, JJA, MJJ, AMJ and MAM), were built to examine the predictability of spring rainfall. Preliminary results (Table 5, Table 6) indicate significant predictive skill (around 70 percent) for whole-MDB spring rainfall at lead times of up to 6 months. These skills are far higher than those achieved with linear models.

An example of the classification tree for spring rainfall is shown in Figure 29. This illustrates the regression tree and the probability density functions (PDFs) from which a break point between states and a skill score are determined. Following this is a discussion of the details of the predictive regression trees.

Precipitation in spring

During El Niño events (Southern Oscillation Index (SOI) less than –2.48; see Figure 29) the state of the sea-surface temperature anomalies in the Indonesian Throughflow (ITF) region determines the extent and severity of negative precipitation anomalies across eastern Australia. This interaction between the Pacific (represented by the SOI) and the Indian Oceans (represented by the ITF) is important in distinguishing the driest years. A dry state of the MDB is related by the classification tree (Figure 29) to a negative SOI (less than –2.48) in conjunction with cool sea-surface temperature anomalies in the ITF less than –0.58 °C). The combination of El Niño with cool sea-surface temperature anomalies in the eastern Indian Ocean results in Terminal Node 4 (Figure 29) which has average rainfall in the MDB of 287.4 mm/year, with significant negative rainfall anomalies over the eastern two-thirds of the continent, with the largest anomalies along the Great Dividing Range and in northern Tasmania. The distribution (Figure 30) of rainfall in Terminal Node 4 shows that there is a 90 percent chance of MDB rainfall of less than 394 mm/year when the SOI less than –2.48 and ITF sea surface temperature less than –0.58 °C. The mean squared error of this state (terminal node on the tree), in conjunction with the PDF, shows that the variation of the cases around the mean is small.

A wet state or terminal node is defined when the SOI greater than or equal to –2.48 and NINO3 sea surface temperature is less than –0.97 °C. Multiple splits on the same variable, in this case on measures of El Niño – Southern Oscillation (ENSO), suggest a linear relationship between the predictand and predictor variables. This is the extreme La Niña group, which combines a neutral or positive SOI with the coolest SST anomalies in the equatorial Pacific Ocean, and displays positive rainfall anomalies over all of eastern Australia. The largest anomalies are on the east coast and over the Great Dividing Range, while some negative anomalies are evident over western Tasmania. The distribution of Terminal Node 7 (Figure 30) shows that when the SOI is greater than –2.48 and NINO3 is less than –0.97 °C, there is a 73 percent chance of rainfall greater than 619.56 mm/year in the MDB. The grouping of cases in Terminal Node 7 is more widespread, as indicated by the mean squared error and the PDF, due to the influence of 3 years that had low rainfall (296, 261 and 453 mm/year).

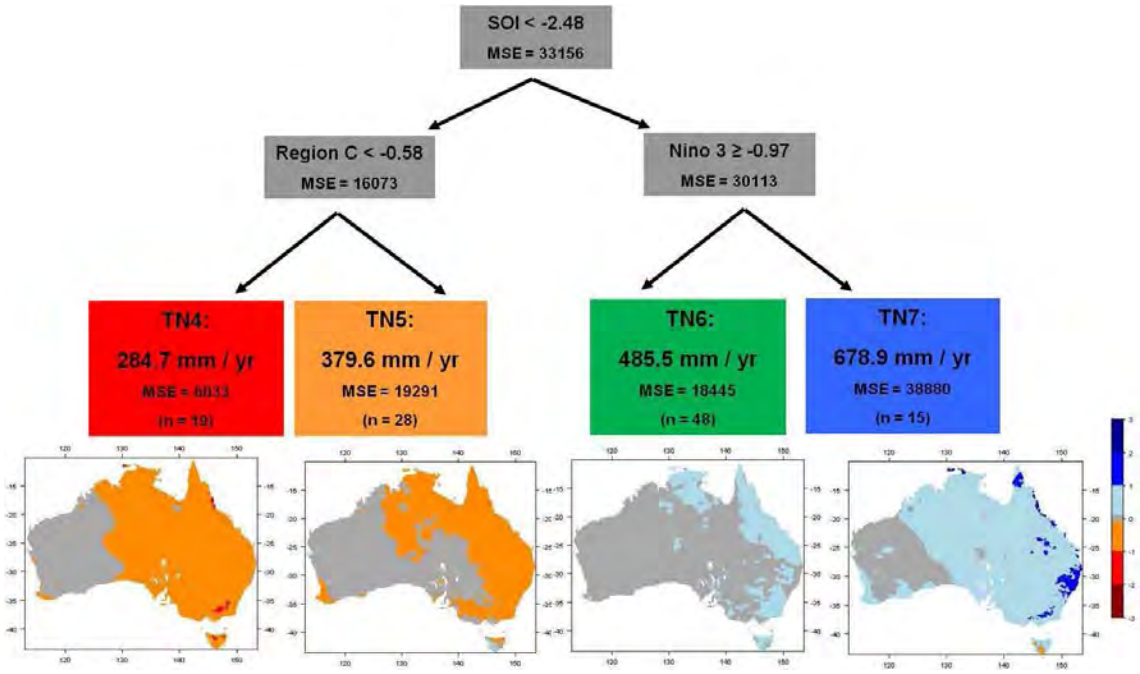

Figure 29. Regression tree for precipitation in spring based on all Indo-Pacific forcings. Anomalies are calculated against the full record and expressed in mm/day in the composite plots. Region C is the Indonesian Throughflow (ITF) region.

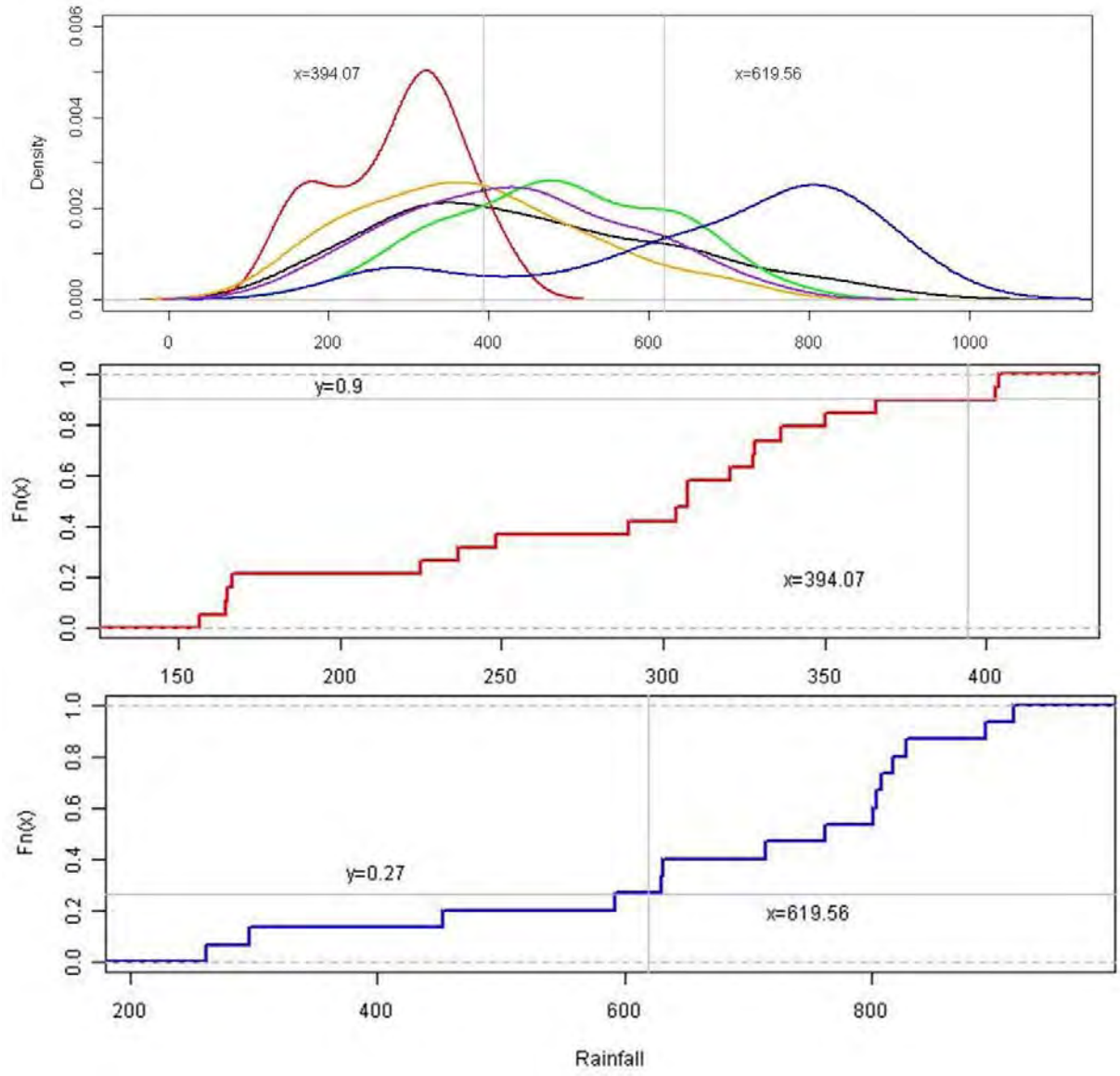

Figure 30. Probability density functions and cumulative density functions for observed MDB rainfall when the classification model predicts that the MDB rainfall falls into one of the four states represented by the coloured boxes in Figure 29. The coloured lines in this figure correspond to these boxes. The black line in the top panel shows the probability density function for the entire observed MDB rainfall or the sum of all classified states..

Predictions of Murray–Darling Basin spring rainfall

Regression trees were constructed that use Indo-Pacific variability in preceding months to classify MDB rainfall in spring which gives information about the antecedent Indo-Pacific conditions that are associated with dry and wet conditions in spring. The skill score of the predictive models indicates how well Indo-Pacific variability in preceding months predicts MDB rainfall in spring.

The details of spring rainfall predictions of the dry terminal nodes can be seen in Table 5. Taking the simultaneous regression tree as an example (September through November, Table 5), it shows that if the September through November values of the SOI are less than –2.48 and sea surface temperature in the ITF is less than –0.58 °C, then there is a 90 percent chance (skill score = 0.9) that rainfall in the MDB will be less than 394 mm/year. This break point separates the bottom 43 percent of MDB spring rainfall. Generally it can be said (with a level of certainty given by the skill score) that given particular Indo-Pacific conditions in a preceding season, spring rainfall in the MDB will be below the break point.

Table 5. Skill scores and decision rules for dry terminal nodes. Mean Murray–Darling Basin rainfall for September through November is 451 mm/year, and median Murray–Darling Basin rainfall for September through November is 421 mm/year.

Season	Indo-Pacific conditions	Mean rainfall in node (mm/year)	Break point (mm/year)	Skill score (0 – 1)	September-November rainfall percentile
September-November	**SOI** < –2.48 *and* **Region C** < –0.58°C	285	394	0.9	43rd
August-October	**SOI** < –0.03 *and* **Region C** < –0.80°C	264	372	1	41st
July-September	**NINO3** ≥ –0.73°C *and* **SOI** < 0.003	354	429	0.76	52nd
June-August	**NINO3** ≥ –0.58°C *and* **Region C** < –0.03°C	364	412	0.67	45th
May-July	**NINO3** ≥ –0.41°C *and* **Region C** < –0.17°C	340	420	0.77	49th
April-June	**NINO3** ≥ –0.41°C *and* **NWS** < –0.01°C	355	412	0.74	45th
March-May	**NINO3** ≥ 0.00°C *and* **NINO3** < 0.61°C	372	520	0.84	67th

The simultaneous and August through October trees use the SOI for the first split and Region C (the Indonesian throughflow) as the second split. The skill scores for these terminal nodes are the highest and the percentiles of rainfall they predict are the lowest, showing there is high certainty for a small rainfall prediction. Trees built with a larger lag have NINO3 as the primary split showing that the low-frequency oceanic mode has greater predictability at a longer lag. The mean rainfall in these terminal nodes is larger (greater than 300 mm/year) and the skill scores are lower (less than 0.8). The exception is March through May, which classifies a dry terminal node with mean rainfall of 372 mm/year on a linear split of NINO3. While the skill score for this terminal node may be high (0.84), the break point determined from the PDF of rainfall in each terminal node is also high. As the distributions of the wet and dry terminal nodes overlap in this model, a large break point is selected, less than 520 mm/year, and only the bottom two-thirds (67th percentile) of rainfall can be determined based on the state of the Indo-Pacific region in March through May. The most useful season for prediction, based on the information in Table 5, is April through June. In this season, there is a 74 percent chance that spring rainfall will be in the bottom 45th percentile when April-June values of NINO3 are greater than –0.41°C and the north-west shelf (NWS) is less than –0.01°C. This season is the most useful because it combines a large lag with high certainty and, although still large, the smallest percentile of rainfall.

The details of the regression trees for predicting wet cases in spring can be seen in Table 6. The regression trees give more useful predictions of the wet terminal nodes compared to the dry node as a much smaller percentile of rainfall is predicted with high certainty. For example, in May through July if NINO3 is less than –0.41°C and the Tripole Index is less than 0.01 then there is an 85 percent chance that spring rainfall in the MDB will be more than 737 mm/year (top 9th percentile). The simultaneous (September through November) and 1-month lag (August through October) predictions are based on the SOI but the second split is also based on ENSO (NINO3). This shows that wet conditions in these two seasons can be classified solely on ENSO with high skill and a high break point (which separates the top quarter of the rainfall distribution). All other seasons require information from both the Pacific and Indian oceans except July through September which only splits on NINO3; however, the skill in this season is low, suggesting that information from both ocean basins results in more skilful predictions.

Table 6. Skill scores and decision rules for wet terminal nodes. Mean Murray–Darling Basin rainfall for September through November is 451 mm/year. Median Murray–Darling Basin rainfall for September through November is 421 mm/year

Season	Indo-Pacific conditions	Mean rainfall in node (mm/year)	Break point (mm/year)	Skill score (0 – 1)	September-October rainfall percentile
September-November	**SOI** ≥ –2.48 *and* **NINO3** < –0.97°C	679	620	0.73	23rd
August-October	**SOI** ≥ –0.03 *and* **NINO3** < –0.81°C	642	588	0.72	25th
July-September	**NINO3** < –0.73°C	648	651	0.53	16th
June-August	**NINO3** < –0.58°C *and* **TPI** < 0.20	702	641	0.72	17th
May-July	**NINO3** ≤ –0.41°C *and* **TPI** < 0.01	797	737	0.85	9th
April-June	**NINO3** < –0.41°C *and* **DMI** ≥ –0.07	618	558	0.63	27th
March-May	**NINO3** < –0.00°C *and* **DMI** ≥ 0.14	630	496	0.71	37th

Linear modelling

In parallel work, a linear model has been applied relating a single-point water balance property w(t) (e.g. rainfall, soil moisture or total runoff) and a set of N lagged climate modes $a_n(t-L_n)$ (e.g. ENSO, Indian Ocean Dipole (IOD) or STR-I):

$$w(t) = \sum_{n=1}^{N} x_n a_n \left(t - L_n\right)$$

where x_n is a set of N weights which constitute the model parameters, and L_n is the time lag corresponding to the maximum absolute correlation between the climate mode and the water balance property. As a test case, the model was applied to the Adelong catchment, using 100 years of soil moisture data provided by AWAP and a 100-year time series of 11 climate indices. The weights were determined using the Singular Value Decomposition technique, using a moving time window of 30 months on a seasonal basis. The model with the resulting weights was able to account for approximately 30 percent of the variance in the soil moisture time series. The time-varying weights showed a marked step change around 1940. This preliminary work raised the following questions:

For a given catchment, which climate indices can be excluded based on the statistical significance of the correlation between the index and the water balance property?

How long should the moving time window be?

What is the origin of the step change around 1940? Is it an artefact of the meteorological input to AWAP?

To answer these questions, the model inversion has been applied at continental scale for the 245 AWRC drainage basins. Sample results have been generated (e.g. Figure 31) and efforts have since moved the modelling platform to the R language to allow greater flexibility in the choice of statistical methods.

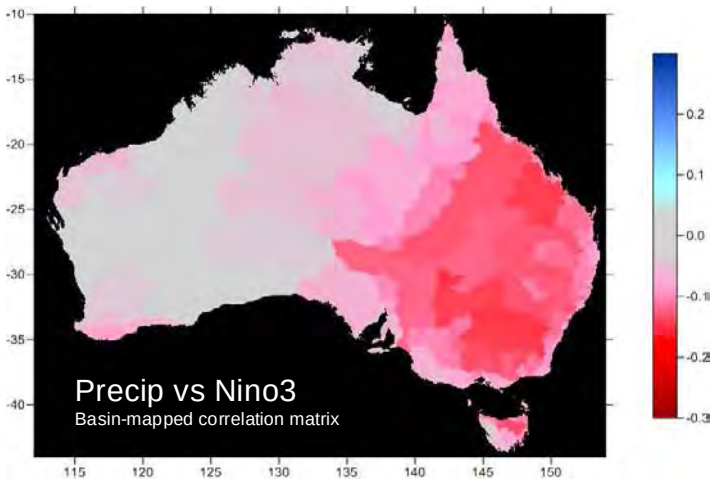

Figure 31. Correlation of monthly precipitation time series for each of the 245 Australian Water Resources Council drainage basins with the Nino 3 climate index

Understand the relationship between hydrological drivers and responses

This activity has been a key area of achievement for Project 1.2. Through work by Vanessa Haverd (with support from Peter Briggs and Mike Raupach), we have now developed a modelling framework called CableDyn. This is based on AWAP but replaces the simple water balance model for AWAP (WaterDyn) with the model CABLE-SLI-CASACNP, developed from CABLE. CABLE-SLI-CASACNP includes far more sophisticated descriptions of critical biological processes (such as the effect of water stress, temperature changes and CO_2 changes on evapotranspiration) than WaterDyn. Key findings from this work include:

- Without tuning, CABLE-SLI-CASACNP performs as well as or better than WaterDyn for predicting local discharge at annual to decadal time scales
- In three test catchments, CABLE-SLI-CASACNP has been used to analyse the sensitivity of water balance responses (local discharge, transpiration, soil evaporation, wet canopy evaporation) to perturbations in hydrometeorological drivers
- The sensitivity of local discharge to temperature ranges from –4 to –9 percent per °C across the three catchments; results are strongly dependent on the concurrent water vapour perturbation
- Sensitivity of local discharge to precipitation is consistent with an amplification factor (proportional response/proportional forcing perturbation) of 3 for the wetter catchments to 8 for the drier catchment. This is the "rainfall-runoff amplifier"
- Rising CO_2 increases discharge by 0.5 to 2 percent per ppm CO_2, the result of decreased stomatal conductance and hence decreased transpiration as CO_2 increases. This is a significant effect. However, additional feedbacks associated with plant growth and structure are likely to modify this result, with overall consequences that are under investigation in current work.

Sensitivity of the water balance to meteorological drivers

We have applied a process-based land surface model (CABLE-SLI-CASACNP) continentally at 0.05° spatial resolution and hourly time resolution with monthly outputs. The model prognoses the coupled fluxes and stores of carbon, water and energy, using the following driver data:

- daily Bureau of Meteorology AWAP Version 3 meteorological data (downscaled to hourly resolution): precipitation, air temperature, solar radiation and vapour pressure
- deseasonalised global atmospheric CO_2 concentration
- monthly woody and grassy leaf area index, derived by decomposing time series of remotely-sensed fraction of absorbed photosynthetically-active radiation
- monthly fraction cover for woody vegetation.

As an illustration of the model output, we show in Figure 32 the total evapotranspiration rates for 1990–2009, aggregated by season and for the whole year.

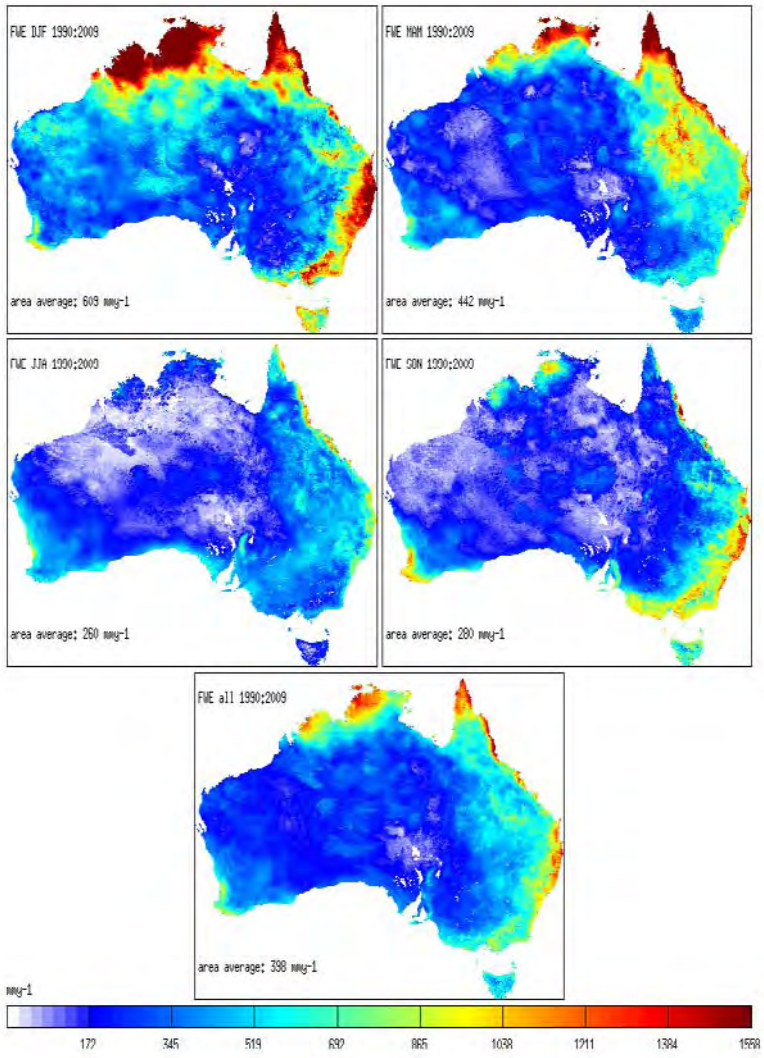

Figure 32. Evapotranspiration in mm/year for four seasons December through February, March through May, June through August, and September through November and for the whole year. Illustrative output from the CABLE-SLI-CASACNP model

We have selected three contrasting catchments for this study (Table 7) from the six nominally unimpaired catchments (Figure 33) used for AWAP parameter estimation in the upper Murrumbidgee basin (Raupach et al. 2009). The analysis is readily extendable to the entire continent or any region thereof. The meteorological drivers investigated are listed in Table 8. Sensitivities were evaluated using model runs performed with and without the listed perturbation for each driver. Sensitivities are reported as relative changes in flux per unit change in driver or as amplification factors, depending on the driver. The temperature perturbation necessitated a concurrent perturbation in atmospheric water vapour. This was prescribed by applying a perturbation to the relative humidity of –0.015 per °C, based on analysis of 1950–2010 AWAP meteorological data for the six Murrumbidgee catchments (Figure 33). The relative humidity and temperature data (on days with no precipitation) were binned by modelled evaporative fraction, and simple linear regression was used to estimate the slope (Figure 34). Analysis of all data together produced a slope of –0.015 per °C ($R^2 = 0.64$).

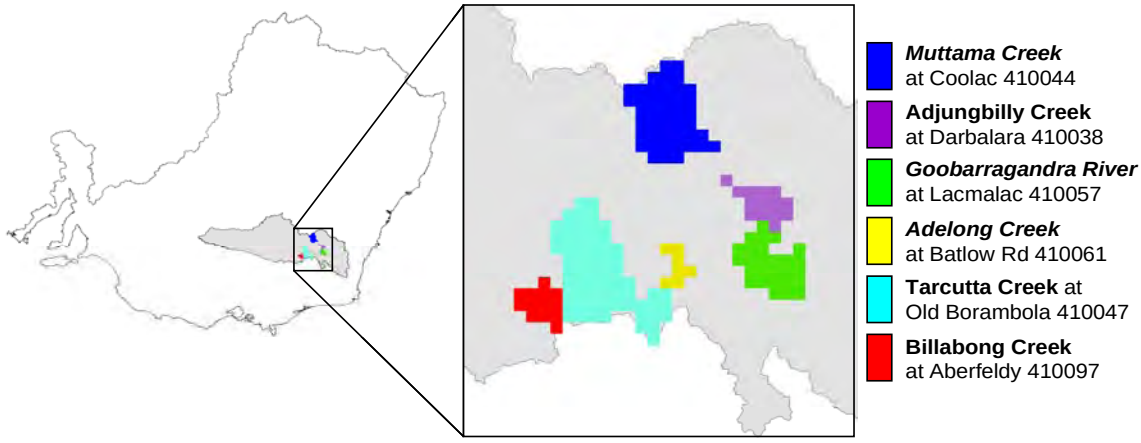

Figure 33. Six nominally unimpaired catchments in the upper Murrumbidgee basin, defined as the drainage areas (at 0.05° grid resolution) upstream of named river gauging stations. The three italicised catchments were used here for sensitivity analyses. Meteorology data for all six were used to determine relative humidity–temperature relationships

Table 7. Catchments used in sensitivity analysis.

	Woody cover	Mean annual precipitation	Muttama Creek
	%	1950–2010 (mm/year)	
Muttama Creek	69	1220	427
Goobarragandra River	53	1052	290
Adelong Creek	27	677	62

Table 8. Meteorological drivers used in the sensitivity analysis

Driver	Perturbation	Measure of flux sensitivity
Temperature	+1 ℃	Relative change in flux per ℃
Precipitation	–10%	Amplification (relative change in flux/relative change in driver)
Solar radiation	–10%	Amplification factor (relative change in flux/relative change in driver)
Wind speed	–10%	Amplification factor (relative change in flux/relative change in driver)
CO_2	10 ppm	Relative change in flux per ppm

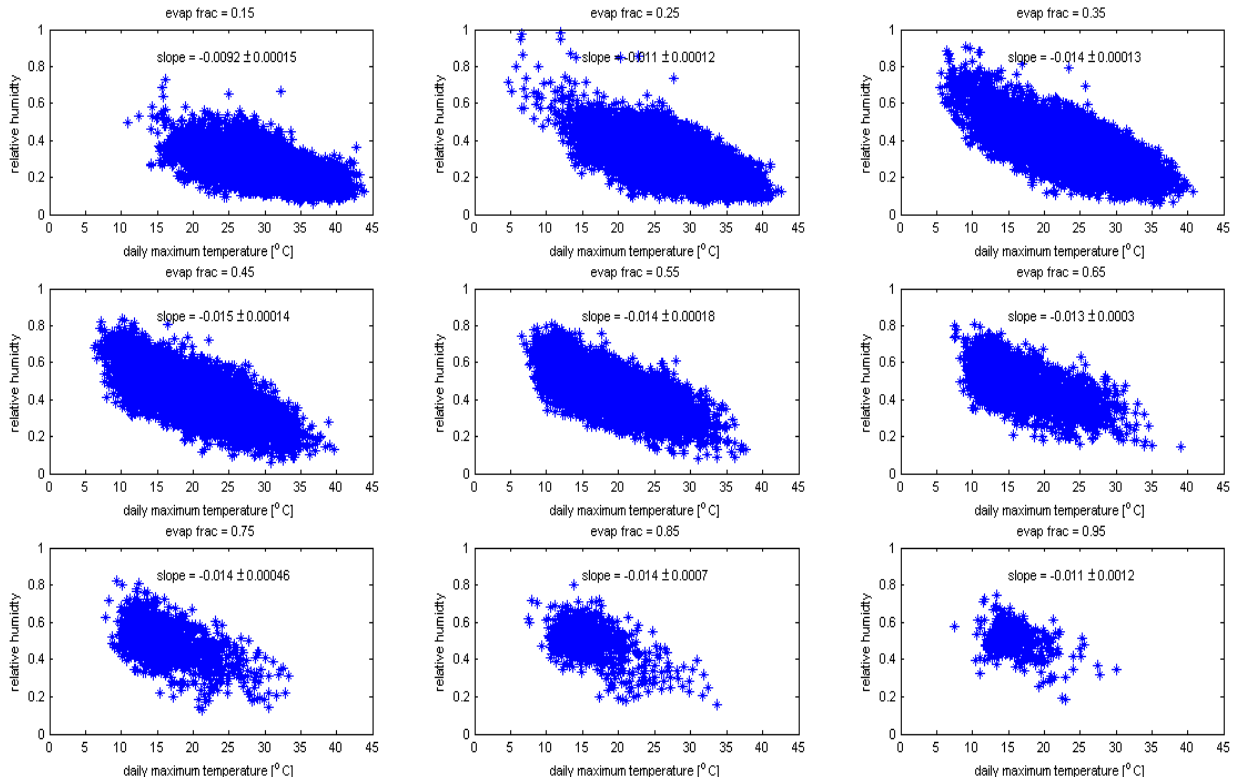

Figure 34. Scatter plots of relative humidity (derived from maximum daily temperature and daily 3:00pm vapour pressure) versus maximum daily temperature from six Murrumbidgee catchments (Adelong Creek, Goobarragandra River, Muttama Creek, Billabong Creek, Adjungbilly Creek and Tarcutta Creek) for 1950–2010. The data from all catchments have been combined and then sorted into nine bins according to evaporative fraction (centred on evaporative fractions of 0.15, 0.25, … 0.95). This bins correspond to increasing wetness as indicated by the evaporative fraction. Slopes pertain to linear regression lines (not plotted). The negative slopes quantify an empirical mean relationship between relative humidity and daily maximum temperature. In sensitivity tests of hydrometeorological responses to temperature perturbations, this relationship was used to quantify the concurrent perturbation in atmospheric water vapour that accompanies the temperature perturbation

Modelled and measured time series of annual streamflow (1955–2010) for the three catchments are shown in Figure 35. The model has not been tuned, yet nonetheless captures 77 to 91 percent of variance in the data producing linear regression slopes of 1.0 to 1.2, indicating that it is a credible tool for analysing the meteorological sensitivity of discharge at annual to decadal timescales.

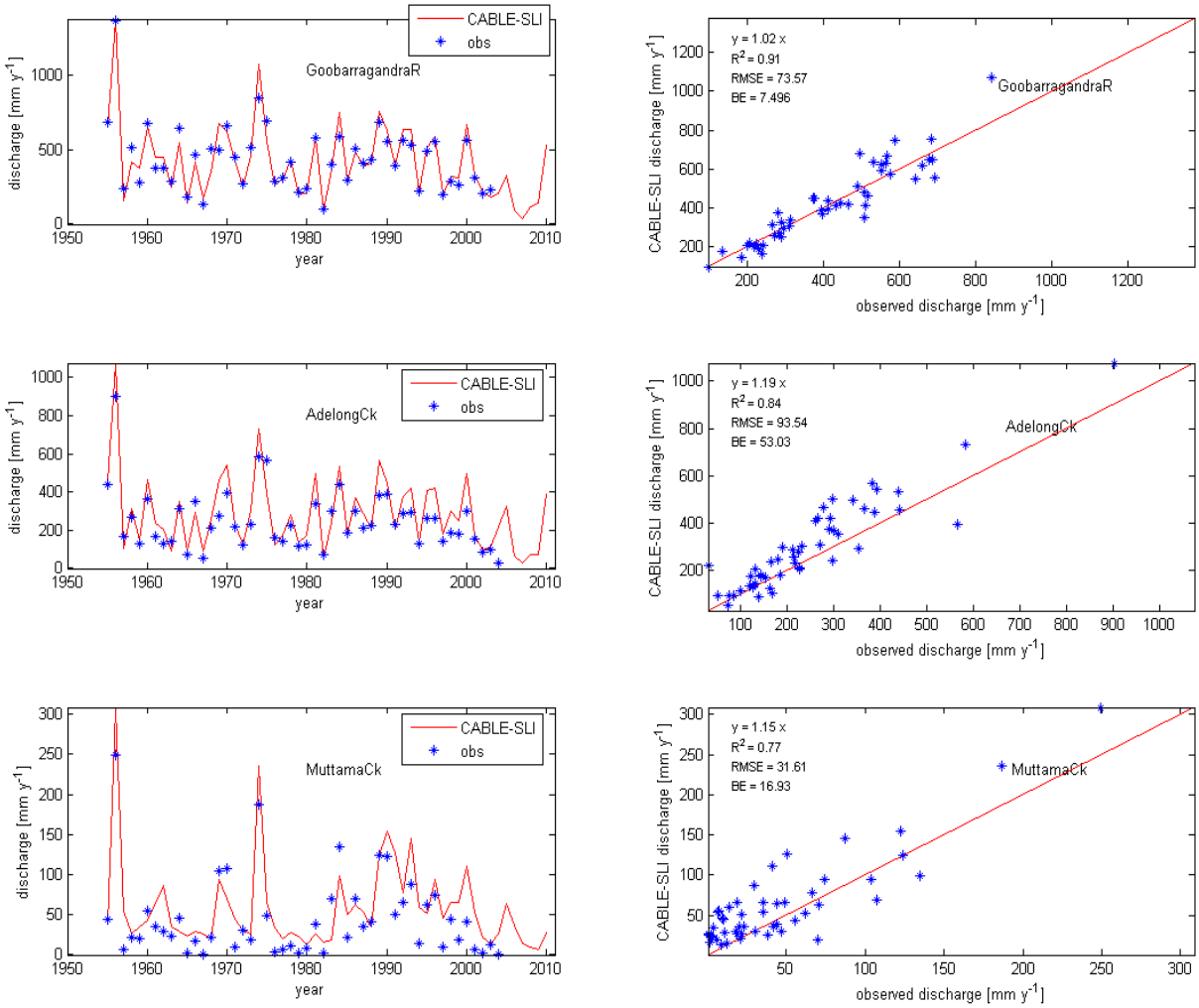

Figure 35. Annual discharge (modelled and observed) for three catchments.

Figure 36 shows the sensitivity of each of four water balance components (discharge (FWDis); soil evaporation (FWSoil); transpiration (FWTra); and wet canopy evaporation (FWwc)) to each of the five drivers that may influence the water balance for the three catchments. Results here are derived from long-term (1950–2010) mean fluxes (Note again here that sensitivities are expressed as amplification factors for precipitation, solar radiation and windspeed, and as relative change per °C for temperature and per ppm for CO_2). We see that discharge is the most sensitive of all the fluxes here, and that Muttama Creek, the driest catchment, is generally much more sensitive than the other two. Key results for each driver are:

- temperature
- Sensitivity ranges from –4 to –9 percent per °C across the three catchments.
- Results are strongly dependent on the concurrent water vapour perturbation, as indicated by the error bars, corresponding to the range of sensitivities corresponding to a range of (relative humidity verus temperature) slopes from –0.018 $°C^{-1}$ to –0.012 $°C^{-1}$.
- Soil evaporation and transpiration increase with increasing temperature due to increased evaporative demand.
- Wet canopy evaporation decreases with temperature due to enhanced dew formation (attributable to the increased slope of the saturated vapour pressure curve).
- precipitation

- The amplification for discharge is around 3 for the wetter catchments but much higher at 8 for Muttama Creek.
- solar radiation
- The amplification for discharge ranges from –0.7 to –0.2 and arises from the positive amplification of evaporation, particularly the transpiration component.
- wind speed
- The amplification for discharge ranges from –0.7 to –0.2 (similar to the solar radiation case) and is also driven largely by the positive amplification of transpiration.
- CO_2
- CO_2 amplifies discharge by 0.5 to 2 percent per ppm CO_2, which is the result of decreased stomatal conductance and hence decreased transpiration as CO_2 increases.

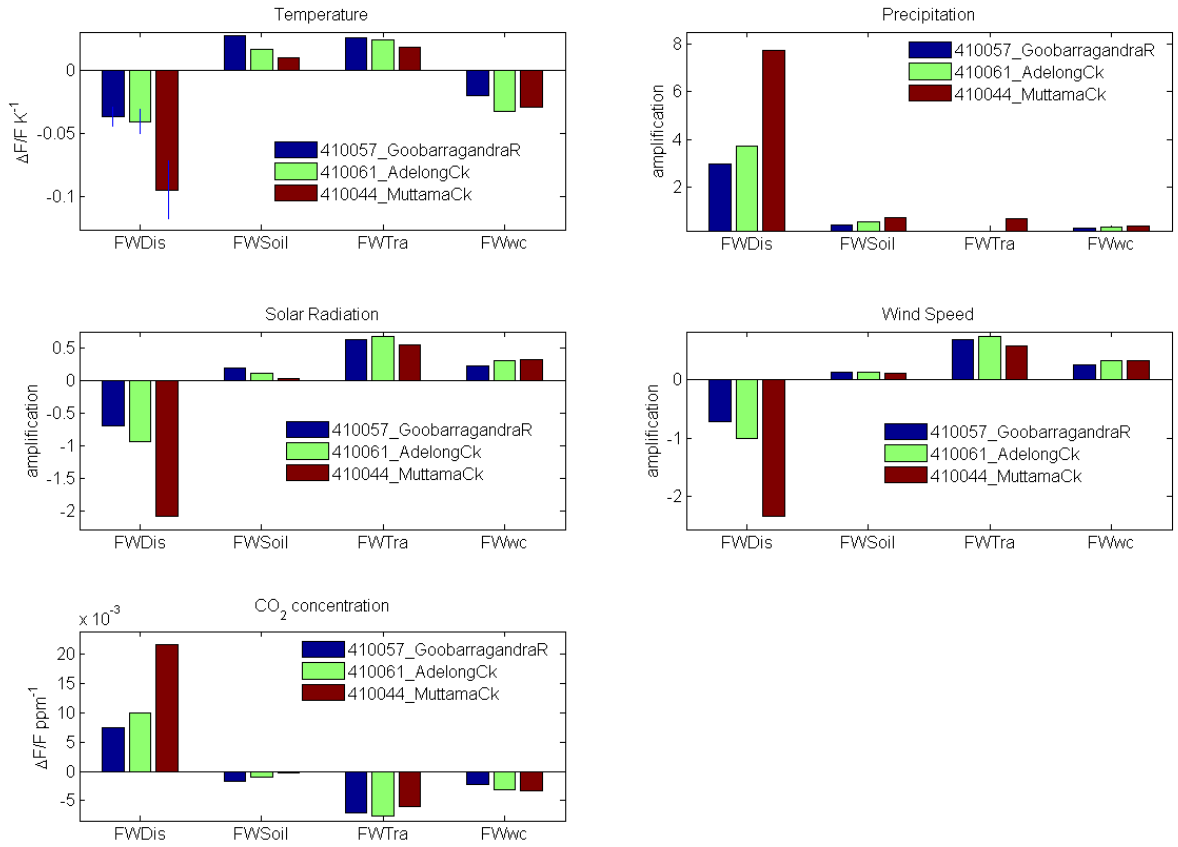

Figure 36. Sensitivity of long-term mean (1950–2010) water balance components (discharge (FWDis), soil evaporation (FWSoil), transpiration (FWTra), and wet canopy evaporation (FWwc)) to meteorological drivers for three catchments.

Figure 37 shows time series of the sensitivities of annual discharge to the meteorological drivers for the three catchments. The sensitivities are not only highly variable between catchments, but also vary significantly from year to year, with higher (absolute) values occurring in years of low discharge. The reasons for this temporal variability in sensitivity are closely related to the spatial variability in the sensitivity of mean discharge to rainfall, which ranges from 3 to 8 with increasing catchment dryness as noted above (Figure 36, upper left panel).

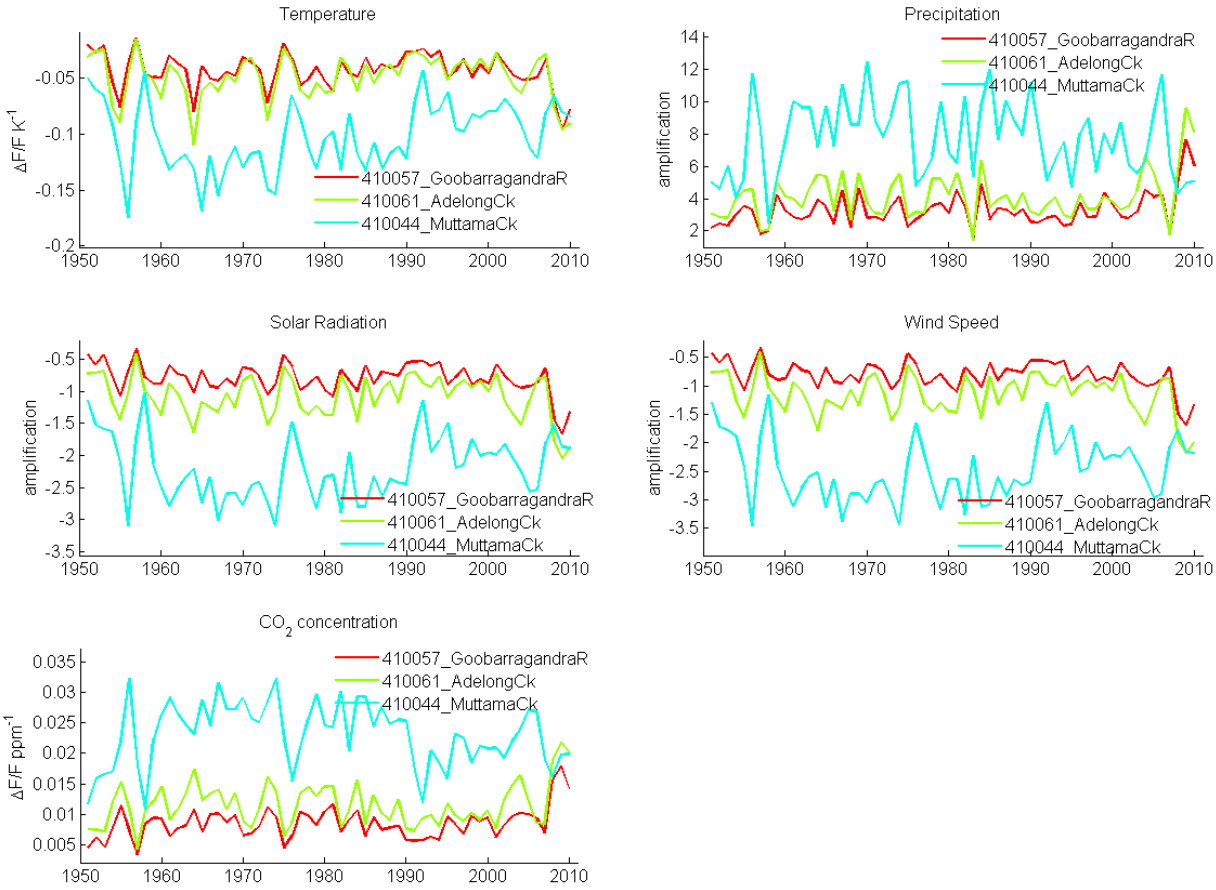

Figure 37. Sensitivity of annual discharge to meteorological drivers.

Conclusions

Work in Project 1.2 has delivered results in three areas.

Develop, maintain and document the Australian Water Availability Project gridded hydrometeorological data

Release of research-quality monthly historical time series and all spatial parameter datasets, for the continent and a SEACI subset, along with area-average AWAP time series for the 245 AWRC drainage basins and major drainage divisions, available to SEACI partners.

Improved metadata.

Successful AWAP validation against GRACE gravimetric data (independent work).

Model statistical climate–water relationships using Australian Water Availability Project gridded data

In work by Kirien Whan, CART and random forest analyses were used to classify spring whole-MDB hydrometeorological state (the whole-MDB average rainfall and upper-layer soil moisture in September through November against the Indo-Pacific sea-surface temperatures up to 6 months previously – that is, whether sea-surface temperatures provide predictive skill at lead times of up to 6 months. Preliminary results indicate significant predictive skill (around 70 percent) for whole-MDB spring rainfall at lead times of up to 6 months. These skills are far higher than those achieved with linear models.

Understand the relationship between hydrological drivers and responses

This work now uses a modelling framework called CableDyn. This framework is based on AWAP but replaces the simple water balance model for AWAP (WaterDyn) with the model CABLE-SLI-CASACNP, developed from CABLE the CSIRO land surface model developed over many years. Compared to WaterDyn, CABLE-SLI-CASACNP includes far more sophisticated descriptions of critical biological processes, such as the effect of water stress, temperature changes and CO_2 changes on evapotranspiration.

Without tuning, CABLE-SLI-CASACNP performs as well as or better than WaterDyn for predicting local discharge at annual to decadal time scales.

In three test catchments, CABLE-SLI-CASACNP has been used to analyse the sensitivity of water balance responses (local discharge, transpiration, soil evaporation and wet canopy evaporation) to perturbations in hydrometeorological drivers.

The sensitivity of local discharge to temperature ranges from –4 to –9 percent per °C across the three catchments; results are strongly dependent on the concurrent water vapour perturbation.

Sensitivity of local discharge to precipitation is consistent with an amplification factor (proportional response/proportional forcing perturbation) of 3 for the wetter catchments to 8 for the drier catchments.

Rising CO_2 increases discharge by 0.5 to 2 percent per ppm CO_2, the result of decreased stomatal conductance and hence decreased transpiration as CO_2 increases. This is a significant effect.

Work next year will focus on the third area.

Links to other projects

The Project 1.2 component *Understanding the relationship between hydrological drivers and responses* has natural linkages with Project 2.2. Significant advancement of this discussion has been somewhat dependent on the progress of the CableDyn model upgrade, which is now largely complete. Discussions with Project 2.2 ensured coordination of material for this report and it is anticipated that closer collaboration in the coming year will assist towards resolving the question of attribution.

CHAPTER 4: PROJECT 2.1

Climate change projections

Dewi Kirono, Jin Teng, David Kent, Francis Chiew, Marie Ekstrom and David Post (CSIRO)

Bertrand Timbal and Yang Wang (BoM)

Abstract

The research in Project 2.1 builds on results from Phase 1 of SEACI to improve global climate model assessment and selection for hydrological applications and to investigate and account for the relative uncertainties in the different components for modelling the impact of climate change on runoff.

There were two activities in 2010/11. Activity 1: (i) assessed the ability of the global climate models from the Intergovernmental Panel on Climate Change Fourth Assessment Report to represent a range of selected climate variables and large-scale climate drivers using a consistent approach so that the results can be compared; (ii) developed a selection framework to identify 'better' performing models that can potentially be used for downscaling modelling to obtain future climate series suitable to drive hydrological models; and (iii) explored the implications of weighting and/or selecting models for future rainfall projections for SEA. Research in Activity 1 showed that:

- According to the M-statistic of Watterson (2009) skill-score: (i) all 24 global climate models can reasonably represent the spatial distribution of the mean and coefficient of variations of examined climate variables (mean sea level pressure, rainfall, temperature and potential evapotranspiration, but the models are not as goods in representing the spatial distribution of the trend; (ii) some models are consistently good across all examined large-scale climate drivers and rainfall inter-annual variability, but many models are not.
- Based on the initial assessment results and the framework developed here, the following eight selected models can be considered as the 'better' performing ones and may be used for future downscaling modelling:
    - first selection: CSIRO-MK3.0, MIROC3.2-medres
    - second selection: CGCM-T47, CSIRO-MK3.5, IPSL-CM4, INM-CM3.0, MRI-CGCM2.3, CNRM-CM3.
- The annual rainfall projections for the weighted global climate models (based on the M-statistic of rainfall) are relatively similar to the median projections of the unweighted 24 models. However, the median annual rainfall projections from the eight selected models are drier than the median of all 24 models. The range (10^{th} to 90^{th} percentile) of the annual rainfall projections from the eight selected models is no smaller than that from all 24 models. For winter and spring, however, the range of uncertainty from the eight selected models is smaller than that from all 24 models.
- Activity 2 assessed the relative merits of different downscaling methods and the relative uncertainties of various components in modelling the impact of climate change on runoff. Three components that were examined were global climate model projections, downscaling methods and hydrological modelling. In 2010/11:
- Initial steps were taken to set up the Weather Research Forecasting (WRF) system as a dynamical downscaling tool to complement existing downscaling methodologies within SEACI. Since the system has multiple options for the physics parameterisations, it is necessary to choose between many of these parameterisations. A 36-member physics parameter ensemble (PPE) was

investigated, and two members of the ensemble were identified as better performers for future downscaling work.

- Analyses of hydrological modelling suggested that at least 10 years of streamflow data are needed for the model calibration to represent hydroclimate variability adequately, and that calibrating hydrological models against the more recent data gives better streamflow predictions.
- Analyses on the use of the perturbation downscaling method (a combination of pattern and daily scaling methods) showed that it should be used cautiously for global warming scenarios higher than 2.0 °C (in its current derivation). The assessment showed that the analogue method underestimates rainfall and therefore the modelled runoff. The use of an inflation factor to scale all the daily rainfalls to match the observed 1961-2000 seasonal means ('match-mean') produced rainfall and modelled runoff that are similar to the observed annual means. However, there are differences in the daily analogue and observed rainfall distribution, sufficient to result in modelled daily and mean runoffs that are different to the values modelled using observed rainfall. The range in the modelled change in future runoff (for the period 2046-2065 relative to 1960-2000) modelled using rainfall from the analogue downscaling informed by the 11 global climate models (i.e. CGCM3.1(T47), CNRM-CM3, CSIRO-MK3.0, CSIRO-MK3.5, GFDL-CM2.0, GFDL-CM2.1, GISS-ER, IPSL-CM4, MIROC3.2-medres, MPI-ECHAM5, MRI-CGCM2.3.2) (after applying 'match-mean' inflation factor) is smaller than the range of modelled runoff using rainfall from the daily scaling perturbation method. It appears that the analogue method moderates the climate-change impact on rainfall and runoff results, and this issue needs to be investigated further, particularly when the large-scale rainfall is often the major predictor in the analogue method. The analogue method can be useful for hydrological-impact studies over large regions. However, more research is required for the analogue method and the necessary corrections to produce daily rainfalls that are sufficiently similar to the observed daily rainfall for direct use in hydrological models. In climate change impact simulations informed by global climate models, there is also a need to improve the bias correction of predictor variables from the models.

Background

The main goal of the research in Theme 2 is to improve hydroclimate projections for SEA. The research in Theme 2 is at the climate–water interface, and its link to climate science and hydrological modelling science is shown schematically in Figure 38.

Hydrological models are generally tailored for specific applications, and are developed and calibrated using local data. There are two main steps involved in estimating the impact of climate on future runoff characteristics and water availability. The first step uses global climate model projections and downscaling models to obtain future catchment-scale climate series to drive hydrological models. Project 2.1 carries out research in this area. The second step involves driving hydrological models with future climate series to estimate future runoff. This may require adapting models to account for changes in the rainfall–temperature–runoff relationship and changes in the dominant hydrological processes in a drier, warmer environment with higher levels of carbon dioxide (CO_2). Project 2.2 carries out research in this area. Both projects in Theme 2 are closely related to – and use information from – the projects in Theme 1.

The research in Project 2.1 builds on results from Phase 1 of SEACI to improve the assessment and selection of global climate models for hydrological applications and to investigate and account for the relative uncertainties in the different components for modelling the impact of climate change on runoff. This will lead to more reliable and updated future catchment-scale climate series to drive hydrological models in climate change impact studies.

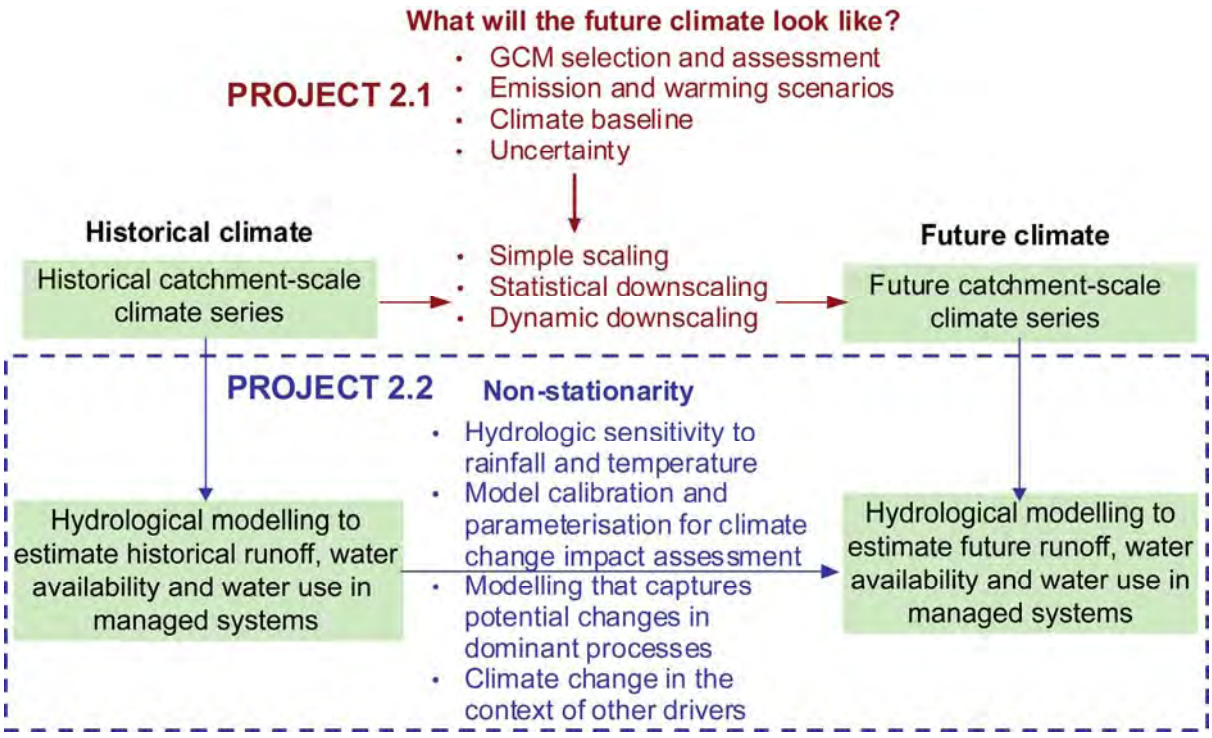

Figure 38. Schematic representation of the approach to modelling the impact of climate change on runoff.

Objectives

Assessment of global climate models and the implications for rainfall projections in the SEACI region

Assess the ability of global climate models of the Intergovernmental Panel on Climate Change Fourth Assessment Report to reproduce observed climate variables and important atmospheric–oceanic drivers of rainfall in SEA (as identified in Theme 1). Explore the implications of weighting and/or selecting global climate models in rainfall projections.

Investigation of uncertainty in climate–water projections

Assess the relative uncertainties in the three main components in modelling the impact of climate change on future runoff, namely global climate model projections, downscaling methods and hydrological modelling.

Methods

Assessment of global climate models and the implications for rainfall projections in the SEACI region

Twenty-four global climate models in the IPCC database were assessed. Researchers examined the ability of these models to reproduce observed seasonal climate variables and important atmospheric–oceanic drivers of rainfall in SEA (as identified in Theme 1).

- The climate variables that were examined included mean sea-level pressure, air temperature, rainfall, and estimated potential evapotranspiration. The sea-level pressure was assessed over Australia, while the other variables were each assessed over the Murray–Darling Basin and over each of the three climate regions within the SEACI region as defined in Timbal and Fernandez (2009), i.e. the northern Murray–Darling Basin, eastern sea-board and south-west of eastern Australia. The ability of each model to represent the spatial pattern of observed monthly, seasonal and annual mean of climatology, coefficient of variability and long-term trend was quantified using the M-statistic of Watterson (2008) for three different periods (1961–1990, 1975–2004 and 1996–2007) for mean sea-level pressure, air temperature, and potential evapotranspiration, and for four different periods for rainfall (1900–2000, 1961–1990, 1975–2004 and 1996–2007). As a result, for rainfall as an example, there are 816 metrics of assessment (four regions, 17 temporal scales, three characteristics and four time periods) for each of the global models. All the results are available for researchers who wish to select/weight GCMs using their preferred considerations and/or thresholds.

- Inter-annual rainfall variability is a characteristic that is important for hydrological impact studies. The representation of this characteristic was assessed by comparing the areal monthly mean of modelled SEA rainfall to the observed rainfall. The extent of the SEA region follows that used by Timbal (2010). Researchers assessed the ability of each model in representing the inter-annual variability with respect to the mean, coefficient of variability and extremes (10^{th} and 90^{th} percentile), as quantified by the correlation coefficient between the model and the observations.

- One of the atmospheric–oceanic characteristics that was assessed in detail is the sub-tropical ridge (STR). The STR is one of the key drivers of rainfall in SEA (Drosdowksy, 2005, Timbal et al., 2010). The mean state and variability of STR-I and STR-P was diagnosed and compared to observations, and the best-performing global climate models were identified using four tests. The methods are discussed in detail in Kent et al. (2011). Current research is assessing the ability of models to represent other drivers (El Niño – Southern Oscillation, Indian Ocean Dipole and Southern Annular Mode) and their teleconnections with rainfall in SEA; this work is expected to be finished in the next year. In 2010/11, an independent study by Irving et al. (2010) assessed the ability of global models to represent ENSO in the context of climate projections over the Pacific region. In addition, Fredericksen et al. (2011) assessed their ability to represent the changes in the Southern Hemisphere weather system in the context of attribution studies of rainfall changes over southern Australia. Results from these two independent studies have been synthesised to complement results from this project.

- In this project, researchers then developed a framework to identify 'better' performing global models that may be used for downscaling modelling (second activity). The first step was to test applicability, i.e. to check whether the global climate models provides daily data required by the daily scaling and analogue downscaling techniques that are applied in Activity 2. The second step was to test reliability based on the results of the above assessment:

- The global model was considered to represent climate variables well if its multi-metric mean of M-statistic is greater than 0.5 for each of the climate variables (sea-level pressure, air temperature, rainfall, and estimated potential evapotranspiration.

- The global model was considered to have a good representation of:
    - STR if it passes three out of four tests as described in Kent et al. (2011)
    - ENSO if it is within the top 75 percent among the 24 global climate models as described in Irving et al. (2010)
    - changes in the Southern Hemisphere weather system if it is strongly correlated to observed changes (defined as having a correlation coefficient greater than 0.5) in baroclinic instability and Phillips criterion as described in Fredericksen et al. (2011).
- The global model was considered to represent inter-annual variability well if it has positive significant correlation coefficient with the observed monthly climatology, coefficient of variability and extremes (10^{th} to 90^{th} percentiles).

The final step was to select the global climate models that pass three to four of the above five tests (i.e. climate variables, STR, ENSO, changes in Southern Hemisphere weather system and inter-annual rainfall variability). This threshold was chosen arbitrarily, but to ensure an adequate number (i.e. more than one) model was selected. This framework has been defined for the needs of this project; other researchers may wish to select models differently but still use the quantitative assessment results from this project. More detailed description of this framework is available in Kirono et al (2011). It is worth noting that the requirement for models to have the required data for Analogue downscaling techniques and to have potential evapotranspiration data may lead to a number of good GCMs being eliminated by the selection process. The researchers therefore also identified models that have the potential to be used in the future but which currently do not have the required data (as depicted in Table 9).

Investigation of uncertainty in climate–water projections

Using limited data in 2009/10, research in Project 2.1 suggested that: (i) the largest uncertainty in projecting future water availability comes from global climate model projections; (ii) the variability in simulations using different downscaling methods is about half the range of variability associated with future projections from the different global models; and (iii) the variability in runoff simulations using different lumped conceptual rainfall-runoff models is small compared to that associated with the global climate model projections and downscaling methods (Chiew et al., 2010; Teng et al., 2011a). The research in Project 2.1.-Activity 1 is focused on improving the interpretation of model projections, which is likely to reduce the range of global model projections used for modelling of the impact of climate change on future runoff. However, the uncertainty in the hydrological modelling is likely to be higher when non-stationarity in dominant hydroclimate processes is accounted for. This is largely investigated in Project 2.2. In addition, researchers investigated whether hydrological models should be calibrated using more recent data or using long historical records to account for decadal hydroclimate variability and a changing climate.

Building on previous research and working closely with Activity 1 and Project 2.2, the focus for Activity 2 in 2010/11 was to better understand and quantify the uncertainties associated with the different downscaling methods. The runoff projections obtained from different downscaling methods were compared: (i) to assess the suitability of these methods for hydroclimate projections across SEA; and (ii) to investigate the uncertainty sourced from downscaling methods. These results – in combination with those from the first activity and Project 2.2 – will lead to updated and improved projections of future runoff across SEA.

Initially, the hydroclimate projections were generated using global climate model rainfall downscaled to 0.05° grids using the perturbation method (a combination of pattern and daily scaling methods). The 114 years of daily future runoff projections were generated for four global warming scenarios:

- 1.0 °C and 1.3 °C, which represent median and high global warming scenarios for 2030, respectively
- 2.0 °C and 3.3 °C, which represent median and high global warming scenarios for 2060, respectively.

An analogue downscaling method developed by the Australian Bureau of Meteorology was also assessed for its suitability in studying the impact of climate change on runoff over very large regions. The analogue model defines a daily weather type by relating large-scale atmospheric predictors to observed rainfall. This

method has been used to successfully downscale point and gridded rainfall across Australia and to study rainfall trends across south-east and south-west Australia. Using this analogue method, three time slices of global climate model daily rainfall – one historical (1961–2000) and two future (2046–2065, 2081–2100) – were downscaled from 11 models to 0.05° (~5 km) grid cells to cover SEA. The downscaled gridded rainfall was used to drive two widely used hydrological models (Sacramento (Burnash et al., 1973) and SIMHYD (Chiew et al., 2002)) and results were compared with the runoff modelled using observed and pattern scaled rainfall.

To complement existing downscaling methods within SEACI, initial steps were taken in 2010/11 to set up the WRF system as a dynamical downscaling tool. Researchers investigated which options for key physics parameter schemes (e.g. planetary boundary scheme, cumulus scheme, micro-physics scheme and radiation scheme) perform optimally in terms of capturing observed rainfall, temperature and mass-field for SEA. A 36-member PPE was run for four case studies representing four different rainfall events, each centred in a 2-week window. Experiments were delayed due to a model version upgrade which warranted a complete re-run of experiments with the new version. Metrics based on mean sea-level pressure, minimum surface temperature, maximum surface temperature, rainfall and wind speed were used to identify the ensemble member with the best performance across the four case studies. Four different ranking methodologies were used to reflect different priorities when ranking the data.

Results

Assessment of global climate models and the implications for rainfall projections in the SEACI region

Figure 39 shows the observed and modelled spatial distribution of annual rainfall and potential evapotranspiration (only for the global climate models which have evapotranspiration data). Some models can reproduce the spatial distribution of the mean annual rainfall, and some models tend to be much drier or wetter than the observations. Some models can reproduce the spatial pattern of the annual coefficient of variability, although these models tend to underestimate the observed values. The observed linear trends are not very well reproduced by most models. All of these comments also apply to potential evapotranspiration. The ability of each model to represent the spatial distribution of each variable was quantified using the M-statistic of Watterson (2008) as summarised in Figure 40. Therefore, the M-statistic for each of the assessment metrics, for each climate variable, for each of the 24 global models are available and multi-metrics-mean of M-statistic for each of the climate variables are summarised in Table 9. Some findings include the following:

- As shown in Figure 40 and Figure 41, overall all 24 global climate models represent climate variables well over the MDB. Mean climatology is best represented and long-term trend is least well represented. This finding also applies for all other regions (e.g. the eastern sea-board) (not shown here).
- For the mean and the coefficient of variability, ranges of the M-statistic are similar regardless of the time period (Figure 41). For the rainfall trend, the global models represent the rainfall trend in the recent period (1996–2007) better than in the other periods. This is in regard not only to the MDB (as shown in Figure 41) but also for other regions (not shown here).
- For rainfall, the M-statistics for the MDB have a strong positive correlation to those for other regions (northern Murray–Darling Basin, eastern sea-board and south-west of eastern Australia; not shown here) suggesting that assessment over the MDB is representative of assessments over different climate regions within the SEACI region.

With regard to the inter-annual rainfall variability, Figure 42 shows the observed and modelled values for monthly mean, coefficient of variability and extremes (10^{th} to 90^{th} percentiles) over the SEA region. Qualitatively, this Figure suggests that some models can reproduce the inter-annual pattern of those three

characteristics but some models cannot. Quantitatively, Table 9 (coloumn 5-8) shows the correlation coefficient (R) between the model and the observations. Some models (e.g. CNRM-CM3 and ECHAM) perform consistently well (with R of > 0.6) while others (e.g. GFDL-CM2.1 and NCAR-PCM) do not perform consistently well (suggested by its positive and negative R) across all inter-annual characteristics that were examined.

In terms of climate drivers, some models consistently pass the test (therefore are good) across all the examined climate drivers but many models are not (Table 9). The former include CSIRO-MK3.0, MIROC3.2-medres, CSIRO-MK3.5, MIROC3.2-hires, NCAR-CCSM and ECHAM-MPI (see also Table 10). If we were to apply the selection framework described previously, the global climate models that may be considered for further downscaling modelling (in Activity 2) are as listed in Table 10.

Figure 43 shows projected changes in annual rainfall per degree of global warming based on different sets of experiments: all 24 global climate models (unweighted), all 24 models (weighted by the rainfall M-statistic summarised in Table 10) and eight selected models (listed under 'First selection' and 'Secondary selection' in Table 10). This figure shows that:

- The median projections suggest decreasing rainfall over most of the region, regardless of the set of experiments.
- The annual rainfall projections from the weighted models are relatively similar to the median projections from the unweighted 24 models, except in the north-east where the weighted models suggest a decrease in rainfall and in the north-west where the weighted models suggest a lesser degree of drying.
- The median annual rainfall projections from the eight selected models are drier than the median of all 24 models (unweighted). The range (10^{th} to 90^{th} percentile) of the annual rainfall projections from the eight selected models is no smaller than that from all 24 models. This is also the case for summer and autumn rainfall projections. For winter and spring, however, the projection from the eight selected models is drier (with smaller uncertainty) than that from all 24 models (not shown here). However, for the 10^{th} percentile range, the selected models suggest a larger degree of drying in comparison to the all 24 models.

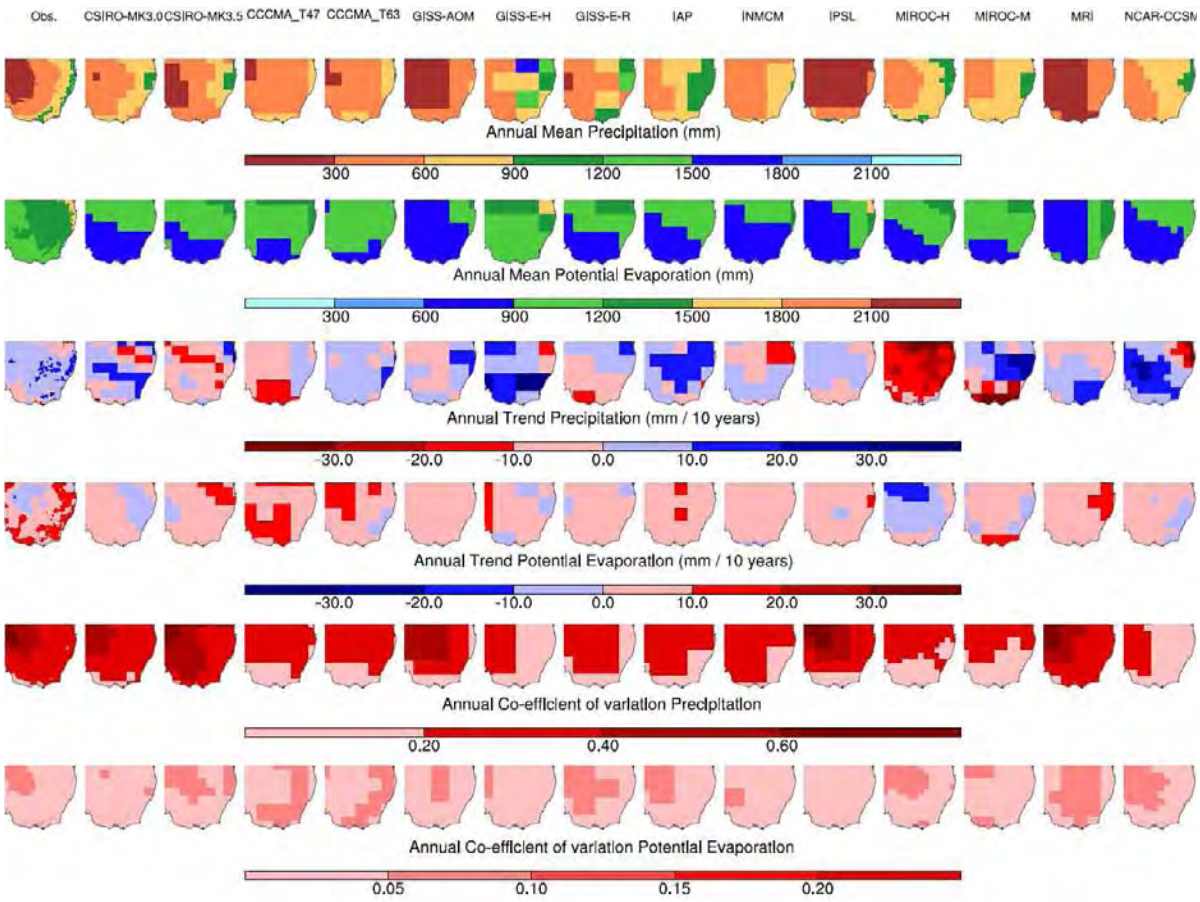

Figure 39. Spatial distribution of observed and modelled statistics of annual rainfall and potential evapotranspiration (PET) for 1951–2006. Each of these spatial distributions has been quantitatively assessed using the M-statistic of Watterson (2008)

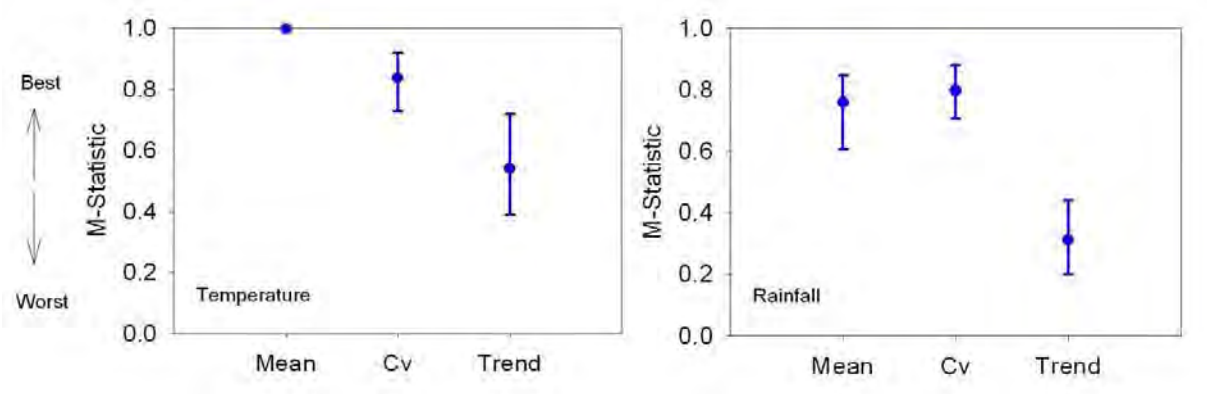

Figure 40. Overall performance, represented by the M-statistic of Watterson (2008), of 24 global climate models for annual temperature and annual rainfall measures over the Murray–Darling Basin. Results are indicated as box plots showing the median and 10th to 90th percentile of 24 models

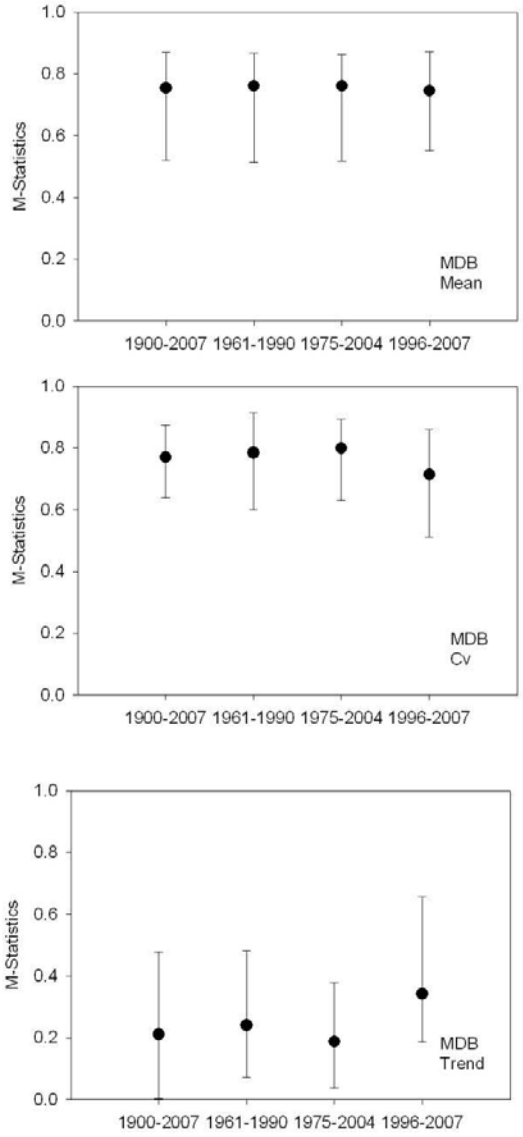

Figure 41. Overall performance, represented by the M-statistic of Watterson (2008), of all 24 global climate models for annual rainfall measures over the Murray–Darling Basin for different periods. Results are indicated as box plots showing the median and 10th to 90th percentile of 24 models

Table 9. Summary of the reliability of 24 global climate models

Model	Spatial Pattern of Climate Variables[1]				Temporal pattern or Interannual variability of rainfall[2]				Drivers for rainfall in SEACI region							
									Sub Tropical Ridge or STR[3]					ENSO Rank[4]	SH[4]	
	MSLP	P	T	PET	Mean	CV	90th perc.	10th perc.	Test 1	Test 2	Test 3		Test 4		300hPa zonal velocity	Phillips criterion
											I	P				
BCCR-BCM2.0	0.634	0.584	0.731	No data	0.877	0.963	0.552	0.826	PASS	PASS	PASS	FAIL	FAIL	13	FAIL	FAIL
CGCM3.1 (T47	0.626	0.652	0.780	0.446	0.626	0.971	0.213	0.816	FAIL	FAIL	PASS	FAIL	FAIL	8	PASS	FAIL
CGCM3.1 (T63)	0.633	0.648	0.784	0.526	0.879	0.938	0.761	0.873	FAIL	FAIL	PASS	FAIL	FAIL	4	PASS	FAIL
CNRM-CM3	0.630	0.586	0.788	No data	0.898	0.874	0.612	0.909	PASS	FAIL	FAIL	FAIL	FAIL	15	FAIL	FAIL
CSIRO-MK3.0	0.632	0.575	0.726	0.444	0.607	0.738	0.235	0.768	PASS	PASS	PASS	PASS	PASS	6	PASS	FAIL
CSIRO-MK3.5	0.635	0.530	0.741	0.458	-0.74	0.071	-0.789	-0.396	PASS	PASS	PASS	PASS	PASS	1	PASS	FAIL
ECHAM5/MPI-OM	0.630	0.558	0.710	No data	0.828	0.872	0.682	0.824	PASS	PASS	PASS	PASS	FAIL	9	FAIL	FAIL
MIUB-ECHO	0.631	0.572	0.754	No data	0.715	0.831	0.648	0.746	PASS	FAIL	PASS	PASS	PASS	19	NO DATA	NO DATA
IAP-FGOALS-g1.0	0.627	0.576	0.761	0.471	-0.203	0.770	-0.663	0.192	FAIL	PASS	PASS	FAIL	PASS	21	PASS	PASS
GFDL-CM2.0	0.626	0.529	0.727	No data	0.857	0.874	0.515	0.804	PASS	FAIL	PASS	FAIL	FAIL	3	FAIL	FAIL
GFDL-CM2.1	0.632	0.559	0.743	No data	-0.12	0.805	-0.429	0.726	PASS	PASS	PASS	FAIL	FAIL	5	FAIL	FAIL
GISS-AOM	0.602	0.505	0.757	0.461	0.975	0.850	0.820	0.922	PASS	FAIL	PASS	FAIL	PASS	24	FAIL	FAIL
GISS-EH	0.615	0.550	0.738	0.483	0.864	0.959	0.654	0.877	FAIL	FAIL	FAIL	FAIL	FAIL	22	NO DATA	NO DATA
GISS-ER	0.614	0.550	0.735	0.432	0.941	0.883	0.628	0.936	PASS	FAIL	PASS	PASS	PASS	23	PASS	PASS
INGV-SXG	0.613	0.583	0.757	No data	-0.498	0.479	-0.761	-0.210	Not assessed	Not assessed	Not assessed	Not assessed	Not assessed	10	PASS	FAIL
INM-CM3.0	0.628	0.569	0.771	0.4727	0.853	0.631	0.798	0.725	PASS	PASS	PASS	FAIL	FAIL	20	FAIL	FAIL
IPSL-CM4	0.619	0.487	0.797	0.472	0.804	0.706	0.636	0.837	FAIL	FAIL	PASS	FAIL	PASS	14	PASS	FAIL
MIROC3.2.(hires)	0.627	0.584	0.788	0.448	-0.027	0.901	-0.736	0.538	PASS	PASS	PASS	FAIL	PASS	11	PASS	PASS
MIROC3.2(medres)	0.620	0.557	0.739	0.485	-0.679	0.828	-0.791	-0.562	PASS	PASS	PASS	FAIL	PASS	17	PASS	PASS
MRI-CGCM2.3.2	0.637	0.485	0.799	0.452	-0.357	0.217	-0.370	-0.141	PASS	PASS	PASS	FAIL	PASS	2	FAIL	FAIL
NCAR-CCSM	0.644	0.579	0.748	0.443	-0.417	0.627	-0.660	0.041	PASS	PASS	PASS	PASS	PASS	18	FAIL	PASS
NCAR-PCM	0.633	0.564	0.738	0.637	0.716	0.834	0.380	0.786	PASS	PASS	PASS	FAIL	PASS	16	FAIL	FAIL
UKMO-HadCM3	0.633	0.589	0.727	No data	-0.212	0.653	-0.673	0.512	PASS	FAIL	FAIL	FAIL	PASS	7	FAIL	FAIL
UKMO-HadGEM1	0.639	0.602	0.752	No data	-0.803	0.825	-0.816	-0.457	PASS	PASS	FAIL	PASS	PASS	12	PASS	PASS

1)expresed as the average of multiple M-Stat from different matrix of assessment, i.e. (i) temporal unit (annual/Seasonal/Monthly); (ii) geographical unit (MDB/NMDB/ESB/SWEA, see Timbal and Fernandez, 2008 for the definition of the region) and (iii) for different measure (mean, coefficient of variability and linear long-term trends). See Watterson (2008) for M-Stat calculation. M-Stat of 1 represents a perfect match between the model and the observation spatial patterns. Assessment for MSLP is conducted over Australia region while for others they are conducted over the SEACI region (MDB, NMDB, ESB, SWEA). M-Stat of each matrix of assessments are available upon request.

2)expressed as linear correlation coefficient (*R*) between temporal pattern of the observed and the GCM. Positive values of 1 represents a perfect match between the temporal pattern of the model and the observation.

3) "FAIL/PASSES" indicates that the model fails/passes a test. Models that pass test 1 exhibit a good annual-cycle over a band that touches 140°E and is narrower than 40° in longitude. Test 2 examines the Euclidean distance from the observed annual cycle (pass if < 0.6, the distance of the NCEP cycle from the BoM cycle). Test 3 (STR-I left, STR-P right) fails if a models inter-annual variability does not resemble the observed, models must fail both STR-I and -P to fail test 3 overall. Test 4 assesses the spatial correlation of the modeled and observed STR intensity/rainfall correlation (pass if r > 0.3, significant at □=0.9). See Kent et al (2011) for more detail.

4) Rank of ENSO performance according to Irving et al (2011) who considered the strength and frequency of ENSO.

5) Performance in representing the changes in the Southern Hemisphere Weather System. The model is deemed to be good if the model has a strong correlation to observed changes (defined as correlation coefficient of >0.5), for at least the two periods being analysed, in either baroclinic instability or in Phillips criterion as described in Fredericksen et al (2011)

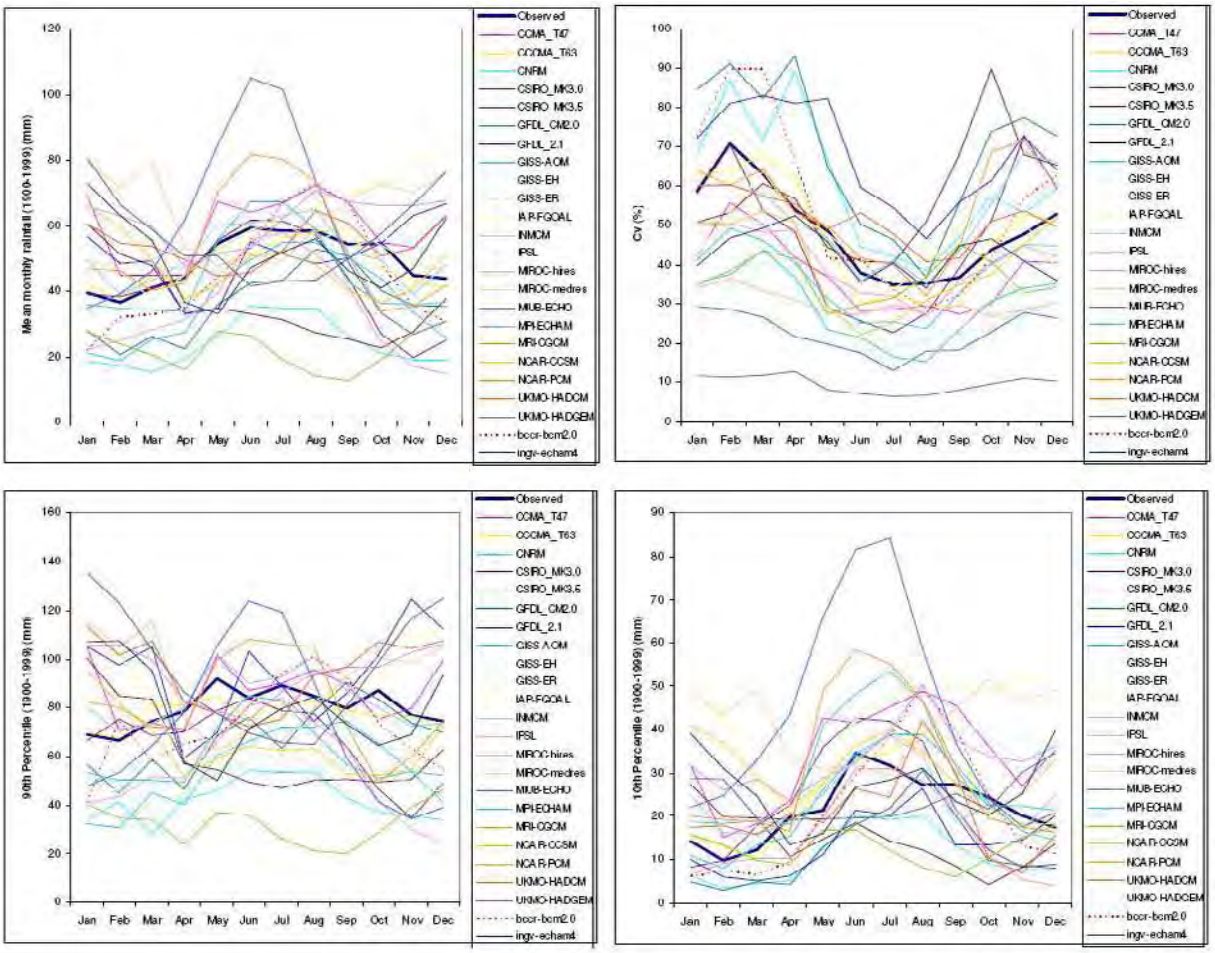

Figure 42. Observed and modelled inter-annual variability of rainfall characteristics (mean, coefficient of variability and extremes) in south-eastern Australia

Table 10. Selected global climate models, based on the selection framework developed here, that can be considered in future downscaling modelling in SEACI. Definition of a 'good' model is described in either the 'Method' section, in Table 9 or in Kirono et al. (2011).

Global climate model	Climate variables	Climate characteristics			Inter-annual rainfall variability
		STR	ENSO	SH	
First selection					
CSIRO-MK3.0	Good	Good	Good	Good	Good
MIROC3.2-medres	Good	Good	Good	Good	Good
Secondary selection					
CGCM-T47	Good	Poor	Good	Good	Good
CSIRO-MK3.5	Good	Good	Good	Good	Poor
IPSL-CM4	Good	Poor	Good	Good	Good
INM-CM3.0	Good	Good	Poor	Poor	Good
MRI-CGCM2.3	Good	Good	Good	Poor	Poor
CNRM-CM3	Good	Poor	Good	Poor	Good
Has potential					
MIROC3.2.-Hires (No analogue data)	Good	Good	Good	Good	Good
NCAR-CCSM (No analogue data)	Good	Good	Good	Good	Good
GFDL-CM2.0 (No PET)	Good	Good	Good	Poor	Good
ECHAM-MPI (No PET)	Good	Good	Good	Good	Poor
NCAR-PCM (No PET)	Good	Good	Good	Poor	Good
UKMO-HadCM3 (No PET)	Good	Good	Good	Poor	Good
GFDL-CM2.1 (No PET)	Good	Poor	Good	Poor	Good

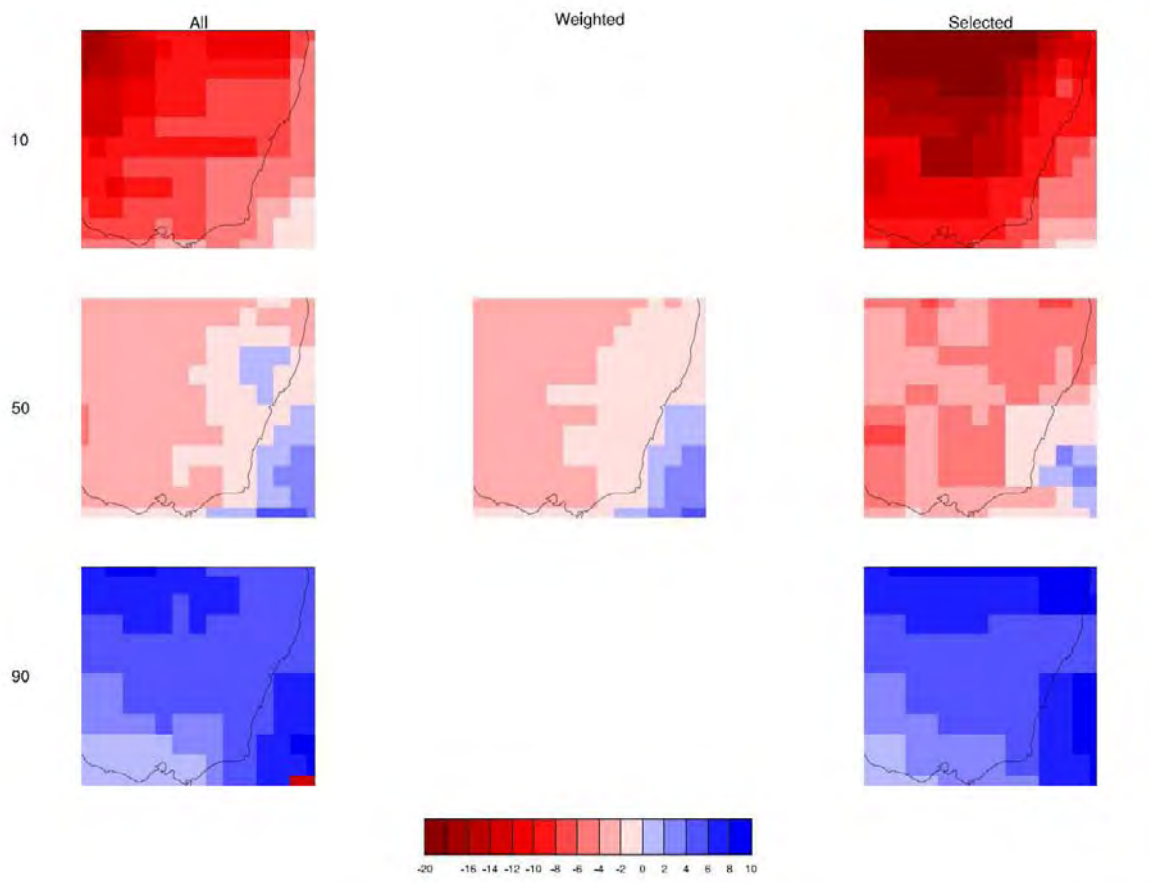

Figure 43. Spatial distribution of percentage changes in annual rainfall per degree global warming based on different sets of experiments: all 24 global climate models (unweighted), all 24 global climate models (weighted by the rainfall M-statistic summarised in Table 9), and eight selected global climate models (listed under 'First selection' and 'Secondary selection' in Table 10)

Investigation of uncertainty in climate–water projections

More detailed results from the WRF downscaling modelling can be found in Evans et al. (2011) and the summary showed that:

- Differences between the members of the PPE are much smaller for relatively weak weather systems than for strong or extreme weather systems
- No single member of the PPE performed best for all cases, all variables and all metrics, although some options clearly performed better than others when considering individual metrics
- Using the four ranking systems, two ensemble members could be identified as better performers in comparison to the total PPE. However, a possibly more robust way of using the rankings is to identify those combinations that should be avoided

Results from the investigation of uncertainty in hydrological modelling and downscaling methods include the following:

- At least 10 years of streamflow data are needed for the model calibration to represent hydroclimate variability adequately. The results also show that calibrating hydrological models against more recent data gives better streamflow predictions (Teng et al., 2011b). These modelling protocols lead to improved understanding of the modelled response of streamflow to climatic conditions.
- Results from analysing the runoff projections derived for the four global warming scenarios show that the perturbation method should be used cautiously for global warming scenarios higher than 2.0 °C. This is because the pattern scaling factors were obtained from SRES A1B global climate

model experiments up to 2100, with a simulated global-average temperature rise of less than 2.0 °C. Using this method for global warming greater than 2.0 °C extrapolates the pattern scaling regression outside the range of actual data and the confidence in the results are therefore lower. The vast majority of changes in runoff in response to increases in global average temperature are reasonably linear. However, small projected changes in rainfall may result in non-linear changes in runoff when global average temperature increases, particularly when rainfall increases in one season but decreases in another. At larger spatial scales, when averaging across a number of climate-model grid cells, differences in response between different grid cells mean that the overall regional runoff response to increases in global average temperature can be non-linear. The implications are that regional-scale analyses of changes in runoff due to climate change require rainfall-runoff models to be run for each projected increase in global average temperature and simple linear approximations can only be used with prior knowledge of the nature of the relationship (Post et al., 2011).

- The analogue downscaling method underestimates the variance and mean in rainfall. This underestimation is amplified in runoff. Maps in Figure 44 show that the historical runoff modelled using the rainfall downscaled from 11 global climate models is underestimated across the whole region for every model.
- A correction factor was applied to every 0.05° grid cell to improve the variance of rainfall ('variance-corrected'). However, the factor is not able to correct the mean seasonal rainfall and therefore the runoff is still underestimated. Figure 45 shows the comparison of summer (DJF) and winter (JJA) rainfall and runoff distributions for one grid cell (in Melbourne). The analogue rainfall was downscaled using NCEP/NCAR re-analysis datasets which were used in developing and validating the analogue method.
- Another set of correction factors was applied to force the analogue seasonal mean rainfall to match the observed values ('match mean'). The result for the same grid cell in Melbourne shows that the modelled runoff is overestimated (Figure 45). Table 11 summarises the mean annual and seasonal runoff averaged across the whole region modelled from observed rainfall and analogue rainfall with different inflation factors. The mean annual runoff, and to a lesser extent mean seasonal runoff, across the whole region is in agreement with the runoff modelled using observed rainfall (Figure 46, Table 11). However, the extreme high daily runoff (Q1, shown as daily runoff that is exceeded 1 percent of the time) and low-flow characteristic (low-flow days, shown as number of days per year when runoff is less than 0.1 mm) are not well captured using this downscaling method.
- The range in the modelled change in future runoff (for the period 2046-2065 relative to 1960-2000) modelled using rainfall from the analogue downscaling informed by the 11 global climate models (after applying 'match-mean' inflation factor) is somewhat smaller than the range of in modelled runoff using rainfall from the daily scaling perturbation method (Figure 47). It appears that the analogue method moderates the climate change impact on rainfall and runoff results and this issue needs to be investigated further, particularly when the large-scale rainfall is often the major predictor in the analogue method.

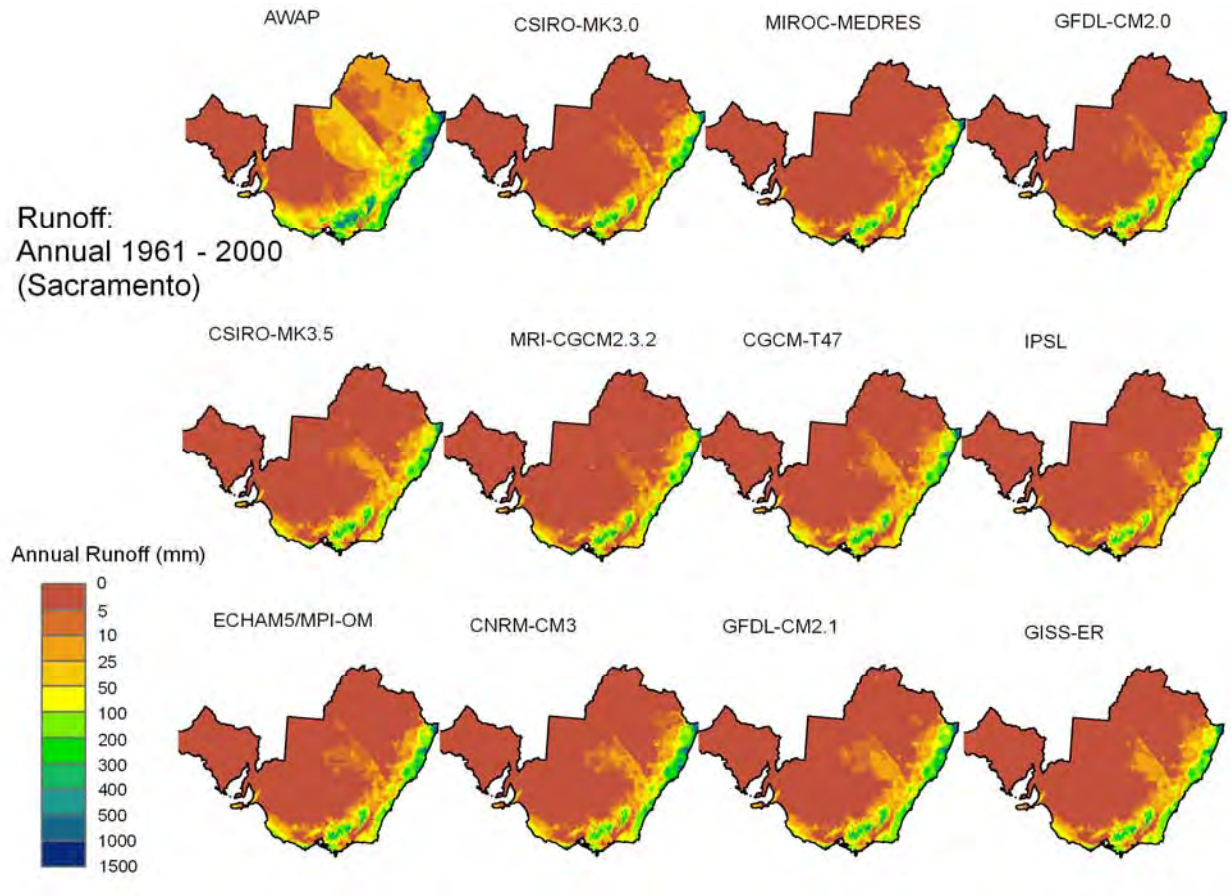

Figure 44. Spatial distribution of mean annual runoff modelled using observed rainfall (Australian Water Availability Project) and rainfall downscaled using the analogue method from 11 global climate models

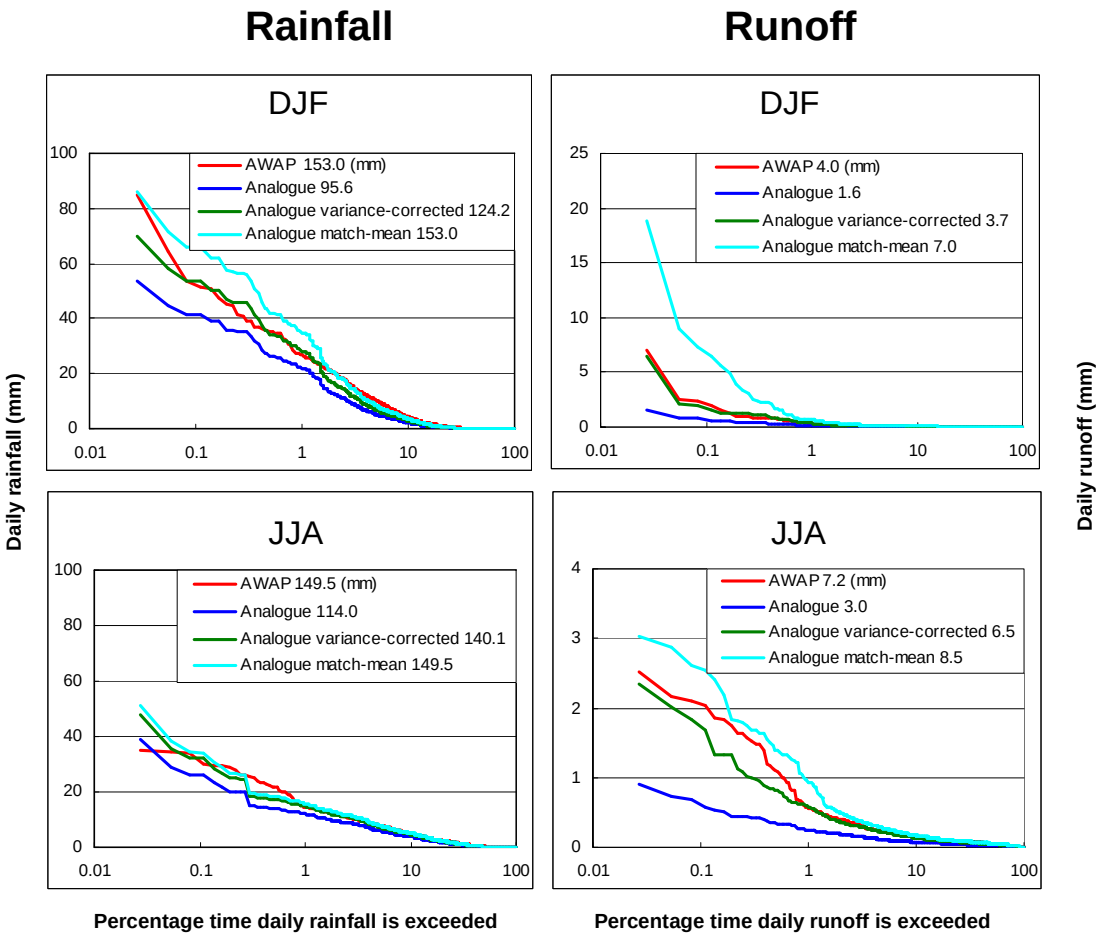

Figure 45. Plots showing rainfall and runoff distributions for one grid cell (in Melbourne) from observed, analogue downscaling, analogue downscaling with an inflation factor to improve the variance, and analogue downscaling with inflation factor to match the seasonal means. The seasonal mean rainfall and runoff are shown in the legend in each plot

Table 11. Mean annual and seasonal runoff averaged across the whole region modelled using different rainfall inputs

Method	Annual	December-February	March-April	June-August	September-November
AWAP	50.0	9.9	12.8	17.0	10.3
NNR 'variance-corrected'	38.4	7.4	9.4	13.7	7.8
NNR 'match mean'	51.8	10.1	12.4	18.3	10.9

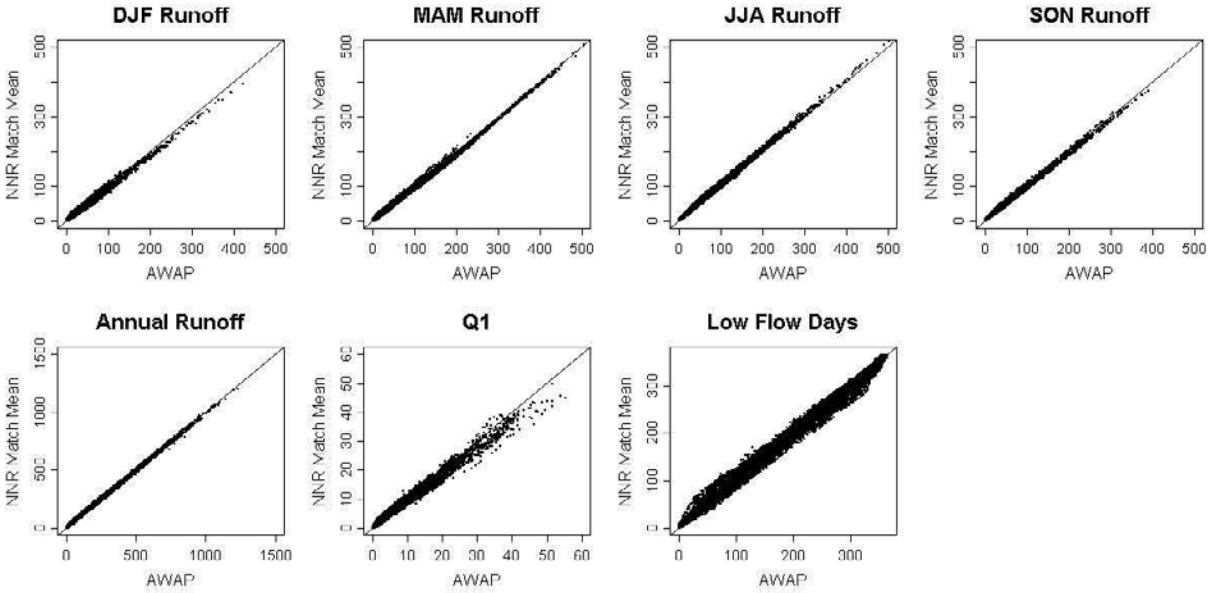

Figure 46. Scatter plots comparing runoff as represented by the Australian Water Availability Program and modelled using the analogue downscaling method for rainfall estimation with inflation factors (with regard to mean) for major runoff characteristics

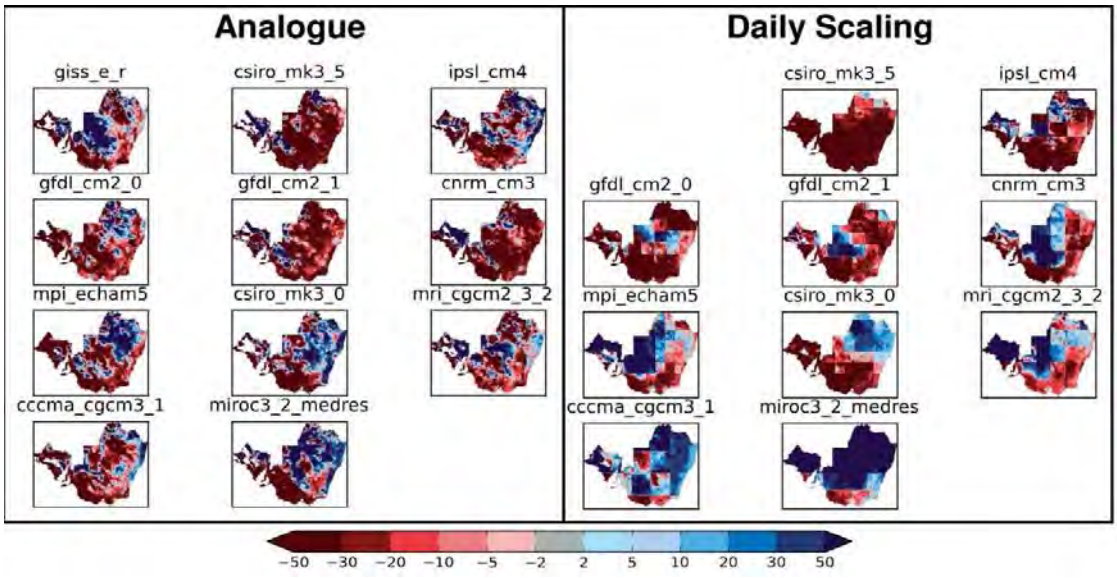

Figure 47. Change in future mean annual runoff for the period 2046-2065 relative to 1960-2000 as modelled using daily scaling and analogue downscaling methods informed by 11 global climate models

Conclusions

The research in Project 2.1 builds on results from Phase 1 of SEACI to improve the assessment of global climate models and selection for hydrological applications, and to investigate and account for the relative uncertainties in the different components for modelling the impact of climate change on runoff. This will lead to more reliable and updated future catchment-scale climate series to drive hydrological models in climate change impact studies, and will result in a reduction of associated uncertainties.

There were two activities in 2010/11. Activity 1 assessed the representation of the climate variables and large-scale drivers in GCMs from the IPCC AR4 and the implications for future rainfall projections for SEA. The study showed that:

- All 24 global climate models can generally represent the spatial pattern of climate variables (rainfall, temperature, potential evapotranspiration and mean sea level pressure). Some models are consistently good in representing all examined large-scale climate states and rainfall inter-annual variability, but many models are not.
- For future downscaling modelling, the following models are recommended:
    - 'first selection': CSIRO-MK3.0, MIROC3.2-medres
    - 'second selection': CGCM-T47, CSIRO-MK3.5, IPSL-CM4, INM-CM3.0, MRI-CGCM2.3, CNRM-CM3.
- When the skill scores on rainfall performance were used to weight each of global climate models the annual rainfall projections from the weighted models are relatively similar to the median projections from the unweighted 24 models. However, the median annual rainfall projections from the eight selected models are drier than the median of all 24 models. The range (10^{th} to 90^{th} percentile) of the annual rainfall projections from the eight selected models is no smaller than that of all 24 models. For winter and spring, however, the range of uncertainty from the eight selected models is smaller than that from all 24 models. This framework has been defined for the needs of this project; other researchers may wish to use a different approach in the selection of global climate models but still use the quantitative assessment results from this project.

The second activity assessed the relative merits of different downscaling methods and relative uncertainties of the three main components in estimating the impact of climate change on runoff (global climate models projections, downscaling methods and hydrological modelling). In 2010/11:

- A 36-member PPE was investigated, and two ensemble members were identified as better performers for future WRF downscaling work.
- At least 10 years of streamflow data were shown to be needed for the calibration of hydrological models to represent hydroclimate variability adequately. Calibrating hydrological models against more recent data gives better streamflow predictions.
- Analyses on the use of the perturbation downscaling method (a combination of pattern and daily scaling methods) showed that it should be used cautiously for global warming scenarios higher than 2.0 °C (in its current derivation).
- Historical and future climate series based on daily scaling and analogue downscaling methods have been completed (11 global climate models for 1960–2000, 2046–2065 and 2081–2100). Historical and future runoff series have also been derived using the Sacramento rainfall-runoff model with climate input from the analogue downscaling technique. The assessment showed that the analogue method underestimates rainfall and therefore the modelled runoff. The use of an inflation factor to scale all the daily rainfalls to match the observed 1961-2000 seasonal means ('match-mean') produced rainfall and modelled runoff that are similar to the observed annual means. However, there are differences in the daily analogue and observed rainfall distribution, sufficient to result in modelled daily and mean runoffs that are different to the values modelled using observed

rainfall. The range in the change in future runoff (for the period 2046-2065 relative to 1960-2000) modelled using rainfall from the analogue downscaling informed by the 11 global models (after applying 'match-mean' inflation factor) is somewhat smaller than the range of modelled runoff using rainfall from the daily scaling perturbation method. It appears that the analogue method moderates the climate change impact on rainfall and runoff results and this issue needs to be investigated further, particularly given that the large-scale rainfall is often the major predictor in the analogue method. The analogue method can be useful for hydrological impact studies over large regions. However, more research is required for the analogue method and the necessary corrections to produce daily rainfall estimates that are sufficiently similar to the observed daily rainfall for direct use in hydrological models. In climate change impact simulations informed by global climate models, there is also a need to improve the bias correction of predictor variables from the models.

Links to other projects

Project 2.1 is strongly linked to Theme 1 and Project 2.2. The global climate model assessment and selection is carried out in the context of the major drivers for rainfall in SEA identified in Theme 1 and the hydrological modelling in Project 2.2. The more accurate and updated future catchment-scale climate series (and associated uncertainties) from Project 2.1 will be used to drive the hydrological models in Project 2.2 and elsewhere to improve prediction of climate change impact on future runoff.

CHAPTER 5: PROJECT 2.2

Hydroclimate impacts for south-eastern Australia

Cuan Petheram, Nick Potter and Lu Zhang

Abstract

The research in Project 2.2 builds on results from Phase 1 of SEACI to enhance knowledge of climate–water processes in a changing climate, and to use this to improve models for predicting the impact of climate change on water availability.

There were two activities in Project 2.2 in 2010/11. Activity 1 undertook an empirical analysis on 34 unimpaired catchments in SEA that had more than 40 years of available data and less than 1 month of missing data during the recent drought (1997-2008). The median year of streamflow commencement was 1946. The first component of the first activity examined changes in the relationship between rainfall, temperature and streamflow and the sensitivity of streamflow to rainfall and temperature.

Firstly, regression analysis was used to test whether the annual rainfall–streamflow relationship during the drought was statistically different from the pre-drought rainfall–streamflow relationship. It was found that 22 catchments had significantly different rainfall–streamflow relationships during the recent drought compared to the pre-drought time period. Out of the 34 catchments, 18 were found to have significantly different rainfall – maximum temperature relationships during the recent drought compared to the pre-drought time period. However, the spatial coherence between these was fairly low, suggesting that while increased temperatures did play a role in reducing streamflow during the recent drought, other subsidiary features of the recent drought were also important.

We then estimated the sensitivity of annual streamflow to annual rainfall and daily maximum temperature using a multiple regression approach. The calculated streamflow sensitivities (multiplication factors) to rainfall mostly lie within the range of about 1.5 to 3.5, i.e. a 10 percent decrease in rainfall leads to a 15 to 35 percent decrease in streamflow. The mean of all of the statistically significant streamflow sensitivities to maximum temperature is –0.186, i.e. a 1 degree increase in daily maximum temperature leads to a 1.86 percent decrease in streamflow. However, larger (i.e. more negative) sensitivities were seen in catchments with smaller increases in maximum temperature during the drought. In those catchments with average maximum temperature anomalies during the drought greater than 0.6 ^{o}C, the average sensitivity to temperature was somewhat smaller at –0.116.

Multiplying the sensitivity factors by the observed rainfall and maximum temperature anomalies for each catchment yields a proportional break-up of the observed streamflow reduction. Averaged over all catchments, weighted by the catchment area, we estimated that of the average 46 percent reduction in streamflow observed across the catchments, 65 percent was accounted for by reduction in annual rainfall during the recent drought, 7 percent was accounted for by increased annually averaged daily maximum temperature, and 28 percent was unexplained.

The second component of the Activity 1used traditional hydrological empirical techniques to investigate which components of the catchment water balance may have changed during the drought. During the drought a statistically significant change (reduction) in daily rainfall occurred between the 10th and 40th percentiles. Very high daily rainfall percentiles (i.e. 1st percentile) during drought were not found to be statistically different from those prior to the drought. However, about 80 percent of the catchments in the southern half of the SEACI region exhibited a statistically significant difference (reduction) in the 1st

percentile of daily runoff. One explanation may be that in small catchments, a statistically significant reduction in very high runoff percentiles (1st percentile) during the drought without a corresponding reduction in very high daily rainfall percentiles (less than 1st percentile) may be evidence for a deepening of the unsaturated zone and more negative soil-water tensions, and hence smaller areas of – and less frequently occurring – saturated overland flow.

The percentage reduction in slow flow during the drought was very strongly correlated with the percentage reduction in streamflow during the drought (correlation coefficient of 0.90). Over the reduced area of the southern SEACI region, no correlation was evident between long-term mean annual rainfall and the percentage reduction in rainfall during the recent drought (–0.06) – the majority of catchments in the southern SEACI region having experienced a reduction in rainfall during the drought of between 15 and 22 percent. This finding suggests that runoff-generating processes have changed to a greater extent in the low-rainfall catchments of the southern SEACI region than in the high-rainfall catchments. More than 70 percent of catchments in the southern SEACI region exhibited a statistically significant change (reduction) in recession coefficient *a,* while approximately 50 percent of catchments in the northern SEACI region exhibited a statistically significant change (reduction) in *a*. These results suggest that during the recent drought there was a change to the aquifer storage – outflow relationship in these catchments.

Activity 2 sought to develop a conceptual understanding for the change in the rainfall-runoff relationship. Seventeen candidate catchments were identified that had streamflow and groundwater level data prior to and during the recent drought. Results are only presented for Axe Creek and Sugarloaf Creek, but these catchments typify the behaviour observed in the other 15 catchments. Both Axe Creek and Sugarloaf Creek showed a significant reduction in mean annual runoff, annual runoff coefficient (proportion of rainfall that becomes runoff) and annual slow flow coefficient (proportion of rainfall the exhibits a 'delayed' runoff response) and an increase in observed case where flows ceased, as well as evidence of a 'hydrological persistence' where runoff is dependent upon the climate in previous years. The 'hydrological memory' appears to increase as the drought progresses. This is most clearly seen in the cease-to-flow cases where consecutive years of similar rainfall result in an ever-increasing cease-to-flow and that individual years of low rainfall prior to the drought show no or only a small cease-to-flow (less than 10 percent).

For both catchments, a conceptual rainfall-runoff model was calibrated well (daily NSE > 0.85) over the 1975 to 1996 period and then used to simulate streamflow over the entire observed record. The models simulated runoff in the years prior to 1975 well (daily NSE > 0.8). However, during the drought the models simulated runoff poorly and model performance declined as the drought progressed. Coincident with the above observations, groundwater levels in both catchments showed a decline since 1997. Prior to 1997, groundwater levels were in a pseudo-steady state, but by the end of 2008 they had yet to achieve a new steady state. Observations of cease-to-flow and electrical conductivity of the streamflow provide strong evidence that the reduction in groundwater levels has resulted in a reduction in baseflow to the river. It is thought, however, that the majority of the reduction in streamflow in these catchments was due to an unprecedented deepening and drying of the unsaturated zone. Collectively these results strongly suggest a change in hydrological behaviour during the recent drought and that the behaviour may have continued to change as the drought progressed. However, continued investigation is warranted. This is because conceptualising reasons for the change in rainfall-runoff relationship was confounded by uncertainty over the change in number of farm dams during the recent drought and the limited ability of conceptual rainfall-runoff models to simulate low-flow processes well.

Background

The main goal of the research in Theme 2 is to improve hydroclimate projections for SEA. The research is at the climate–water interface, and its link to climate science and hydrological modelling science is shown schematically in Figure 38.

Hydrological models are generally tailored for specific applications, and are developed and calibrated using local data. There are two main steps involved in estimating climate impact on future runoff characteristics and water availability. The first step uses global climate model projections and downscaling models to obtain future catchment-scale climate series to drive hydrological models. Research in this area is carried out under Project 2.1. The second step involves driving hydrological models with future climate series to estimate future runoff. This may require adapting models to account for changes in the rainfall–temperature–runoff relationship and changes in the dominant hydrological processes in a drier, warmer environment with higher levels of carbon dioxide (CO_2). Research in this area is carried out under Project 2.2. Both projects in Theme 2 are closely related to, and use information from, the projects in Theme 1.

Researchers in Project 2.2 are building on results from Phase 1 of SEACI to enhance knowledge of climate–water processes and modelling. That research leads to more accurate and updated estimates of the impact of climate change on catchment water yield and streamflow, and also reduces associated uncertainties. This report summarises results from two activities in the second year of this 3-year project.

Objectives

Empirical analysis: quantification of the decline in rainfall and streamflow in catchments with long streamflow records in south-eastern Australia

- Investigate potential changes in relationships between rainfall, temperature and streamflow.
- Investigate potential changes to dominant hydrological processes through a low-flow analysis.

Towards a conceptual understanding of changes in dominant hydrological processes

- Conceptualise changes to hydrological behaviour and runoff-generating processes.

Method and results

Catchment selection

For the purposes of the empirical analysis, we required long, mostly complete time series of observed streamflow data. From the gauging stations available in the SEACI region, we chose a threshold of greater than 40 years of complete data, and less than 30 days of missing data in total between 1997 and 2008. In order to rule out any effects from farm dams or land-use changes (forestry, agriculture or bushfires), a visual examination of each catchment was performed with Google Earth. Several catchments were deemed to have excessive potential for land-use signals in the streamflow data, and so were excluded. In total, 34 catchments remained (Table 12). Of these, 14 lie on the eastern coast of New South Wales outside the Murray–Darling Basin (MDB), and 20 lie within the MDB, principally in the southern MDB. The median year of streamflow data commencement is 1948.

Daily maximum temperature and rainfall data for each catchment were obtained from SILO. Missing streamflow data were infilled using the Sacramento lumped conceptual rainfall-runoff model (Burnash et al. 1973), calibrated over the entire period of record. Averaged across all catchments, weighted by the catchment area, the study area has seen a 15 percent reduction in annual rainfall during 1997–2008 compared to the pre-1997 data, a 46 percent reduction in annual streamflow, and a 0.6 ºC increase in annually averaged daily maximum temperature.

Table 12. Streamflow gauging data sets used for the empirical analysis.

Gauge reference	Catchment name	State	Area (km^2)	Start date	Centred latitude	Centred longitude
201001	Oxley At Eungella	NSW	214	1947	–28.4	153.2
203002	Coopers Ck At Repentance	NSW	61	1920	–28.6	153.4
203005	Richmond At Wiangaree	NSW	709	1943	–28.4	152.9
203010	Leycester At Rock Valley	NSW	174	1951	–28.6	153.1
204017	Bielsdown Ck At Dorrigo Nos.2 & 3	NSW	76	1947	–30.4	152.7
204030	Aberfoyle At Aberfoyle	NSW	199	1951	–30.2	151.8
204031	Mann At Shannon Vale	NSW	344	1951	–29.9	151.8
204033	Timbarra At Billyrimba	NSW	987	1951	–29.4	152.2
204034	Henry At Newton Boyd	NSW	400	1951	–29.9	152.1
204037	Clouds Ck At Clouds Ck	NSW	63	1952	–30.1	152.6
205006	Nambucca At Bowraville	NSW	430	1959	–30.6	152.7
208006	Barrington At Forbesdale (Causeway)	NSW	602	1945	–32.0	151.6
218001	Tuross At Tuross Vale	NSW	89	1948	–36.3	149.5
222007	Wullwye Ck At Woolway	NSW	519	1949	–36.3	148.9
401210	Snowy Creek R At Below Granite Flat	VIC	417	1933	–36.7	147.4
401215	Morass Creek R At Uplands	VIC	539	1930	–36.9	147.8
401216	Big R At Joker Creek	VIC	366	1935	–36.9	147.4
403213	Fifteen Mile Creek R At Greta South	VIC	226	1959	–36.8	146.3
405205	Murrindindi R At Murrindindi Above Colwells	VIC	109	1940	–37.5	145.6
405212	Sunday Creek R At Tallarook	VIC	336	1946	–37.3	145.1
405214	Delatite R At Tonga Bridge	VIC	355	1948	–37.1	146.3
405215	Howqua R At Glen Esk	VIC	374	1948	–37.2	146.4
405217	Yea R At Devlins Bridge	VIC	363	1955	–37.5	145.4
405219	Goulburn R At Dohertys	VIC	707	1955	–37.4	146.2

Gauge reference	Catchment name	State	Area (km^2)	Start date	Centred latitude	Centred longitude
405226	Pranjip Creek R At Moorilim	VIC	818	1958	–36.8	145.4
405227	Big R At Jamieson	VIC	632	1959	–37.4	146.0
405228	Hughes Creek R At Tarcombe Road	VIC	479	1959	–37.0	145.4
406213	Campaspe R At Redesdale	VIC	644	1954	–37.2	144.5
410024	Goodradigbee R At Wee Jasper (Kashmir)	NSW	990	1915	–35.3	148.7
410026	Yass R At Yass	NSW	1237	1916	–35.0	149.2
410044	Muttama Creek R At Coolac	NSW	1061	1939	–34.8	148.1
410057	Goobarragandra R At Lacmalac	NSW	663	1958	–35.4	148.5
410062	Numeralla R At Numeralla School	NSW	676	1948	–36.4	149.4
418014	Gwydir R At Yarrowyck	NSW	819	1956	–30.5	151.5

(a) (b)

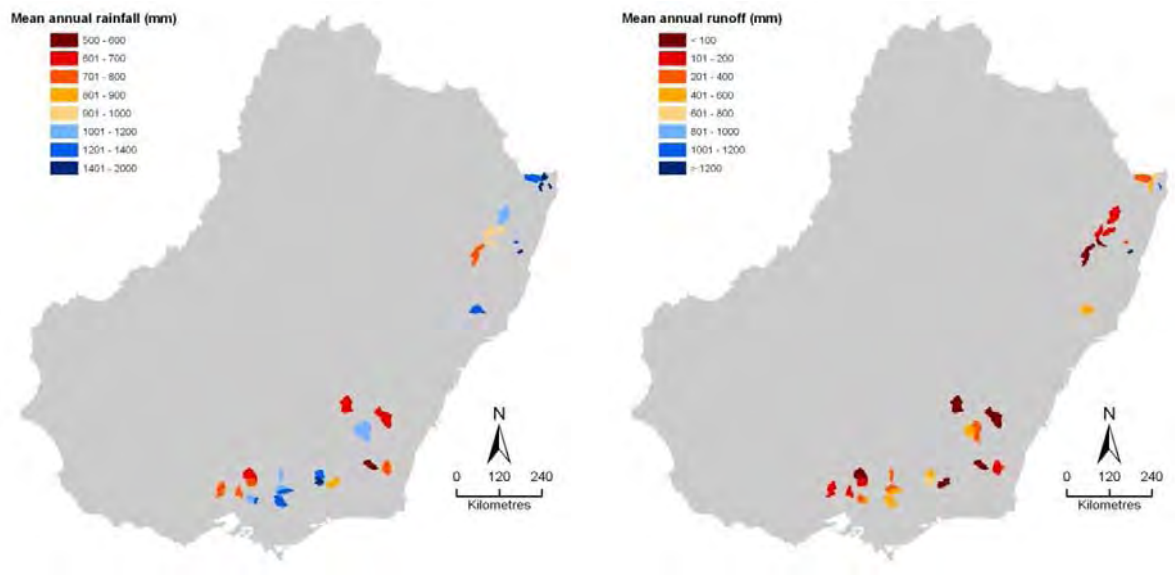

Figure 48. Mean annual rainfall (a) and runoff (b) of selected catchments in south-eastern Australia.

Empirical analysis: quantification of the decline in rainfall and streamflow in catchments with long streamflow records in south-eastern Australia

Investigate potential changes in relationships between rainfall, temperature and streamflow

Changes in the rainfall–streamflow relationship

First we tested whether the annual rainfall–streamflow relationship during the drought was statistically different from the pre-drought rainfall–streamflow relationship. A difference in the relationship indicates that streamflow has been lower than expected based on annual rainfall alone. In this case, some of the subsidiary features of the drought (such as increased temperatures, increased potential evapotranspiration, changes to the seasonal distribution of annual rainfall, surface water – groundwater interactions, changes to land use, etc.) may be hydrologically important in explaining the low streamflow during the recent drought.

Simple functional relationships between annual rainfall and evapotranspiration have long been recognised. Perhaps the best known is Budyko's (1974) relationship. Other similarly shaped curves have been proposed both before and since Budyko's (see, for example, Choudhury, 1999; Arora, 2002; Zhang et al., 2004). To first order, annual evapotranspiration generally follows these curves quite well. Annual streamflow can then be estimated from these relationships by assuming mass balance, i.e. that the sum of annual streamflow and evapotranspiration is approximately equal to annual rainfall.

These curves use the dryness index (i.e. the ratio of annual potential evapotranspiration to annual rainfall) rather than annual rainfall by itself to predict streamflow, but the relatively low rate of inter-annual variability in potential evapotranspiration in many catchments make rainfall–streamflow relationships (i.e. without any use of annual potential evapotranspiration) almost as good, particularly in semi-arid regions. Zhang et al.'s (2001) curve, as well as the tanh function (Grayson et al., 1996), are examples of such an approach.

One drawback of many of the rainfall–streamflow relationships described above is that in most cases statistical tests on the curve parameters are difficult to perform. For this reason, we considered a linear regression between annual rainfall and Box-Cox transformed annual streamflow data (Figure 49). Optimising the parameter using a maximum-likelihood procedure (see, for example, Myers, 1990) allows for a linear relationship between annual rainfall and streamflow (Box-Cox parameter equal to one) in higher rainfall catchments, and non-linear relationships similar to the tanh function (Box-Cox parameter close to zero) for lower rainfall catchments. Specifically, we considered the following linear model:

$$\hat{Q}_i = \alpha_{\text{pre}-97}.I_{\text{pre}-97} + \alpha_{\text{post}-97}.I_{\text{post}-97} + \beta.P_i + \varepsilon_i \quad (1)$$

where $\hat{Q}_i$ is transformed annual streamflow, $I_{\text{pre}-97}$ and $I_{\text{post}-97}$ are pre-1997 and post-1997 indicator variables, and P_i is annual rainfall. An F-test can be used to test the null hypothesis that the intercepts are equal:

$$H_0 : \alpha_{\text{pre}-97} - \alpha_{\text{post}-97} = 0 \quad (2)$$

Note that the Box-Cox transform is monotonic (i.e. large values of streamflow correspond to large values of transformed streamflow). This means that $\alpha_{\text{post}-97} < \alpha_{\text{pre}-97}$ implies that the rainfall–streamflow relationship is lower during 1997–2008 compared to the pre-drought period (Figure 49).

(a) (b)

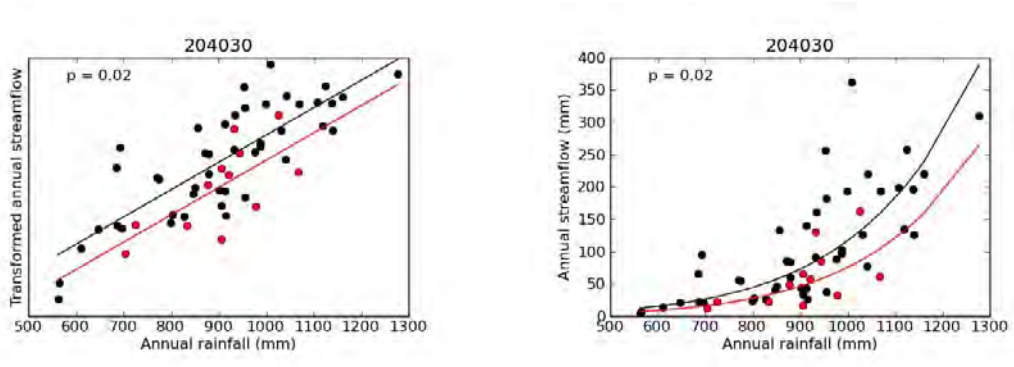

Figure 49. Testing the annual rainfall–streamflow relationship (example catchment 204030 with maximum-likelihood Box-Cox parameter of 0.1). The linear relationship between annual rainfall and transformed streamflow is shown in (a), and the corresponding relationship between annual rainfall and un-transformed streamflow is shown in (b). Red points and curves are for 1997–2008 data; black points and curves are for pre-1997 data.

We found that 22 catchments had significantly different rainfall–streamflow relationships during the recent drought compared to the pre-drought time period (Table 13). This suggests that for a given annual rainfall amount, the annual streamflow amount is significantly less (as in Figure 49). Or in other words, observed annual streamflow is significantly lower than the 'expected' amount based on the annual rainfall and the long-term relationship between rainfall and streamflow.

Table 13. Number of catchments with significantly different rainfall–streamflow relationships and rainfall – maximum temperature (Tmax) relationships.

		Rainfall vs. Streamflow		
		Significantly different	Not significantly different	Total
Rainfall vs. maximum temperature	Significantly different	13	5	18
	Not significantly different	9	7	16
		22	12	34

Changes in the rainfall–daily maximum air temperature relationship

In general, at monthly and annual timescales, rainfall and average maximum temperature are inversely related (i.e. high temperatures are associated with low rainfall and vice versa; e.g. Nicholls, 2004). Data analysis has revealed a trend for higher mean annual maximum temperature for a given mean annual rainfall in SEA (Nicholls, 2004; Cai and Cowan, 2008). Next we tested whether the rainfall–maximum temperature relationship was significantly different during the recent drought.

In contrast to the annual rainfall–streamflow relationships described above, the relationship between annual rainfall and annual average maximum temperature is linear (see Figure 50). Thus the Box-Cox transform is not needed for the temperature data:

$$T_{\max,i} = \alpha_{\text{pre–97}}.I_{\text{pre–97}} + \alpha_{\text{post–97}}.I_{\text{post–97}} + \beta.P_i + \varepsilon_i \quad (3)$$

where $T_{\max,i}$ is annually averaged daily maximum temperature, with the null hypothesis given again by Equation (2) to determine whether the intercepts differ significantly before and during the drought.

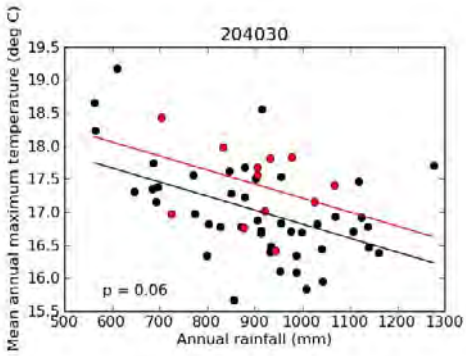

Figure 50. An example of the relationship between annual rainfall and annually averaged maximum temperature for catchment number 204030. Red points and line are for 1997–2008 data; black points and line are for pre-1997 data

Out of the 34 catchments, 18 were found to have significantly different rainfall–maximum temperature relationships (Table 13) during the recent drought compared to the pre-drought time period. In these catchments, residual temperature (in the sense of Nicholls, 2004) has thus been significantly higher during the recent drought.

However, the relationship between different rainfall–streamflow and different rainfall–maximum temperature relationships does not appear to be highly correlated. Although the majority of catchments have significantly different rainfall–streamflow relationships and significantly different rainfall– maximum temperature relationships, several catchments have only one significantly different relationship. In fact the chi-squared test statistic for a test for independence on Table 13 is 0.95, which is much less than the 5 percent critical value of 3.8. This may be because some of those catchments with significantly higher residual maximum temperature during the recent drought may have low sensitivity of streamflow to changes in temperature. Conversely, the significantly different rainfall–streamflow relationships seen in some catchments may be due to other factors such as changed rainfall seasonality and changes in surface–subsurface connectivity. Spatially, those catchments with significantly different rainfall–streamflow relationships are primarily located around the southern MDB, while those catchments with significantly different rainfall– maximum temperature relationships are more uniformly spread across the SEACI region (Figure 51).

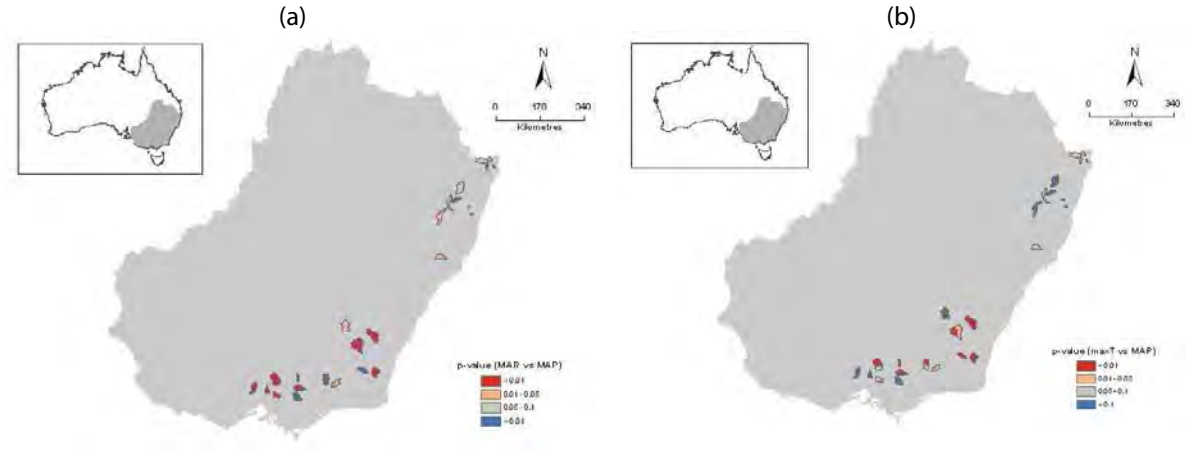

Figure 51. Statistical significance of tests for differing rainfall–streamflow relationships during the drought (left-hand panel) and differing rainfall– maximum temperature relationships (right-hand panel)

Sensitivity of annual streamflow to annual rainfall and maximum temperature

There are a few different approaches to estimating the climate elasticity of streamflow (i.e the sensitivity of streamflow to climate variables). One approach is to use calibrated rainfall-runoff or process-based models to directly measure the sensitivity of streamflow to changes in rainfall and temperature (Chiew, 2006; Potter and Chiew, 2009). Alternatively, sensitivities can be calculated analytically from rainfall–streamflow relationships (such as those based on Budyko's curve (Budyko, 1974) described above, e.g. Arora, 2002; Milly and Dunne, 2002). These approaches, however, rely on model assumptions. Data-based approaches – either parametric (e.g. Vogel et al., 1999) or non-parametric (e.g. Sankarasubramanian et al., 2001) – allow for estimation of streamflow sensitivity without the need for model assumptions. The effect on streamflow of changes in maximum temperature is less easily estimated. This is because there is considerable correlation between rainfall and temperature (Figure 50) and any effect from residual temperature is generally much less apparent than the direct effect of changes in rainfall.

Here we follow the approach of Vogel et al. (1999) and estimate the sensitivity of annual streamflow to annual rainfall and maximum temperature using a multiple regression approach. Regression is ideally suited to this problem as any correlation between annual rainfall and annual average air temperature is incorporated into the parameter estimation procedure. However, as before, we include a Box-Cox transform on the annual streamflow data.

In semi-arid catchments, the relationship between annual rainfall and annual streamflow can be far from linear (e.g. Figure 49). Fitting a linear regression without first transforming streamflow in these catchments can result in negative predicted streamflow. Thus in low-rainfall years, streamflow predicted from rainfall alone will be much smaller than observed streamflow, resulting in a large residual. But in low-rainfall years, the temperature anomaly is typically large and so data from these years will exert a large and erroneous influence on the estimate of streamflow sensitivity to temperature.

We first transform streamflow using the Box-Cox transform to get $\hat{Q}_i$. We then calculate the relative differences in transformed annual rainfall $\delta P_i = \left(P_i - \overline{P}\right)/\overline{P}$ and the annual Tmax anomaly $\Delta T_{\max,i} = T_{\max,i} - T_{\max}$. Then, for the pre-drought data only, we fit the linear model:

$$\hat{Q}_i = \hat{\eta}_P \delta P_i + \hat{\eta}_T \Delta T_{\max,i} + \varepsilon_i \qquad (4)$$

In this way, the regression coefficients $\hat{\eta}_P$ and $\hat{\eta}_T$ can be interpreted as the sensitivity of transformed streamflow to rainfall differences and maximum temperature anomalies, with the other variable held constant. However, these estimates are not directly useable as they relate to transformed streamflow.

To obtain estimates of the sensitivity of rainfall and maximum temperature to un-transformed streamflow, we first calculate the expected value of un-transformed streamflow for average rainfall and average annual temperature:

$$E\left(Q_i \mid \delta P_i = 0, \Delta T_{\max,i}\right) \tag{5}$$

$$E\left(Q_i \mid \delta P_i, \Delta T_{\max,i} = 0\right) \tag{6}$$

To ensure that these estimates from the inverse Box-Cox transform are unbiased (Miller,1984 discusses this problem), we use the plug-in density method (see Collins, 1991). Then we define the rainfall elasticity of streamflow η_P as the least-squares slope between δP_i and $\delta Q_i - E\left(Q_i \mid \delta P_i = 0, \Delta T_{\max,i}\right)$, and the temperature elasticity of streamflow η_T as the least-squares slope between $\Delta T_{\max,i}$ and $\delta Q_i - E\left(Q_i \mid \delta P_i, \Delta T_{\max,i} = 0\right)$. Note that if the streamflow data were not transformed initially (or equivalently the Box-Cox transform parameter is 1), then $\hat{\eta}_P = \eta_P$ and $\hat{\eta}_T = \eta_T$.

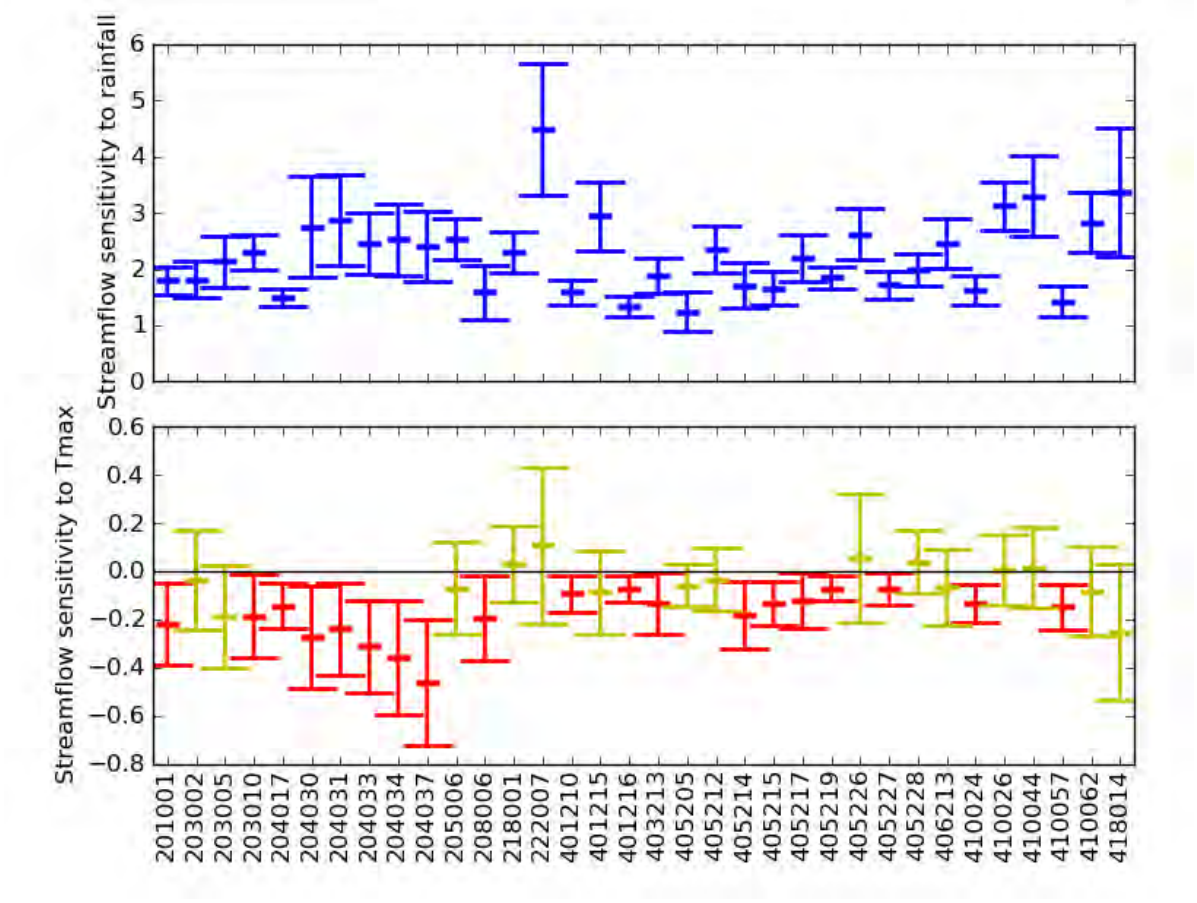

Figure 52. Estimated streamflow sensitivities to rainfall η_P and to maximum temperature η_T. For all catchments (Table 12). Mustard-coloured ranges for η_P contain zero and are thus not statistically significant

The calculated streamflow sensitivities to rainfall are shown in Figure 52. Most lie within the range of about 1.5 to 3.5, consistent with other estimates in SEA (Chiew, 2006; Potter et al., 2008). As the estimates are least-squares regression estimates, confidence intervals for these sensitivities are straightforward to calculate, and these are shown as well. The uncertainty is generally larger for larger values of the elasticity. This is due to the greater variability of streamflow in these catchments. Nevertheless, all values of η_P are statistically significant. Larger values of η_P are located in drier catchments. These catchments also tend to have larger absolute (i.e. more negative) values of η_T, and this is consistent with theoretical results for streamflow sensitivity to rainfall and potential evapotranspiration (Dooge et al., 1999; Milly and Dunne, 2002).

In contrast, the streamflow sensitivity to maximum temperature is not statistically significant in 15 of the 34 catchments. These are shown in mustard in Figure 52. The mean of all of the statistically significant values of η_T is −0.186 (i.e. a 1 degree increase in average daily maximum temperature leads to a 18.6 percent reduction in streamflow). However, more negative values of η_T are located in those catchments that have seen the least increase in average maximum temperature during the drought (less than 0.6 ºC). In those catchments with average maximum temperature anomalies greater than 0.6 ºC, average η_T is −0.116.

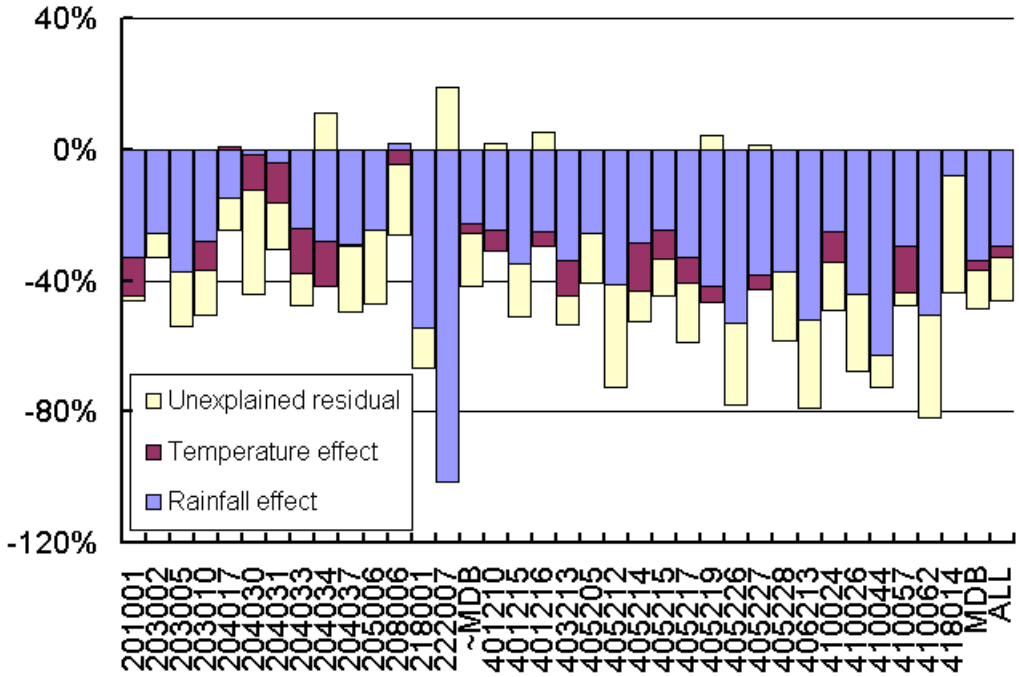

Figure 53. Proportion of observed streamflow reduction explained by streamflow sensitivity factors for all catchments considered (Table 12).

Next, we look at the reduction in streamflow during 1997–2008 compared to the pre-drought data for each catchment. Multiplying the sensitivity factors by the observed rainfall and maximum temperature anomalies for each catchment yields a proportional break-up of the observed streamflow-reduction (Figure 53). Here, a temperature effect is only included if the sensitivity η_T is statistically significant. Averaged over all catchments, weighted by the catchment area, we obtain estimates for the rainfall and maximum temperature effect on streamflow for all catchments, those in the MDB, and those outside (Table 14).

Table 14. Estimate of the effect of the observed reduction in rainfall and the observed increase in maximum temperatures during the recent drought (1997–2008). The first percentages show reductions from the long-term mean; the bracketed percentages are the proportion of the observed reduction in streamflow.

Region	Rainfall effect		Temperature effect		Residual		Total
Outside MDB	−23%	(55%)	−3%	(7%)	−16%	(38%)	−42%
MDB	−34%	(69%)	−3%	(7%)	−11%	(24%)	−48%
All	−30%	(65%)	−3%	(7%)	−13%	(28%)	−46%

Potential changes to dominant hydrological processes through a low-flow analysis

In the previous Section we reported a 46 percent weighted average reduction in streamflow across 34 selected catchments (Table 14). Sixty-five percent of this was accounted for by a reduction in rainfall and 7 percent to changes in temperature. The remaining 28 percent unexplained residual may be due to changes in seasonality and inter-annual variability of rainfall; land management (e.g. change in farm dams); or changes in hydrological processes. A popular line of thought has been that changes to dominant hydrological process due to an extended drought are most likely to be manifested in those processes associated with long-term storages (e.g. in the unsaturated and saturated zone). Hence this empirical analysis focused on parameters associated with low-flow processes, such as baseflow and groundwater recession constants.

Assessment of changes in rainfall and streamflow percentiles and cease-to-flow

The runoff, rainfall, runoff coefficient and daily percentiles of rainfall and runoff for each season and each year of observed records were computed for each of the 34 catchments. The non-parametric Wilcox test was applied to the resulting seasonal and annual time series, to assess whether the median value was significantly different during the recent drought (1997–2008) compared to the prior period (pre-1997).

Figure 54 shows that all catchments in the southern half of the SEACI region, except for one, exhibited a statistically significant reduction in median annual runoff during the drought and more than 80 percent of these catchments exhibited a statistically significant change in their median runoff coefficient. Across all southern SEA catchments, a statistically significant difference was also observed for daily runoff percentiles between 10 and 60 (Figure 55). The two catchments in the southern SEACI region that did not show a statistically significant difference for the 1st and 5th percentiles of daily runoff (Figure 55) were the two wettest catchments (Figure 48). With one exception, catchments in the northern part of the region did not consistently exhibit a significant change in hydrological behaviour across multiple metrics. The spatial pattern of results presented in this Section is consistent with the spatial patterns observed in the previous Section.

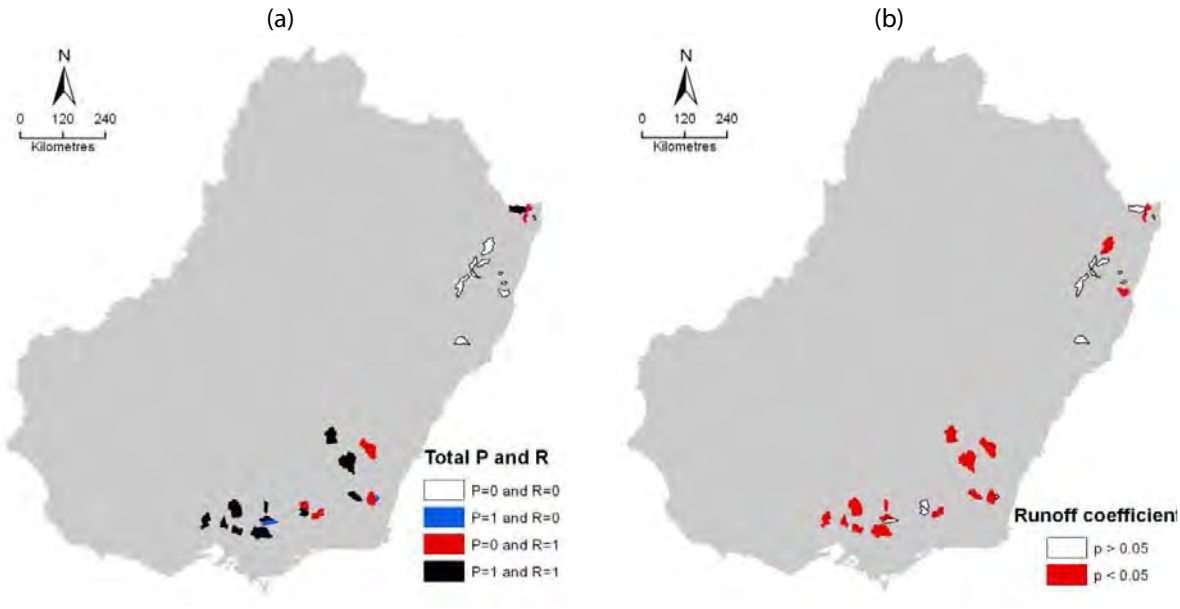

Figure 54. (a) Comparison of median annual rainfall (P) and runoff (R) during the recent drought and prior to the recent drought. '1' indicates a result that is statistically significant ($p<0.05$) and '0' indicates a result that is not statistically significant. For example in those catchments shaded red the median annual rainfall was not statistically significantly different during the recent drought and prior to the recent drought, but the median annual runoff was statistically significantly different. (b) Comparison of median annual runoff coefficient during the recent drought and prior to the recent drought

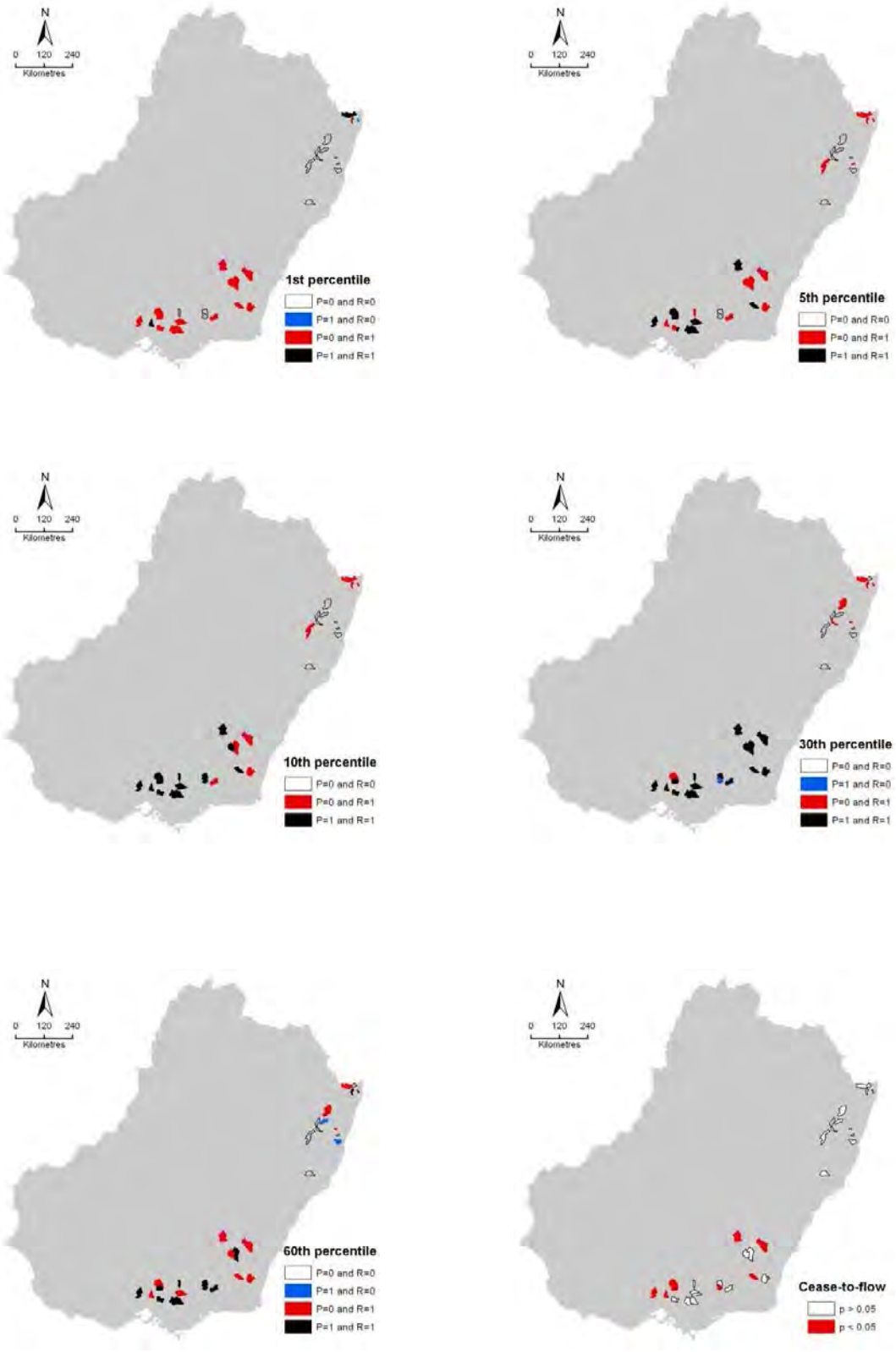

Figure 55. Comparison of median daily rainfall percentiles (P) and runoff percentiles (R) during the recent drought and prior to the recent drought. '1' indicates a result that is statistically significant ($p<0.05$) and '0' indicates a result that is not statistically significant.

Figure 55 illustrates that there was no statistically significant difference between the very high daily rainfall percentiles (1st percentile) observed during the drought and those observed prior to the drought. The statistically significant change in daily rainfall occurred between the 5th and 40th percentiles. Notably, about 80 percent of catchments in the southern half of the region exhibited a significant difference in the 1st percentile of daily runoff during the drought compared to that observed prior to the drought. One possible explanation is that in small catchments, a statistically significant reduction in very high runoff percentiles (1st percentile) during the drought without a corresponding reduction in very high daily rainfall percentiles (less than 1st percentile) may be evidence for a deepening of the unsaturated zone and more negative soil water tensions, and hence smaller areas of and less frequently occurring saturated overland flow. However, it is difficult to definitively attribute cause, because of the confounding effect of farm dams, which are said (anecdotally) to have increased in number during the recent drought, and the implied assumption that very high daily runoff percentiles are the result of very high daily rainfall percentiles. However, this anecdotal evidence is tempered by a recent study (GA, 2008) which indicates that across the southern parts of the MDB, farm dams increased in number by only 6 to 9 percent between 1994 and 2005, though this figure may vary locally. At the time of analysis, complete SEA farm dam details for 2005 were unavailable. These data have since been sourced and in the future the likely influence of farm dams on streamflow will be assessed on a catchment-by-catchment basis.

Cease-to-flow was designated as being flow less than 0.1 ML/day (the threshold for accurately measuring flow using a V-notch weir). Approximately 40 percent of the catchments in southern SEA show a statistically significant difference in the cease-to-flow metric during and prior to the recent drought. All of these catchments had a low mean annual rainfall (Figure 48); about 40 percent of them were ephemeral prior to the drought and about 60 percent ephemeral during the drought. Of the remaining catchments in southern SEA, about 30 percent were ephemeral prior to the drought, but only 25 percent were ephemeral during the drought. Catchments that exhibited significant change in cease-to-flow behaviour during the drought were already intermittently experiencing a surface-water to groundwater disconnection due to low mean annual recharge and rainfall.

Trends in annual streamflow and slow flow

In a recent assessment of slow flow at 141 sites in the MDB, CSIRO (2010b) used a Generalised Additive Model, which accounts for the effects of exogenous influences (rainfall and seasonality were chosen as explanatory variables). They found a downward trend in 95 percent of gauges analysed, of which 66 percent were statistically significant at the 5 percent level. However, it is likely that groundwater extraction was taking place in many of these catchments and the authors concluded that the downward trends were most likely due to land-use change or groundwater extraction. Here trends in baseflow were examined in our 34 unimpeded catchments, which were selected in part to exclude notable groundwater extraction and forestry.

The task of separating baseflow (sub-surface flow) from river discharge data has many practical difficulties (Appleby, 1970; Kirchner, 2003) and a variety of methods exist (Nathan and McMahon, 1990; Chapman, 1999; Eckhardt, 2005). This study used the Lyne and Hollick digital filter (Grayson et al., 1996). The quick and slow flow responses resulting from the application of this method have little physical reality, hence the slow flow component is not necessarily equivalent to baseflow (i.e. it could be delayed surface runoff). Despite this limitation the filter has been widely applied and there is a considerable body of data available for comparative purposes (e.g. Lacey, 1996). Here two values for the alpha term were trialled, 0.925 and 0.98 (as per CSIRO 2010b). While they resulted in different quantities of 'slow flow', the trends and proportions prior to and during the drought were the same.

The percentage reduction in slow flow during the drought was very strongly negatively correlated (–0.82 using Spearman rank correlation) to the long-term mean annual rainfall for the 34 catchments, which was a stronger negative correlation than that between the percentage reduction in streamflow and long-term mean annual rainfall (–0.72; Table 15). The percentage reduction in slow flow during the drought was very

strongly correlated with the percentage reduction in streamflow during the drought (correlation coefficient of 0.90).

Examining only those catchments located in southern SEA, the percentage reduction in slow flow during the drought was very strongly negatively correlated (–0.84) with long-term mean annual rainfall, which was a slightly weaker correlation than the correlation between the reduction in streamflow and long-term mean annual rainfall (–0.88). For these catchments, the correlation between the percentage reductions in baseflow during the drought was very strongly correlated with the percentage reduction of streamflow during the drought (0.96).

Notably, over the reduced area of southern SEA, no correlation was evident between long-term mean annual rainfall and the percentage reduction in rainfall during the recent drought (–0.06) – the majority of catchments in southern SEA experienced a reduction in rainfall during the drought of between 15 and 22 percent. This finding suggests that runoff-generating processes have changed to a greater extent in the low-rainfall catchments of the southern basin than in the high-rainfall catchments. This is consistent with previous observations that rainfall-runoff elasticities are highest in catchments with low runoff coefficients (Chiew, 2006). Prior to the drought, many lower-rainfall catchments already demonstrated a disconnection between the groundwater and surface water as evidenced by periods of cease-to-flow and hence are thought to be particularly susceptible to years of low rainfall. They are also more likely to have lower relief and be less incised than the higher-rainfall catchments resulting in different patterns, depths and groundwater flow paths.

Table 15. Correlation matrix between annual rainfall, stream flow and slow flow using Spearman-ranked correlation method. Green squares show correlation values for all 34 selected catchments. Yellow squares show correlation values for catchments in southern SEACI region.

Parameter	Mean annual rainfall (mm)	Percentage reduction streamflow	Percentage reduction slow flow	Percentage reduction rainfall
Mean annual rainfall (mm)	1	–0.72	–0.82	–0.17
Percentage reduction streamflow	–0.88	1	0.90	0.50
Percentage reduction slow flow	–0.84	0.96	1	0.36
Percentage reduction rainfall	–0.06	0.23	0.20	1

Figure 56 illustrates that slow flow during the recent drought was significantly different ($p<0.05$) in all the catchments in the southern SEACI region, but was significantly different in only a few of the northern catchments.

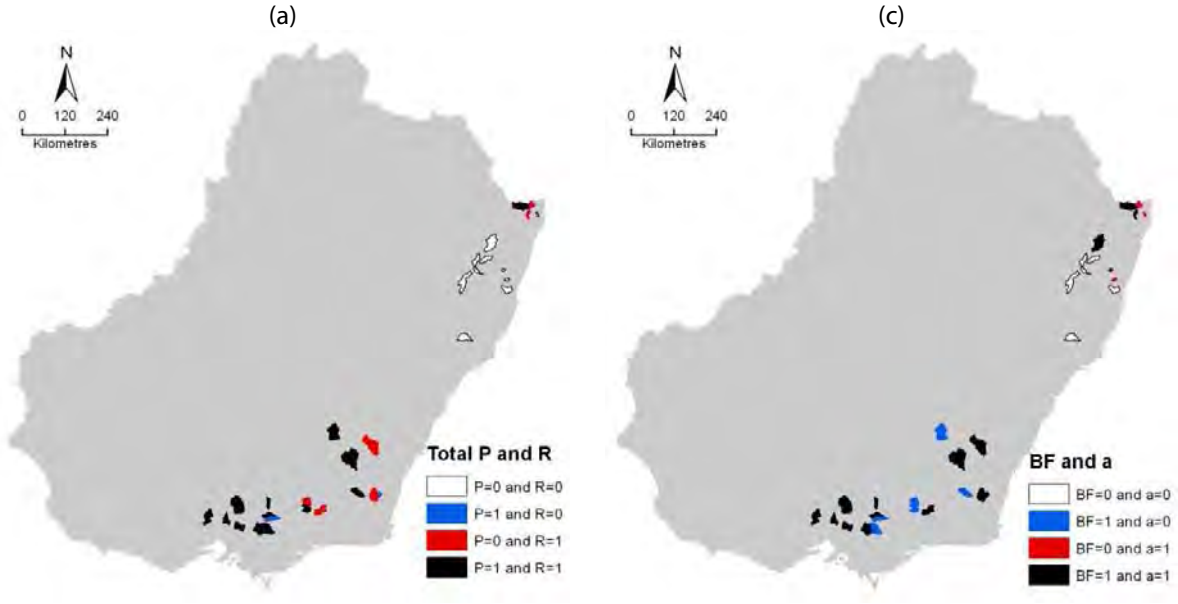

Figure 56. (a) Comparison of median annual rainfall (P) and runoff (R) during and prior to the recent drought. '1' indicates a result that is statistically significant ($p<0.05$) and '0' indicates a result that is not statistically significant. (b) Comparison of median annual slow flow (BF) and recession constant (a) during and prior to the recent drought. '1' indicates a result that is statistically significant ($p<0.05$) and '0' indicates a result that is not statistically significant.

Hydrograph recession analysis

Hydrograph recessions reflect the aquifer storage – outflow relationship of an aquifer. Analysis of flow recession curves enables the groundwater reservoir to be characterised. In engineering hydrology applications, a single linear model (Equation 7) is typically used to model flow recessions:

$$Q_t = Q_0 \times \exp(\frac{-t}{k}) \tag{7}$$

where Q_t is the discharge at time *t*, Q_0 the initial discharge and *k* the retention constant.

In theory, changes in computed *k* over time indicate changes to the characteristics of the groundwater reservoir. The attraction of using a linear model is its simplicity and that the retention constant *k* has the dimension of time. Therefore *k* can be interpreted as being representative of residence or turnover time for water in the aquifer. However, many studies have found that the underlying assumption of Equation 7 – that the storage is proportional to the outflow – does not hold (Wittenberg, 1994; Moore, 1997). A similar finding was noted in this study, with most catchments exhibiting non-linear behaviour. As a consequence, there was a correlation between the lengths of the recessions and *k*, with those years typified by short recessions having low values of *k* and those years with long recessions having high values for *k*. For this reason we used a non-linear model as described by Equation 8:

$$Q_t = Q_0 \left[1 + \frac{(1-b)Q_0^{1-b}}{ab} t \right]^{\frac{1}{(b-1)}} \tag{8}$$

The first step in this analysis was to identify suitable data pairs and group them by season and/or year. Data pairs were selected such that $Q_t > Q_{t-1}$ and that the total catchment average rainfall on the two preceding days was <1 mm. The parameter *b* in Equation 8 was set to 0.5 based on the results from theoretical and experimental studies (Wittenberg, 1999). Parameter *a* in Equation 8 was then optimised to each set of data pairs in each season/year. Wittenberg (1999) argues that even if the 'true' value of *b* is not exactly met, the assumption of *b*=0.5 would be more physically based and better fitting for the majority of river basins than the linear reservoir.

More than 70 percent of catchments in the southern SEACI region exhibited a statistically significant change (reduction) in recession coefficient *a* (Figure 56). Approximately 50 percent of catchments in the northern SEACI region exhibited a statistically significant change (reduction) in *a*. These results suggest that during the recent drought there was a change in the aquifer storage – outflow relationship of these catchments. Those catchments in Figure 56 that indicate a statistically significant change in slow flow, but not in recession coefficient *a,* either have a very low or very high mean annual rainfall. In the low-rainfall catchments the recession coefficient is very low (much less than 1) indicating negligible surface water – groundwater connectivity, but rather bankflow return (i.e. water that may have infiltrated into the river bank returning to the river once the river stage has declined) following an event.

Towards a conceptual understanding of changes in dominant hydrological processes

Conceptualised changes to hydrological behaviour and runoff-generating processes

Petrone et al. (2010) surmised that in the south-west Western Australia, a new hydrological regime has developed in many catchments over the recent record. These authors undertook a trend and change point analysis of streamflow data from south-west Western Australia. Trend tests showed a significant decline in annual rainfall and runoff between 1950 and 2008, with corresponding change points for both rainfall and streamflow in the late 1960s or mid-1970s. Over the more recent record (1989–2008), however, streamflow decline was observed as a step change but rainfall did not show a significant downward trend.

Excluding the potential for changes in land management to have occurred, the results from previous Sections lend support to the supposition that a new hydrological regime may have also occurred in SEA. In an earlier section it was observed that a statistically significant change occurred in the rainfall-runoff relationship in the 80 percent of the catchments in the southern SEACI region and in a later Section we then speculated that a number of consecutive years of below-average rainfall resulted in a deepening of the unsaturated zone and more negative soil water tensions, and hence smaller areas of – and less frequently occurring – saturated overland flow.

This Section focuses on developing a conceptual understanding of hydrological behaviour in selected catchments and identifying evidence for a change in hydrological regime by a weights-of-evidence approach. Without the opportunity or foresight to implement a controlled experiment (requiring many years of resource-intensive monitoring), we note that retrospective analyses such as this are challenged by data limitations. In this study we were limited to routine measurements made by departments in the jurisdictions of the study area and the use of surrogate parameters. For example, in the absence of soil-water measurements, we used information on groundwater levels to infer a change in unsaturated zone thickness and soil water tension. We also used measurements of stream electrical conductivity to infer the absence or presence of groundwater discharge into the stream. In an attempt to provide additional evidence for a change in hydrological behaviour, we calibrated the Sacramento rainfall-runoff model between 1975 and 1996 and then simulated runoff over the entire period of observed record (~1960s–2008). By assessing model performance prior to 1975 and between 1997 and 2008 and comparing with the calibration period, we investigated how well a model calibrated prior to the drought was able to simulate runoff during the drought, compared to an independent period prior to the drought.

Unfortunately, most unregulated catchments in Australia with streamflow data do not have groundwater data of sufficient length or quality, and vice versa. Ultimately, we settled on 17 upland catchments in Victoria for analysis, as these had the most complete data and were also located in that part of the basin that has experienced the greatest reductions in runoff. These catchments had streamflow records prior to and during the drought and groundwater level data, which were taken as part of the dryland salinity programs during the 1980s and 1990s. Groundwater extractions were negligible and catchments were unregulated to the best of our knowledge (based on Google Earth and discussions with hydrogeologists from the Victorian Department of Primary Industry). Unfortunately, as we are still trying to obtain the GeoScience Australia Farm Dam data, we were not able to make a quantitative assessment of the likely impact of farm dams on runoff in each of these catchments. These data will be pursued in 2011/12.

To help develop a conceptual understanding of the relationship between hydrological parameters, key parameters were plotted together on the one Figure. Such Figures were generated for all 17 catchments, but are only shown here for Axe Creek (Figure 57) and Sugarloaf Creek (Figure 58). The data available for these two catchments typify those catchments that had the better quality data.

From top to bottom, Panel #1 shows mean annual rainfall (blue), mean annual runoff (green), simulated runoff (pink), and number of days in each year with streamflow data (orange). Panel #2 shows a monthly rainfall mass-residual curve (blue), annual runoff coefficient (black), and slow-flow runoff coefficient using 0.98 for alpha (brown). Panel #3 shows daily runoff (green), cease-to-flow (i.e. flow less than 0.1ML/day, red), and simulated cease-to-flow (pink). Panel #4 shows groundwater levels (red, brown, green) and manually sampled EC (orange points), box plots of manually sampled EC for each year, and continuous EC (orange line). Panel #5 shows groundwater levels (red, brown, green) and non-linear recession coefficient *a* (black points).

In both catchments, there was a significant reduction in mean annual runoff, annual runoff coefficient and annual slow-flow coefficient, and an increase in observed cease-to-flow. Close examination of these data indicates that a 'hydrological persistence' is evident, where runoff depends upon the climate in previous years. The 'hydrological persistence' appears to increase as the drought progresses. This is most clearly seen in the cease-to-flow where consecutive years of similar rainfall result in an ever-increasing cease-to-flow and individual years of low rainfall prior to the drought show no or only a small cease-to-flow.

The Sacramento conceptual rainfall-runoff model achieved a good calibration over the 1975 to 1996 period (daily Nash Sutcliffe Efficiency (NSE) greater than 0.85 and bias less than 0.02) in both catchments. In the case of Axe Creek, the model simulated runoff in the 10 years prior to 1975 well (daily NSE=0.81 and bias=0.044). However, during the drought the model simulated runoff poorly (daily NSE=0.4 and bias 1.105). A similar result was observed for Sugarloaf Creek, where the model simulated runoff in the 2 years prior to 1975 well (daily NSE=0.85 and bias=0.1; though it should be noted this time frame is too short to objectively assess model performance), but the model skill was considerably poorer over the drought period (daily NSE=0.62 and bias=3.338). In both catchments, model performance declined as the drought progressed. These results suggest a change to the hydrological behaviour of these catchments had occurred since 1997 and that the relationship may have continued to change as the drought progressed. Again, it should be noted, however, that an increase in farm dams over the drought period would have a similar effect on model performance and that conceptual rainfall-runoff models typically model low-flow events more poorly than high-flow events (e.g. see Panel #3 for both catchments).

Coincident with the above observations, groundwater levels in both catchments declined since 1997, though this is best seen in Axe Creek due to the smaller depth-to-watertable scale and having groundwater levels closer to the surface. Prior to the drought, groundwater levels were in a pseudo-steady state, but with many consecutive years of below-average rainfall, groundwater levels steadily declined and had not attained a new steady state. The decline in groundwater levels in Axe Creek is highly likely to be responsible for the steady increase in cease-to-flow through a lack of surface water – groundwater connection and change in the aquifer storage–outflow relationship (as shown by the recession constant *a*). Evidence for this is that in other very low-rainfall years prior to the drought (e.g. 1982, which had the lowest annual rainfall since 1965) the percentage cease-to-flow was zero; in the following summer (1983) which had a higher-than-average mean annual rainfall the cease-to-flow increased, but only to about 10 percent. Anomalously

high stream EC observations were also recorded for 1982. Sugarloaf Creek exhibited a similar pattern even though it appears to have a shorter groundwater residence time compared to Axe Creek, where the peak cease-to-flow coincides with a year of low rainfall. Further evidence for a disconnection between the surface water and groundwater systems in Axe Creek can be seen in the reduction in streamflow EC in 2003, despite very low-rainfall years, which prior to this resulted in high streamflow EC. It is surmised that post-2003 groundwater contribution to streamflow is limited to bankflow return shortly after an event as evident by the low streamflow EC and small recession coefficient *a*.

Results presented here, however, indicate that slow flow has declined at roughly the same proportion as total flow across most catchments in SEA and that slow flow was a relatively small proportion of total streamflow. Hence it is thought that only a small component of the reduction in streamflow was due to a reduction in slow flow, which is often used as an analogy for baseflow. Declining groundwater levels, however, strongly imply a deepening of the unsaturated zone and more negative soil water tensions, which – as mentioned earlier – would be likely to result in smaller areas of and less frequently occurring saturated overland flow.

While the focus of discussion here has been on Axe Creek and to a lesser extent Sugarloaf Creek, these observations hold true for the other 15 catchments. The results presented strongly suggest a change in hydrological behaviour during the recent drought and that the behaviour may have continued to change as the drought progressed (and groundwater levels further decreased). However, further investigation is warranted. This is because the interpretation of hydrological behaviour in these catchments is confounded by uncertainty over the change in farm dam number and volume during the recent drought and the inability of conceptual rainfall-runoff models to simulate low-flow processes well.

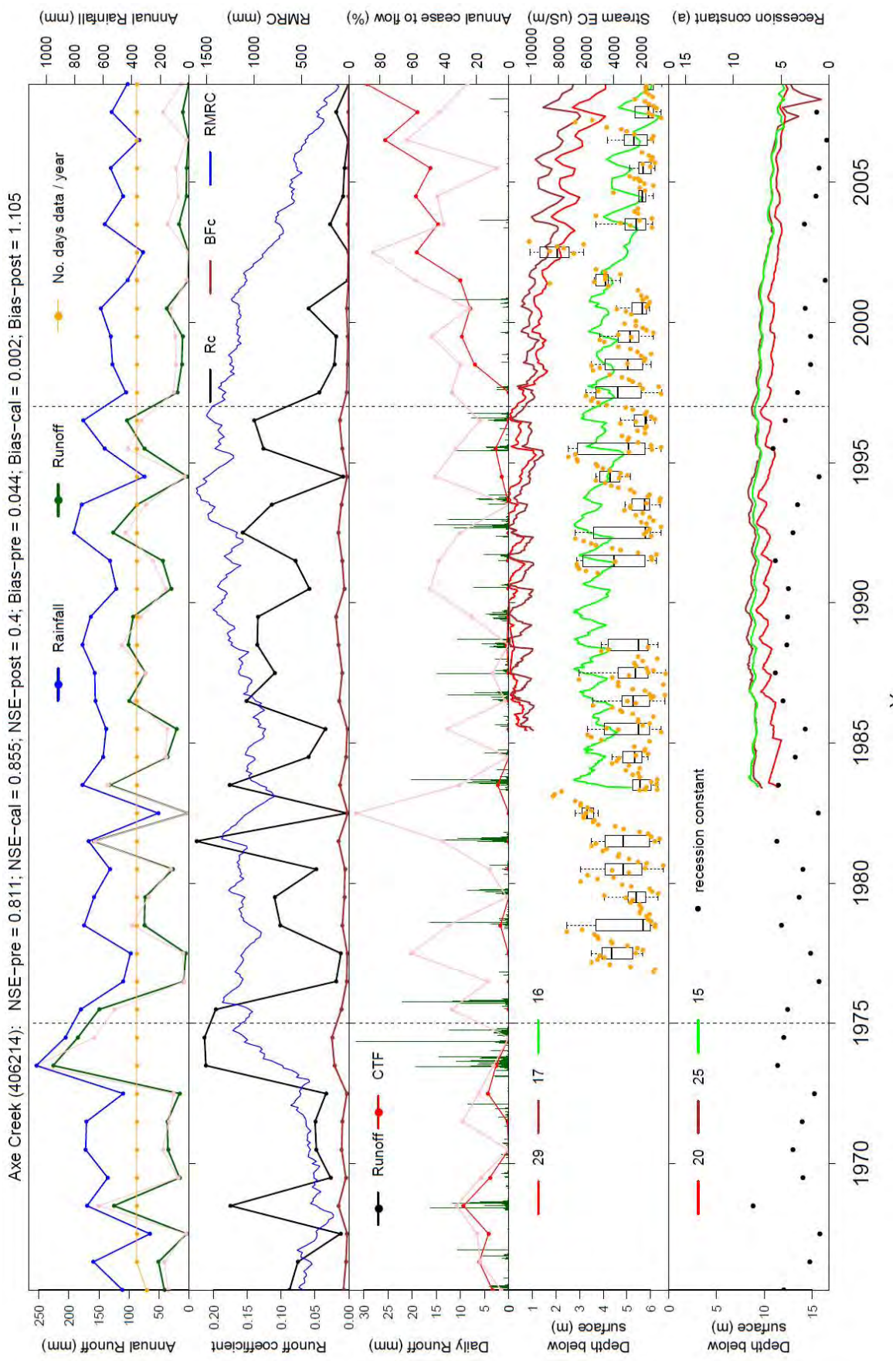

Figure 57. Hydrological metrics for Axe Creek.

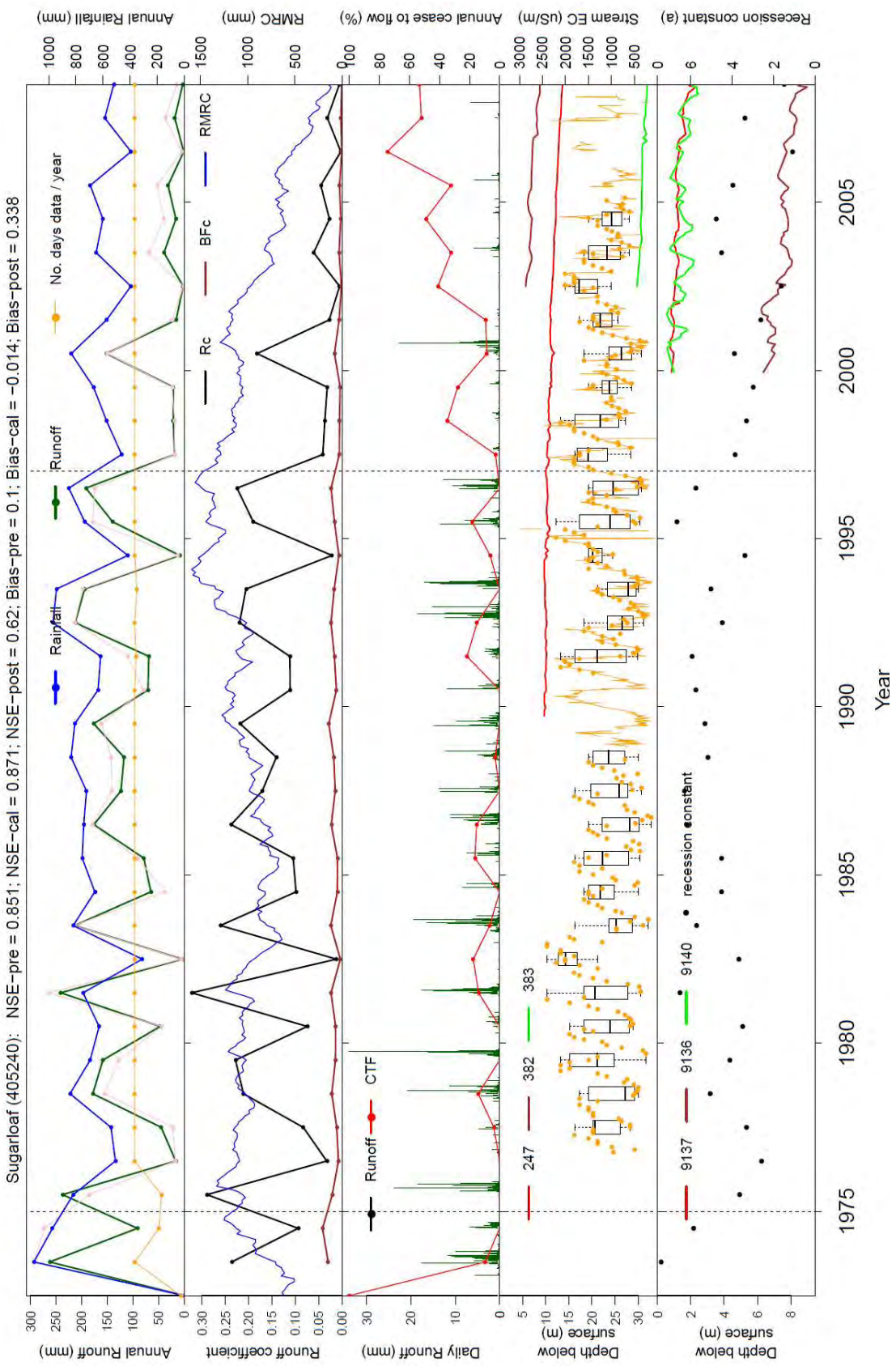

Figure 58. Hydrological metrics for Sugarloaf Creek

Conclusions

There were two studies in Project 2.2 in 2010/11. The first component of the first study examined changes in the relationship between rainfall, temperature and streamflow and the sensitivity of streamflow to rainfall and temperature. We found that:

- Rainfall–streamflow relationships and rainfall–maximum temperature relationships appear to be different during the recent drought compared to the long-term pre-drought period.
- The spatial coherence between these are fairly low, suggesting that while increased temperatures did play a role in reducing streamflow during the recent drought, other subsidiary features of the recent drought were important.
- Using a multiple regression approach, an average 46 percent reduction in streamflow was observed across the catchments, 65 percent of which was accounted for by reduction in annual rainfall during the recent drought, 7 percent was accounted for by increased annually averaged daily maximum temperature and 28 percent was unexplained.

The second component of the first study used traditional hydrological empirical techniques to investigate which components of the catchment water balance may have experienced change during the drought. We found that:

- During the drought, a statistically significant change (reduction) in daily rainfall occurred between the 10th and 40th percentiles.
- Very high daily rainfall percentiles (i.e. 1st percentile) during drought were not found to be statistically different from those prior to the drought, but about 80 percent of catchments in the southern half of the SEACI region exhibited a statistically significant difference (reduction) in the 1st percentile of daily runoff. This lends support for a deepening and 'drying' of the unsaturated zone and hence smaller areas of – and less frequently occurring – saturated overland flow.
- Runoff-generating processes changed to a greater extent in the low-rainfall catchments of the southern SEACI region than in the high-rainfall catchments. The percentage reduction in slow flow was very strongly correlated with the percentage reduction in total streamflow.
- More than 70 percent of catchments in the southern basin exhibited a statistically significant change (reduction) in recession coefficient *a* suggesting that during the recent drought there was a change in the aquifer storage – outflow relationship in these catchments.

The second study sought to develop a conceptual understanding for the change in the rainfall-runoff relationship. It was found that:

- Conceptual rainfall-runoff models calibrated between 1975 and 1996 simulated runoff in the years prior to 1975 well but simulated runoff increasingly poorly over the course of the drought.
- Prior to 1997, groundwater levels were in a pseudo-steady state, but during the drought they did not achieve a new steady state. Observations of cease-to-flow and streamflow EC provide strong evidence that the reduction in groundwater levels has resulted in a reduction in baseflow to the river.
- It is thought, however, that the majority of the reduction in streamflow in these catchments was due to an unprecedented deepening and drying of the unsaturated zone. Declining groundwater levels strongly imply a deepening of the unsaturated zone and more negative soil-water tensions, which would be likely to result in smaller areas of and less frequently occurring saturated overland flow.

Collectively, these results strongly suggest a change in hydrological behaviour during the recent drought and that the behaviour may have continued to change as the drought progressed. However, continued investigation is warranted. This is because conceptualising reasons for the change in rainfall-runoff relationship was confounded by uncertainty over the change in number of farm dams during the recent drought and the inability of conceptual rainfall-runoff models to simulate low-flow processes well. These confounding factors will be addressed in 2011/12 as part of the model development component of the work.

Links to other projects

Both projects in Theme 2 are closely related to, and use information from, the projects in Theme 1. The future climate input data used in Project 2.2 were derived in Project 2.1.

CHAPTER 6: PROJECT 3.1

Advancing seasonal predictions for south-eastern Australia

Eun-Pa Lim, Harry Hendon, Sally Langford and Oscar Alves

Abstract

This study assesses the improvements in seasonal climate forecasts for south east Australia (SEA) using the upgraded Bureau of Meteorology Predictive Ocean Atmosphere Model for Australia (POAMA2) compared to the previous POAMA1.5 system (POAMA1.5b). The main upgrades of POAMA2 are an improved method to initialise the ocean model and an improved method to generate the ensemble of forecasts. An ensemble of forecasts is made from slightly perturbed initial conditions and using three slightly different versions of the model in order to account for forecast uncertainty due to model errors and due to the sensitive dependence on the initial conditions, whose accurate depiction is limited by observational uncertainty. This comparative assessment is based on a set of re-forecasts for the period 1980-2010. The assessment focuses on improvements in forecast accuracy and other measures of forecast quality such as reliability (the average agreement between forecast probabilities and mean observed frequency of occurrence), sharpness (the tendency to forecast probabilities near zero or 100 percent) and resolution (ability of the forecasts to resolve events into different outcomes).

Compared to POAMA1.5b, POAMA2 demonstrates improved skill in predicting El Niño conditions in the Pacific and the Indian Ocean Dipole phenomenon especially the ocean surface temperatures in the eastern Indian Ocean (the eastern pole of the IOD). Both the IOD and El Niño are primary drivers of climate variations in SEA, and therefore, good climate predictions in SEA are predicated upon good predictions of these key drivers. One of the model versions of POAMA2 uses an explicit mean-state bias correction, which results in an improved representation of the effects of El Niño across SEA but unfortunately also results in slightly reduced ability to predict El Niño conditions in the Pacific.

Taking the benefits of improved ocean initial conditions and the improved method to generate forecast ensembles, POAMA2 demonstrates improved forecast accuracy for SEA for all seasons except for late autumn. Importantly, POAMA2 shows improved forecast reliability compared to POAMA1.5b. However, POAMA2 forecasts are far from being perfectly reliable. Calibration (post-processing) of the forecasts is shown to improve reliability but degrades sharpness. Multi-model ensemble forecasts using POAMA2 and 3 models that contributed to the European Union ENSEMBLES project are shown to be a good way of improving accuracy, reliability, and resolution without sacrificing sharpness.

Background

The Bureau of Meteorology makes seasonal climate forecasts using a coupled atmosphere ocean climate model (POAMA). The POAMA forecast system is continually being developed and has been recently upgraded to version POAMA2. The key upgrades over the older version POAMA1.5b are: (i) an improved initialisation of the ocean using the POAMA Ensemble Ocean Data Assimilation System (PEODAS; Yin et al., 2010); and (ii) an improved method of ensemble generation (increasing the ensemble to 10 members each from 3 slightly different versions of the model to better account for forecast uncertainty due to model error). The new ensemble generation strategy was motivated by SEACI1 work that showed that the seasonal climate forecasts from the older POAMA1.5 suffered from low reliability.

Objectives

- Assess improvements in forecast quality for SEA using POAMA2 compared to POAMA1.5b.
- Assess the forecast model's representation and prediction of the main mechanisms of climate variability that provide seasonal predictability of climate in SEA so as to guide future model development and to provide insight as to the degree that systematic model error is acting to limit forecast skill.
- Explore benefits for improved reliability by calibration (post-processing) of forecasts from POAMA2 and by combining POAMA2 forecasts with other available international model forecasts into a multimodel ensemble and provide uncalibrated and calibrated forecasts to Project 3.2.

Methods

Based on results of SEACI1 that indicated low reliability of the POAMA1.5 seasonal climate forecasts, a new ensemble generation strategy for POAMA2 was developed in order to improve forecast reliability. The strategy adopted three slightly different versions of the model in order to better represent forecast uncertainty due to model errors. One model version used exactly the same model physics as POAMA1.5b. The other two model versions used a slightly modified treatment of shallow convection (which helped to reduce model drift) but differed only in that an explicit bias correction was applied in one version in order to further limit climate drift. For each of the three model versions of POAMA2, 10 ensemble members were generated from slightly different initial ocean conditions provided by the new ocean assimilation system PEODAS. The ocean perturbations sample forecast uncertainty due to sensitivity to the initial state. In contrast, a single ensemble of 10 members was generated from POAMA1.5b. The set of re-forecasts (referred to as hindcasts) were generated from the first of each month for the period 1960-2010 (for POAMA2) and 1980-2010 for POAMA1.5b. The forecast duration was nine months. The comparison here focuses on the common period 1980-2010. Some limited comparison is also made to forecasts from three models that contributed to the EU ENSEMBLES projects.

Monthly mean forecasts from the models were verified against observed monthly mean analyses of sea-surface temperature, mean sea-level pressure, and Australian rainfall provided by Hurrell et al. (2008), NCEP2 (Kanamitsu et al., 2002) and the Australian Water Availability Project (AWAP) <http://reg.bom.gov.au/climate/austmaps/metadata-daily-rainfall.shtml>, respectively. In order to account for the mean model bias (climate drift), monthly mean forecast anomalies were generated by subtracting the model climatology based on the hindcasts 1980-2010. The model climatology is a function of forecast start month and lead time. Observed anomalies for each month and year were similarly developed by subtracting the observed climatology for the period 1980-2010.

Probabilistic forecasts for above/below median SEA Australian rainfall were verified for accuracy using hit rates (proportion of correct forecasts expressed in percentage and for reliability, resolution and sharpness using the construction of attributes diagrams, Figure 59). The ensemble mean forecast was assessed using correlation with the observed anomalies.

In order to provide insight as to the degree that systematic model error is limiting forecast skill and to help guide future model development, the representation and prediction of the main mechanisms of climate variability that provide seasonal predictability of climate in SEA are assessed. The key modes of tropical variability that affect SEA climate are the El Niño phenomenon, which we monitor with the NINO3 SST index (Figure 60a), east-west shifts of El Niño, which we monitor with the Modoki El Niño SST index (EMI) (Figure 60b) , and the Indian Ocean Dipole, which we monitor with the Diople Mode SST Index (DMI) (Figure 60c). We monitor ocean surface temperature variations in the eastern pole of the IOD using the Indian Ocean Dipole east SST index (IODE). Surface temperature variations in the IODE region are thought to be the primary source of tropical convective variability during IOD events that affect Australian climate (e.g. Cai et al. 2011). We also assess the representation and prediction of the dominant mode of extratropical atmospheric variability, the so called Southern Annular Mode (SAM; Figure 60d), which impacts rainfall in the far southern portion of SEA during winter and in the eastern portions of SEA in summer.

The direct rainfall forecasts from POAMA were also calibrated (post-processed) using an inflation of variance technique (Johnson and Bowler, 2009). This technique calibrates each ensemble member forecast to have the same variance as the observation but maintains the original forecast accuracy (i.e the correlation of the ensemble mean forecast with the verification). Calibration improves probabilistic forecast reliability while minimizing root-mean-square error of the ensemble mean forecasts.

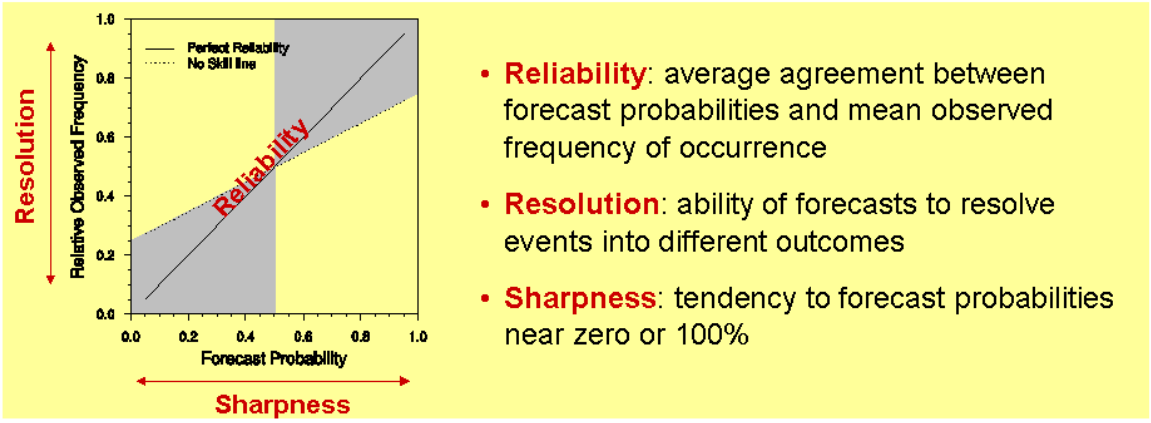

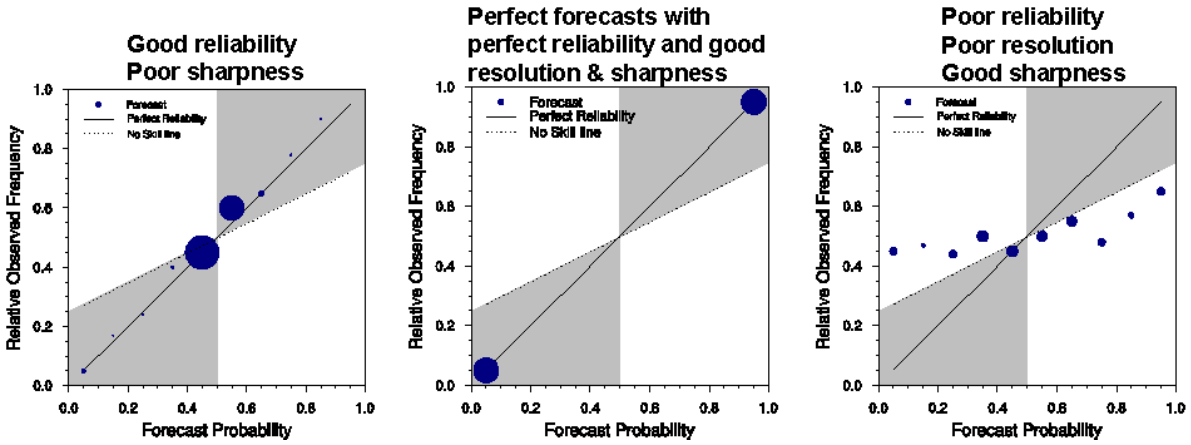

Figure 59. Example attributes diagrams for probabilistic predictions of the occurrence of a above/below median climate event. The size of the dot indicates the number of forecasts in each probability bin. Examples depict a range of reliability, sharpness and resolution, as indicated above each panel

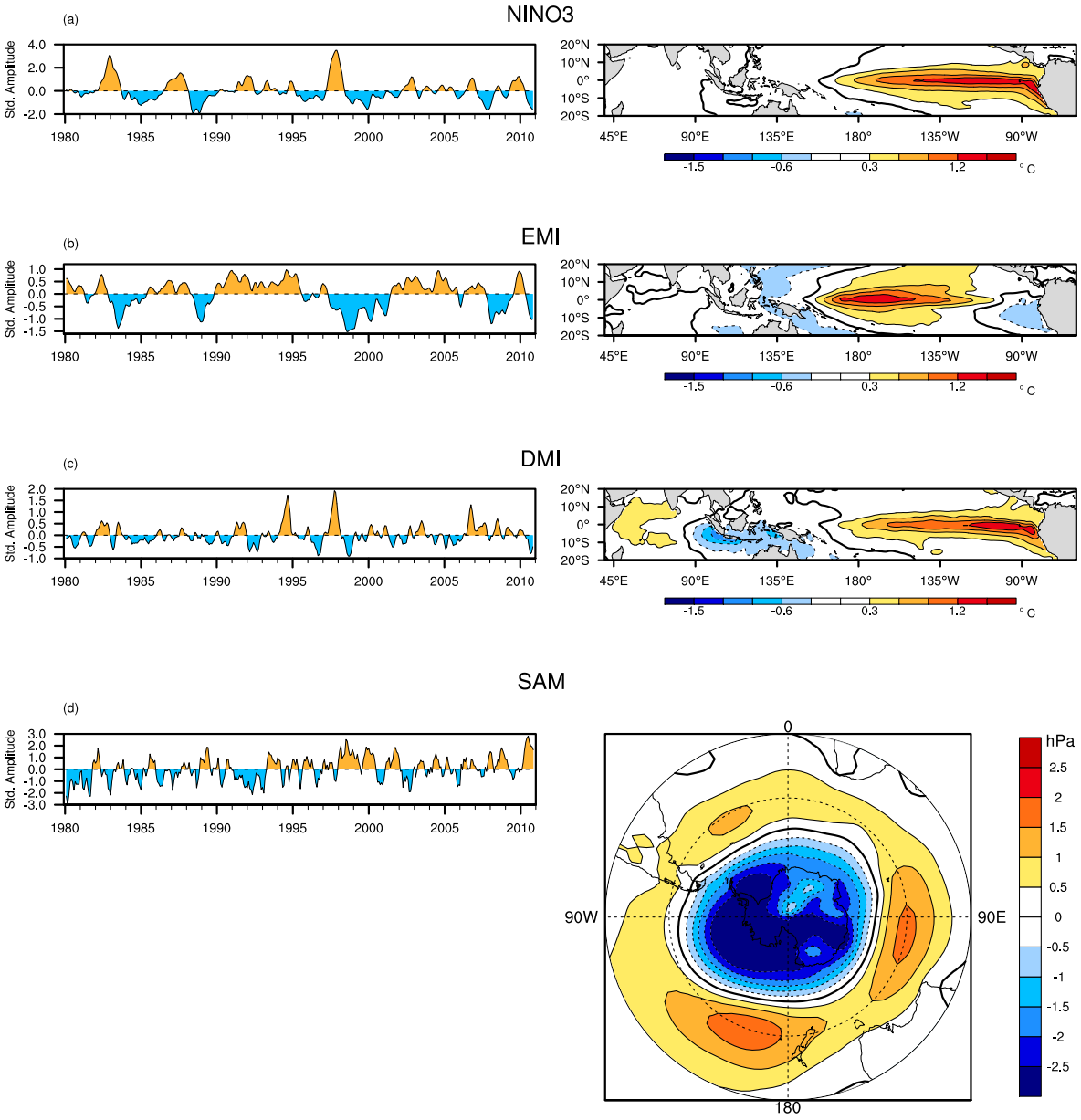

Figure 60. Left panels: Standardized time series of the monthly NINO3, EMI, DMI, and SAM indices based on observation 1980-2010. Right panels: Spatial patterns of the regression onto the time series in the left panels for sea-surface temperature (°C) for NIÑO3, EMI, and DMI, and mean sea-level pressure (hPa) for the SAM. Use of standardized indices means that the displayed spatial patterns have amplitude associated with a one standard deviation anomaly of the associated index

Results

Prior to assessing the POAMA forecasts, we begin by examining the observed relationship of SEA rainfall with El Niño, the IOD, and the SAM. The observed relationships between rainfall in SEA with these modes of climate variability indicates that the IOD (as monitored by the DMI) has the most dominant impact on rainfall across the southern portions of SEA during winter-spring (areas with red shading in Figure 61a). The influence of the two different types of El Niño is distinctive over SEA: eastern Pacific El Niño, as monitored by the NIÑO3 SST index, has the dominant impact on rainfall in the southern portions of SEA during late spring-early summer (green shades in Figure 61a), whereas central Pacific El Niños, as monitored by the EMI index, have the strongest impact on rainfall in the northern portion of SEA during late autumn-spring (blue shades in Figure 61a). The magnitude of the correlation between mean rainfall over SEA and these indices (Figure 61b) confirms the dominance of the IOD (as monitored by the DMI) on winter and spring rainfall. Noting that the IOD and El Niño are strongly related to each other in spring, the influence of El Niño, as measured by NINO3 SST index, is comparable to the IOD in this season. However, based on Cai et al. (2011), we now understand that the impact of El Niño on rainfall in southern portions of SEA in spring is largely produced via the co-varying surface ocean temperatures in the Indian Ocean associated with the IOD. So, the apparently strong impact of El Niño as indicated in Figure 61b means that forecasts of SEA rainfall during El Niño will be limited by the ability to predict the IOD.

(a) (b)

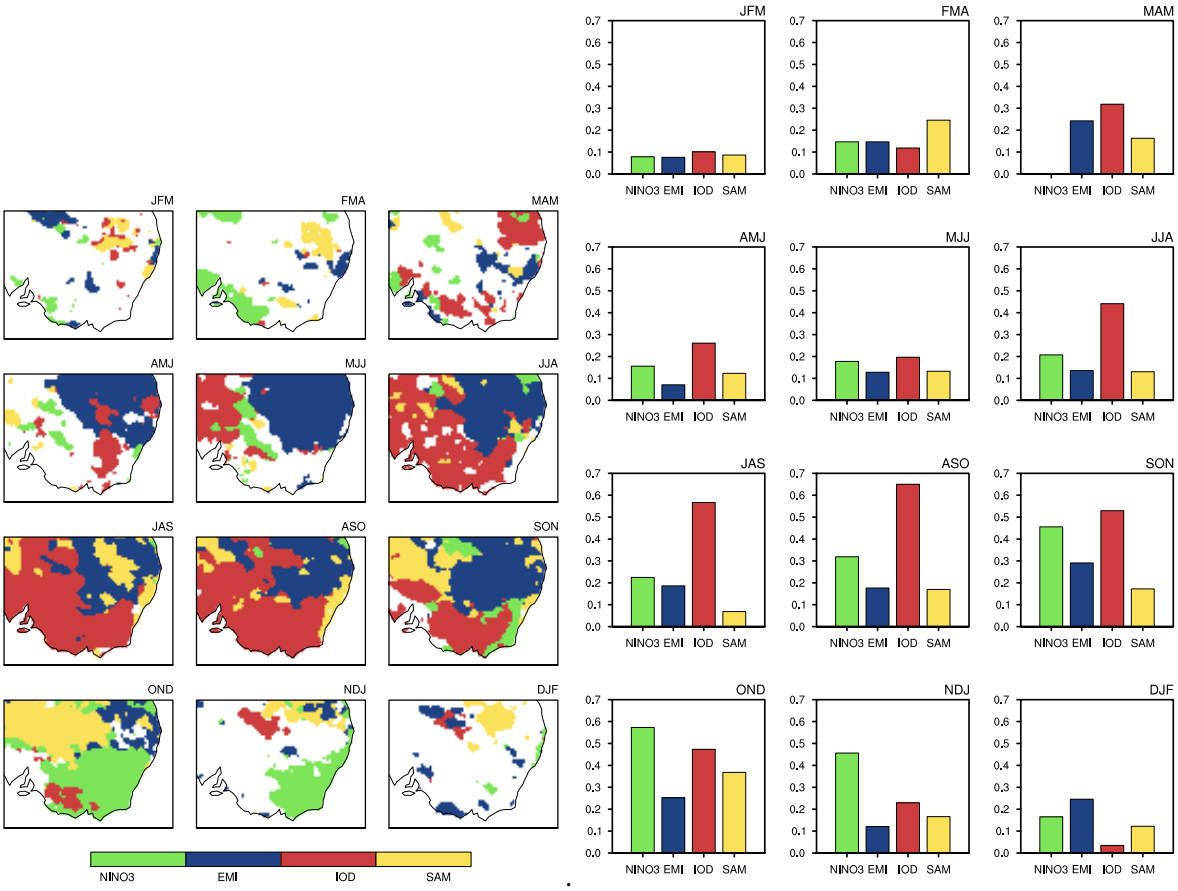

Figure 61 (a) Shading indicates which index (NINO3, EMI, DMI or SAM) has the largest correlation with observed rainfall 1980-2010. Correlations were computed for the indicated 3 month mean seasons. (b) The magnitude of the correlation between the mean rainfall over south-eastern Australia and each of the indices.

The ability to predict the key modes of variability that affect SEA rainfall is assessed by scoring the forecasts of the NINO3, EMI, and DMI SST indices and the SAM index. Here, forecast accuracy is assessed using the correlation of the ensemble mean forecast of these indices with the verifying analysis (Figure 62). For this analysis, forecasts and verifying analysis are for 3-month means. Forecasts from POAMA2 show a good improvement in accuracy compared to POAMA1.5b for prediction of the occurrence of El Niño, as monitored by the NINO3 SST index, at all lead times to 9 months. A more modest improvement in predicting east-west shifts of El Niño is evident for the EMI. The improvement in predicting NINO3 SST index is found regardless of the starting month for the forecast (Figure 63a), whereas the improvement in predicting east-west shifts of El Niño using the EMI SST index is limited for forecasts initialised in the second half of the year (Figure 63b). In contrast to the improvement for prediction of El Niño, the prediction of the IOD is less skilful in POAMA2 than POAMA1.5b, as evidenced by the lower correlation for the DMI index (Figure 62c). Nevertheless, forecasts initialised prior to the maturation of the IOD in September through November have better skill in POAMA2 than POAMA1.5b especially at longer lead times (Figure 63c). In addition, skill in predicting the sea surface temperature in the eastern Indian Ocean, as monitored with the IODE SST index, is significantly higher in POAMA2 than POAMA 1.5b for forecasts initialised after July (Figure 63d). Because the surface temperature variations in the eastern Indian Ocean are a primary source of atmospheric variability over SEA (e.g. Cai et al. 2011), this improved prediction of the IODE SST index provides hope for improved prediction of SEA climate with POAMA2.

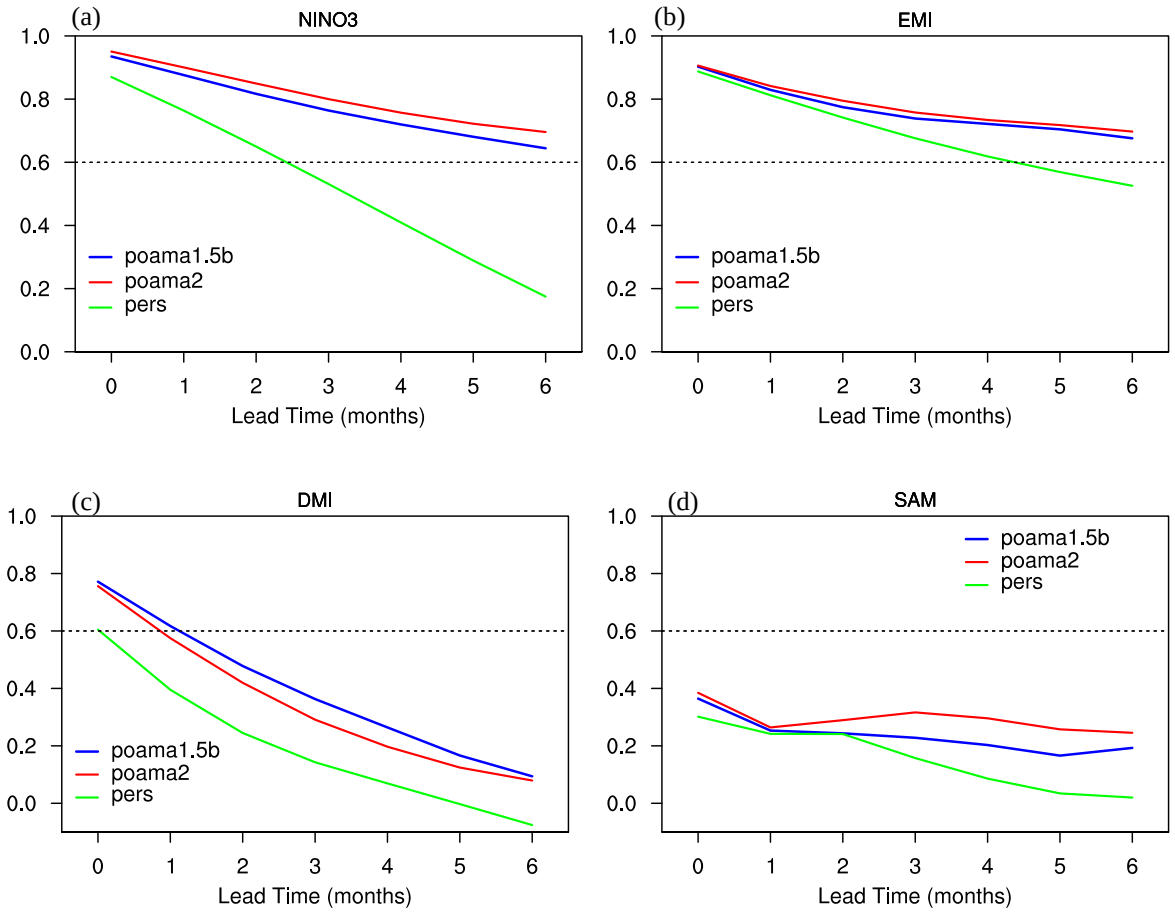

Figure 62. Forecast accuracy as measured by correlation of the ensemble mean forecast with the verifying observations as a function of forecast lead time for the (a) NINO3; (b) EMI, (c) DMI, and (d) SAM indices. Forecasts scores from POAMA2 are in red, from POAMA1.5b in blue and a reference persistence forecast is in green. Forecasts and verification are for 3 month means

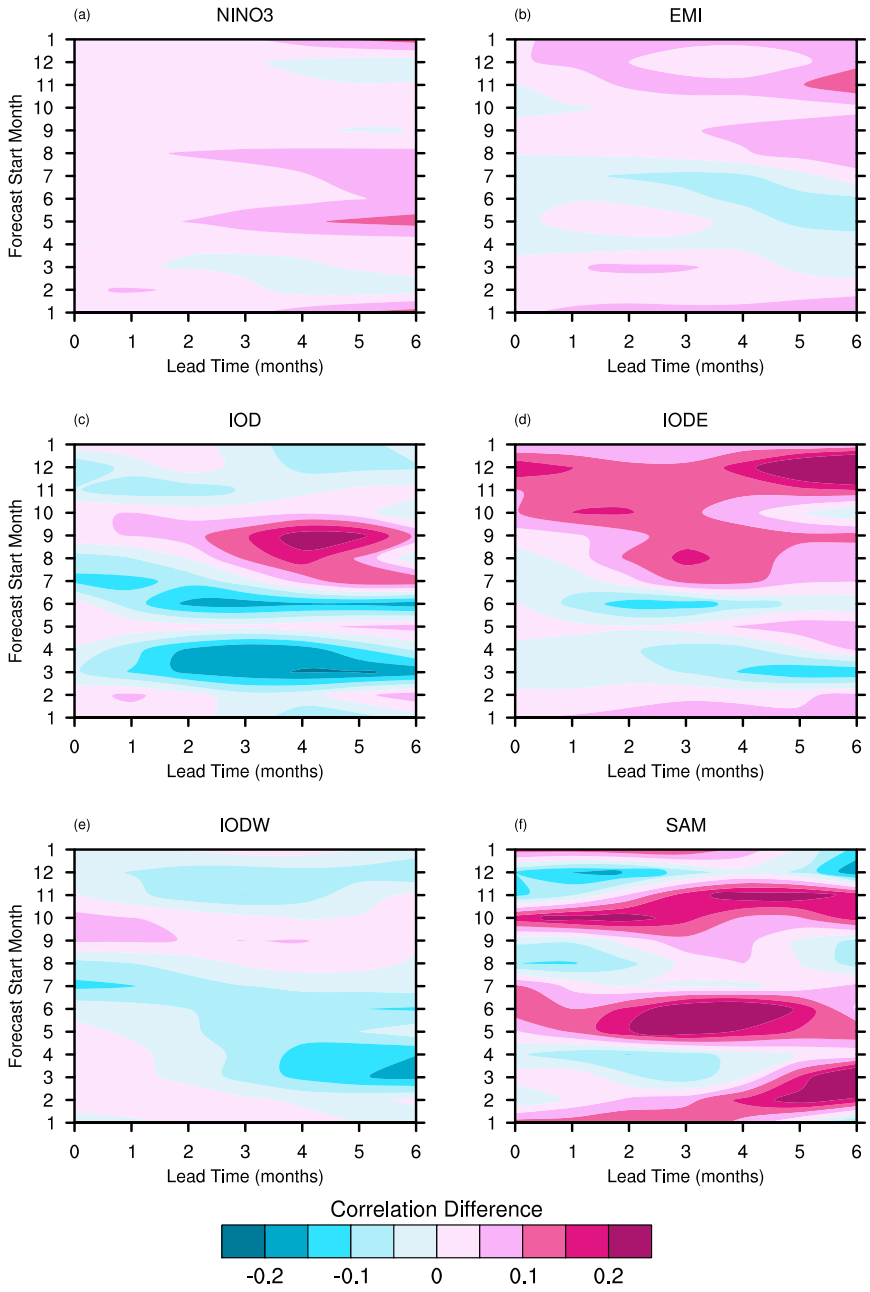

Figure 63. Difference in forecast accuracy between POAMA2 and POAMA1.5b as measured by difference in the correlation of the ensemble mean prediction with verifying observations as a function of forecast start time and lead time for the (a) NINO3; (b) EMI, (c) DMI, (d) IODE SST index, (e) IODW SST index, and (f) the SAM index. Pink (blue) color shadings indicate the increase (decrease) of forecast accuracy by POAMA2 compared to POAMA1.5b

POAMA2 provides improved seasonal prediction of the SAM after lead time 1 month (Figure 62d), although the level of forecast skill is, not-surprisingly low (i.e., we do not expect high skill for predicting the SAM at long lead time because the SAM is primarily an internal mode of variability in the atmosphere with a characterstic decorrelation time of ~10 days). Nonetheless, we made a preliminary investigation of the feasibility of predicting the monthly SAM. The monthly SAM can be skilfully predicted by POAMA2 in the first month of the forecasts and is better than a persistence forecast (Figure 64), indicating that the POAMA model is able to represent some aspects of the future evolution of the SAM that depend on the initial conditions (presumably mainly due to atmospheric initial conditions). However, we also see that forecasts of the SAM that verify in late spring months are feasible by POAMA2 for lead times up to 8 months, which we attribute to the association of the SAM with El Niño in this season (L'Heureux and Thompson, 2006).

Consequently, spring season mean SAM is predictable by POAMA2 with a lead time of up to 3 months (Figure 64b).

Figure 65 provides a summary of the predictive capability of POAMA2 for the key modes of climate variability that influence SEA rainfall. Predictive skill for eastern and central Pacific ENSO is very high throughout the year and at lead times to at least 3 months. On the other hand, the predictive skill for the IOD and the SAM is highly seasonal, but higher skill is found in the seasons when IOD and SAM are important to rainfall in SEA (winter to spring for IOD and late spring for SAM).

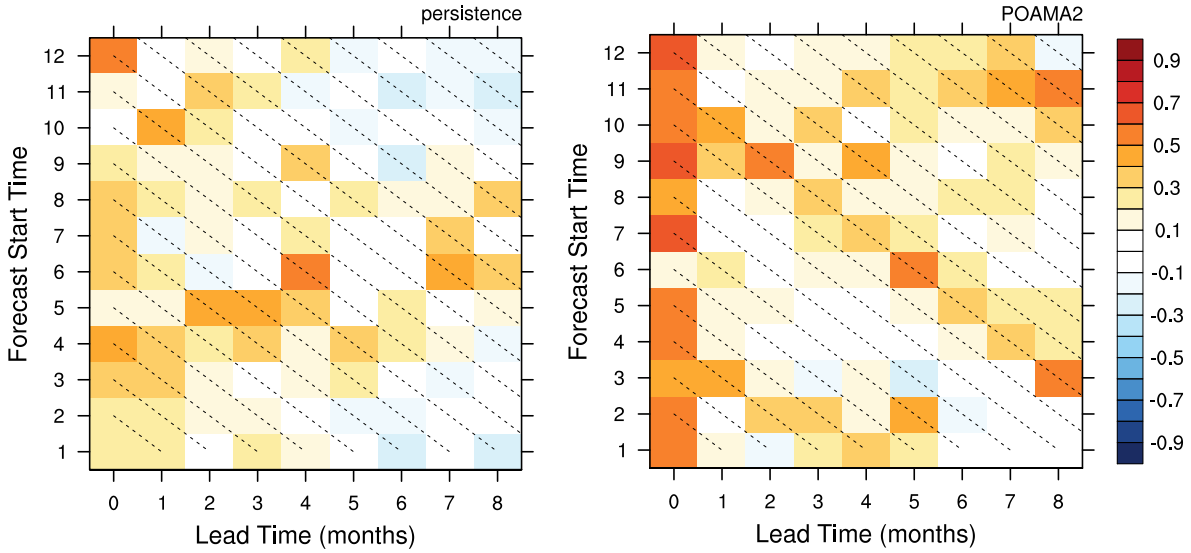

Figure 64. Forecast accuracy for predicting the monthly SAM index using a persistence forecast (left) and POAMA2 (right). Forecast accuracy, as a function of start month (ordinate) and lead time in months (abscissa), is measured using correlation of the ensemble mean forecast with the verification. Sloping dotted lines indicate a constant verification time (as indicated by the intersection of the lines with the ordinate)

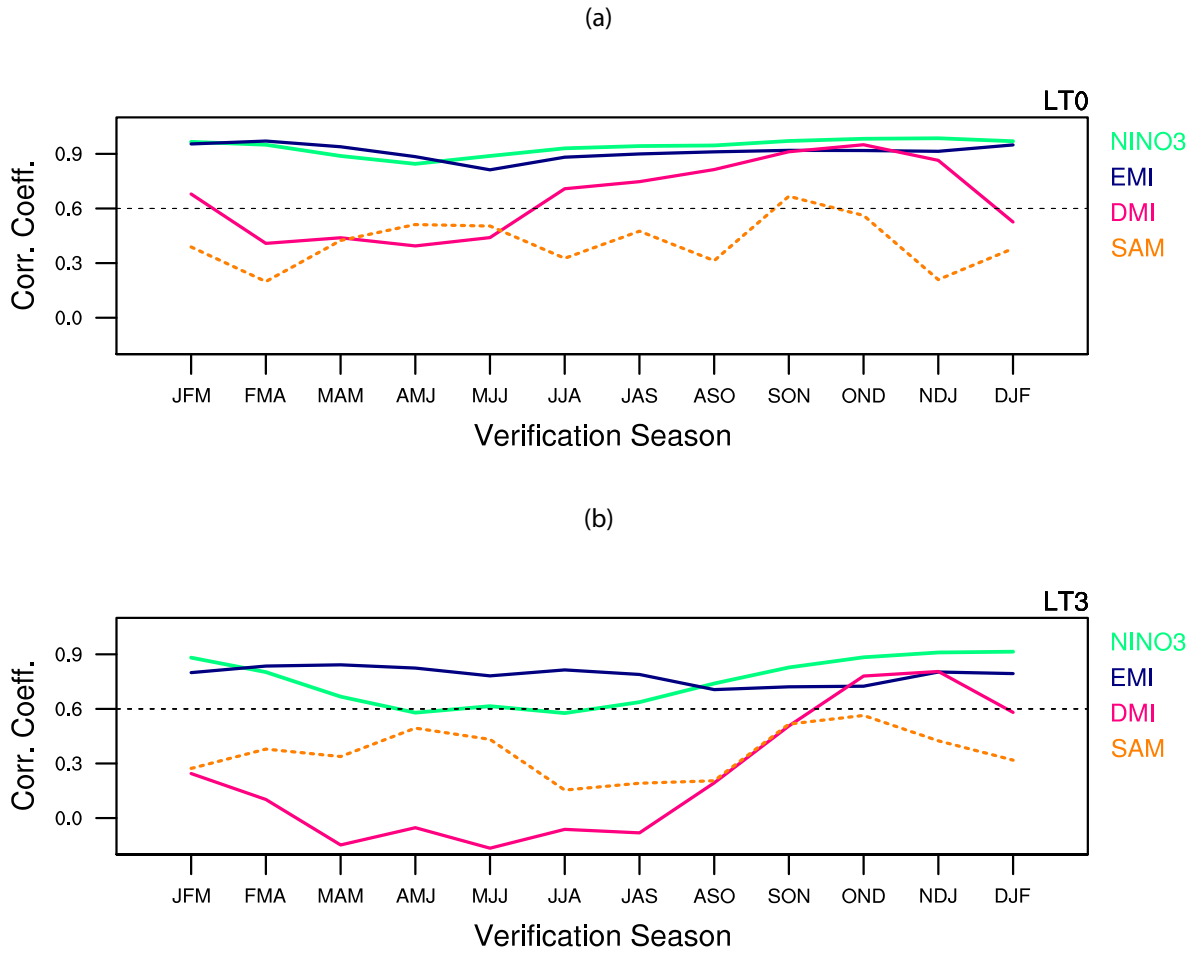

Figure 65. Forecast accuracy, as measured by correlation of the ensemble mean prediction with the verifying analysis, for the NINO3, EMI, and IOD SST indices and the SAM index for 3 month mean data at lead time (a) zero month and (b) 3 month.

In SEACI1 and SEACI1P, it was shown that the systematic surface cold bias over the entire tropical Pacific and warm bias off the west coast of South America in the POAMA1.5b model results in a westward shift of the maximum variability of sea-surface temperature associated with El Nino, thus hindering the skilful prediction of different types of ENSO and their impact on Australian rainfall using POAMA1.5b (Hendon et al., 2009). In developing POAMA2, we attempted to reduce the model's mean surface temperature bias using two distinct approaches. We used a slightly different treatment of shallow convection that resulted in slightly less model drift. However, to more fully alleviate the model drift, we also used an explicit flux correction that virtually eliminated all of the drift in the surface climate. In particular, the flux correction effectively removes the cold bias in the tropical Pacific, thereby improving the model's ability to distinguish the spatial patterns of ocean surface temperature associated with eastern Pacific and central Pacific El Niños. The predicted patterns of SST variation associated with eastern Pacific El Niño and central Pacific El Niño using the flux-corrected version of the model are more similar to their observed counterparts than are those from the non-flux corrected version of the model (*not shown). Both versions of the model, however, continue to produce patterns of surface temperature variation for the two types of El Niño that are more similar to each other than is observed (Figure 66).*

Flux correction is also seen to improve the representation of the impact of El on Australian rainfall, especially in winter and at short lead times (Figure 67). In the non-flux corrected version of the model, the model's representation of the impact of eastern Pacific El Niño (as monitored with the NINO3 SST index) on rainfall becomes spuriously positive at lead times 1 month and longer (Figure 67a). Flux correction at least postpones this spurious impact to lead times beyond 2 months. And, the impact on rainfall by central Pacific El Niño (as monitored by the EMI) is better simulated to lead times of at least 3 months (Figure 67b). These improvements in the representation of the impact of El Niño on Australian rainfall appear to improve the predictive skill for rainfall in north-east SEA, where El Niño has the largest impact on rainfall in winter (Figure 67c).

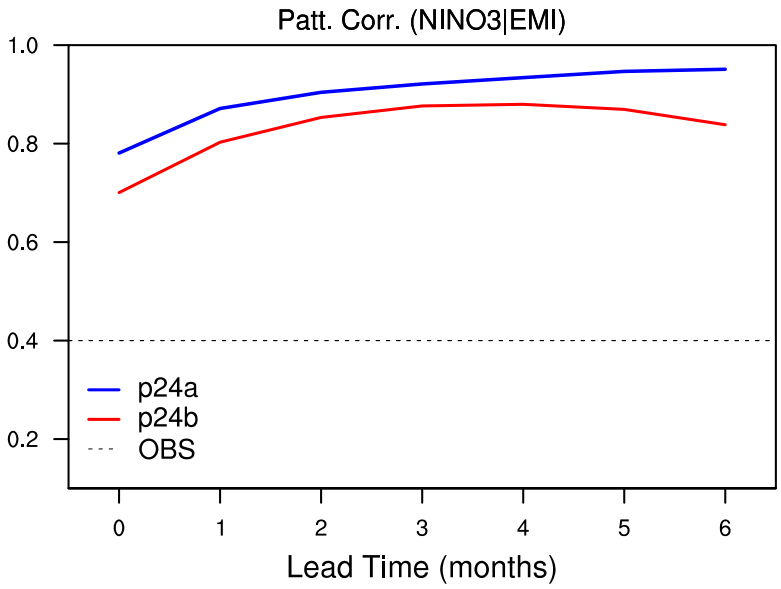

Figure 66. Pattern correlation between eastern Pacific and central Pacific El Niños from non-flux corrected forecasts (p24a;blue), flux corrected forecasts (p24b;red) and based on observations (dotted). The correlations from POAMA are shown as a function of forecast lead time (months)

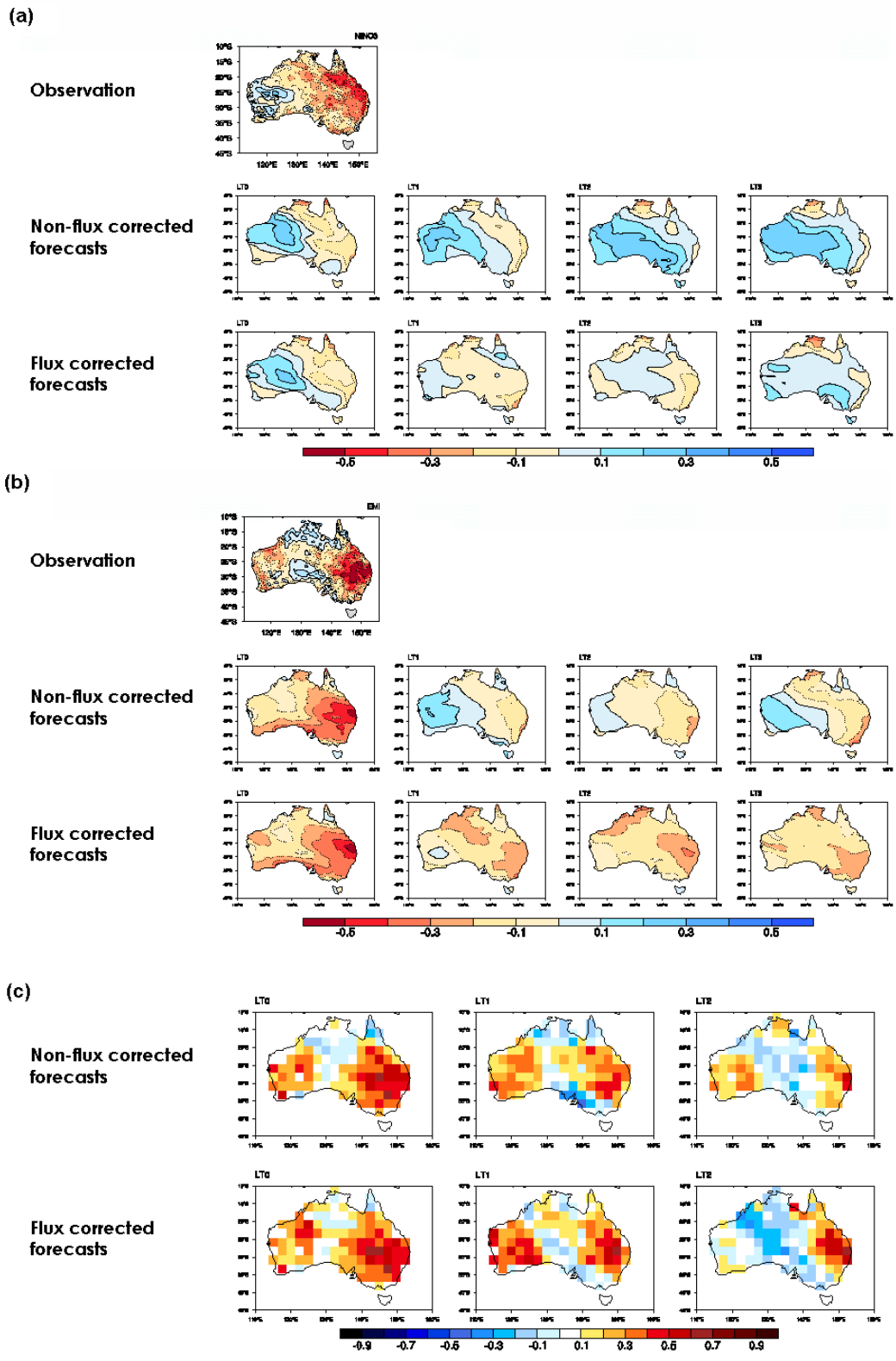

Figure 67. Correlation of Australian rainfall in June-July-August with (a) the NINO3 index and (b) the El Niño Modoki Index (EMI). In (a) and (b) correlation based on observation is compared to non-flux-corrected and flux-corrected forecasts at lead times of zero to 4 months over 1980–2010. (c) Predictive skill (as measured by correlation of ensemble mean forecast) of winter rainfall at lead times from zero to 2 months

Finally, flux correction improves the mean position and intensity of the STR over eastern Australia in all seasons except for summer (not shown). Despite all these benefits of flux correction for depiction of variability within the forecasts, flux-corrected forecasts are not as skilful as non-flux-corrected forecasts in predicting the occurrence of El Niño and the IOD. Therefore, the final configuration of the POAMA2 ensemble generation method combined forecasts from three different versions of the model: non-bias-corrected, reduced bias by altered model physics, and explicit bias correction.

We now compare forecast skill for predicting SEA rainfall using POAMA2 and POAMA1.5b. Seasonal rainfall for SEA is skilfully predicted both POAMA1.5b and POAMA2 for all seasons except late autumn and summer, as seen by hit rates for the prediction of above median (also called proportion correct or percent consistent score) greater than 55 percent over the majority of the region for lead time 1 month (Figure 68). Hit rates exceeding 50 percent are evident for forecasts to 3 months lead time for the later part of the year (late winter to early summer; not shown). Although hit rates are comparable between POAMA1.5b and POAMA2, POAMA2 has overall higher skill. Furthermore, POAMA2 has improved reliability (Figure 69), especially if forecasts for the entire country are considered (not shown). Forecast reliability can be further improved by post processing (calibration with an inflation of variance method; right hand panels in Figure 69) but at the expense of reduced sharpness and, to a lesser degree, reduced resolution.

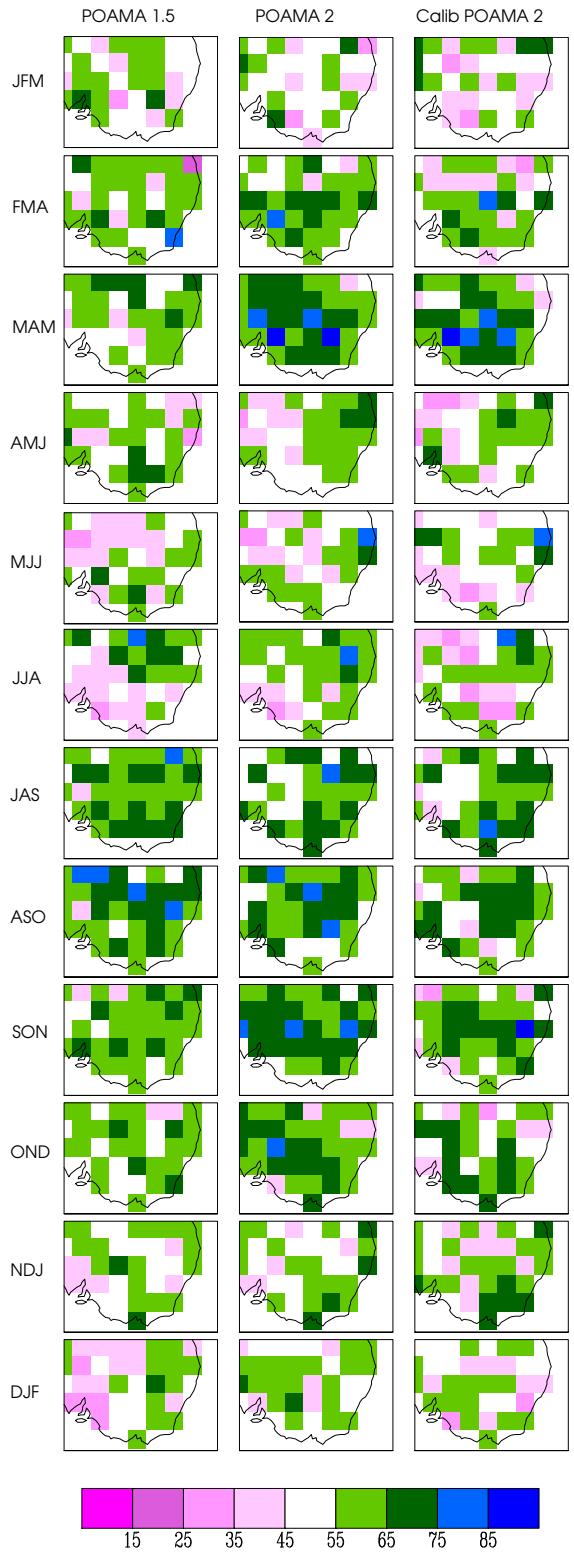

Figure 68. Hit rates (proportion of correct forecasts expressed in percentage) for predicting seasonal rainfall to be above median in POAMA1.5, POAMA2 and calibrated POAMA2 at a lead time of 1 month

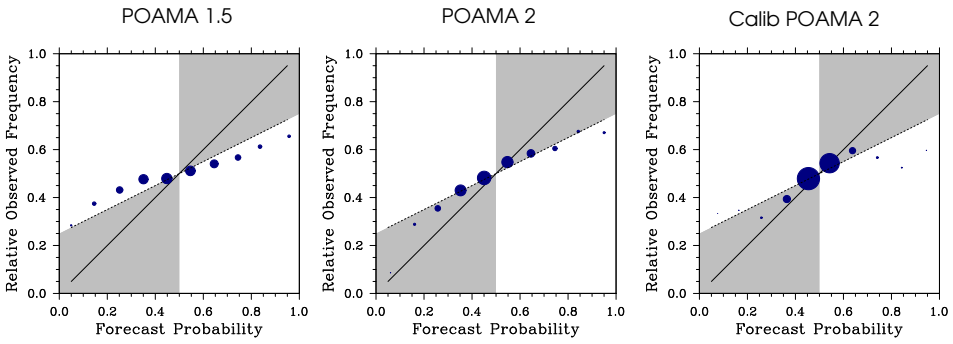

Figure 69. Attributes diagrams of POAMA1.5b, POAMA2 and calibrated POAMA2 forecasts of above-median rainfall, over all grid points of south-eastern Australia for all 12 seasons in 1980–2006 at a lead time of 1 month. Perfectly reliable forecasts should line up with the diagonal line. Forecasts in the grey areas are considered to be reliable, as they are correct in predicting the occurrence or non-occurrence of an event and their errors are smaller than a climatological forecast. The size of dots represents forecast frequency in each probabilistic forecast category

Finally, we compare the rainfall forecasts from POAMA2 to those from 3 models that contributed to the EU ENSEMBLES project (Weisheimer et al., 2009) in order to assess common successes/failures and to understand the benefit of true multi-model ensembles for Australian rainfall forecasts. This investigation suggests that as a single model, the ECMWF system3 has slightly higher skill for predicting Australian rainfall than any of the three single versions of POAMA2, whereas other ENSEMBLE models show similar or less skill than the single versions of POAMA2. However, the full 30 member ensemble of POAMA2 forecasts presents comparable or even slightly higher skill than ECMWF system3 over SEA in terms of both hit rates and reliability (Figure 70). Hit rates and reliability of predicting rainfall in SEA can be further increased beyond the best single model or POAMA2 if a multi-model average is created consisting of POAMA2 and the forecasts from the ECMWF, UK Met Office and Meteo-France forecast systems. In particular, this multi-model approach not only improves forecast reliability but also forecast resolution and sharpness, which are the forecast qualities that are difficult to increase unless independent information is added to the forecast system (Stephenson et al., 2005; Doblas-Reyes et al., 2006). For instance, statistical calibration improves forecast reliability but tends to reduce forecast sharpness while the multi-model ensemble improves all of them (Figure 70b). Therefore, given the current capability of dynamical models, the multi-model ensemble approach is likely to be the best way of improving seasonal predictive skill and quality for regional climate.

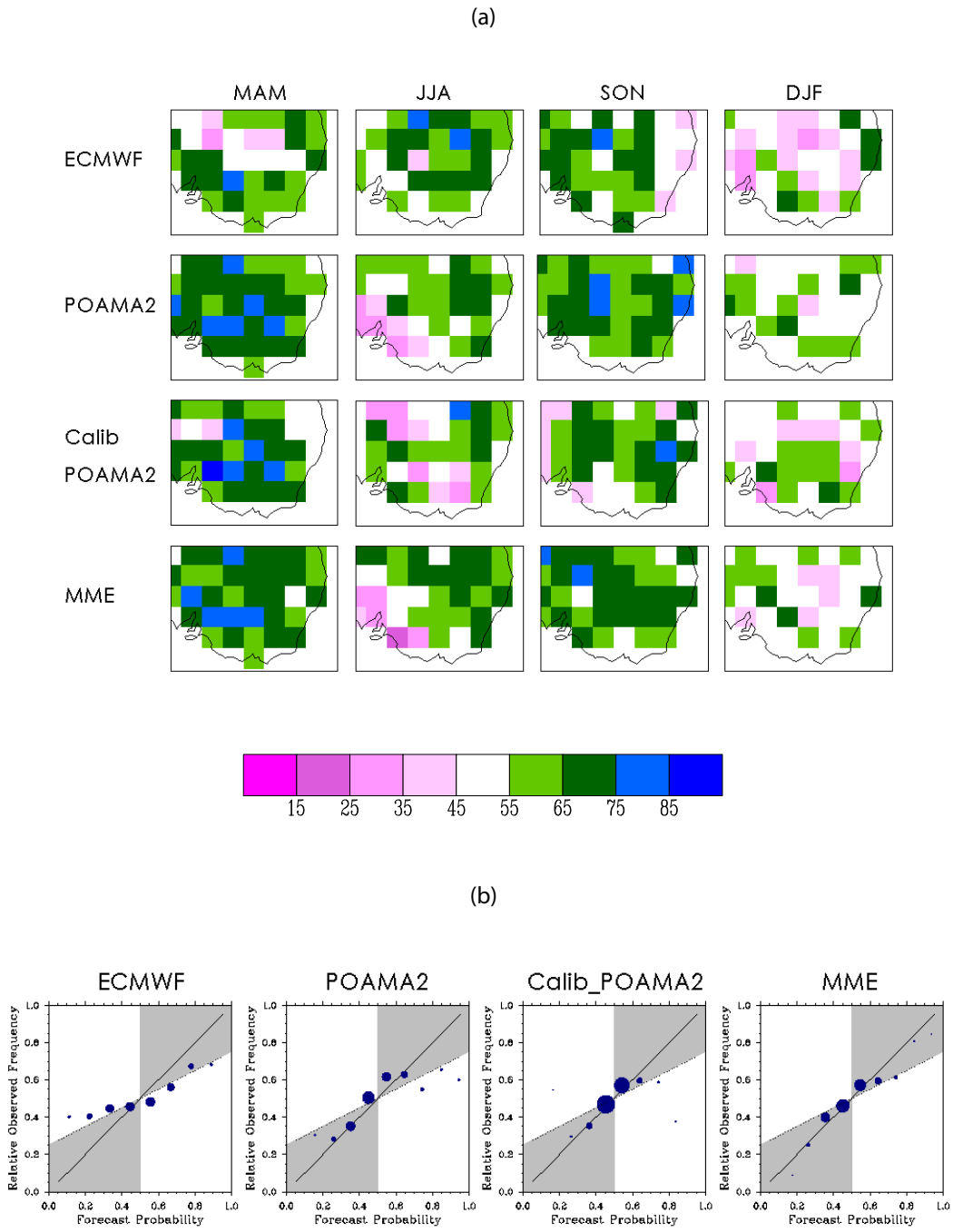

Figure 70. (a) Hit rates and (b) attributes diagrams for predicting seasonal rainfall over south-eastern Australia to be above the median at a lead time of 1 month for four models: the European Centre for Medium-Range Weather Forecasts system 3 (ECMWF), POAMA2, calibrated POAMA2, and a multi-model ensemble system consisting of POAMA2, ECMWF, UK Met Office, and Meteo-France forecast systems. Forecasts over all grid points of SEA for the four major seasons in (a) are used in (b)

Conclusions

As part of a continuous effort to improve the seasonal forecasting capability using the POAMA forecast system, a major upgrade has been made to POAMA (POAMA2) by improving the ocean initial conditions and the ensemble generation strategy. The improved ocean initial conditions, which are the source of long lead seasonal predictability, are provided by the new POAMA Ensemble Ocean Data Assimilation System (PEODAS). The new ensemble generation strategy produces a 10 member ensemble from 3 slightly different versions of the model. By combining three different model versions, forecasts from POAMA2 obtain the benefit of a multi-model approach (e.g. improved reliability without loss of sharpness) that offsets model errors.

Our investigation shows that POAMA2 has improved skill compared to POAMA1.5b for predicting the occurrence of different types of El Niño in the Pacific and for predicting sea-surface temperature variations in the eastern Indian Ocean associated with the IOD. El Niño and the IOD are key sources of rainfall variability in SEA in winter and spring, so this improvement in the prediction of the occurrence of El Niño and the IOD is a positive step toward improved prediction of SEA climate. POAMA2 also shows improved prediction of the SAM compared to POAMA1.5b, although the level of forecast skill remains relatively low except for late spring. Skilful prediction of SAM in the late spring is indicated to a lead time of 3 months, which we attribute to the association of the SAM with El Niño in this season.

The explicit flux-correction adopted in one version of POAMA2 effectively eliminates the tropical Pacific cold bias of the earlier versions of POAMA. This improved simulation of the mean state leads to better simulation of spatial patterns of sea-surface temperature variations associated with different types of El Niño, thus resulting in a more faithful representation of the impact of El Niño on SEA rainfall. Although forecasts from the bias corrected version of POAMA demonstrate improved representation of the relationship of Australian rainfall with El Niño, the predictions of the occurrence of El Niño and the IOD are not as accurate as those from the non-flux corrected models. This result emphasizes the need to improve the representation of the mean state in future versions of the POAMA system but it also indicates that more work is required to understand what is controlling forecast skill for El Niño.

Forecast skill from POAMA2 is comparable but slightly improved to that from POAMA1.5b in regard to forecast hit rates for rainfall exceeding the median over SEA. POAMA2 forecasts also have slightly better reliability due to the improved ensemble generation approach (this is much more apparent if all Australian land points are considered). Forecast reliability can be further improved by calibrating the forecasts with an inflation of variance technique. Although this technique significantly improves forecast reliability, it does so at the expense of forecast sharpness. Hence, there is no substitute for continued reduction in model error in order to improve forecast quality. The analysis of the representation of the relationship of the key modes of tropical variability with Australian rainfall indicates that forecast skill is being limited by model error and the upper limit of forecast skill has yet to be achieved. The systemtic westward shift of El Niño variability in the model contributes to this error, however there are probably other factors involved as well (e.g. bias in the latitudinal profile of the zonal wind) that need to be identified in order to progress the development of future versions of POAMA.

Finally, we have assessed the seasonal forecasts from three of the models that contributed to the ENSEMBLES project (ECMWF, UK Met Office and Meteo-France). Seasonal forecasts of Australian rainfall from these systems are comparable in skill to those from POAMA2, while a multimodel forecast based on POAMA2 and these three models is overall the best forecast both in terms of accuracy and also reliability and sharpness. Until key model errors are eliminated in the POAMA system, a multi model approach appears to be the optimal method for providing regional climate forecasts with good forecast accuracy, reliability, resolution and sharpness. Nonetheless, the good progress from POAMA1.5b to POAMA2 suggests that it is feasible that accurate and reliable forecasts can be produced by a future version of POAMA.

Links to other projects

This project is linked to Project 3.2, which plans to use downscaled and calibrated POAMA outputs to drive a hydrological model for streamflow predictions and to Project 1.1 explores the mechanism of climate variability in SEA..

CHAPTER 7: PROJECT 3.2

Hydrological application of seasonal predictions

QJ Wang, David Robertson and Prafulla Pokhrel

Abstract

Previous work undertaken through SEACI established forecasting models by selecting predictors that use observed catchment and climate indices to represent the:

- catchment condition at the forecast time
- climate during the forecast period.

In the second year of Phase 2 of SEACI, methods for incorporating the output of dynamic hydrological and climate models into the Bayesian joint probability modelling approach for seasonal streamflow forecasting have been investigated. Simulations from a dynamic hydrological model that represent the catchment condition at the forecast time were used to replace the selected predictors representing catchment condition at the forecast time, while seasonal rainfall forecasts from a dynamic climate model were used to replace selected predictors representing climate during the forecast period. These methods were evaluated for 21 catchments in eastern Australia that experience a wide range of hydrological and climate conditions.

For catchment condition, replacing the selected predictors with hydrological model simulations resulted in little change in the predictive skill, reliability and robustness of streamflow forecasts. However, the use of hydrological modelling output for operational forecasting is attractive in that it eliminates the need for selecting predictors. As a result, it reduces the computational requirements to establish forecast models, and skill estimates based on forecasts of historical events are not artificially inflated, as can be the case with predictor selection.

For climate, replacing the selected predictor with seasonal rainfall forecasts produced by a dynamic climate model produced mixed results, with increases in predictive skill of streamflow forecasts for some seasons and decreases in others. Bayesian model averaging over forecasting models that consider a range of climate predictors – including both climate indices and POAMA rainfall forecasts – appears to be an appropriate technique to produce forecasts that capture the strengths of all candidate predictors. However, the efficacy of Bayesian model averaging has yet to be appraised for seasonal streamflow forecasting and will require further research.

A highlight of the project is the adoption of the Bayesian joint probability modelling approach and current research results by the Bureau of Meteorology. The Bureau officially commenced issuing seasonal streamflow forecasts for 21 locations in SEA to the public in December 2010.

Background

Forecasts of future seasonal streamflows are potentially valuable to a range of water managers and users, including irrigators, urban and rural water-supply authorities, environmental managers and hydroelectricity generators. Such forecasts can inform planning and management decisions to maximise returns on investments and available water resources and to ensure security of supply (Plummer et al., 2009).

Previous SEACI research has led to the development of a statistical method, the Bayesian joint probability (BJP) modelling approach, for forecasting seasonal streamflows at multiple sites (Wang et al., 2009; Wang and Robertson, 2011). The BJP approach uses a multivariate distribution to model the joint distribution of future streamflows and their predictors such as antecedent streamflows, El Niño – Southern Oscillation (ENSO) indices, and other climate indices. The model parameters and their uncertainties are inferred from historical data using a Bayesian method. Occurrences of zero streamflows are treated as censored data, having unknown precise values but equal to or below zero, in model parameter inference. The parameters are then used to produce joint probabilistic forecasts of streamflows at multiple sites for future events. Censored predictor values are augmented to 'known' values, and negative values in streamflow forecasts are converted to zero.

A rigorous predictor selection method has also been established which selects predictors using the pseudo-Bayes factor, a measure of the predictive performance of forecasting models. Predictors representing the catchment condition at the forecast time are selected from a pool of indices comprising antecedent streamflow and rainfall totals based on their ability to predict streamflows. Predictors representing the climate during the forecast period are selected from a pool of climate indices based on their ability to forecast rainfall. The final forecasting models combine the selected predictors to jointly forecast seasonal streamflow and rainfall at multiple sites.

The observed indices used as predictors are simple and cannot fully describe the complexity of conditions at the time of forecast or how those conditions may evolve during the forecast period. Dynamical hydrological and climate models explicitly simulate the detailed dynamics of catchment or climate processes and therefore output from these models may better reflect the true sources of predictability. In the second year of Phase 2 of SEACI, work has focused on developing and evaluating methods for using the output of dynamic hydrological and climate models in the BJP modelling approach.

Objectives

The overall project objectives are to:

- further develop and evaluate the BJP modelling approach for seasonal streamflow forecasting
- incorporate dynamic climate and hydrological modelling into the BJP modelling approach
- transfer the technology for practical applications.

Specific objectives of the project in 2010/11 were to:

- develop methods to incorporate dynamic climate and hydrological modelling into the BJP modelling approach
- evaluate the performance of forecasts made using the developed methods on catchments experiencing a range of climate and hydrological conditions typical of SEA
- transfer the technology of the BJP modelling approach for applications in SEA.

Methods

Forecasts of seasonal (3-month) streamflow totals were produced on the first day of each month using the BJP modelling approach. The output of dynamic hydrological and climate models was incorporated into the BJP modelling approach in a manner consistent with the operational application. A dynamic hydrological model was used to produce simulations that represent only the catchment condition at the forecast time, while rainfall forecasts from a dynamic climate model were used to represent the climate during the forecast period. The impact on predictive skill, reliability and robustness of replacing the selected predictors with dynamic model outputs was assessed incrementally: first by replacing the catchment condition predictor, and then by replacing the climate predictor.

The monthly water balance model, WAPABA (Wang et al. 2011), was used to produce simulations that represent only the catchment condition at the forecast time. These simulations were obtained by running the model to the forecast date using observed forcing data, to initialise the state variables, and then for the subsequent 3 months using monthly climatology mean forcing data. Variation in the simulated 3-month streamflow totals for a given month is solely due to differences in the initial conditions of the soil moisture and groundwater storages and not related to the climate forcing during the simulation period. Forecasts of 3- month streamflow totals were produced using the BJP modelling approach using the WAPABA simulations and total streamflow for the previous month to replace the selected predictors representing catchment condition at the forecast date. Total streamflow for the previous month was included as a predictor as a form of data assimilation.

Forecasts from POAMA, the Australian Bureau of Meteorology's dynamic seasonal climate forecasting model (Lim et al., 2010), were used to represent climate during the forecast period. Forecasts of 3-month rainfall totals from POAMA 2.4a were used to replace the selected climate predictors in the seasonal streamflow forecasting models that used WAPABA simulations to represent catchment condition at the forecast time.

The skill, reliability and robustness of streamflow forecasts were assessed using a cross-validation procedure. A new procedure was developed to produce cross-validation WAPABA simulations that allow the calibration of WAPABA parameters over a wide range of flow and climate conditions, while ensuring data for the forecast period had minimal influence on the calibrated parameters. WAPABA was calibrated using the entire data record except for the forecast year of interest and 2 years on either side (5 years in total). Simulations that represent only catchment condition at the forecast time were produced for the entire record and subsequently used in the BJP modelling approach to produce forecasts for the year of interest. This calibration, simulation and forecasting process was repeated for all years in the historical record.

The performance of the streamflow forecasts (produced using the BJP modelling approach) and the output of dynamic climate and hydrological models were evaluated for 21 catchments in eastern Australia covering a wide range of climate and hydrological conditions including some catchments outside the SEACI region.

Effort was also devoted to transferring the developed methods to the Bureau of Meteorology to support the improvement of the national service of seasonal streamflow forecasting.

Results

The skill of streamflow forecasts produced using the BJP modelling approach varies with catchment and season. Forecasts are more skilful for perennial streams in catchments that have large and active soil and groundwater storages and therefore long memory, for example inflows into Dartmouth and Hume reservoirs (Figure 71). Over SEA, forecasts tend to be the most skilful for spring and summer seasons when the annual hydrograph is receding. During these seasons, forecast streamflows are dominated by baseflows derived

from catchment soil and groundwater storages. The catchment condition predictors provide a good approximation of condition of these storages. Forecasts are least skilful when the dominant source of streamflows during the forecast period is concurrent rainfall. This occurs for autumn seasons over SEA when catchments are wetting up and the annual hydrograph is rising. The forecast probability distributions are reliable, with differences between the forecast probabilities corresponding to observed frequencies of events being within the range expected by sample variability. In general, the streamflow forecasts appear to be robust with minimal conditional bias with respect to time and forecast event size. However, temporal biases do appear in some catchments for autumn forecasts made after the late 1990s.

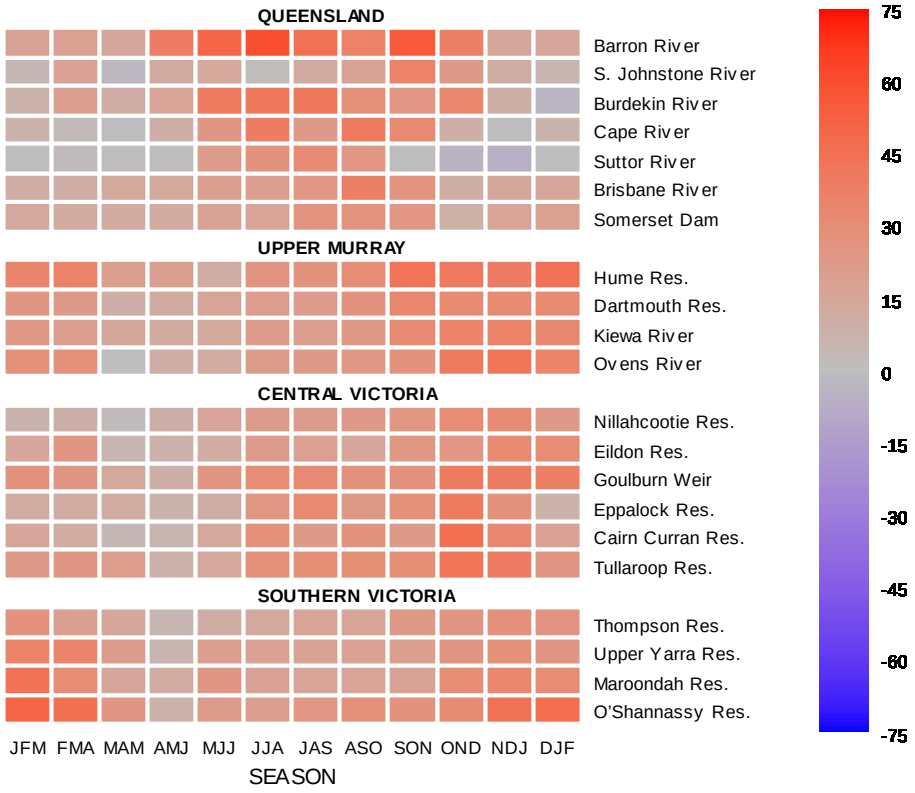

Figure 71. Skill scores based on root-mean-square error in probability for cross-validation forecasts made using selected predictors for the period 1950–2008 for a sample of catchments in eastern Australia. Positive skill scores (red shading) indicate an improvement over a forecast made using the historical distribution of seasonal streamflow

Replacing the selected predictors representing the catchment condition at the forecast time with WAPABA simulations produces little change in the average skill, reliability and robustness of streamflow forecasts for all catchments and seasons (Figure 72). The predictive skill scores typically change by less than 10 percent for individual catchments and seasons. Over SEA, improvements in skill scores tended to occur for forecasts made between May and December, which suggests that the WAPABA simulations represent the catchment condition at the forecast time better that the selected predictors. The use of WAPABA simulations for operational forecasting is attractive in that it eliminates the need for selecting predictors related to the initial catchment condition. As a result, it reduces the computational requirements to establish forecast models,

and skill estimates based on forecasts of historical events are not artificially inflated as can be the case with predictor selection.

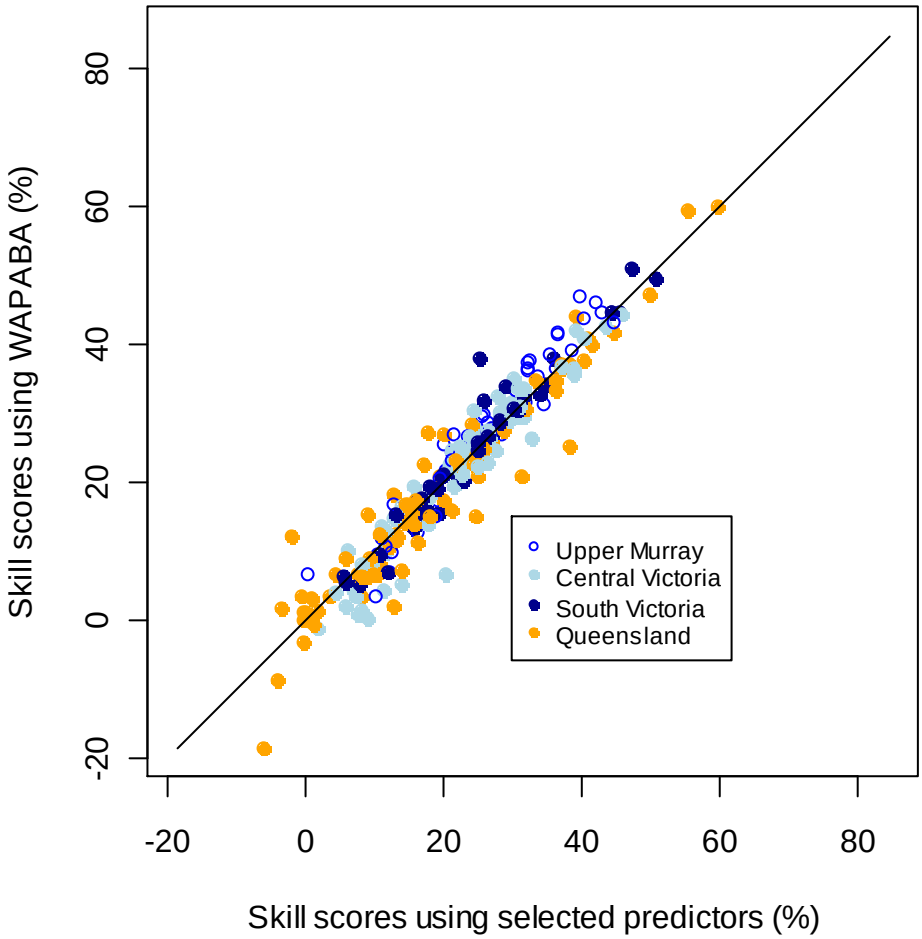

Figure 72. Changes in skill scores based on root-mean-square error in probability when replacing selected predictors representing catchment conditions at the forecast time with WAPABA simulations and total streamflow for the previous month. Each point represents a single forecast location and season. Points above the 1:1 line represent an improvement in predictive skill

Replacing the selected climate predictors with forecasts of 3-month rainfall totals from POAMA produces no change in the average root-mean-square error in probability skill score for all seasons and catchments. However, the changes for individual seasons at some locations are as much as ± 30 percent, with changes exceeding ±10 percent for many seasons and locations (Figure 73). The increases in predictive skill arise when POAMA has skill in forecasting rainfall. This corresponds to forecasts made in March and between June and October for catchments in SEA. When POAMA rainfall forecasts are not skilful, they only add noise to the streamflow forecast and hence decrease the skill of streamflow forecasts. However, even when POAMA does have skill in forecasting rainfall, it does not always outperform the selected climate predictor. A hierarchical Bayesian model averaging (BMA) approach has been developed which can merge forecasts made using different predictors in such a way that that combines their strengths. The use of the hierarchical BMA approach for combining streamflow forecasts made using climate indices and all three sub-versions of POAMA is currently being evaluated.

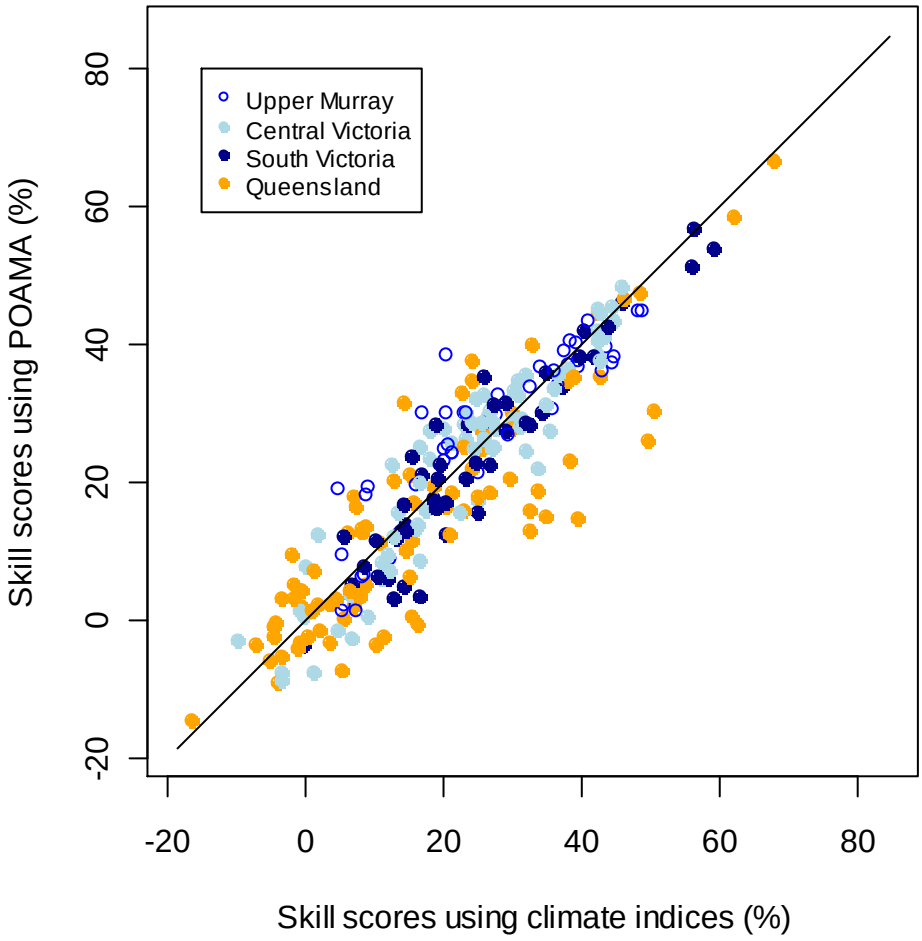

Figure 73. Changes in skill scores based on root-mean-square error in probability from replacing selected predictors representing climate during the forecast period with forecasts of 3-month rainfall totals from POAMA. Each point represents a single forecast location and season. Points above the 1:1 line represent an improvement in predictive skill

One of the highlights of this project (and the complementary seasonal streamflow forecasting project under the Water Information Research and Development Alliance (WIRADA) between CSIRO and the Bureau of

Meteorology) is the adoption of the BJP modelling system and current research results by the Bureau of Meteorology. A seasonal streamflow forecasting service, including a website, was developed in a collaboration between the Bureau, CSIRO and water managers. The Bureau's Extended Hydrological Prediction team officially commenced issuing public operational forecasts for 21 locations in south east Australia in December 2010 (see <http://www.bom.gov.au/water/ssf/index.shtml>). An experimental forecasting service is currently offered for five other catchments in eastern Australia. These forecasts are produced using the BJP modelling system and the forecast verification systems developed through SEACI and WIRADA research. The website provides a suite of forecast products. Figure 74 shows one of the products.

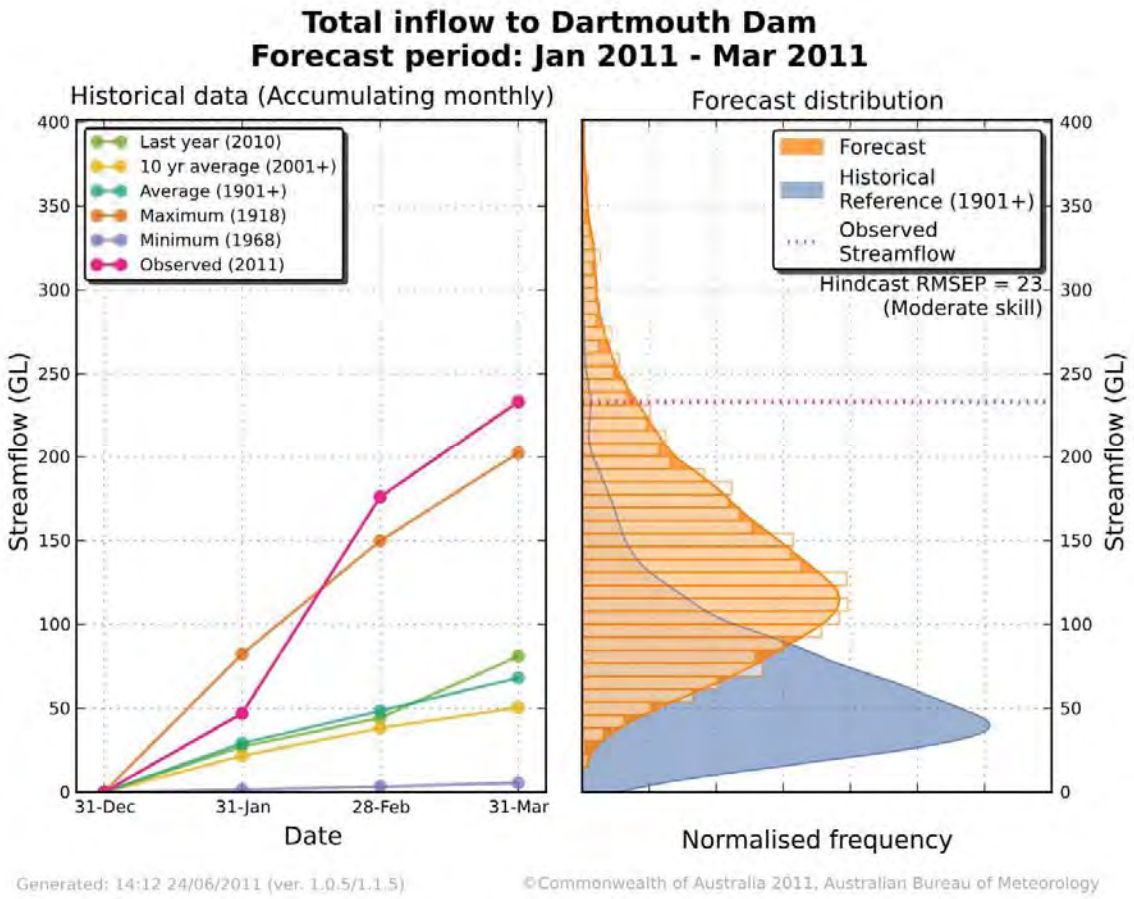

Figure 74. Seasonal streamflow forecast issued by the Bureau of Meteorology for total inflows to Dartmouth Dam for January to March 2011. The probabilistic forecast was produced by using the Bayesian joint probability modelling approach

Conclusions

Operational implementation of the BJP modelling approach establishes forecasting models by selecting predictors that represent the two sources of streamflow predictability the:

- catchment condition at the forecast time
- climate during the forecast period.

Research completed during the second year of Phase 2 of SEACI has established methods to incorporate the output of dynamic hydrological and climate models into the BJP modelling approach in a manner consistent with the operational application. Simulations from a dynamic hydrological model that represent the catchment condition at the forecast time were used to replace the selected predictors representing catchment condition at the forecast time, while seasonal rainfall forecasts from a dynamic climate model were used to replace selected predictors representing climate during the forecast period. These methods were evaluated for 21 catchments in eastern Australia that experience a wide range of hydrological and climate conditions.

For catchment condition, replacing the selected predictors with hydrological model simulations resulted in little change in the predictive skill, reliability and robustness of streamflow forecasts. However, the use of hydrological modelling output for operational forecasting is attractive in that it eliminates the need for selecting predictors. As a result, it reduces the computational requirements to establish forecast models, and skill estimates based on forecasts of historical events are not artificially inflated, as can be the case with predictor selection.

For climate, replacing the selected predictor with seasonal rainfall forecasts produced by a dynamic climate model produced mixed results, with increases in predictive skill of streamflow forecasts for some seasons and decreases in others. Bayesian model averaging over forecasting models that consider a range of climate predictors – including both climate indices and POAMA rainfall forecasts – appears to be an appropriate technique to produce forecasts that capture the strengths of all candidate predictors. However, the efficacy of BMA has yet to be appraised for seasonal streamflow forecasting and will require further research.

A highlight of the project is the adoption of the BJP modelling approach and current research results by the Bureau of Meteorology. The Bureau officially commenced issuing seasonal streamflow forecasts for 21 locations in SEA to the public in December 2010.

Links to other projects

This project and WIRADA Project 4.2 ('Seasonal to long-term water forecasting and prediction') represent a joint effort in developing seasonal streamflow forecasting methods and tools for adoption by the Bureau and key water management agencies in Australia.

The project has a strong linkage with Project 3.1 in Phase 2 of SEACI in two ways. The first is the use of dynamic climate model predictions for streamflow forecasting. The second is the use of the Bayesian joint probability method for calibration of climate model predictions to overcome bias and reliability problems and for combining dynamic modelling with empirical modelling to improve rainfall predictions.

The project also draws on results from Project 1.1 in Phase 2 of SEACI, especially results on climate drivers.

CHAPTER 8: NEXT STEPS

Research has progressed well in the second year of Phase 2 of SEACI. All projects are on track, already producing some very useful research findings, and all should continue producing innovative research and useful outputs for the remainder of Phase 2 of SEACI and beyond.

This Chapter summarises proposed research directions for 2011/12. Progress against these research directions will be reported in the SEACI 2 Synthesis Report due to be released in September 2012.

Theme 1: Understanding past hydroclimate variability and change in south-eastern Australia

Research in Project 1.1 has led to a better understanding of the factors that influence climate and streamflow in south-eastern Australia (SEA). In 2011/12, work on understanding the SEA rainfall decline will continue with a new focus on daily rainfall. Research will also continue on the role of the meridional circulation in affecting the climate of SEA. Following on from the analysis of the ability of the CCSM3 model to reproduce the expansion of the Hadley cell and strengthening of the STR only if anthropogenic forcings are included in the model, this analysis will now be carried out with two additional models in order to strengthen this result. In addition, the ACCESS model will be used to investigate the response of the meridional circulation to different patterns of oceanic warming and other possible drivers. Finally, the role of the Australian monsoon in influencing the ongoing autumn rainfall deficit across SEA will be further investigated.

Research in Project 1.2 will focus on using the CableDyn model to attribute observed hydrological responses to changes in major hydrometeorological drivers such as precipitation, temperature, CO_2, wind and radiation. As part of this, the relationship between temperature and humidity will be investigated in order to explore its impact on the sensitivity of the water balance. Similarly, the role of CO_2 will be explored by examining feedbacks that occur through biological and ecological processes such as vegetation structure and functioning.

Theme 2: Long-term hydroclimate projections in south-eastern Australia

Researchers in Project 2.1 will continue assessing the ability of global climate models to represent a range of important climate drivers and their relationship to rainfall across SEA. Additionally, the implications for climate projections of selecting and/or weighting a subset of global climate models will be further investigated. A range of downscaling methods including daily scaling, analogue downscaling, WRF dynamic modelling, and NHMM statistical downscaling will be assessed to investigate the relative uncertainties in the downscaling process. All of this information will be synthesised to inform the development of future climate series suitable for use in hydrologic modelling in SEA.

Research in Project 2.2 will continue to explore the nature of the rainfall-temperature-streamflow relationship. In particular, the sensitivity of streamflow to temperature will be assessed by applying techniques (which have previously indicated a ~30 percent reduction in streamflow to a 1°C temperature rise) to the 34 catchments selected in 2010/11. Additionally, the 17 catchments with streamflow and groundwater data will be investigated further through a seasonal analysis and an assessment of the impact of farm dams, as well as determining how they have responded to the 2010/11 floods. Finally, the above information will be synthesised in order to investigate how to adapt hydrological models to represent these processes.

Theme 3: Seasonal hydroclimate prediction in south-eastern Australia

Research in 2010/11 has shown that POAMA2 has good skill in predicting key climate drivers, especially those associated with ENSO. The very high rainfall received in 2010 provides an opportunity to assess the lead time at which the 2010 La Nina event could have been predicted, as well as the role of other predictable and unpredictable components of the climate that contributed to the very high rainfall received. The ability to represent extremely wet conditions months in advance would have enormous benefits to operational management of water in SEA.

Research carried out in 2010/11 showed that using outputs from POAMA2 to represent climate during the forecast period produced mixed results, with increases in predictive skill in some seasons and decreases in others. Research in 2011/12 will focus on the use of Bayesian model averaging to select a range of candidates to form multiple forecast models. The candidates will include climate indices from the Pacific, Indian, and extra-tropical regions as well as POAMA predictions. This should lead to improved skill in forecasting seasonal streamflows across SEA.

LIST OF PUBLICATIONS ARISING FROM SEACI RESEARCH IN 2010/11

Project 1.1

Cai W, van Rensch P, and Cowan T (in press) Influence of global-scale variability on the subtropical ridge over southeast Australia, *Journal of Climate*, doi: 10.1175/2011JCLI4149.1.

Cai W, van Rensch P, Cowan T and Hendon HH (2011) Teleconnection pathways of ENSO and the IOD and the mechanisms for impacts on Australian rainfall. *Journal of Climate* 24, 3910–3923.

Project 1.2

Briggs PR, Paget M, King EA, Haverd V, Trudinger CM, Raupach MR (2011) CSIRO AWAP Run 26c Historical Monthly and Annual Model Results for 1900-2011/02: AWAP 26c using improved Bureau of Meteorology AWAP Version 3 meteorological data. Data announcement 5/7/2011. pp. 9.

Briggs PR, Raupach MR, Haverd V, King EA, Paget M, Trudinger CM (2011) *Spatially varying parameters for CSIRO AWAP modelling*. Technical Report, CSIRO Marine and Atmospheric Research, Canberra, pp. 22.

Ummenhofer CC, Sen Gupta A, Briggs PR, England MH, McIntosh PC, Meyers GA, Pook MJ, Raupach MR, and Risbey JS (2010). Indian and Pacific Ocean influences on Southeast Australian drought and soil moisture. *Journal of Climate* 24, 1313–1336, doi:10.1175/2010JCLI3475.1.

Project 2.1

Kirono DGC, Chiew FHS and Kent DM (2010) Identification of best predictors for forecasting seasonal rainfall and runoff in Australia. *Hydrological Processes* 24(10), 1237–1247, doi:10.1002/hyp.7585.

Teng J, Chiew FHS, Vaze J and Post DA (2011) Calibration of hydrological models for medium term streamflow prediction in a changing climate. In: *Hydro-climatology: Variability and Change*. Proceedings of symposium J-H02 held during IUGG2011 in Melbourne, Australia, July 2011. IAHS Publication 344, 221–226, IAHS Press, Wallingford, UK.

Teng, J., Vaze, J., Chiew, F.H.S., Wang, B., Perraud, J-M. (2011). Estimating the relative uncertainties sourced from GCMs and hydrological models in modelling climate change impact on runoff. Journal of Hydrometeorology, doi: 10.1175/JHM-D-11-058.1.

Vaze J, Teng J, Chiew FHS (2010) Assessment of GCM simulations of annual and seasonal rainfall and daily rainfall distribution across south-east Australia. *Hydrological Processes* 25(9), 1486–1497, doi:10.1002/hyp.7916.

Project 2.2

Chiew FHS, Young WJ, Cai W and Teng J (2010) Current drought and future hydroclimate projections in southeast Australia and implications for water resources management, *Stochastic Environmental Research and Risk Assessment*, 24(4), 601–612, doi:10.1007/s00477-010-0424-x.

Post DA, Teng J, Chiew FHS, Wang B, Vaze J and Marvanek S (2011) Non-linearity of the runoff response across south-eastern Australia to increases in global average temperature. In: *Hydro-climatology: Variability and Change.* Proceedings of symposium J-H02 held during IUGG2011 in Melbourne, Australia, July 2011. IAHS Publication 344, 188–194, IAHS Press, Wallingford, UK.

Project 3.1

Charles A, Hendon HH, Wang QJ, Robertson D, and Lim EP (in press) Comparison of techniques for the calibration of coupled model forecasts of Murray Darling Basin seasonal mean rainfall, CAWCR Technical Report.

Langford S, Hendon HH, and Lim EP (2011) *Assessment of POAMA's predictions of some climate indices for use as predictors of Australian rainfall*, CAWCR Technical Report No.031, The Centre for Australian Weather and Climate Research. Available online at < http://www.cawcr.gov.au/publications/technicalreports/CTR_031.pdf>.

Lim EP, Hendon HH, Alves O, Yin Y, Wang G, Hudson D, Zhao M and Shi L (2010) *Dynamical seasonal prediction of tropical Indo-Pacific SST and Australian rainfall with improved ocean initial conditions*. CAWCR Technical Report No.032, The Centre for Australian Weather and Climate Research. Available online at <http://www.cawcr.gov.au/publications/technicalreports/CTR_032.pdf>.

Lim EP, Hendon HH, Anderson DTL, Charles A and Alves O (2011) Dynamical, statistical-dynamical and multi-model ensemble forecasts of Australian spring season rainfall. *Monthly Weather Review* 139, 958–975, doi:10.1175/2010MWR3399.1.

Yin Y, Alves O and Oke P (2011) An ensemble ocean data assimilation system for seasonal prediction. *Monthly Weather Review*, 139, 786–808, doi:10.1175/2010MWR3419.1.

Project 3.2

Wang QJ and Robertson DE (2011) Multisite probabilistic forecasting of seasonal flows for streams with zero value occurrences. *Water Resources Research*` 47, W02546, doi:10.1029/2010WR009333.

Robertson DE, Wang QJ, Pagano TC, Haparachchi, HAP (2011) Using water balance model output to represent initial catchment conditions in statistical forecasting of seasonal streamflows, 34th IAHR World Congress, International Association of Hydro-Environment Engineering and Research, Brisbane, Australia, June 26 to July 1 2011.

Robertson DE, Wang QJ, Schepen A, Peaty T, Zhou S, Perkins J, Shin D, Plummer N, Allie S (2010) Evaluation of the Bayesian joint probability modelling approach to seasonal streamflow forecasting for inflows into Melbourne Water and Hydro Tasmania storages, CSIRO Water for a Healthy Country National Research Flagship.

Non-project specific

Cai W, Sullivan A, Cowan T, Ribbe J, and Shi G (2011) Simulation of the Indian Ocean Dipole: A relevant criterion for selecting models for climate projections, *Geophysical Research Letters*, 38, 27 L03704, doi:10.1029/2010GL046242.

Fu G and Charles SP (2011) Statistical downscaling of daily rainfall for Southeastern Australia, Hydro-climatology: Variability and change. In: *Hydro-climatology: Variability and Change.* Proceedings of symposium J-H02 held during IUGG2011 in Melbourne, Australia, July 2011. IAHS Publication 344, 69–74, IAHS Press, Wallingford, UK.

Roff G, Thompson DWJ, and Hendon H (2011) Does increasing model stratospheric resolution improve extended-range forecast skill?, *Geophysical Research Letters* 38, L05809, doi:10.1029/2010GL046515.

Smith I and Timbal B (2010) Links between tropical indices and southern Australia rainfall, *International Journal of Climatology*, doi:10.1002/joc.2251.

REFERENCES

Appleby VC (1970) Recession and baseflow problem. *Water Resources Research* 6:5, 1398–1403.

Archer CL and Caldeira K (2008) Historical trends in the jet streams. *Geophysical Research Letters*, 35, doi:10.1029/2008GL033614.

Arora VK (2002) The use of the aridity index to assess climate change effect on annual runoff. *Journal of Hydrology*, 265,164-177.

Birner T (2010) Recent widening of the tropical belt from global tropopause statistics: Sensitivities. *Journal Geophysical Research*, 115, D23109. doi: 10.1029/2010d014664.

Briggs PR, Paget M, King EA, Haverd V, Trudinger CM and Raupach MR (2011a) CSIRO AWAP Run 26c historical monthly and annual model results for 1900–2011/02: AWAP 26c using improved Bureau of Meteorology AWAP Version 3 meteorological data. Data announcement 5/7/2011.

Briggs PR, Raupach MR, Briggs PR, Haverd V, King EA, Paget M and Trudinger CM (2011b) Spatially varying parameters for CSIRO AWAP modelling. CSIRO Marine and Atmospheric Research, Canberra.

Budyko MI (1974), Climate and Life, Academic Press, New York, USA.

Burnash, R. J. C., Ferral, R. L. & McGuire, R. A. (1973) A Generalised Streamflow Simulation System – Conceptual Modelling for Digital Computers, Joint Federal and State River Forecast Center, Sacramento, Technical Report.

Cai W (2006) Antarctic ozone depletion causes an intensification of the Southern Ocean supergyre circulation, *Geophysical Research Letters*, 33, L03712, doi:10.1029/2005GL024911.

Cai W and Cowan T (2008) Dynamics of late autumn rainfall reduction over south-eastern Australia, *Geophysical Research Letters*, 35, L09708, doi:10.1029/2008GL033727.

Frederiksen JS and Frederiksen CS (2007) Inter-decadal changes in Southern Hemisphere winter storm track modes, *Tellus*, 59 A, 559–617.

Cai W, Rensch PV, Cowan T and Hendon HH (2011) Teleconnection pathways for ENSO and the IOD and the mechanism for impacts on Australian rainfall. *Journal of Climate*, doi: 10.1175/2011JCLI4129.1.

Chapman (1999) A comparison of algorithms for stream flow recession and baseflow separation. *Hydrological Processes* 13, pp. 701-714.

Chiew FHS, Kirono DGC, Kent DM, Frost AJ, Charles SP, Timbal B, Nguyen KC and Fu G (2010) Comparison of runoff modelled using rainfall from different downscaling methods for historical and future climates. *Journal of Hydrology* 387, 10–23.

Chiew, F. H. S., Peel, M. C. & Western, A. W. (2002) Application and testing of the simple rainfall-runoff model SIMHYD. in Singh, V. P. & Frevert, D. K. (eds.), *Mathematical models of small watershed hydrology and applications* (Littleton, Colorado, USA: Water Resources Publication), 335–367.

Choudhury, B.J. (1999) Evaluation of an empirical equation for annual evaporation using field observations and results from a biophysical model. *Journal of Hydrology*, 216, 99-110.

CSIRO (2010a) Program Annual Report 2009/10. South Eastern Australian Climate Initiative (SEACI). CSIRO, Australia.

CSIRO (2010b) Baseflow Assessment for the Murray-Darling Basin. Water for a Healthy Country Flagship report, CSIRO, Australia.

Doblas-Reyes FJ, Hagedorn R, Palmer TN and Morcrette J-J (2006) Impact of increasing greenhouse gas concentrations in seasonal ensemble forecasts. *Geophysical Research Letters* 33, L07708, doi:10.1029/2005GL025061.

Drosdowsky, W., 2005, The latitude of the subtropical ridge over eastern Australia: The L index revisited, *International Journal of Climatology*, *25*, 1291–1299, 10.1002/joc.1196.

Eckhardt K (2005) How to construct recursive digital filters for baseflow separation. *Hydrological Processes* 19, 507–515.

Evans JP, Ekstrom M and Ji F (2011) Evaluating the performance of a 36 member of WRF physics ensemble over South-East Australia. Submitted to Climate Dynamics.

Frederiksen CS, Frederiksen JS, Sisson JM and Osbrough SL (2011) Australian winter circulation and rainfall changes and projections. International *Journal of Climate Change Strategies and Management* Paper 4, Vol 3, issue 2.

Fu Q, Johanson CM, Wallace JM and Reichler T (2006) Enhanced mid-latitude tropospheric warming in satellite measurements, *Science*, 312, 1179.

GA (2008) Mapping the growth, location, surface area and age of farm dams in the Murray-Darling Basin. Geoscience Australia. March 2008.

García-García D, Ummenhofer CC and Zlotnicki V (2011) Australian water mass variations from GRACE data linked to Indo-Pacific climate variability. *Remote Sensing of Environment,* 115, 2175–2183.

Grayson RB, Argent RM, Nathan RJ, McMahon RA, Mein RG (1996) Hydrological recipes. Estimation Techniques in Australian Hydrology. Cooperative Research Centre for Catchment Hydrology, Australia, Canberra.

Hendon HH, Lim E-P, Wang G, Alves O and Hudson D (2009) Prospects for predicting two flavours of El Niño. *Geophysical Research Letters*, 36, L19713, doi:10.1029/2009GL040100.

Hu Y and Fu Q (2007) Observed poleward expansion of the Hadley circulation since 1979, *Atmospheric Chemistry Physics*, 7, 5229–5236.

Hurrell JW, Hack JJ, Shea D, Caron JM and Rosinski J (2008) A new sea surface temperature and sea ice boundary data set for the Community Atmosphere Model. *Journal of Climate*, 21, 5145–5153, doi: 10.1175/2008JCLI2292.1.1.

Irving D, Perkins S, Brown JR, Sen Gupta A, Moise A, Murphy B, Muir L, Colman R, Power S, Delage F, Brown JN (in press). Evaluating global climate models for climate change projections in the Pacific Island region. Climate Research, doi: 10.3354/cr01028.

Johnson C and Bowler N (2009) On the reliability and calibration of ensemble forecasts. *Monthly Weather Review* 173,1717–1720.

Jones DA, Wang W and Fawcett R (2009) High-quality spatial climate data-sets for Australia. *Australian Meteorological and Oceanographic Journal* 58, 233–248.

Kajikawa Y, Wang B, and Yang J (2010) A multi-time scale Australian monsoon index, *International Journal of Climatology*, 30, 1114–1120.

Kanamitsu M, Kistler RE, Reynolds RW, Yang SK, Hnilo JJ, Fiorino M and Potter GL (2002) NCEP/DOE AMIP-II Reanalysis (R-2). Bull. Amer. Meteor. Soc., 83, 1641–1643.

Kent DM, Kirono DGC, Timbal B and Chiew FHS (2011) Representation of the Australian sub-tropical ridge in the CMIP3 models. Revised version submitted to *International Journal of Climatology*.

Kirchner JW (2003) A double paradox in catchment hydrology and geochemistry. *Hydrological Processes* 17, 871-874.

Kirono DGC, Kent DM, Chiew FHS and Teng J (2011) GCM Evaluation and selection for climate change impacts assessment in South Eastern Australia. Greenhouse 2011 Conference, Cairns, 4-8 April 2011.

Lacey GC (1996) Relating baseflow to catchment properties. A scaling approach. Cooperative Research Centre for Catchment Hydrology Report 96/8, Australia.

L'Heureux ML and Thompson DWJ (2006) Observed Relationships between the El Niño–Southern Oscillation and the Extratropical Zonal-Mean Circulation. *Journal of Climate*, 19, 276–287.

Lu J, Deser C and Reichler T (2009) Cause of the widening of the tropical belt since 1958. *Geophysical Research Letters*, 36, L03803, doi:10.1029/2008GL036076.

Marshall GJ (2003) Trends in the Southern Annular Mode from observations and reanalyses. *Journal of Climate*, 16, 4134-4143.

Miller DM (1984) Reducing Transformation Bias in Curve Fitting. *The American Statistician,* 38, 124–126.

Milly PCD and KA Dunne (2002) Macroscale water fluxes. 2. Water and energy supply control of their interannual variability. *Water Resources Research*, 38, 1206, doi:10.1029/2001WR000760.

Munier S, Becker M, Maisongrande P and Cazenave A (2011) Evaluation of groundwater storage variations in various large aquifers using GRACE data. *Geophysical Research Letters*. Submitted.

Nathan RJ, McMahon TA (1990) Evaluation of automated techniques for base flow and recession analyses. *Water Resources Research*, 26 (7),1465–1473.

Nicholls N (2004) The changing nature of Australian droughts. *Climate Change*, 63, pp. 323–336.

Nicholls N (2009) Local and remote causes of the southern Australian autumn-winter rainfall decline, 1958-2007. *Climate Dynamics*, DOI 10.1007/s00382-009-0527-6.

Petrone KC, Hughes JD, Van Niel TG, Silberstein RP (2010) Streamflow decline in southwestern Australia, 1950-2008. *Geophysical Research Letters,* 37, L1140, doi:10.1029/2010GL043102.

Plummer N, Tuteja NK, Wang QJ, Wang E, Robertson DE, Zhou S, Schepen A, Alves O, Timbal B and Puri K (2009) A seasonal water availability prediction service: Opportunities and Challenges, in 18th World IMACS/MODSIM Congress, edited, Modelling and Simulation Society of Australia and New Zealand Inc., Cairns.

Post DA, Teng J, Chiew FHS, Wang B, Vaze J and Marvanek S (2011) Non-linearity of the runoff response across south-eastern Australia to increases in global average temperature. In: Hydro-climatology: Variability and Change. Proceedings of symposium J-H02 held during IUGG2011 in Melbourne, Australia, July 2011. IAHS Publication 344. IAHS Press, Wallingford, UK.

Raupach MR, Briggs PR, Haverd V, King EA, Paget M and Trudinger CM (2009) Australian Water Availability Project (AWAP): CSIRO Marine and Atmospheric Research Component: Final Report for Phase 3. CAWCR Technical Report No. 013. Australia, pp. 67.

Robertson DE and Wang QJ (2010) Selection of predictors for the Bayesian joint probability approach to seasonal streamflow forecasting, *Journal of Hydrometeorology*,

Sankarasubramanian A, Vogel RM, and Limbrunner JF (2001) Climate elasticity of streamflow in the United States. *Water Resources Research*, 37, 1771–1781.

Seidel DJ and Randel WJ (2007) Recent widening of the tropical belt: Evidence from tropopause observations. *Journal Geophysical Research*, 112, doi:10.1029/2007JD08861.

Stephenson DB, Coelho CADS, Doblas-Reyes FJ and Balmaceda M (2005) Forecast assimilation: A unified framework for the combination of multimodel weather and climate predictions. *Tellus*, 57A, pp. 253–264.

Teng J, Vaze J, Chiew FHS, Wang B and Perraud JM (2011a) Estimating the relative uncertainties sourced from GCMs and hydrological models in modelling climate change impact on runoff. Submitted to *Journal of Hydrometeorology*. doi: 10.1175/JHM-D-11-058.1.

Teng J, Chiew FHS, Vaze J and Post DA (2011b) Calibration of hydrological models for medium-term streamflow prediction in a changing climate. In: Hydro-climatology: Variability and Change. Proceedings of symposium J-H02 held during IUGG2011 in Melbourne, Australia, July 2011. IAHS Publication 344. IAHS Press, Wallingford, UK.

Timbal B and Fernandez E (2009) Improved detection of the recent rainfall decline across SEA including its seasonality and spatial characteristics. SEACI Final Report for Project 1.2.1P, Australia. Available online at <http://www.seaci.org>.

Timbal B (2009) The continuing decline in south-east Australian rainfall: update to May 2009. *CAWCR Research Letters*, 2, 4-10, July 2009.

Timbal B (2010) A discussion on aspects of the seasonality of the rainfall decline in south-eastern Australia. *CAWCR Research Letters*, 4, pp. 20–33.

Timbal, B., J. Arblaster, K. Braganza, E. Fernandez, H. Hendon, B. Murphy, M. Raupach, C. Rakich, I. Smith, K. Whan, and M. Wheeler, 2010, Understanding the anthropogenic nature of the observed rainfall decline across South Eastern Australia, *Tech. rep.*, CAWCR Research report.

Vaze J, Chiew F, Perraud J-M, Viney N, Post D, Teng J, Wang B, Lerat J and Goswami M (2011) Rainfall-runoff modelling across southeast Australia: datasets, models and results. *Australian Journal of Water Resources*, 14 (2), pp. 101-116.

Vogel RM, Wilson I, and Daly C (1999) Regional regression models of annual streamflow for the United States. *Journal of Irrigation and Drainage Engineering*, 125, pp. 148–157.

Watterson IG (2008) Calculation of probability density function for temperature and precipitation change under global warming. Journal of Geophysical Research 113: D12106.

Wang B, Kang I-S and Lee J-Y (2004) Ensemble Simulations of Asian–Australian Monsoon Variability by 11 GCMs, *Journal of Climate*, 17, 803–818.

Wang QJ, Robertson DE and Chiew FHS (2009) A Bayesian joint probability modelling approach for seasonal forecasting of streamflows at multiple sites, *Water Resource Research*, 45, pp. 18.

Wang QJ and Robertson DE (2011) Multisite probabilistic forecasting of seasonal flows for streams with zero value occurrences, *Water Resources Research*, 47, W02546, doi:10.1029/2010WR009333.

Weisheimer A, Doblas-Reyes FJ, Palmer TN, Alessandri A, Arribas A, Deque M, Keenlyside N, MacVean M, Navarra A and Rogel P (2009) ENSEMBLES: A new multi-model ensemble for seasonal-to-annual predictions—Skill and progress beyond DEMETER in forecasting tropical Pacific SSTs. *Geophysical Research Letters*, 36, L21711, doi:10.1029/2009GL040896.

Wittenbery H (1999) Baseflow recession and recharge as nonlinear storage processes. *Hydrological Processes* 13, pp. 715-716.

Yin Y, Alves O and Oke P (2011) An ensemble ocean data assimilation system for seasonal prediction. *Monthly Weather Review*, 139, pp. 786–808.

Zhang L, Hickel K, Dawes WR, Chiew FHS, Western AW, and Briggs PR (2004) A rational function approach for estimating mean annual evapotranspiration. *Water Resources Research*, 40, W02502, doi:10.1029/2003WR002710.

Zhang L, Dawes WR, and Walker GR (2001) Response of mean annual evapotranspiration to vegetation changes at catchment scale. *Water Resources Research*, 37, pp. 701–708.

For more information:

Email **seaci@csiro.au**
Visit **www.seaci.org**

National Research FLAGSHIPS
Water for a Healthy Country

CSIRO

Australian Government
Department of Climate Change and Energy Efficiency
Bureau of Meteorology

MURRAY–DARLING BASIN AUTHORITY

State Government Victoria
Department of Sustainability and Environment